PROCEEDINGS
OF THE PAKISTAN ACADEMY OF SCIENCES:
A. Physical and Computational Sciences

PAKISTAN ACADEMY OF SCIENCES
ISLAMABAD, PAKISTAN

HEC Recognized, Category Y

PROCEEDINGS
OF THE PAKISTAN ACADEMY OF SCIENCES:
A. Physical and Computational Sciences

CONTENTS

Research Articles

Pakistan Academy of Sciences

Research Article

Design of Power Monitoring and Electrical Control Systems to Support Energy Conservation

Fransiscus Yudi Limpraptono[1*], Eko Nurcahyo[1], Mochammad Ibrahim Ashari[1], Erkata Yandri[2], and Yahya Jani[3]

[1]Department of Electrical Engineering, National Institute of Technology Malang,
Jl. Raya Karanglo, Km. 2, Malang 65143, Indonesia
[2]Graduate School of Renewable Energy, Darma Persada University, Jl. Radin Inten 2,
Pondok Kelapa, East Jakarta 13450, Indonesia
[3]Department of Urban Studies, Malmö University, Nordenskiöldsgatan 1,
21119 Malmo, Sweden

Abstract: The increasing demand for electrical energy and the decreasing supply of fossil fuels in recent years have increased the cost of electrical energy. So that the culture of saving electrical energy is a habit that must be cultivated in the community. On the other hand, energy-saving behavior cannot be realized massively without a support system that can control energy use. With these concerns, it is necessary to develop a method that encourages a culture of saving electrical energy. This paper proposes a system that supports active energy efficiency methods that can support an energy-efficient culture. This system is an electric power monitoring system that is integrated with a smart electrical panel that continuously monitors the use of electrical energy and can control electrical loads automatically, record electricity usage, provide comprehensive reports and analyze energy usage. The method used to carry out this research is research and development. This research has produced a prototype of electrical power control and monitoring system that has a smart panel based on a raspberry PI 3 and PZEM-004t power energy meter. The monitoring system performs and executes automatic control of electrical loads. The system can also provide reports in the form of data monitoring in daily, weekly, monthly or annual period. From the test results, it can be concluded that the system can work well. This research is expected to contribute to providing a system that can support government efforts in saving energy.

1. INTRODUCTION

The massive development of energy conversion technologies and the invention of various equipment that ease human activities leads to a significant increase in energy usage involving electricity. With the continuous increase of energy consumption, the price of electric energy is getting more expensive [1, 2]. This condition is worsened by the declining supply of fossil fuel as the main resource for power generations.

The increase in energy price and energy consumption encouraged the government to improve the culture of saving electrical energy [3–5]. Moreover, the environmental concern such as pollution and gas emission has also motivated the energy-saving promotion. The saving energy campaign can be started by using the electrical energy in the residential and building premises wisely [6]. According to the obtained data from the previous researches, it was observed that the energy requirement in the building absorbs 40% of the total world energy needs. In Indonesia specifically, the building sector requires about 50 % of total energy expenditure and more than 70 % of overall electricity consumption [7]. As a consequence of high energy consumption, the building sector

in Indonesia contributes to 30 % of greenhouse gas emissions [8]. According to the United States Department of Energy, building premises contribute to 40 % of the country's major energy consumption and 40 % of CO_2 emissions [9]. In a crowded urban environment, this trend is much higher. The buildings in New York City contribute 75 % of city energy consumptions [10].

The needs of electrical energy in commercial buildings are mostly for heating or cooling, ventilation, air conditioning (HVAC), and lighting. With the increase of energy prices and environmental issues of fossil fuel energy supplies, many researchers have been developing the use of alternative and renewable energy to promote green energy [11, 12].

Energy efficiency can be achieved by optimizing the use of lighting systems and implementing lighting system design in proportion with the room functionalities. Most importantly, the operation of heating/ cooling systems and ventilation should be controlled continuously according to the actual needs [13]. To make sure efficient consumption of electrical energy, effective power metering, and monitoring systems are required. The power metering and monitoring systems would provide important information to the owners and operators correlating to the performance of building energy consumption. An effective metering and monitoring system can involve tenants, property managers, and owners in measuring energy consumption. Hence, substantial actions can be implemented immediately to maintain the use of energy in an efficient way. The integrated energy management and monitoring system are sufficient to improve energy efficiency. An effective measurement and monitoring system may bring 10 % direct energy savings and hence reduce the operational costs of the building [14].

Promotion of energy saving in residential and building premises should also be included in communication strategies since it is understood mainly by experts and industry, but not by commons [15]. To reduce the electrical energy consumption through the improvement of the habit of energy saving, the Indonesian government issued the Regulation of the Minister of Energy and Mineral Resources (ESDM) on Electricity Energy Saving. It states that all office buildings must implement the electricity energy-saving program on the air conditioning system, lighting system, and other supporting equipment. Some references in the implementation of the policy are by using energy-efficient appliances, the implementation of a good energy management system, and change the behavior of people who live in the building [14].

There are two approaches in the efforts of energy efficiency, namely passive and active energy efficiency. Passive energy efficiency activities can be done by installing and using energy-saving equipment and efforts to correct power factors. Passive energy efficiency is a fundamental effort for energy conservation. However, the passive approach alone is not sufficient to reach the desired level of energy efficiency. It needs a system that can support energy efficiency with the method of active approach. Energy efficiency requires an active approach such as load control, system automation, and monitoring of energy consumption to obtain a better saving energy scheme which eventually results in a better energy efficiency performance [16–18].

The electric energy efficiency of the active approach method requires an electrical energy monitoring system that must have the ability to provide reports and data analysis and be able to communicate with various devices. This system is connected to an electric load distribution panel which is capable of recording power consumption and being able to control the electrical load automatically. More importantly, the system must be able to connect with a number of separate measuring equipment, transmit data between devices, store measurement data, and produce the various analyses required for decision making. On the other hand, with the rapidly growing field of information and communication technology, the system is required to use effective communication methods such as IP-based, autodial, and connection with mobile devices or smartphones.

So far, it is costly to implement the monitoring system with the required capabilities as described. Therefore, the implementation of the saving-energy monitoring system is limited. This research proposed a system that supports active energy efficiency method which can help the energy-saving cultures. Low-cost power monitoring and

energy management system is designed for building premises. The proposed system is connected with a distribution panel in each building and equipped with a communication protocol for remote monitoring purposes. It has some advantages features involved the ability to control the electric load automatically, record the use of electric power, provide comprehensive reports and analyze the use of energy.

2. MATERIALS AND METHODS

2.1 Research Methods

To develop a smart-panel system for power consumption control and monitoring, the research and development (R&D) method is conducted in this paper. The proposed method mainly consists of two parts; the development of a smart-panel prototype and the development of application software that would be used to control and monitor energy consumption. The initial stage of smart-panel prototype development is hardware and software design. Followed by the realization of the obtained design to develop the smart panel. The next stage is testing and calibrating the developed smart-panel to obtain a proper design and parameter control setting.

The second part of the method is to design software applications for controlling and monitoring energy consumption. In this stage, the comprehensive application software was developed to control and monitor the electrical parameter involving the energy consumption accurately. The final step is integrating the developed smart-panel dan application software before employed the smart-panel to the real test system.

2.2 System Design

This research addressed the efficient design of a prototype system to support the conservation of electrical energy. The designed system has smart and low-cost features. It comprises several smart panel units, a local computer network (LAN), database server as data storage, web server containing application of system controller, and a power monitoring display. The proposed monitoring design is depicted in Figure 1.

The design of the server-based system is embedded system Raspberry PI 3, which has low power, low price, small size, and high performance. An open-source operating system was implemented to reduce the cost. The monitoring system is responsible for recording the electrical energy consumption in a building and monitoring electrical quantities such as voltage, current, power factor, and electrical power. The monitoring system performs and executes automatic control of electrical loads that have been set by the operator. The system can also provide reports in the form of data monitoring in daily, weekly, monthly or annual period. Real-time reports are displayed on the dashboard power monitoring system. That dashboard is situated on a strategic location that can be seen by building users as part of an active approach method of energy conservation.

Smart panels are part of the system that serves as a power distribution panel. The architecture of the proposed smart panel is depicted in Figure 2. Smart panels are controlled by an embedded system Raspberry Pi 3, which has a Broadcom BCM2837B0, Cortex-A53 (ARMv8) 64-bit 1.4 GHz processor, with the Storage Capacity of 1GB LPDDR2 SDRAM. It has 2.4 GHz wireless LAN and 5 GHz IEEE 802.11 b/g/n/ac, Bluetooth 4.2. Besides, it has Gigabit Ethernet, 40- pin GPIO, 4 USB 2.0 ports, and HDMI. Raspberry Pi uses the Raspbian Linux-based operating system, which comes with several applications such as Apache web server and MySQL database. Raspberry Pi is expanded with I/O port expander MCP23017, so it can add 16 bits of the I/O port. The interface of MCP23017 chip with Raspberry pi using I2C line.

The panel is controlled by a programmed Raspberry Pi embedded system to control the electrical load. Smart panels are also capable of communicating with the server over a computer network, hence it can either send or receive commands from the server. The smart panel contains an embedded system that will be in charge of reading input signals from all push buttons and activating a switch contactor that will turn on or offload directly. Also, the smart panel has a measuring instrument of electrical quantities that continuously records the consumption of electric power.

The design of the smart panel prototype has 16 inputs and 16 outputs. The input unit is used to read the push button status that serves to turn on and off the electrical load. The output unit is used to connect or disconnect the electrical load. The switch circuit on the output unit employs a G3MB-202P solid-state relay. Both the input and output unit circuits are protected by optical isolation to avoid the inclusion of undesired electrical voltage The proposed smart panel design implements a PZEM-004t power energy meter for electrical power measurement. This module can measure voltage, current, active power, and electrical energy. PZEM-004 can store data when power is

off and able to communicate with the controller unit through the serial port. The implemented design of the smart panel is depicted in Figure 3.

3. RESULTS AND DISCUSSION

3.1 Power Meter Unit Test Results

The validation of the designed power meter is carried out by comparing the performance of the proposed metering design to the standard power meters. Three different loads were considered in the experimental setup. It was monitored that the PZEM-004T module provided high accuracy measurement
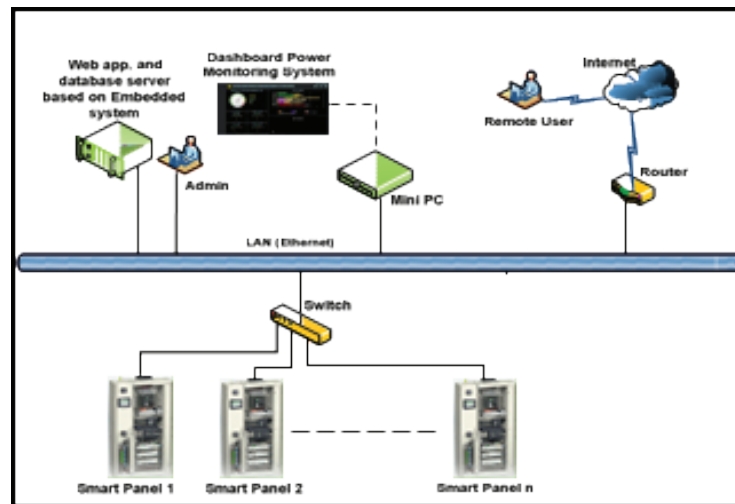
Fig. 1. Smart Panel and Power Monitoring System
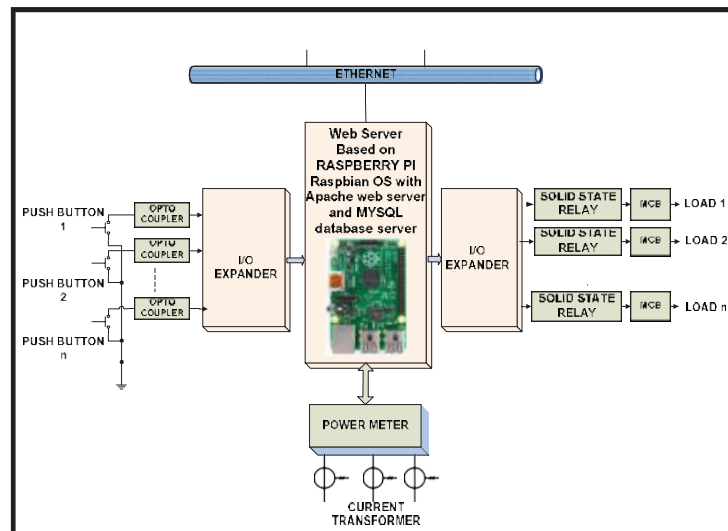
Fig. 2. Architecture of the Smart Panel
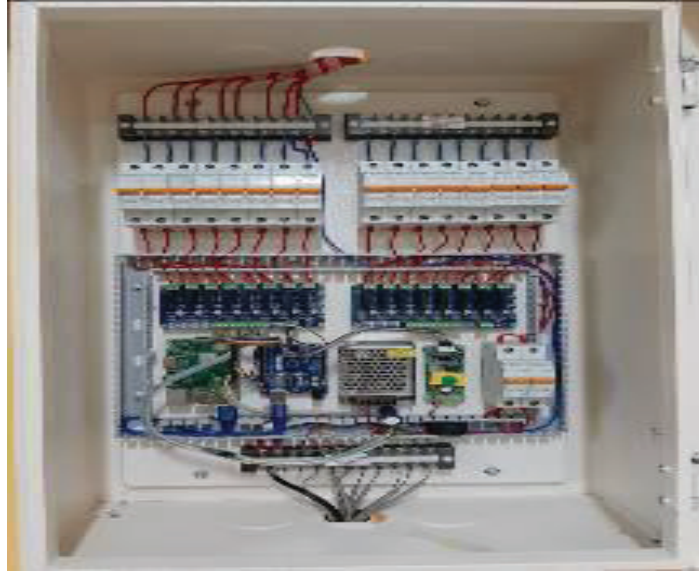
Fig. 3. Smart Panel.
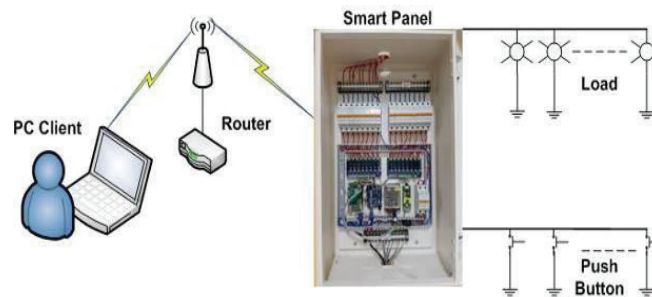
Fig. 4. Diagram of Power Monitoring and Control System Unit Testing

results. Therefore the proposed measurement module was suitable for measuring current and power. For current and power measurements, it has an average error of 0 %. While for voltage measurements, the average error is around 0.04.

3.2 Power Monitoring and Control System Test Results

The power Monitoring and Control System unit is tested with a monitor and controls the load remotely. The experimental setup is shown in Figure 4.

Initially, the experimental procedures was conducted by remotely open the Power Monitoring website with a web browser hence a web page would appear as shown in Figure 5.

To enter the Power Monitoring web application, each user must log in first. If the login procedure is successful then the user can see a set of application features. The users would see the usage of electrical power from each panel. The measured electrical powers were displayed in graphical form with the option to select the data period on a daily, weekly, monthly and annual basis. The right-hand side of the dashboard displayed the voltage and the current for each panel. While the bottom side of the dashboard displayed the graph for cosφ.

The testing of load control features can be done by entering the system control menu. The web page display of the control system page is shown in Figure 6.

Each panel has 16 push buttons, according to the design of the smart panel. Loads can be turned "on" or "off" through each of these pushbuttons. In addition, the load can also be turned "off" or "on" automatically by scheduling the load activities.
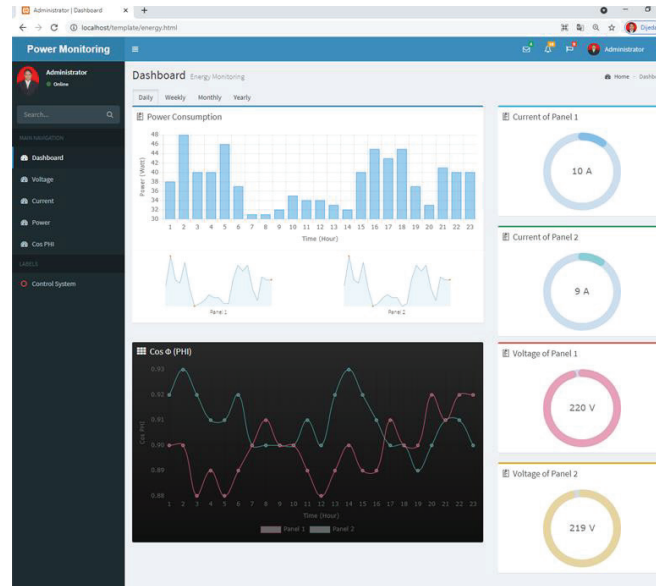
Fig. 5. Remote Power Monitoring System
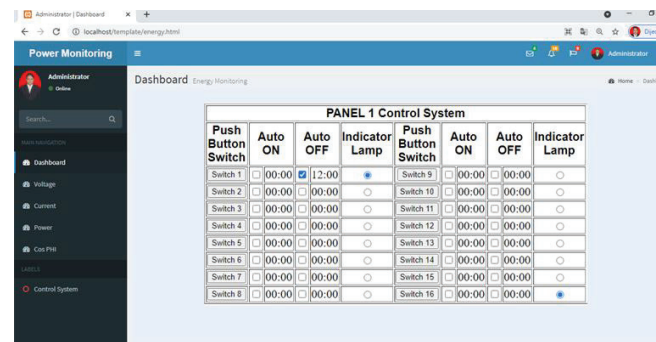
Fig. 6. Remote Control System

Each load has an auto ON and auto OFF menu that can be set by the user.

4. CONCLUSION

This paper presents research on power monitoring and electrical load control systems to support the conservation of electrical energy. From the experimental results, it can be concluded that the system can work well. The power meter unit can function properly with high accuracies. A small error of 0.04 % was observed for voltage measurement. While the measurement of current and electrical power resulted in an error of 0 %. The power monitoring system can work well and can record and display power usage at any time. The load control system can also function well to control load activity remotely and automatically. This research is expected to contribute to providing a system that can support government efforts in saving energy.

5. ACKNOWLEDGEMENTS

6. CONFLICT OF INTEREST

The authors declare no conflict of interest.

7. REFERENCES

1. Anindhita., I. Rahardjo., I. Fitriana., R.E.P. Dewi., E. Siregar., N. Niode., Yudiartono., A. Sugiyono., La Ode., W.P.T. Wijaya., A.K. Paminto, and N. Gustriani. *Indonesia Energy Outlook 2018: Sustainable Energy for Land Transportation, 134 (4). BPPT, Jakarta, Indonesia* (2018).

2. P.G. Adinurani, R.H. Setyobudi, S.K. Wahono, M. Maizirwan, A. Nindita, E. Purbajanti, S.S. Harsono, A.R. Malala, L.O. Nelwan, and A. Sasmito. Ballast weight review of capsule husk *Jatropha curcas* Linn. on acid fermentation first stage in two-phase anaerobic digestion. *Proceedings of the Pakistan Academy of Sciences B. Life and Environmental Sciences.* 54 (1): 47–57 (2017).

3. K. Suwansit., B. Konsombut., P. Hankongkaew, and T. Tantidham, PMA: Power Monitoring Application for Android. In: *2014 Third ICT International Student Project Conference* (ICT-ISPC), p. 69–72 (2014). DOI: 10.1109/ICT-ISPC.2014.6923220

4. E. Yandri, R. Ariati, and R.F. Ibrahim. Improving energy security model through detailing renewable and energy efficiency indicators: A concept for manufacture industry. In: P*roceedings of the SIGER 2017 Universitas Lampung*, p. 9 (2017).

5. E. Yandri., R. Ariati, and R.F. Ibrahim. Meningkatkan keamanan energi melalui perincian indikator energi terbarukan dan efisiensi guna membangun ketahanan nasional dari daerah [Improve energy security through detailed indicators of renewable energy and efficiency in order to build national resilience from the regions]. *Jurnal Ketahanan Nasional* 24(2): 239–260 (2018). [in Bahasa Indonesia]. DOI: 10.22146/jkn.30999

6. S. Farooq and I. Yaqoob. Awareness towards efficiency of green and conventional building materials used in Pakistan. *Proceedings of the Pakistan Academy of Sciences A. Physical and Computational Sciences* 56 (3): 75–84 (2019).

7. EECCHI. *Buku pedoman energi efisiensi untuk desain bangunan gedung di Indonesia* [Energy efficiency guidebook for building design in Indonesia]. Dirjen EBTKE, Jakarta (2012), [in Bahasa Indonesia].

8. H. Berchmans., S. Suaib., I. Agustina., R. Panjaitan, and W. Winne, *Panduan penghematan energi di gedung pemerintah* [Guidelines for saving energy in government buildings]. USAID Indonesia Clean Energy Development (ICED Project), Jakarta (2014).

9. US DoE. *2011 Buildings energy data book.* U.S. Department of Energy, US, p. 286 (2012).

10. NYC Gov. *PlanYC: New York City local law 84 benchmarking report,* NYC Government, NY (2012).

11. A. Nizami., J. Ali, and M. Zulfiqar. Climate change is real and relevant for sustainable development, an empirical evidence on scenarios from North-West Pakistan. *Sarhad Journal of Agriculture,* 36(1): 42–69 (2020). DOI: 10.17582/journal.sja/2020/36.1.42.69

12. H.H. Senousy and S.A. Ellatif. Mixotrophic cultivation of *Coccomyxa subellipsoidea* microalga on industrial dairy wastewater as an innovative method for biodiesel lipids production. *Jordan Journal Biology Sciences* 13(1):47–54 (2020)

13. D. Delek., P. Zenzerovic, and V. Sucic, Home automation-an educational prototype. In: Proceeding of the 23rd International DAAAM Symposium, 23(1): 0727–0732, 2012.

14. ESDM. *Peraturan Menteri ESDM Nomor 13 tahun 2012 tentang Penghematan Pemakaian Tenaga Listrik* [Minister of Energy and Mineral Resources regulation number 13 of 2012 concerning saving the use of electric power], ESDM, Jakarta (2012).

15. J. Makijenko., J. Burlakovs., J. Brizga, and M. Klavins. Energy efficiency and behavioral patterns in Latvia. *Management of Environmental Quality,* 27 (6):695–707 (2016). DOI:10.1108/MEQ-05-2015-0103

16. J. Genet and C. Schubert. *Designing a metering system for small and medium-sized buildings.* Technical Report SEMED310007EN, SE, p. 52. (2011).

17. S. Ahmad., M.H. Zafar., M. Ashraf., I. Khan., and F.Q. Khan. Energy-efficient TDMA based clustering scheme for WSN. *Proceedings of the Pakistan Academy of Sciences: A. Physical and Computational Sciences* 55 (3): 53–65 (2018).

18. K. Abdullah., A.S. Uyun., R. Soegeng., E. Suherman, H. Susanto., R.H. Setyobudi., J. Burlakovs, and Z. Vincēviča-Gaile. Renewable energy technologies for economic development. *E3S Web of Conference* 188(00016): 1–8 (2020). DOI:10.1051/e3sconf/202018800016

Pakistan Academy of Sciences

Research Article

Lighting Enhancement of Classrooms in Heritage School Buildings Based on the Greenship Rating Tools

Susan Susan[1*], and Rani Prihatmanti[2]

[1]Department of Interior Architecture, Universitas Ciputra, CitraLand CBD Boulevard, Made, Sambikerep, Surabaya 67219, Indonesia
[2]Programme Architecture, School of Housing, Building & Planning, Universiti Sains Malaysia, Penang 11800, Malaysia

Abstract: This study aims to suggest some strategies for improving the quality of lighting in adaptive reuse buildings. Recently, several concerns have been raised about the lighting environment of heritage buildings that have been adaptively reused for a different function. These changes may lead to a problem for the occupants of the building, particularly on the indoor lighting quality. It is regarded as one of the most affected variables in the building of heritage that is adaptively reused. Green Building Council Indonesia (GBCI) has been concerned about this issue, particularly to the requirements related to lighting power density and control, visual comfort, outside view, and daylight. The purpose of this research is therefore to suggest some strategies for improving the quality of lighting in the two classrooms of two heritage schools in Surabaya, Indonesia, based on the Greenship Interior Space rating tool. There are three credits for lighting power density and control, and one credit for visual comfort criteria. By performing light mapping measurements, calculations, and computer simulation, this analysis is qualitative. To capture the condition of the classrooms examined, building observation was also performed. The observation shows that the existing condition gains four credits only. If adopted, the strategies proposed could achieve eight credits, which is covers 80% of the assessment points. The higher credits achieved reflect a better lighting environment and better value for energy efficiency and conservation.

Keywords: Adaptive Reuse, Energy Efficiency, Green Building, Lighting Quality, Visual Comfort.

1. INTRODUCTION

Adaptive reusing a building is a common practice to prolong the lifespan of a building. The heritage building is a legacy from the past which could not be replaced once lost. It is also a source of reference for the next generation, therefore these highly significant value properties must be sustained. However, some buildings are not purposely built for the same purpose in the future. A problematic condition to the indoor environment could be created by these alterations. These alterations will significantly affect the occupants, particularly their well-being and productivity. According to Prihatmanti and Bahauddin [1, 2], there is a risk for occupants' dissatisfaction in an adaptively reused building. This is due to the limitation of the heritage conservation practice which must comply with the

guidelines. One of the most affected factors found in the adaptively reused building is indoor lighting. An appropriate amount of light will lead to fewer work errors, better safety, and lower absenteeism level. Hence, it will significantly affect the work performance of the building occupants [3, 4].

Some green building organizations, including the Green Building Council Indonesia (GBCI), have the arising concern to this condition. Previously, green building rating tools are used as parameters to design green buildings. Since the paradigm of sustainability has shifted, these rating tools are currently used to assess non-green buildings as well, including heritage buildings. Greenship, which was developed by the Green Building Council Indonesia has six rating tools: Appropriate Site Development, Energy Efficiency and Conservation,

Water Conservation, Material Resources and Cycle, Indoor Air Health and Comfort, Building and Environment Management. There are three criteria related to the lighting environment, which are placed under two rating tools, (i) Lighting power density and control is placed under Energy Efficiency and Conservation; (ii) Visual comfort, outside view and daylight, are placed under Indoor Health and Comfort.

Energy used for lighting systems consumes 20 % of whole-building energy consumption. The usage of an energy-saving lamp will give a significant impact on the environment as well as on the building's operational cost. An energy-saving lamp will lead to less renewable energy consumption and reduce environmental pollution. Based on previous research, a building that uses an occupancy sensor saves 20 % to 26 % of lighting energy compared to a building with a manual system [3].

Several studies about lighting in a learning environment have been conducted. According to Susan and Prihatmanti [6], the lighting environment has a crucial role in affecting students' contentment and academic performance. Research on student awareness of higher education classrooms explains that the learning environment is influenced by physical attributes, including temperature, acoustic, lighting, daylight, and air quality [7]. This is also emphasized by Samani, a learning environment must provide an appropriate lighting quality to increase the motivation to learn and enhance the students' learning performance [8]. Another previous study conducted by Axarli and Tsikaloudaki also stated that the pupil's academic performance and well-being are significantly depending on the quality of the luminous environment [9]. The student performance is significantly correlated with the lighting quality in their classroom [10]. Related to this, a good lighting environment is significant to motivate the students for a better learning process. This is also addressed by Bluyssen et al. that exposure to poor lighting could cause short and long-term health impacts [11].

Adaptively reused buildings, particularly heritage buildings, are being reused into different functioned which is different from their original purpose. This could create occupants' discomfort due to the inappropriate space planning for the new purpose [1]. The lighting condition must be adjusted to comply with the occupants' activity as well as the need of saving energy. Therefore, this paper focuses on investigating the lighting performance and proposes suggestions to enhance the lighting environment, based on the Greenship Rating Tools.

2. MATERIALS AND METHODS

Regarding the issue of lighting environment, the Green Building Council Indonesia has been highlighting this matter. The current rating tool has put lighting as an important factor that gives a significant chance to reduce operational cost, reduce
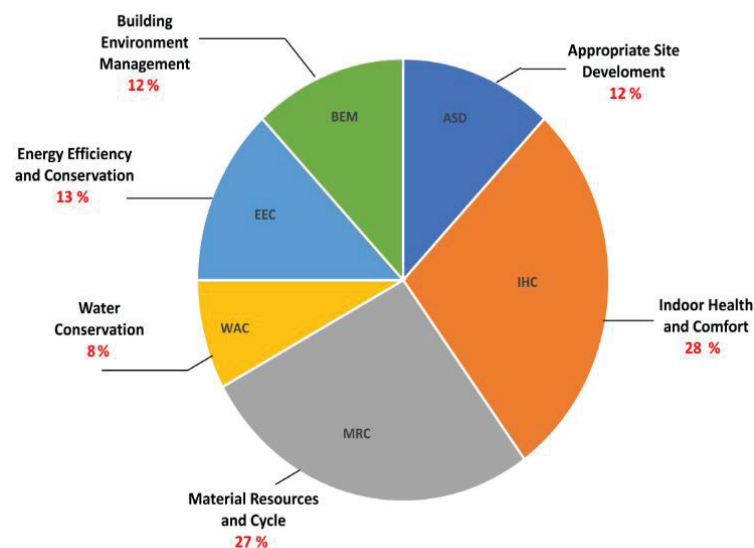
Fig. 1. Greenship Interior Space Rating Tools [5].

the greenhouse effect, and improve occupants' performance. As mentioned before, there are three criteria related to lighting performance, which are listed in Figure 2 [5]. Those are lighting power density and control, visual comfort, and outside view and daylight.

2.1 Lighting Power Density and Control Criteria

The Lighting Power Density and Control criteria aim to build an understanding regarding the consequence of energy saving on a built environment [9]. Based on the Greenship rating tools, the benchmark for these criteria is listed in Figure 3 [5].

Based on the Standard National Indonesia (SNI)/Indonesian National Standard, the maximum amount of lighting power density for a classroom is $13 \, \text{W m}^{-2}$ [12]. There are potential strategies that can be applied to achieve the targets: first, lighting power density can be reduced by applying interior finishes with high reflectance value; second, a daylighting system must be maximized to save energy; third, applying daylighting sensor that integrates with the building's artificial lighting system; fourth, option for lamps with higher efficacy, such as fluorescent and LED; fifth, the lighting armature must be selected based on the distribution characteristic, high efficiency, and the ability to reduce glare.

2.2 Visual Comfort Criteria

The lighting source on a working plane could be received from daylight and artificial light. In all circumstances, daylight is much-preferred compare to artificial light. However, if daylighting is insufficient to fulfill the building's requirement, artificial lighting must be provided. Daylighting and artificial lighting must be designed carefully, where excessive daylight could cause discomfort glare as well as disability glare [13]. On the contrary, the amount of artificial lighting which does not fulfill the standard could cause visual discomforts such as red-eye, eye irritation, blurred view, and difficulty in reading any objects. It is also has been studied by Lee, Moon, and Kim that visual comfort is strongly affecting the mood [14].

According to the GBCI, the main objective of the Visual Comfort criteria is to provide a suitable lighting quality in the designated workplace to enhance the productiveness and well-being of the users [5]. Based on the standard given by the local agency, any classroom should provide 350 lx as its illumination standard [10]. The benchmark for these criteria according to the Greenship rating tool is listed in Figure 4 [5].

2.3 Outside View and Daylight Criteria

Eye fatigue can be reduced by providing an outdoor view for the occupants. Those who have access to the outdoor view show symptoms of reduced stress level, less frustration, more patient, and higher performance [15, 16]. Meanwhile, maximizing the daylight could give good impacts such as improve occupants' health, provide better lighting quality, as well as saving cost and energy for artificial lighting. Hwang and Kim also agreed that daylight is proven for improving the occupants' comfort in an indoor environment [14]. Hence, the Outside View and Daylight criteria are required to be calculated. These criteria aim to reconnect the indoor to the outdoor area by providing an outside view as well as daylight into the indoor space. This will increase the occupants' satisfaction, in terms of comfort and productivity. The benchmark based on the Greenship rating tool for the outside view and daylight is listed in Figure 5 [5].

3. RESULTS AND DISCUSSION

3.1 Observation

There are two heritage schools selected for this study. The selection criteria are based on the heritage significance of the studied buildings. Those schools are Santa Maria Senior High School and

Code	Criteria	Credits
EEC 3	Lighting Power Density and Control	5
IHC 6	Visual Comfort	3
IHC 7	Outside View and Daylight	2

Fig. 2. Greenship criteria for lighting system and environment [5].

No.	Benchmark	Credits	
1A	Save 20 % in lighting systems with more efficient lighting power or total lighting power, as described in Energy Conservation Lighting System SNI 03-6197-2000.	1	5
	or		
1B	Save 40 % in lighting systems with more efficient lighting power or the total lighting power, as described in SNI 03-6197-2000 (Energy Conservation Lighting System).	2	
	or		
1C	Save 60 % in lighting systems with more efficient lighting power or the total lighting power, as described in SNI 03-6197-2000 (Energy Conservation Lighting System).	3	
2A	Use 100 % electronic ballast	1	
	or		
2B	Meet the 2A benchmark and save energy using an integrated lighting sensor and/or a built-in occupancy sensor and/or person power.	2	

Fig. 3. Benchmark for lighting power density and control [5].

No.	Benchmark	Credits	
1	Utilizing a lighting system with illumination in compliance with SNI 03-6197-2000 of Energy Conservation in Lighting System.	1	3
2	Provide at least 90 % of individuals, with individual reachable lighting settings (switch), and or provide all users in multi-occupant room/area with a lighting control system.	1	
3	Provide integrated automatic curtains/blind to the natural lighting control system.	1	

Fig. 4. Benchmark for visual comfort based on the Greenship rating tool [5].

No.	Benchmark	Credits	
1	75 % floor area used is oriented horizontally to outside view, limited by transparent wall and if drawn a straight line, then the transparent wall with a lower threshold is at a maximum of 0.90 m above the floor.	1	2
2	Optimal use of natural light to meet a minimum of 75 % of floor area used to achieve the natural light intensity for at least 300 lx.	1	

Fig. 5. Benchmark for outside view and daylight based on the green ship rating tool [5].

St. Louis Senior High School. Due to the historical significance. These schools are classified by the Surabaya City government regulation No. 5/2005 as national heritage buildings. Currently, both schools consist of the original heritage building and the newly built annex building. The annex building is newly built to accommodate the increasing number of students enrolled annually.

The first case study is the Santa Maria High School. The location of this school is Raya Darmo Street Surabaya. The studied classroom is 56.88 m^{-2} in size and facing to the South. According to the site observations conducted, there are four windows in total (1.8 m × 1.0 m in size; 1.8 m above the ground) which are located two in the North and two in the South wall. The second case study is the St. Louis Senior High School. Its location is in Polisi Istimewa street Surabaya. According to the observation, the studied classroom is 82.96 m^{-2} in size, facing North, located in the front part of the original building which is facing the main road as well as the parking area. High openings were also present and located in the North, East, and South wall.

The assessment which is applied based on the lighting criteria from Greenship Interior Space showed that the existing classrooms only obtained four credits from a total of 10 credits listed in lighting-related criteria.

Buildings can contribute energy savings from the lighting system. There are six lamps in each studied classroom. The lamps on the studied buildings are general fluorescent lamps 36 W for Santa Maria Senior High School and 58 W for St. Louis Senior High School. This proposed lighting system will create brighter classrooms, with 3.8W m^{-2} and 4.2 W m^{-2} lighting power density, as well as saving energy up to 71 % and 68 % respectively. This strategy will give the classrooms three credits. However, the current lighting system does not use 100 % electronic ballast as well as the integrated lighting sensor, and/or integrated occupancy sensor, and/or individual control by the means of saving energy. This decision has made both buildings lose another credit provided in these criteria.

Illuminance level was also measured, both for daylighting and artificial lighting conditions.

According to the measurements taken, the illuminance level at Santa Maria Senior High School falls between 10 lx to 45 lx on daylighting and between 42 lx to 91 lx for artificial lighting conditions. While at St. Louis Senior High School, it falls between 26 lx to 105 lx and 47 lx to 150 lx respectively. Unfortunately, the illuminance levels in both schools were below the standard of SNI, which has to be 350 lx. This means that the buildings studied do not comply with the first benchmark of visual comfort. According to the GBCI, a lighting control system on a multi-occupant room or area should be provided which is accessible to all users. This resulted in the buildings obtained another one point from the second benchmark of visual comfort.

According to the building observation conducted, the high openings in Santa Maria Senior High School were made from a wooden frame and glazed by tinted glass. The openings were at 1.8 m above the floor and located on eye level. This resulted in a restricted view to the outside. However, due to the glare and thermal concerns, the openings are covered by an internal shading device. An internal shading device also restricts the occupants to access the outside view. These conditions have prevented the buildings from obtaining another credit provided on the criteria of the outside view. Thus, both buildings could not obtain credit from the daylight criteria as well. As explained previously, daylight illuminance levels in both classrooms are ranged between 10 lx to 105 lx. There is no optimal use of natural light to reach 75 % of the floor area to obtain the intensity of light for at least 300 lx. The natural light intensity for 100 % area is below 300 lx.

3.2 Analysis and Design Proposed

3.2.1 Lighting Power Density and Control

Based on the SNI, the maximum lighting power density for a classroom is 13 W m^{-2}. To achieve the optimum savings on lighting power density, the studied classrooms require lamps with higher efficacy. Philips TL-D 36W/33-640 1SL/25 with 100 % electronic ballast (eco passport: certified with energy efficiency label B) is proposed to be used in both classrooms. This research also proposes to add the numbers of lighting points, to make better lighting distribution. The number of lighting points

Fig. 6. The classroom condition and site plan of Santa Maria Senior High School.

Building of the studied classroom
Studied classroom

Fig. 7. The classroom condition and site plan of St. Louis Senior High School

at Santa Maria Senior High School was adjusted from 6 points to 12 points. Meanwhile, at St. Louis Senior High School, the numbers of lighting points were adjusted from 6 to 18. The lighting power density after the adjustment is tabulated in Table 1.

The treatment conducted to the classrooms at Santa Maria Senior High School and St. Louis Senior High School are 7.59Wm^{-2} and 7.81Wm^{-2} lighting power density, as well as saving energy 42 % and 40 % respectively. This system contributes three credits to the Lighting credit from each classroom. Another 1 credit is targeted to be achieved by using an integrated lighting sensor and/

or integrated occupancy sensor and/or individual control to save energy. The planning for this system can be seen in Figure 9 and Figure 10.

3.2.2 Visual Comfort

In this study, the illuminance level is calculated by using the equation in Equation (1) [17]:

$$F = E \times A/Uf \times LLf \qquad (1)$$

Where: F   =   Flux (lumens)
E   = Illuminance (lx)
A   = Area (m2)

Table 1. Lighting Power Density proposed

School Name	Lighting points numbers	Lighting power (W)	Area (m^2)	Lighting power density (W m^{-2})
(a)	(b)	(c)	(d)	(e) = (bxc)/(d)
Santa Maria	12	36W	56.88	7.59
St. Louis	18	36W	82.96	7.81

Code	Criteria	Credits
EEC 3	Lighting Power Density and Control	3
IHC 6	Visual Comfort	1
IHC 7	Outside View and Daylight	0

Fig. 8. Lighting credits for the classrooms
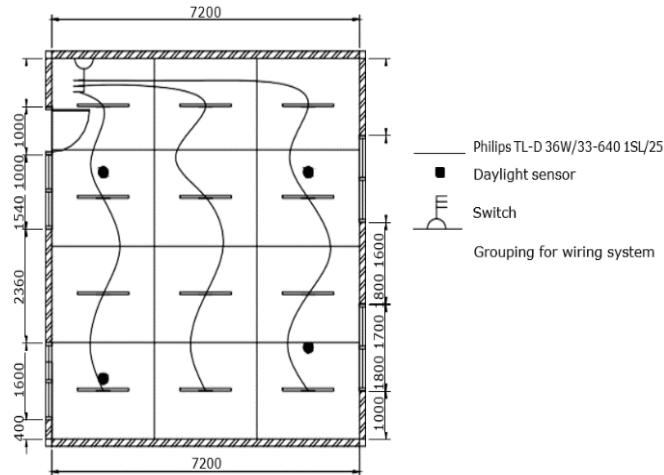
Fig. 9. Sensor and lighting plan for Santa Maria Senior High School
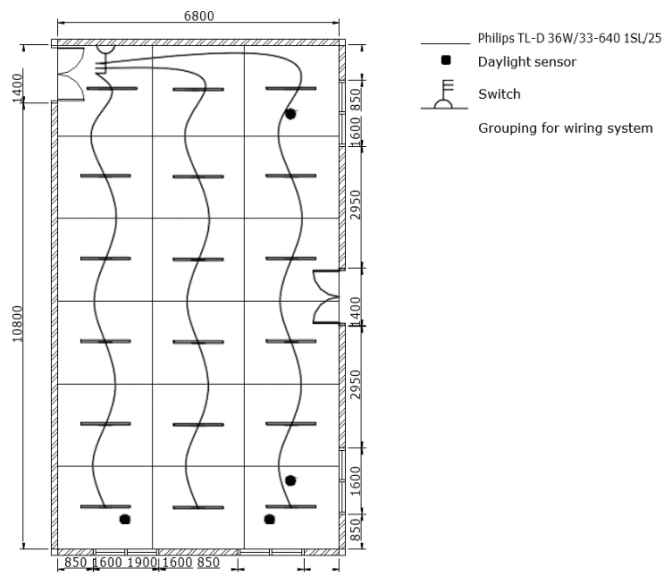
Fig. 10. Sensor and lighting plan for St. Louis Senior High School.

Table 2. Illuminance level proposed

School Name	F (lumens)	Lighting points numbers	Area (m²)	Uf	LLf	E (lx)
(a)	(b)	(c)	(d)	(e)	(f)	(g)
Santa Maria	2850	12	56.88	0.75	0.8	361
St. Louis	2850	18	82.96	0.75	0.8	371

Uf = Utilization factor (0.75)
LLf = Light Loss factor (0.8)

According to the SNI, the illuminance level in both classrooms must reach 350 lx. In this study, Philips TL-D 36W/33-640 1SL/25 with 2 850 lx was proposed to be applied. After the treatment, the illuminance level in both classrooms is above 350 lx, which is 361 lx for Santa Maria Senior High School and 371 lx for St. Louis Senior High School (refer to Table 2). Based on the proposed strategy, as much as one credit is achieved from this treatment.

Another two credits were achieved by providing a lighting control system on multi-occupant room/ area for all users and an automatic curtain to the natural lighting control system. The placement of the lighting control system (switch) can be seen in Figure 9 and Figure 10. The switch must be reachable by all the users. An automatic curtain is also suggested to be applied since it can keep them perfectly aligned to control natural lighting.

3.2.3 Outside View and Daylight

As mentioned previously, the lighting enhancement based on Greenship rating tool is connected to access of outside view. The observation conducted at the Santa Maria Senior High School showed only 34 m^2 (59 %) area can get the access to the outside view (Fig 11), while at the St. Louis Senior High School only 56 m^2 (68 %) area (Fig 12). Nevertheless, there is no treatment proposed for this benchmark, since the building is a heritage building that has certain limitations to conduct major alterations on its façade.

Another credit could be achieved by optimizing the natural light. It has to reach at least 75 % of the total floor area. This will be used to obtain the natural light intensity of at least 300 lx. As mentioned previously, both classrooms have high openings. Theoretically, it could be a good treatment for daylight penetration. Unfortunately, due to glare and thermal problems, the openings are glazed with tinted glass and covered by internal blinds, which are usually closed on daily activities. The minor treatment is to propose a higher illuminance level. Tinted glass could be replaced by low-E glass. Based on the previous benchmark, an automatic curtain is suggested. To overcome

glare and thermal problems when the window is opened, reflective light shelves are proposed. The treatments proposed are then simulated by using the software Velux 3.0.22. The result is illustrated in Figure 13 and Figure 14. The red area showed a higher illuminance level which could reach 600 lx and gradually decreasing towards the center of the room, reaching 300 lx.

3.2.4 Proposed Methods and Recommendations

Table 3 shows the enhancement strategies and the comparison between the previous and proposed methods, which indicates the advantages of the proposed methods to create energy efficiency and comfortability to the users. The Lighting Power Density and Control and Visual Comfort criteria can be achieved to improve the lighting condition of the studied buildings. However, the Outside View and Daylight criteria could not be fulfilled due to no proposed treatment conducted since both buildings are heritage-listed.

To show the difference between before and after the proposed treatment, the credit comparison of the previous condition and the proposed methods is shown in Table 4.

This research provides the suggestion for the Greenship rating assessment. Figure 15 shows the process flowchart that is developed as a reference for lighting designers as well as for the lighting assessors.

The practical application of this research is not only for heritage buildings but can also be applied with suitable modifications in campus buildings, assisted by a good energy management system. [17, 18]. That way, the future research direction will be easier to develop into the concept of ICT-based energy security for smart cities with the support of smart-grid technology.

4. CONCLUSION

The adaptive reusing building is a common practice to preserve a building with high significant value. However, there are many considerations and limitations when it comes to change to a new purpose. This research was conducted in two heritage schools which also adaptive reused
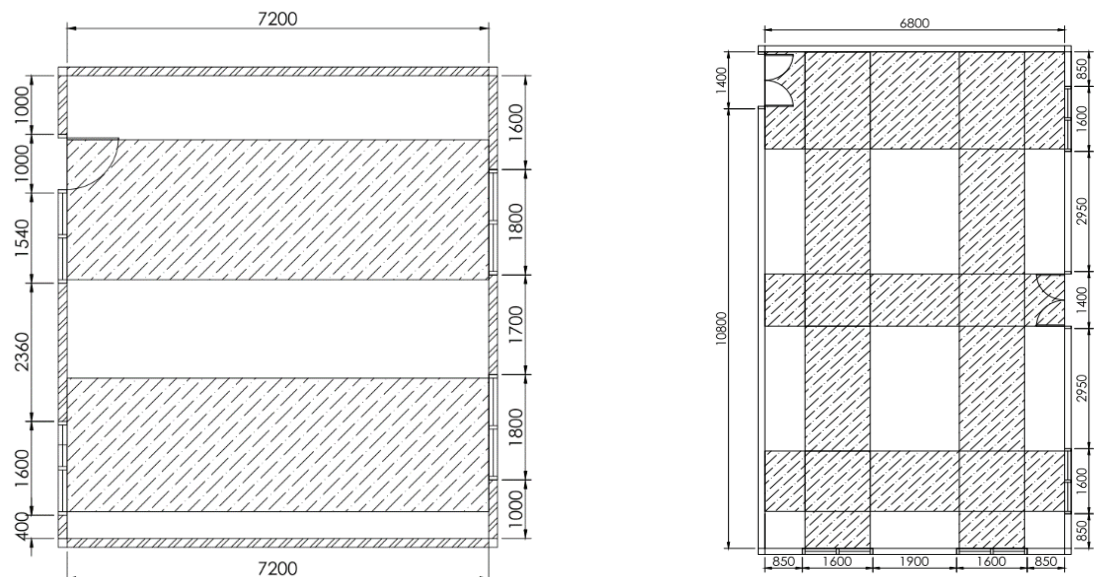
Fig. 12. The area with outside view access at St. Louis Senior High School.
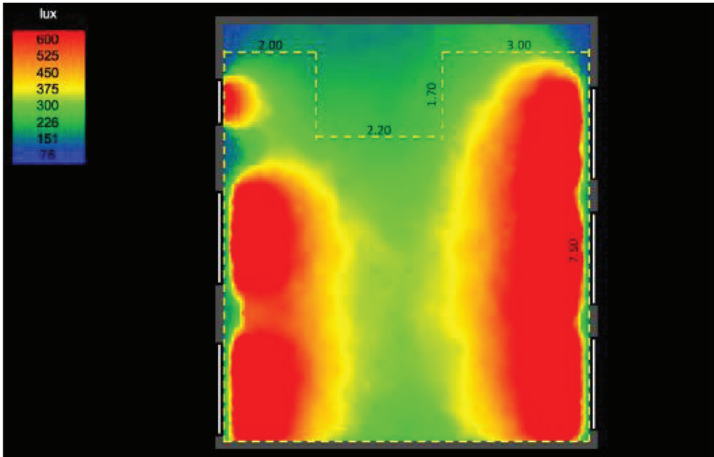
Fig. 13. Daylight simulation result for Santa Maria Senior High School.
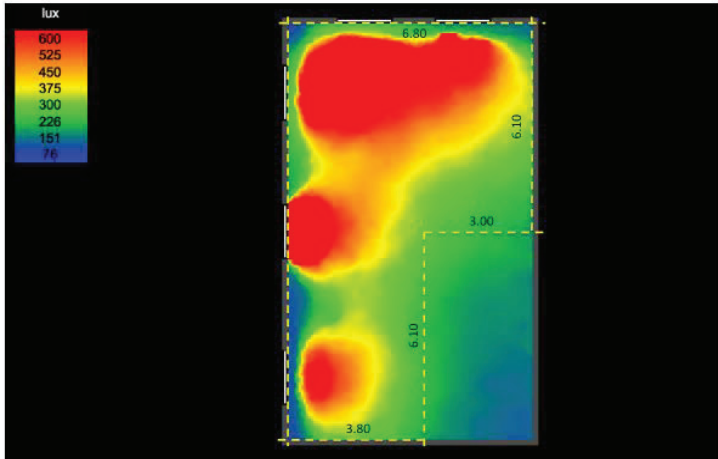
Fig. 14. Daylight simulation result for St. Louis Senior High School.

Table 3. Strategies Comparison of previous condition and the proposed methods

	Before		After	
Criteria	Strategies		Strategies (Proposed Methods)	Application in this Research
Lighting Power Density and Control	Based on SNI, low wattage lamp types		20 % to 60 % savings in lighting systems (low wattage, high flux, high efficacy), 100 % electronic ballast, integrated lighting sensor and/or integrated occupancy sensor, and/or individual control to save energy.	40 % to 42 % savings in the lighting system, 36 W, 2 850 lumens, 100 % electronic ballast, integrated lighting sensor and/or integrated occupancy sensor and/or individual control to save energy.
Visual Comfort	< 150 lx		Based on SNI	Combination of artificial lighting and daylighting, produce illuminance level 361- 371 lx (SNI standard for classroom = 350 lx)
Outside View and Daylight	59 % to 68 % floor area directed horizontally to the outside view and 100 % area has illuminance level <105 lx in daylighting condition.		Additional opening using low-E glass, an automatic curtain.	No treatment is proposed since the studied buildings are heritage-listed.

Table 4. Credit Comparison of previous condition and the proposed methods

	Before		After	
Criteria	Strategies	Credits	Strategies	Credits
Lighting Power Density and Control	Based on SNI, low wattage lamp types	3	40 % to 42 % savings in the lighting system, 36 W, 2 850 lumens, 100 % electronic ballast, integrated lighting sensor and/or integrated occupancy sensor and/or individual control to save energy.	5
Visual Comfort	< 150 lx	1	Combination of artificial lighting and daylighting produce illuminance level 361- 371 lx (SNI standard for classroom = 350 lx)	3
Outside View and Daylight	59 % to 68 % floor area directed horizontally to the outside view and 100 % area has illuminance level <105 lx in daylighting condition.	0	No treatment is proposed since the studied buildings are heritage-listed.	0
	Total credits on the previous condition	4	Total Credits on proposed methods	8
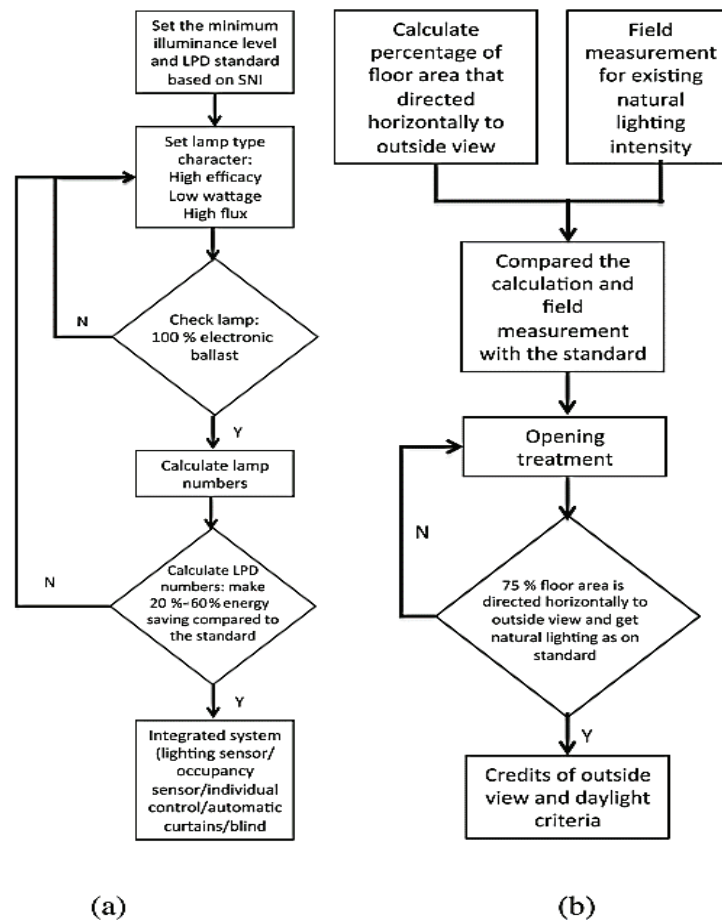
Fig. 15. (a) Lighting Power Density and Visual Comfort assessment flowchart; (b) View and Daylight assessment Flowchart.

from the previous purpose. Two classrooms were assessed based on the lighting quality according to the Greenship Rating Tools. From the measurement conducted, it showed that the amount of light in the studied buildings was inadequate. The indoor light level was below the standard (350 lx). Moreover, according to the Greenship Interior Space lighting criteria, both classrooms only obtained 4 credits from the total 10 credits listed. Several strategies could be implemented in these buildings to obtain more credits on the criteria for lighting systems and the environment. Although the studied buildings are heritage-listed, the occupants' visual comfort should not be neglected.

Further research can be applied by using the whole parameters of Greenship - Indoor Health and Comfort rating tool. The alterations of heritage building's function will affect the occupants, particularly on their well-being and productivity.

Further research on comprehensive criteria of Indoor Health and Comfort will reduce the risk for occupants' dissatisfaction in an adaptively reused building, not only for indoor lighting but also for overall conditions related to indoor health and comfort.

5. ACKNOWLEDGEMENTS

6. CONFLICT OF INTEREST

The authors declare no conflict of interest.

6. REFERENCES

1. R. Prihatmanti, and A. Bahauddin. Impacts of adaptive reuse in the UNESCO listed heritage buildings, George Town, Penang. In: *Retracing Tradition for a Sustainable Future.* The Malaysian Experience, N.F.L. Abdullah, and M. R. Pakri (Ed.). Universiti Sains Malaysia, Penang, Malaysia, p. 80–94 (2013).

2. R. Prihatmani R and M. Susan. Adaptive reuse of heritage building and the impact to the visual comfort: Assessed by the lighting quality. *IPTEK Journal of Proceeding Series,* 3: 127–141 (2017).

3. W.W.J.M. van Bommel, and G J. van den Beld, *Lighting for work: visual and biological effects.* Philips Lighting, The Netherlands, p. 1–17 (2003). DOI: 10.1.1.857.216

4. J.M, Katabaro and Y. Yan. Effects of lighting quality on working efficiency of workers in office building in Tanzania. *Journal of Environment and Public Health,* ID 3476490:1–13 (2019). DOI: 10.1155/2019/3476490

5. GBCI, *Greenship Rating Tool for Interior Space Version* 1.0. Jakarta, Indonesia, (2012).

6. M.Y. Susan and R. Prihatmanti. Daylight characterisation of classrooms in heritage school buildings. *Planning Malaysia,* 15(1): 209–220 (2017). DOI: 10.21837/pm.v15i1.236

7. Z. Yang., B. Becerik-Gerber, and L. Mino, A study on student perceptions of higher education classrooms: Impact of classroom attributes on student satisfaction and performance. *Building and Environment,* 70: 171–188 (2013). DOI: 10.1016/j. buildenv.2013.08.030

8. S.A. Samani. The impact of indoor lighting on students' learning performance in learning environments : A knowledge internalization perspective University of Applied Sciences. *International Journal of Business and Social Science,* 3(24): 127–136 (2012).

9. K. Axarli and K. Tsikaloudaki. Enhancing visual comfort in classrooms through daylight utilization. In: *Clima 2007 Wellbeing Indoors*, p. 1–8 (2007).

10. M. Pinto., R. Almeida., P. Pinho, and L. Lemos. Daylighting in classrooms - the daylight factor as a performance criterion. In: *ICEHCISA*, p. 1–2 (2014).

11. P.M. Bluyssen., S. Janssen., L.H. van den Brink, and Y. de Kluizenaar. Assessment of wellbeing in an indoor office environment. *Building and Environment,* 46(12): 2632–2640 (2011). DOI.: 10.1016/j.buildenv.2011.06.026

12. BSN. *Konservasi Energi pada Sistem Pencahayaan* [Energy Conservation in Lighting Systems]. Badan Standarisasi Indonesia, Jakarta, Indonesia (2010). [in Bahasa Indonesia].

13. W.K.E. Osterhaus, Discomfort glare assessment and prevention for daylight applications in office environments. *Solar Energy*, 79(2): 140–158 (2005). DOI: 10.1016/j.solener.2004.11.011

14. J. Lee., J.W. Moon, and S. Kim, Analysis of occupants' visual perception to refine indoor lighting environment for office tasks. *Energies,* 7(7):4116–4139 (2014). DOI: 10.3390/en7074116

15. P. Leather., M. Pyrgas., D. Beale, and C. Lawrence. Windows in the workplace: sunlight, view, and occupational stress. *Environment and Behavior,* 30(6):739–762 (1998). DOI: 10.1177/001391659803000601

16. L. Lottrup., U. Stigsdotter, H. Meilby, and A.G. Claudi. The workplace window view: A determinant of office workers' work ability and job satisfaction. *Landscape Research,* 40(1): 57–75 (2015). DOI: 10.1080/01426397.2013.829806

17. E. Yandri., R. Ariati., A.S. Uyun., R.H. Setyobudi., O. Anne., H. Susanto, and Z. Vincevica-Gaile. Implementation of walk-through audits for designing energy management system: A first step towards an efficient campus. *IOP Conference Series: Earth and Environmental Science,* 490(012005):1–11(2020). DOI: 10.1088/1755- 1315/490/1/012005

18. S. Farooq and I. Yaqoob. Awareness towards efficiency of green and conventional building materials used in Pakistan. *Proceedings of the Pakistan Academy of Sciences A. Physical and Computational Sciences* 56 (3): 75–84 (2019).

Pakistan Academy of Sciences

Research Article

Optimal Design of Barangay Rogongon Microgrid System

**Anacita Palma Tahud*, Samuelle Jane Dahili Estoperez, Jeryl Manlupig Wayco,
and Noel Regis Estoperez**

Department of Electrical Engineering and Technology, College of Engineering and Technology,
MSU-Iligan Institute of Technology, A. Bonifacio Avenue, Iligan, Philippines

Abstract: In this research, specifically an electrical distribution system design of the proposed microgrid in a remote barangay, Brgy. Rogongon, in Iligan City, is presented. Due to limited access and limited-service electrical utility grid, about 10 % of the Philippine household population at a development disadvantage. Through the project, potential sites for hydropower and solar PV installations as well as distribution pathways were identified using Geographic Information (GIS). Household surveys were conducted to obtain the 5 yr projected load demand and the results are presented in thematic maps. The electrical distribution system of the microgrid was designed and simulated using Just Another Electrical Distribution Network Software (JAED.NS). The system simulation showed an acceptable 5.94 % estimated total system loss which implies that the designed electrical distribution system is feasible.

Keywords: Electrical Distribution, JAED.NS Software, Remote Rural Area, Renewable Energy, Thematic Map.

1. INTRODUCTION

In the Philippines, over 2×10^6 households do not have electricity, with limited access and limited service of only 4 h to 6 h d^{-1} [1], putting them at a developmental. One of these areas is in Region X (Northern Mindanao) with 1 953 sitios remain unenergized [2]. These include sitios in Iligan City, particularly in Barangay Rogongon. The said barangay has the largest land area in the Iligan City with 35 555 ha and a population of 4 870 [3]. Despite having the largest area it appears to be having a very low population density [4] and is 27.5 km away from the city proper [5] and is not yet connected to the electrical utility grid of Iligan City. This fact of the problem lies due to the limited access, services, and the lack of utility grid electrical connection.

Lately, the idea of microgrid has gained recognition turning modern power system expert attentions from centralized power generation to the microgrid system designed in two-way configuration; can deliver excess power into the electric utility grid as well as taking power from the grid and can operate completely separated ("off-grid/islanded") from the utility grid. [6, 7].

Because of the microgrids' capability to address energy access challenges, it is gaining popularity especially in remote rural area regions where high Potential renewable energy sources are available. Renewable energy sources are now recognized globally as an important alternative option in supplying electrical loads of microgrids because of their lesser operating cost, unlike conventional energy. sources [8–10].

This study aims to optimally design the Barangay Rogongon Microgrid. Specifically, this would accomplish the following: determine the load demand profile of the selected sitios of Barangay Rogongon; develop a thematic map of load demand using Geographic Information System (GIS) and design the electrical distribution system using JAED.NS software.

2. MATERIALS AND METHODS

2.1 Study Area

Barangay Rogongon represents about 44 % of the total land area of Iligan City, Philippines. It is situated in the remotest part of Iligan and majority of the inhabitants in the barangay are Indigenous

People (IP), specifically "Higaunons". Majority of the area still has no access to electricity from the present grid, which is a major hindrance to its economic development. The study area is composed of five selected sitios in the barangay (Figure 1) [11].

2.2 System Design and Simulation

The Microgrid Electrical Power System is composed of three parts as the Generation System, Transmission System, and the Distribution System. For the generation system, two renewable energy sources were considered, hydro and solar.

Through the Department of Science and Technology (DOST) – funded project of Mindanao State University – Iligan Institute of Technology (MSU-IIT) entitled "Techno-Economic Feasibility Study of a Microgrid in a Remote Community", potential sites for hydropower and solar PV installation were identified using GIS and Multi-Criteria Decision Making (MCDM) [11].

For the transmission system, the least-cost path from the identified sites to load centers was adapted from the GIS Spatial Analyst-based Transmission line routing [12]. Along with the transmission pathway, the hydropower site, solar-PV site, and

households were mapped using Just Another Electrical Distribution Network Software (JAED. NS). Also, analytic processes like fault analysis and load flow were executed using the JAED.NS.

Household surveys were conducted to determine the 5 yr projected energy demand. With the survey data, an energy assessment [13] was carried out to determine the general patterns of electricity consumption and hence, management of electric load demand. Also, thematic maps using GIS were produced based on the energy demand per sitio.

In designing the electrical distribution system of the microgrid, the requirements and specifications of all components such as the solar PV system equipment, wires, poles, and transformers were determined.

After data preparation and system design determination, simulations were then carried out using the aforementioned electrical distribution software. The designed electrical distribution system of Barangay Rogongon, Iligan City, was modeled and necessary system adjustments were made. System load flow was carried out as well wherein the voltages, currents, and real and reactive power flows in the system under given load
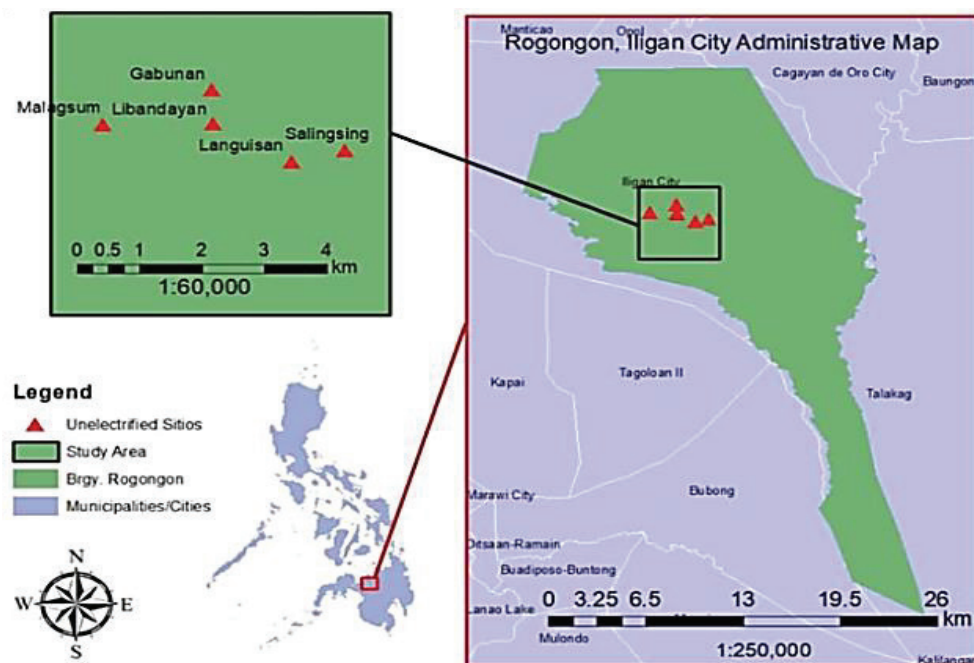
Fig. 1. Map of Barangay Rogongon, Iligan City (with the five selected sitios).

conditions were determined.

Fault analysis was also included which is an important consideration in any power system planning, protection equipment selection, and overall system reliability assessment. Different fault conditions were simulated and the values of short circuit currents were determined.

3. RESULTS AND DISCUSSION

3.1 Load Demand

Based on the conducted household surveys on the five sitios involved in the study, the load demand for the first five years is shown in Table 1 and Figure 2.

3.2 Thematic Map

From the data gathered during the conduct of household surveys, houses were geotagged and mapped using the ArcGIS platform. Figure 3 shows one of the thematic maps generated based on the identified households' load demand profile for the fifth year. As shown, Sitio Salingsing has the greatest demand while Sitio Malagsum shows the lowest.

3.3 Electrical Distribution System of Barangay Rogongon

Figure 4 shows the electrical distribution system of Barangay Rogongon overlaid in Google Earth, with hydro and solar as renewable sources of energy. Included as input data were parameters such as transformer profile, types, and size of distribution line wires, pole structure, and load audit of all five sitios.

3.4 Load Flow and Fault Analysis

The designed electrical distribution system consists of one substation transformer, one generator, six distribution transformers, 109 distribution poles, 12 secondary poles, and 45 households. Load flow analysis was performed as part of the simulation, wherein important data such as voltages, currents, and real and reactive power flows in the system under given load conditions were determined. Figure 5 shows the simulation results.

A feature of JAED.NS called net tracer was used to inspect line connections. As shown in Figure 5, there is no red mark on the wire lines and transformer. This indicates that the system is balanced and not overloaded. Furthermore, simulation results showed an acceptable 5.94 % estimated total system loss. Also, the voltage profile showed the line voltage at the downstream bus of Salingsing to be 12.725 kV. Voltage variation at this bus is 7.79 % which is within the 10 % tolerance on voltage as stipulated in the Philippine Distribution Code.

Figure 6 (a to d) shows the sub-transmission line load curve, distribution line load curve, underbuilt line load curve, and secondary service drop line load curve, respectively. A pattern can be seen in these four graphs wherein the line load curve fluctuates in the peak hour of the system. During these peak hours, consumers tend to use different appliances at the same time thus increasing the electrical demand per household. Other important information was derived from the simulation results such as the

Table 1. Load Demand Profile

Sitio Name	Max demand in Year 1 (VA)	Max demand in Year 2 (VA)	Max demand in Year 3 (VA)	Max demand in Year 4 (VA)	Max demand in Year 5 (VA)
Malagsum	1 504.67	1 518.79	1 518.79	1 518.79	1 518.79
Gabunan	12 888.85	14 342.38	16 384.23	16 869.14	16 869.14
Libandayan	3 710.52	4 884.49	5 936.10	7 044.28	7 044.28
Languisan	3 441.48	3 441.48	3 441.48	3 857.21	3 857.21
Salingsing	8 150.51	8 283.69	15 866.52	15 866.52	17 001.36
Unspecified Sitios	8 385.58	8 947.65	9 378.42	9 378.42	12 577.46
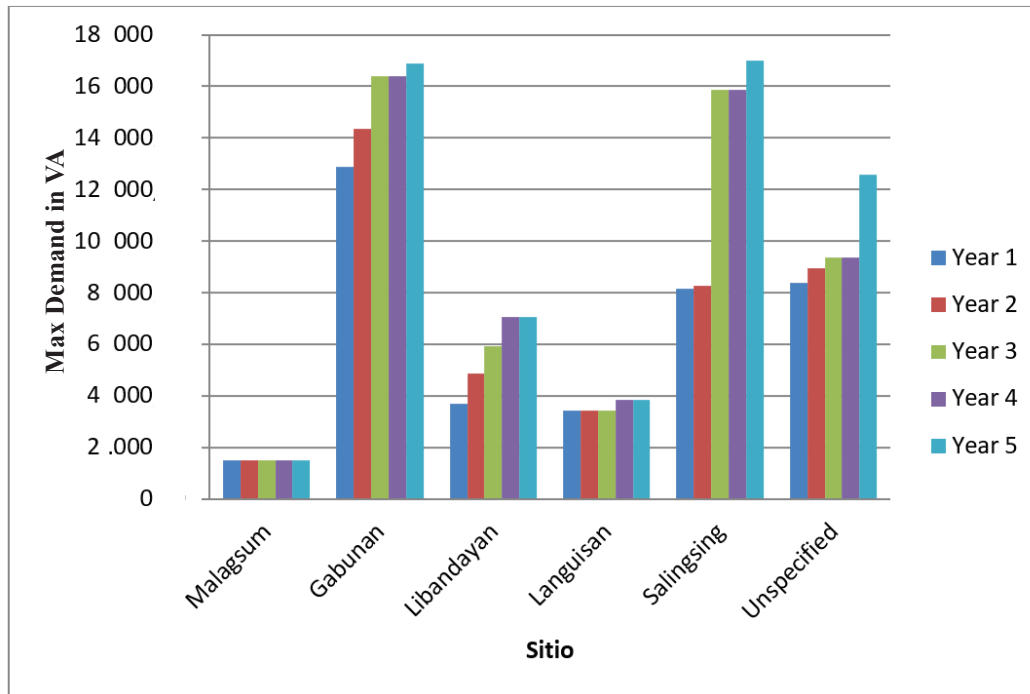
Fig. 2. Comparison of Load Demand Profile for 5 yr.
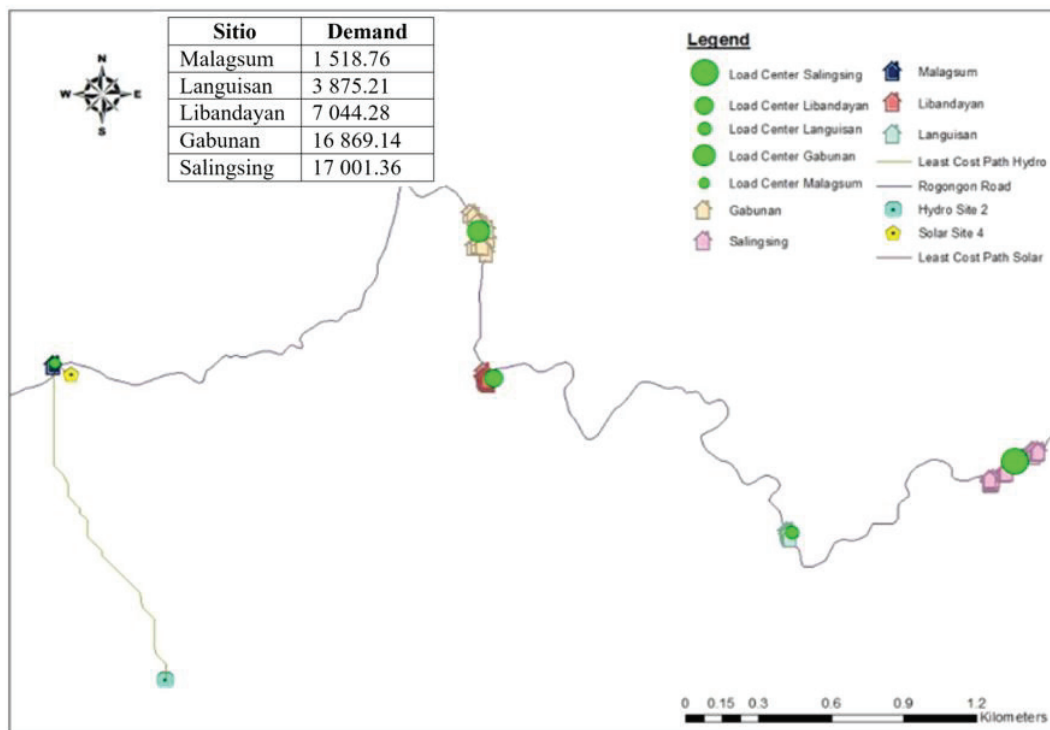
Fig. 3. Fhematic Map of Barangay Rogongon in Year 5.
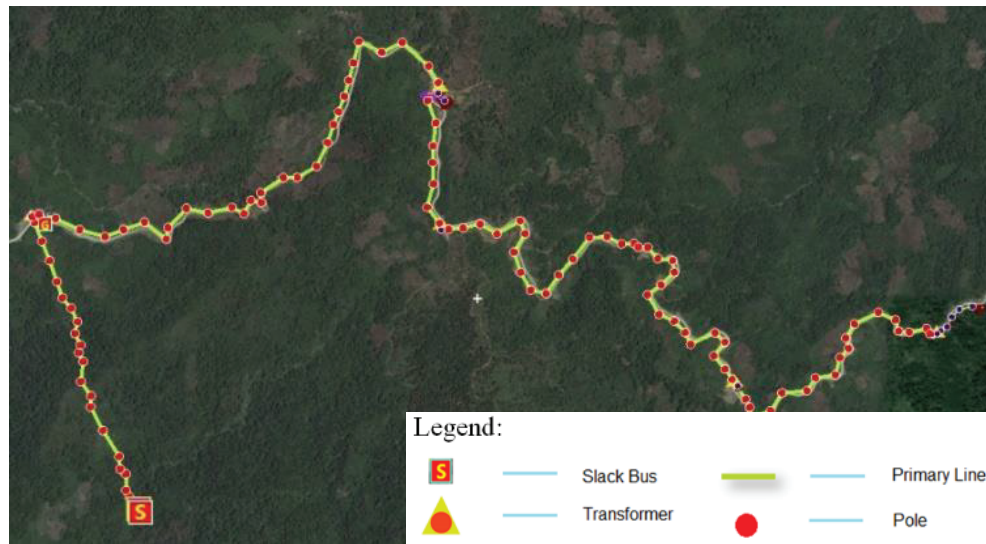
Fig. 4. Hydro and Solar Distribution System of Barangay Rogongon.
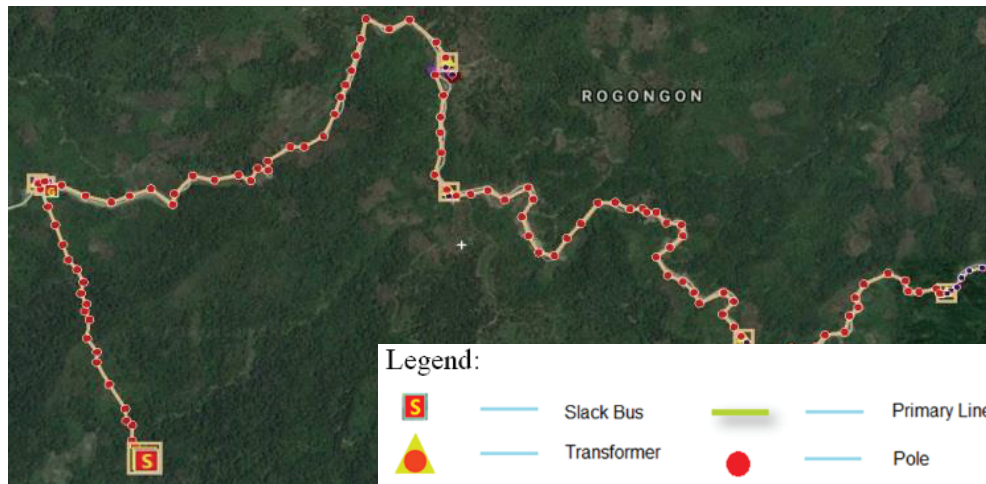
Fig. 5. Simulation Result for Hydro and Solar Distribution System of Brgy. Rogongon

Table 2: Voltage Profile of Rogongon Distribution System

Bus Name	Line Voltage (kV)	Bs Name	Line Voltage (kV)
Reference	13.800	Libandayan	12.738
Malagsum	12.761	Languisan	12.729
Gabunan	12.741	Salingsing	12.725
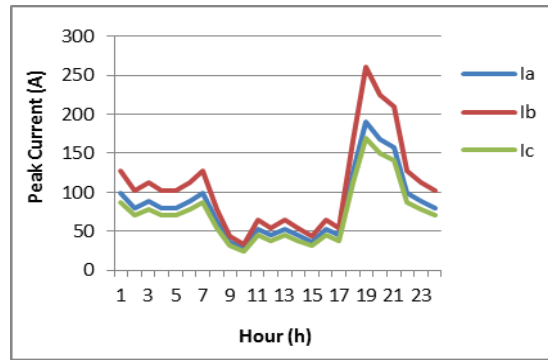
(a)
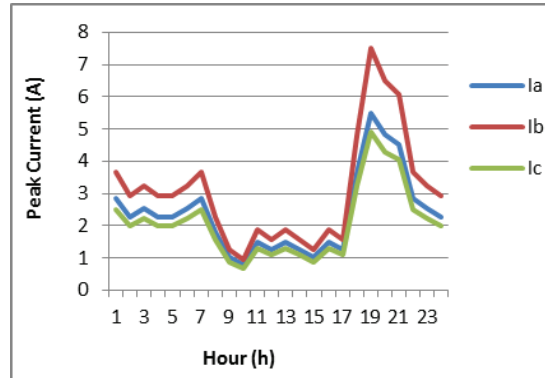
(b)
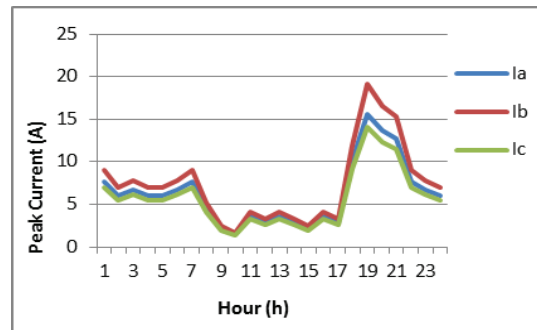
(c)
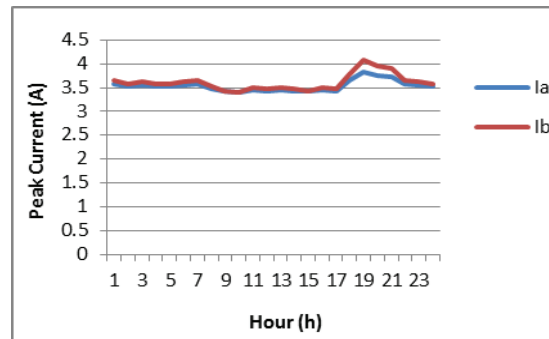
(d)

Fig. 6. Information derived from the simulation results showing: (a) Subtransmission Line Load Curve; (b) Distribution Line Load Curve; (c) Underbuilt Line Load Curve; and (d) Secondary Service Drop Line Load.

design for switch gears, setting of relays, and stability of system operation.

4. CONCLUSION

In this study, the 5 yr expected load demand of the five unelectrified sitios in Barangay Rogongon Iligan City were obtained and thematic maps were created using GIS. The electrical distribution system of the proposed Microgrid System was designed and simulated. After series of modifications, testing, and simulations, the distribution system resulted in an estimated 5.94 % total system loss. The system loss is well within acceptable range which implies that the designed electrical distribution system for Barangay Rogongon is feasible.

5. ACKNOWLEDGEMENTS

6. CONFLICT OF INTEREST

The authors declare no conflict of interest.

7. REFERENCES

1. International Renewable Energy Agency, *Accelerating Renewable Energy Mini-Grid Deployment: A Study on the Philippines* [Online] from https://www.irena.org/-/media/Files/IRENA/Agency/Publication/2017/Oct/IRENA_Philippines_Renewable_Mini-Grids_2017.pdf (2017) [Accessed on 20 June 2019].

2. NEA. *National Electrification Administration,* [Online] from http://www.nea.gov.ph/index.php?option=com_phocadownload&view=sections (2017) [Accessed on 03 December 2018].

3. Philippine Statistics Office, *2010 Census of Population and Housing* [Online] from https://psa.gov.ph/content/population-iligan-city-was-recorded-323-thousand-results-2010-census-population-and-housing (2013) [Accessed on 01 May 2018].

4. Zamboanga. *Zambansa, Rogongon, Iligan City, Lanao del Norte, Philippines* [Online] from https://www.zamboanga.com/z/index.php?title=Rogongon,_Iligan_City,_Lanao_del_Norte,_Philippines (2017) [Accessed on 03 May 2018].

5. Iligan. *Iligan City Government, Iligan Barangays* [Online] from http://www.iligan.gov.ph/city-govt/iligan-barangays/ (2017) [Accessed on 01 May 2018]

6. H.E. Gelani., N. Mashood., D. Faizan, and H. Haseeb. Efficiency comparison of alternating current (AC) and direct current (DC) distribution system at residential level with load characterization and daily load variation. *Proceedings of the Pakistan Academy of Sciences: A. Physical and Computational Sciences* 54 (2): 111–118 (2017).

7. E. Yandri., R.H. Setyobudi., H. Susanto., K. Abdullah., Y.A. Nugroho., S.K. Wahono., F. Wijayanto, and Y. Nurdiansyah. Conceptualizing Indonesia's ICT-based energy security tracking system with detailed indicators from smart city extension. *E3S Web Conferences* 188(00007): 1–7 (2020). DOI: 10.1051/e3sconf/202018800007

8. A.U. Rehman., S. Zeb., H.U. Khan., S.S.U. Shah, and A. Ullah. *Design and operation of microgrid with renewable energy sources and energy storage system: A case study.* 2017 IEEE 3rd International Conference on Engineering Technologies and Social Sciences, (Thailand 2017). DOI: 10.1109/ICETSS.2017.8324151

9. K. Abdullah, A.S. Uyun, R. Soegeng, E.Suherman, H. Susanto, R.H. Setyobudi, J. Burlakovs, and Z. Vincēviča-Gaile. Renewable energy technologies for economic development. *E3S Web of Conference* 188(00016): 1–8 (2020). DOI:10.1051/e3sconf/202018800016

10. H. Hariyanto, D. Parenden, Z. Vincēviča-Gaile2, and P.G. Adinurani. Potential of new and renewable energy in Merauke regency as the future energy. *E3S Web of Conference* 190(00012):1–8 (2021). DOI: 10.1051/e3sconf/202019000012

11. D.A. Badang., C.F. Sarip, and A.P. Tahud. *Geographic Information System (GIS) and Multicriteria Decision Making (MCDM) for Optimal Selection of Hydropower Location in Rogongon, Iligan City.* 2018 IEEE 10th International Conference on Humanoid, Nanotechnology, Information Technology, Communication and Control, Environment and Management (HNICEM),

(Baguio City, Philippines 2018). DOI: 10.1109/ HNICEM.2018.8666266

12. J.V.S. Bondaug and R.V. Irosido. *Geographic Information System (GIS) Spatial Analyst-Based Electric Transmission Line Routing in Rogongon, Iligan City.* [Thesis BS]. Mindanao State University - Iligan Institute of Technology, Iligan City, Philippines (2017)

13. P. Mohanty., K.R. Sharma., M. Gujar, and M. Kolhe. *Solar photovoltaic system applications: A guidebook for off-grid electrification. Springer,* (2016). DOI: 10.1007/978-3-319-14663-8

Pakistan Academy of Sciences

Research Article

Fog-based Intelligent Transportation System for Traffic Light Optimization

Muhammad Rusyadi Ramli*, Riesa Krisna Astuti Sakir, and Dong-Seong Kim

Department of IT Convergence Engineering, Kumoh National Institute of Technology,
61 Daehak-ro, Yangho-dong, Gumi, Gyeongsangbuk-do, 39177, Korea

Abstract: This paper presents fog-based intelligent transportation systems (ITS) architecture for traffic light optimization. Specifically, each intersection consists of traffic lights equipped with a fog node. The roadside unit (RSU) node is deployed to monitor the traffic condition and transmit it to the fog node. The traffic light center (TLC) is used to collect the traffic condition from the fog nodes of all intersections. In this work, two traffic light optimization problems are addressed where each problem will be processed either on fog node or TLC according to their requirements. First, the high latency for the vehicle to decide the dilemma zone is addressed. In the dilemma zone, the vehicle may hesitate whether to accelerate or decelerate that can lead to traffic accidents if the decision is not taken quickly. This first problem is processed on the fog node since it requires a real-time process to accomplish. Second, the proposed architecture aims each intersection aware of its adjacent traffic condition. Thus, the TLC is used to estimate the total incoming number of vehicles based on the gathered information from all fog nodes of each intersection. The results show that the proposed fog-based ITS architecture has better performance in terms of network latency compared to the existing solution in which relies only on TLC.

Keywords: Fog Computing, Reduce Gas Emission, Road Safety, Smart City

1. INTRODUCTION

Intelligent transportation systems (ITS) has been becoming a key aspect to realize the concept of Industry 4.0 and smart city [1, 2]. ITS can bring logistic systems into more efficient. In terms of smart cities, ITS can enhance road safety and lower gas emission [3, 4]. Currently, most ITS architectures are based on cloud computing [5]. In ITS, the network should be reliable and the task should be processed in real-time. Thus, it is still challenging to design an optimal ITS with the current architectures.

Although cloud computing offers some advantages for ITS, its approach naturally conflicts with the principles of ITS. For instance, cloud data centers are generally remote, leading to an unacceptable transmission latency. Alternatively, fog computing can outperform conventional cloud computing, as it brings the cloud closer to the edge (e.g., end-users and devices) to provide low latency

and location awareness for the target systems [6, 7]. Therefore, fog computing can be suitable for handling ITS communications and processes [8].

There have been extensive researches on ITS. However, only a few address fog-based ITS architecture. The researchers surveyed the role of big data analytics to improve the efficiency of fog-based ITS [9]. Some researchers proposed a fog-based system for vehicular ad hoc network (VANET) smart mobility applications [10]. The authors in [11] propose the integration between fog and cloud to enhance the performance of IoT applications, such as smart traffic [12]. Different from the mentioned works, in this paper, the authors propose a fog-based architecture to solve traffic light optimization problems.

The first problem is the dilemma zone problem. In this problem, the vehicle is located between the should-go and the should-stop zone. When the vehicle is in this zone, the vehicle may hesitate

to take action whether to accelerate or decelerate. Furthermore, the vehicle will be more confused when the traffic light is shown a yellow sign and at the same time, the vehicle is in the dilemma zone. This condition may lead to serious traffic accidents. Thus, we consider deploying fog node on each traffic light to overcome this problem. The roadside unit (RSU) node is used to collect the current traffic information (e.g., vehicle's position and vehicle's speed) and transmit it to the fog node. Then, the fog node will estimate and determine the traffic light scheduling based on the gathered information from RSU nodes. Further, they choose fog node to execute this process because it requires to be processed in real-time.

The second problem is to make each intersection able to estimate incoming number of vehicles from its adjacent intersection. We consider the traffic light center (*TLC*) to perform the task of this problem. Specifically, the *TLC* gathers and stores the information such as total number of vehicles that is passing by on each road of intersection from the fog nodes. Then, *TLC* will use these gathered information to estimate the total number of vehicles that will come to the adjacent intersection. Finally, the *TLC* will transmit the estimation results of incoming vehicles to each respected fog node in the adjacent intersection. Therefore, the adjacent intersection aware of the incoming traffic condition.

Based on the explanation above, the role of the fog node in the proposed architecture is to provide a real-time computation process to solve the dilemma zone problem. The *TLC* has similar functionality with the cloud server in which is used to store the global information of the intersection. It makes each intersection aware of the other intersections' traffic conditions. Moreover, it is expected that the proposed method has better performance in terms of network latency compared to the existing solution in which relies only on *TLC*. As for the *TLC*, it is used to estimate the incoming number of vehicles for each intersection. Furthermore, the role of the RSU node is only for providing the current traffic condition. Since the RSU node has a computation constraint, then the collected traffic conditions information will be transmitted and processed on the fog node in which has more capability to conduct the computation process.

2. PROPOSED FOG-BASED ITS ARCHITECTURE

The proposed fog-based architecture consists of three layers which are edge, fog, and cloud layer. The RSU nodes are located in the edge layer. The fog layer comprises traffic lights equipped with a fog node. A fog node can be a switch or router which has an adequate computational capability to perform the task. The Cloud layer, as mentioned above, consists of *TLC*. The wireless communication link is used to connect between the edge and fog layer. The communication between the fog and cloud layer is provided through broadband communication links since it has longer distances. As for the communication between RSU and the vehicle, it could use a vehicle to infrastructure (V2I) communication protocol in which the problem of it is out of this paper scope.

Consider an intersection road that consists of traffic lights such as depicted in Figure 1. These traffic lights are equipped with a fog node. Each traffic light can communicate to the other through a fog node. We assume that the traffic light only able to communicate to each other inside of their domain. The reason lies in the distance between intersections that varies in reality. It thus not feasible to connect each intersection domain by using only fog nodes. Also, the RSU is considered as a node to gather the current zone location and speed of the vehicle. We deploy three RSU nodes (e.g., G-RSU, Y-RSU, R-RSU) on the side road where each node only responsible to monitor its zone. For instance, G-RSU, YRSU, and R-RSU nodes only responsible to gather the traffic information that are located in the should-go, dilemma, and should-stop zone respectively. Furthermore, we also consider *TLC* to connect each of intersection domain. The *TLC* has a similar functionality with the cloud server in which is used to store the global information of the intersection. It makes each intersection aware of the other intersections' traffic conditions. The traffic light scheduling is also implemented by using an algorithm that proposed in our previous work [1].

Second, this paper considers each intersection aware of its adjacent. The *TLC* is used to process the estimation number of incoming vehicles based on the gathered traffic information of the fog node. Then, the estimation results will be transmitted
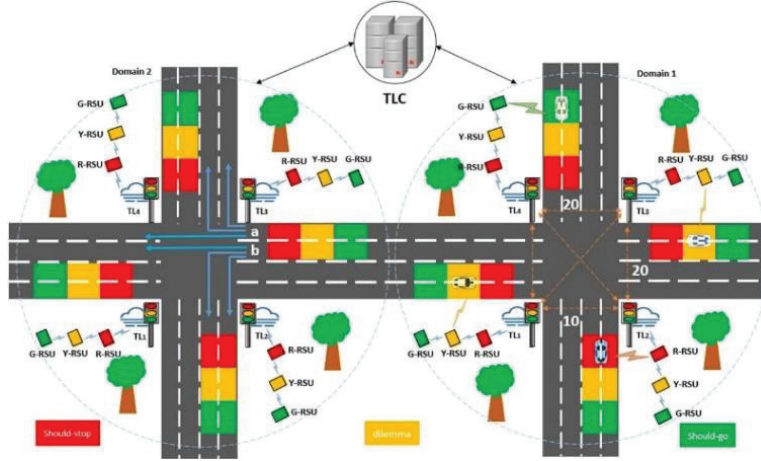
Fig. 1. The architecture of the proposed fog-based ITS for traffic light optimization

to each fog node in the adjacent intersection. Particularly, we assume there are two lanes on the road which are lane a and b. Each vehicle on these lanes may take a left turn, a right turn or a straight forward. The *TLC* table is used to estimate the total vehicle numbers on each lane of the adjacent intersection. Each fog node will transmit the total number of vehicles and store it in the *TLC* table. As shown in Table I, Fog ID, Lane ID, and Number of Vehicles in the *TLC* table represent the location of fog node, lane information, and a number of vehicles in the lane of respected Fog ID. For instance, fog node 3 in Domain 1 is given Fog3-1 as its Fog ID. The lane information of Fog3-1 is denoted by Fog3-1a and Fog3-1b. And the number of vehicles in each lane is stored in the number of vehicles column. This information, later on, will be used to estimate the number of vehicles for the adjacent intersection.

Based on Figure 1. There are a total of 20 vehicles in fog3-1, 20 vehicles in fog4-1, and 10 vehicles in fog 2-1. Then, it can get a total of 50 vehicles in Domain 1. The *TLC* will estimate the number of vehicles for the adjacent intersection which is located in Domain 2. The process of

estimation number can be expressed as Equation (1) and Equation (2)

$$straight\ and\ turning\ right\ = \frac{\frac{20}{2}+20}{20+10+20} = 0.666 \quad (1)$$

$$straight\ and\ turning\ right\ = \frac{\frac{20}{2}+10}{20+10+20} = 0.444 \quad (2)$$

As mentioned above, the total number of vehicles in Domain 1 is 50 vehicles. Then, *TLC* can estimate the current volume of each lane in Fog3-2 as Equation (3) and Equation (4)

$$Estimated\ volume\ in\ Fog3-2a\ =\ 0.666*50\ =\ 30 \quad (3)$$

$$Estimated\ volume\ in\ Fog3-2b\ =\ 0.444*50\ =\ 20 \quad (4)$$

where the *TLC* can estimate the volume of other sections in Domain 2 by using the same mechanism.

3. DELAY ANALYSIS OF FOG-BASED ITS ARCHITECTURE

Taking a situation of intersection road where different total number of vehicles passing by at each section. At first, RSU gathers real-time data based on the current condition of the traffic. Each traffic light waits for the incoming data gathered from the RSU. Then, the data will be processed on the fog node for the traffic light scheduling. There is a condition where the fog node should offload the task to an available node due to the computation storage constraint. In this case, the distributed computing mechanism is needed to avoid congestion on the fog node. It denotes this case as the worst case and

Table 1. An example of vehicle information table of TLC

Fog ID	Lane ID	Number of Vehicles
Fog3-1	Fog3-1a	10
Fog3-1	Fog3-1b	10

is considered as for our future work. Finally, the traffic light optimization results will be transmitted to the *TLC* for the global information of intersection. Therefore, this research illustrates all of these processes as a weighted undirected graph G = (V, E) such as depicted in Figure 2.

In Figure 2, the vertex set of V = {*TL1, TL2, TL3, TL4, TLC*}, where vertex *TLi* and *TLC* denote the fog node in each traffic light of an intersection and *TLC* respectively. Meanwhile, the edge set of E = {*eTL1,TL2, ..., eTLi,TLj, eTLj,TLC*}, where each edge *eTLi,TLj* and *eTLj,TLC* represent the wireless communication link among fog nodes and between fog node and *TLC* respectively. The weight of each edge denoted by *WTLi, WTLj* represent the communication latency between fog node *TLi* and fog node *TLj*. The weight of *WTLj , WTLC* denotes the communication latency between fog node *TLj* and *TLC*. Also, *CTLi* and *CTLC* express the computing capacity of each fog node and *TLC* respectively.

From the above scenario, the service latency for processing the traffic light optimization task on each fog node can be derived as Equation (5)

$$\frac{D_{rsu}}{r_{rsu}} + \frac{D_{TLi}}{C_{TLi}} + W_{TLi,TLj} + \frac{D_{TLC}}{r_{TLC}} + W_{TLj,TLC} \quad (5)$$

where $\frac{D_{rsu}}{r_{rsu}}$ denotes communication latency of RSU. $\frac{D_{TLi}}{C_{TLi}}$ denotes the computation latency of the traffic light optimization process on the fog node *TLi*.

Furthermore, this research considers the transmission latency under the stop-and-wait ARQ protocol. In general, the stop-and-wait ARQ protocol is a basic approach to conduct error control in digital communications in which it offers error and flow control during the transmission. Hence, according to [13], the transmission latency of *WTLi,TLj*, and *WTLj, TLC* under stop and-wait ARQ protocol can be formulated as Equation (6) and Equation (7).

$$W_{TLi,TLj} = \frac{D_{TLi}}{r_{TLj}} \times \frac{1+P_{eTLi}}{1-P_{eTLi}} \quad (6)$$

$$W_{TLj,TLC} = \frac{D_{TLC}}{r_{TLC}} \times \frac{1+P_{eTLC}}{1-P_{eTLC}} \quad (7)$$

where *DTLi* and *DTLC* denote the task that transmitted to the fog node *TLi* and *TLC* respectively. ri and rc denote the transmission rate of the link *eTLi,TLj* and *eTLj,TLC*. PeTLi and *PeTLC* express the packet error rate of the link *eTLi,TLj* and *eTLj,TLC*.

In summary, it can be denoted the delay of the proposed fog-based ITS architecture as Equation (8) and Equation (9)

$$\frac{D_{rsu}}{r_{rsu}} + \frac{D_{TLi}}{C_{TLi}} + \frac{D_{TLi}\,(1+P_{ei})}{r_{TLi}\,(1+P_{ei})} \quad (8)$$

$$\frac{D_{TLC}}{C_{TLC}} + \frac{D_{TLC}\,(1+P_{ec})}{r_{TLC}\,(1+P_{ec})} \quad (9)$$

4. PERFORMANCE EVALUATION

To verify the proposed fog-based ITS architecture, we evaluated the latency in service from the system model that is shown in Figure 1 by using Equation (9). The simulation parameters and metrics are presented in Table 2. According to [14], the delay between IoT nodes (i.e., RSU) and its corresponding fog node, among fog nodes, and between fog nodes and cloud (i.e., *TLC*) are uniformly distributed
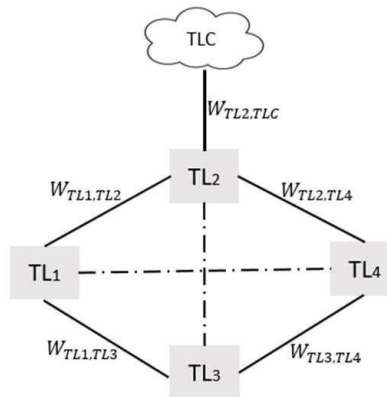
Fig. 2. The weighted undirected graph

between U[1, 2], U[0.5, 1.2], and U[15, 35] ms respectively. Also, it sets 100 Bytes of network length for the task of the first problem, and 500 Bytes for the task of the second problem. This research implemented the proposed fog-based ITS architecture in iFogsim [15] where it is used to describe the network topology and simulate tasks throughout the simulator. The simulation tests were running in the desktop computer equipped with an Intel Core i5-4690 processor, 16 GB of RAM, and Microsoft Windows 10. Furthermore, the researchers tested the proposed fog-based ITS architecture with two different vehicles scenarios which are 30 and 60 cars.

Following in Figure 3, the proposed fog-based ITS architecture can overcome *TLC*-based architecture in terms of latency when it executes the first problem task. There is a correlation between the latency and the number of cars. In conventional *TLC*-based architecture, the latency increased in proportion with the increase of the car's number.

However, It is recommended that the proposed *TLC* architecture should be able to maintain the latency when it was subjected to different scenarios.

The proposed fog-based ITS architecture can achieve latency around 14.74 ms even when 30 cars appeared in the simulation scenario. On contrary, the *TLC*-based architecture obtains around 104.43 ms with the 30 cars that have appeared. When the number of vehicles is increased to 60 cars, the fog-based architecture is still able to maintain its network performance with obtained latency of around 15.64 ms. The *TLC*-based architecture achieves 108.32 ms which significantly higher than the fog-based ITS architecture. Similarly, the proposed fog-based ITS architecture can overcome the *TLC*-based architecture when it executes the task of the second problem. The fog-based ITS architecture can achieve better latency in both 30 and 60 cars scenarios compared to the *TLC*-based architecture.

Table 2. Simulation Parameters and Metrics

Parameters	Values
Number of vehicles in each road segment	30 to 60
Number of traffic lights in each intersection	4
Number of fog nodes in each intersection	4
Weight of normal vehicles	1
Weight of heavily-loaded vehicles	2
Weight of should-go zone & should-stop zone	1
Weight of dilemma zone	2
Length of should-go zone	20 *m*
Length of dilemma zone	30 *m*
Latency between RSU & its fog node (*ms*)	U[1,2]
Latency between each fog node (*ms*)	U[0,5,1,2]
Latency between fog node & TLC (*ms*)	U[15,35]
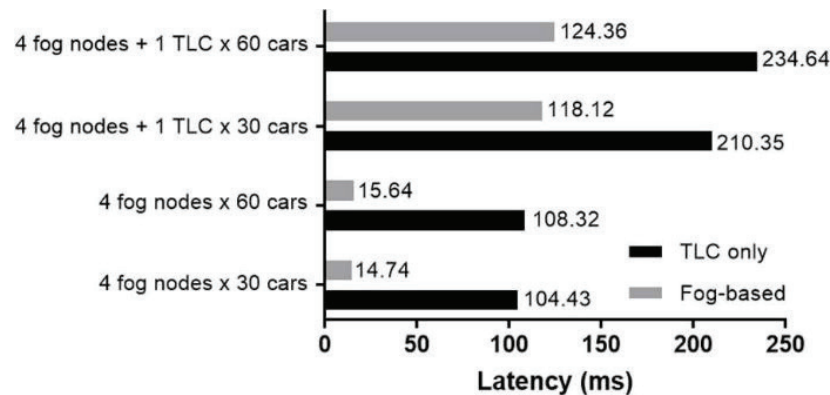
Fig. 3. The latency for executing the first and second problem task

5. CONCLUSION

This research presents a fog-based ITS architecture for traffic light optimization. First, we introduce two traffic light optimization problems that this work wants to tackle. The first problem is executed on the fog node since it requires a real-time process to avoid serious accidents. Then, the estimated number of incoming vehicles is processed in the *TLC*. This is because all of the fog nodes in each intersection can be communicated to the *TLC*. It makes the *TLC* can gather the traffic information of each intersection. Finally, this research verifies the average latency in service of a simulated system by using several scenarios. This research found that the proposed fog-based *ITS* architecture has lower latency compared to the *TLC*-based architecture. In future work, it will analyze the throughput, the operational cost, and the energy consumption of the proposed fog-based ITS architecture. It will also investigate the efficient task distributed mechanism in the worst-case condition such as overcapacity on the fog node.

6. ACKNOWLEDGEMENTS

7. CONFLICT OF INTEREST

The authors declare no conflict of interest.

8. REFERENCES

1. 1. T. Ngo., T. Huynh-The., and D-S. Kim. A novel VANETs-based traffic light scheduling scheme for greener planet and safer road intersections. *IEEE Access* 7: 22175–22185 (2019). DOI: 10.1109/ACCESS.2019.2891250.

2. E. Yandri., R.H. Setyobudi., H. Susanto., K. Abdullah, Y.A. Nugroho., S.K. Wahono., F. Wijayanto, and Y. Nurdiansyah. Conceptualizing Indonesia's ICT-based energy security tracking system with detailed indicators from smart city extension. *E3S Web Conferences* 188(00007): 1–7 (2020). DOI: 10.1051/e3sconf/202018800007.

3. B. Novianto., K. Abdullah., A. S. Uyun., E. Yandri., S.M. Nur., H. Susanto., Z. Vincēviča-Gaile., R.H. Setyobudi, and Y. Nurdiansyah. Smart micro-grid performance using renewable energy. *E3S Web of Conferences* 188(00005): 1–11 (2020). DOI: 10.1051/e3sconf/202018800005.

4. C. Suthaputchakun, and Z. Sun. A novel traffic light scheduling based on TLVC and vehicles' priority for reducing fuel consumption and CO2 emission. *IEEE System Journal* 12: 1230–1238 (2018). DOI: 10.1109JSYST.2015.2500587

5. H. Nasser., Y. Hafeer, and A. Saida. Towards software testing as a service for software as a service based on cloud computing model. *Proceedings of the Pakistan Academy of Sciences A. Physical and Computational Sciences* 55 (4): 1–8 (2018).

6. C. Mouradian., D. Naboulsi., S. Yangui., R.H. Glitho, M.J. Morrow., and P.A. Polakos. A comprehensive survey on fog computing: state-of-the-art and research challenges. *IEEE Communication Survey Tutorials,* 20: 416–464 (2018). DOI: 10.1109/COMST.2017.2771153.

7. M.R. Ramli., P.T. Daely., J-M. Lee., and D-S. Kim, Bio-inspired service provisioning scheme for fog-based industrial internet of things. *IEEE International Conference on Emerging Technologies and Factory Automation* (ETFA), 1661–1664(2019). DOI: 10.1109/ETFA.2019.8869402

8. Khan, S.U., and U. Naeem. Practices for clients in the adoption of hybrid cloud. *Proceedings of the Pakistan Academy of Sciences A. Physical and Computational Sciences* 54 (1): 13–32 (2017).

9. T.S.J. Darwish, and K. Abu Bakar. Fog based intelligent transportation big data analytics in the internet of vehicles environment: Motivations, architecture, challenges, and critical Issues. *IEEE Access*, 6: 15679– 15701 (2018).

10. J. Pereira., L. Richardo., N. Lus., C. Senna., and S. Sargento. Assessing the reliability of fog computing for smart mobility applications in VANETs. *Future Generation of Computer Systems,* 94: 317–332 (2019). DOI: 10.1016/j.future.2018.11.043

11. A. Munir., P. Kansakar, and U. Khan. IFCIoT: Integrated Fog Cloud IoT: A novel architectural paradigm for the future Internet of Things. *IEEE Consumer Electronics Magazine,* 6: 78–82 (2017). DOI: 10.1109/MCE.2017.2684981

12. Nahry., H.R. Agah., A. Thohirin, and N.H.A. Hamid. Modeling the relationship between on-street parking characteristics and through traffic delay. *Proceedings of the Pakistan Academy of Sciences: A. Physical and Computational Sciences* 56 (2): 29–36 (2019

13. X. Ma., H.I. Volos., X. Zheng., J.H. Reed, and T. Bose. A variation-aware approach for task allocation in wireless distributed computing systems. *IEEE Global Communication Conference* (GLOBECOM), 5006–5011 (2013). DOI: 10.1109/ GLOCOMW.2013.6855744

14. A. Yousefpour., G. Ishigaki, and J.P. Jue. Fog computing: Towards minimizing delay in the internet of things. *IEEE International Conference on Edge Computing* (EDGE), 17–24 (2017). DOI: 10.1109/IEEE.EDGE.2017.12

15. H. Gupta., A.V. Dastjerdi., S.K. Ghosh., and R. Buyya. iFogSim: A toolkit for modeling and simulation of resource management techniques in the Internet of Things, Edge and Fog computing environments. *Software: Practice and Experience,* 47: 1275–1296 (2017). DOI:10.1002/spe.2509

Pakistan Academy of Sciences

Research Article

Convolutional Neural Network and Long-Short Term Memory based for Identification and Classification of Power System Events

Mauridhi Hery Purnomo[1*], Vincentius Raki Mahindara[2], Rahmat Fabrianto Wijanarko[2], Agustinus Bimo Gumelar[1], Feri Wijayanto[3], and Yanuar Nurdiansyah[4]

[1]Department of Computer Engineering, Institut Teknologi Sepuluh Nopember, Jl. Teknik Kimia, Keputih, Sukolilo, Surabaya 60111, Indonesia
[2]Department of Electrical Engineering, Institut Teknologi Sepuluh Nopember, Jl. Teknik Kimia, Keputih, Sukolilo, Surabaya 60111, Indonesia
[3]Institute for Computing and Information Science, Radbound University Comenisulaan 4, 6525 HP Nijmegen, The Netherlands
[4]Program Study of Information Technology, University of Jember, Jl. Kalimantan 37, Jember 68121, Indonesia

Abstract: In this present era, power system delivery has to be reliable and sustainable. The growth of demands increasing the complexity of the power system operations. An interrupted power supply must not occur for any reason. Hence, the improvement of the controller and protection devices is mandatory. One of the unnecessary interruptions in the power system is a false trip due to the incorrect setting of the protection devices. Therefore, a method to classify the symptom of the power system based on the voltage, current, and frequency measurements is required. However, since there are a ton of maneuver options and fault types, the number of data becomes complex, enormous, and irregular. This is where deep learning takes place. This paper proposed the use of Convolutional Neural Networks (CNN) combined with Long-Short Term Memory (LSTM) to recognize the categorize the type of events in a medium voltage power distribution network. As CNN's models are great at decreasing frequency variation, LSTM is great for temporal modeling, we take benefit of CNN's and LSTM's complementarity in this study by integrating it into a unified architecture. The simulation results indicate that CNN and LSTM can recognize the symptoms in power system operation with accuracy up to 79 % with a total epoch 350.

Keywords: Artificial Intelligence-based Model, Deep Learning Algorithm, Electrical Protection System, Energy Efficiency, Sustainable Power System

1. INTRODUCTION

As far as the many appealing challenges faced by the industry today, the most critical part is to be able to compete in the market by figuring and shaping the new technology revolution. The successful technology revolution requires a support system. One of the most crucial parts is the power system. It has been a common secret that everyone demands a reliable power system. When the blackout occurs, every second of the power outages leads to an economic loss in every business sector. To tackle this issue, the power system must be fortified with a defensive scheme that considers the possible fault. On the other hand, with the recent trends of distributed energy resources (DER), a lot of intermittent generators penetrate the system that might cause system instability [1–3]. The combination of a bunch of operation schemes and the possibility of distributed generator (DG) penetration equal with no shortage of challenges for the engineers.

A reliable and sustainable power system network means it has a ton of operation maneuvers and a dependable protection system. The operation

and protection of the power system must work independently but with a correlated purpose. The false or unsafe operation during power system maneuver that might be caused by DER penetration [4], sudden load injection or rejection, networks topology variation, and a fault condition shall be anticipated by a proper protection system [5]. However, the protection system shall not limit the flexibility of power system operations. For this particular reason, a trade-off point is compulsory to achieve a robust power system [6]. An illustration regarding the correlation between power system operation and protection is presented in Figure 1.

As the electrical protection device, a relay works by comparing the reading value to a specific threshold and delay time before it trips the circuit breaker (CB) [7]. The relay must work to limit the interruption, diminish the damage of the component involved, and minimize the affected area. If the closest relay to the fault location cannot handle the situation, then it must be backup by another relay that has a greater time and more area banned from the system. The coordination of the relays constructs an electrical protection system.

The fault in the power system could be categorized into two types, i.e., series faults such as an open line condition and shunt faults such as the short circuit condition [8, 9]. It is very easy to distinguish the type of fault in a direct observation by witnessing the broken equipment or conductor. Per contra, if the fault is located in a remote area, then the observation-only can be proceeded by examining the electrical parameters, i.e., voltage, current flow, and frequency. Chiefly, it is impossible to witness every single piece of equipment on the system. This is where the protection device takes place.

The study aims to fill the gap of providing timeless power system monitoring to witness the symptoms by planting an artificial intelligence-based model in electrical protection devices (EPD). The EPD has to be able to determine what is happening in the system and decide the precise action to overcome the situation. This paper intends to show the opportunity of implementing a deep learning computation to solve a protection scheme problem in power system operations. It is known that deep learning has an undoubted performance in terms of image processing [10]. In this case, the pattern of data series based on the simulated power system events will be used as a feature to be extracted. Deep learning is based on the convolutional neural networks (CNN) since its powerful ability to recognize the pattern [11]. The objective is to use CNN to perform an event classification based on large data sets gathered in the operation of medium voltage power system distribution networks. Later, the CNN is combined with the long-short term memory (LSTM) technique to increase the accuracy of recognizing and classifying the power system distribution network symptoms.

2. COMMON PROBLEM ON MEDIUM VOLTAGE POWER SYSTEM DISTRIBUTION NETWORK

2.1 Fault and Fault-like Event in Power System

An event in the electrical system such as ground fault, phase fault, start or cease of electrical machines, and network topology changes has its symptoms. These symptoms are categorized based on the electrical parameter, i.e., frequency, current flow, and voltage. As an illustration, during the event of a short circuit fault, the closest source feeder relay to the fault location will experience a drop voltage
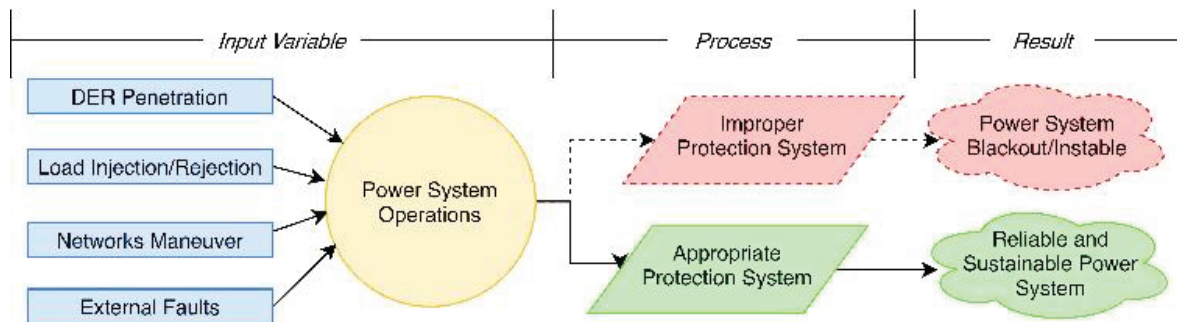
Fig. 1. Reliable and sustainable power system is a result of an appropriate protection system and proper power system operations

followed by increasing current flow and a higher frequency rate at the source site. Meanwhile, in the event of motor starting, the feeder may sense a dip voltage, surge current, and frequency drop. These two events are different even though the symptom of voltage and current is similar.

The fault conditions require CB to trip while it is prohibited to trip during motor starting events. Somehow, due to an improper setting, there is a record of CB trip during the motor starting. This happens quite often in most petrochemical or oil-and-gas companies [12]. The root cause is because the multi-function relay was installed with a default setting and not considering the in-rush condition. As a containment action, the engineer usually broader the setting or disabling to anticipate the drop voltage or the surge current during motor starting. This action comes with a risk that the relay may do not trip when the short circuit occurs during the start process. To validate this hypothesis, time-series data is gathered using a commercial software called ETAP in a transient stability domain.

To set the simulation, the sequence of events is divided into three domains, which are: i) PRE-event, ii) ON-event, and iii) POST-event [13]. To visualize these time domains, Figure 2 represents the voltage, frequency, and current measurements of a feeder that suffering a short circuit condition at t = +1 s.

As shown in Figure 2, PRE-event denoted as the state where there is no switching condition. meaning to say, this domain happens before t = 1 s and might be stated as the normal or basic condition. Meanwhile, ON-event just after the switching. In this domain, the event is happening without any controller react to overcome the events. The ON-event occurs at t = +1 s until any reactions or following events. Regarding that, the EPD must take action or decision during this time domain. The POST-event is any event that happens with regard to the previous events. It could be an opening of CB to clear the fault. However, in this POST event, there is a possibility that the system might go unstable or being stable. This condition is most likely depending on how long the time required of the CB to react.

2.2 Power System Network and The Protection System

The simple system consists of two generators where one of them is considered as a distributed generator (DG). The main transfer bus of this system is an 11 kV that is connected into four different feeders. Every feeder on this system is equipped with a relay that able to observe voltage (V), frequency (f), and current flow (I) in rms. The relay ID is namely A until F as shown in the single line diagram (SLD) Figure 3.

There are several loads connected to the main bus of 11 kV. However, this paper is focused on the 11 kV events only. Several situations that taken into consideration are i) normal condition, ii) three-phase symmetrical (LLL) fault of phase a-b-c in 11 kV, iii) line to line (LL) fault of phase a-b in 11 kV, iv) line to ground (LG) fault of phase a-b in 11 kV, v) the event of DG outage, and vi) direct online (DOL) motor starting of 3 000 kW induction
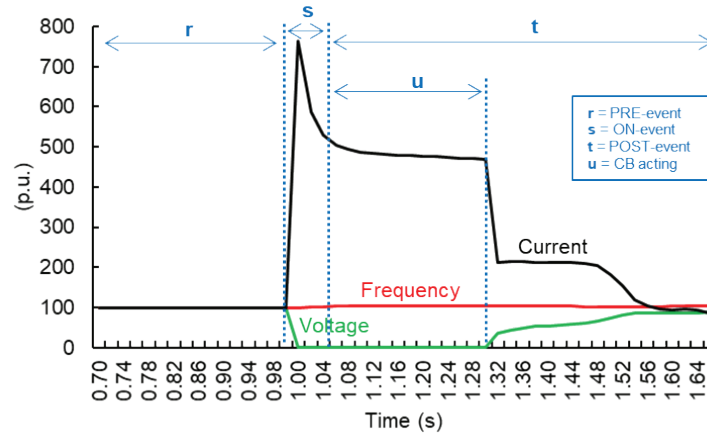
Fig. 2. The sequence of events in the power system on the perspective of voltage, frequency, and current flows

machine. Those six situations will be simulated under several circumstances, such as the penetration of DG and the total load connected.

2.3 Event Classification Based on Convolutional Neural Network (CNN)

2.3.1 CNN Architecture

Recently, Artificial Intelligence (AI) has witnessed a massive development that could bridge the divide between human and machine capacities. This field aims to allow computers to see the environment as people do, to interpret it in the same way, and even to use understanding for many functions such as the identification of images and videos, image analyses and classification, recommendation systems, linguist processing, etc. In power system generation with intelligent electricity meters increasing and the widespread use of power generation technology such as solar panels, we have much information on the use of electricity. This information is a multivariate time sequence of power that could be used in turn for modeling and even predicting future energy usage. The progress made in Artificial Intelligence (AI) by Deep Learning, mainly through one specific algorithm – Convolutional Neural Network (CNN), has been built and improved over the moment. CNN can learn characteristics from sequence information, assist multiple-variate information automatically, and able to immediately generate a multi-step forecasting vector [10]. A CNN is a deep learning algorithm capable of capturing input data, assigning significance (learnable weights and biases) to multiple aspects/objects, and being prepared to distinguish between them [14] Figure 4 depicts the typical CNN block scheme that later will be used on the power system operations.

The fundamental objective in implementing deep learning is to eliminate the complicated and eventually restricting choice of features. The role of a convolutional layer can be articulated merely: it uses a three-dimensional quantity of data to generate a fresh three-dimensional quantity of data.

As shown Figure 5, illustrates the 3D convolution process used in CNNs, and input features are used for the convolution operation. The first convolution layer uses low-level characteristics like edges, rows, and angles. The input is $N \times N \times D$ and is converted with H kernels, each of which

is separately $k \times k \times D$. Convolution of with one kernel generates an output function and separately generates features map with kernels. Each kernel passes one element at a time from the top-left corner. One element will be moved down from the kernel and one item will be passed over again from left to right. This method is performed until the kernel hits the bottom-right corner. If input height and width are equal to 32 and the kernel value is 5, there will be 32 distinctive places from left to correct and 32 distinctive places from top to upper that the kernel can hold. According to these locations, each function in the output will comprise 32×32 ((N-$k+1) \times (N$-$k+1$)) components. To be able to achieve a single component in a single output, multiplier activities between two components are input=($k \times k \times D$) and kernel=($k \times k \times D$) are needed for each place in the sliding window method.

In Figure 6, the same color links are limited to having the same weight at all times. This can be achieved by initializing all the connections within a group with the same weights and by always averaging a group's weight updates before applying them at the end of each backpropagation iteration. This filter produces the output layer of the function map. A neuron is triggered in the feature map where a filter is identified at the respective place in the prior layer to contribute to its activities.

3. RESULTS AND DISCUSSION

3.1 Data Gathering

As stated in Section 2.1. The most crucial part of the electrical circumstances is the ON-event. Therefore, by considering that the relay sampling is one cycle (equal to 20 ms for 50 Hz system) and the relay must react within five cycles, the data consist of five samplings construct by the PRE-event and ON-event as shown in Figure 7.

Says there are five rows of data to be recognized by the CNN, then the first two data consist of the PRE-event data or the normal (basis) condition. When the event is occurring, there will be a deviation between the PRE and ON events. Using the SLD, as shown in Figure 3, the whole relay on the system is assumed able to measure the current, voltage the frequency. Each phase on every feeder will be measured regarding the voltage and current flows in rms value. While the frequency is
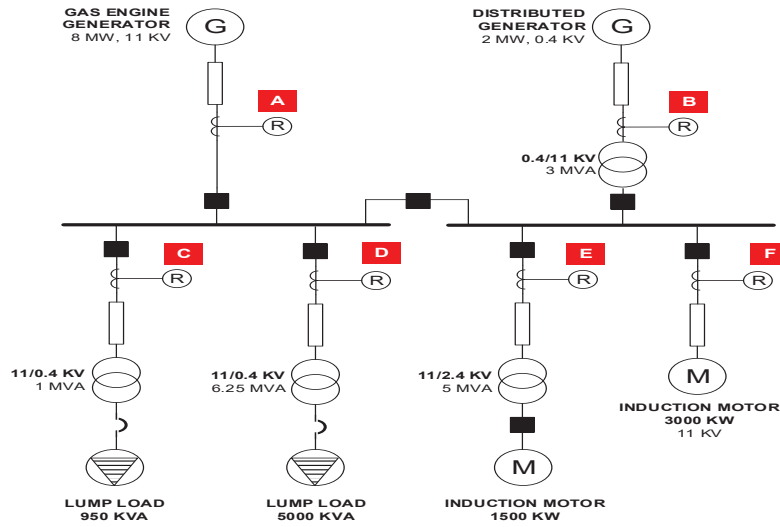
Fig. 3. Single Line Diagram (SLD) being used for the simulation and data gathering.
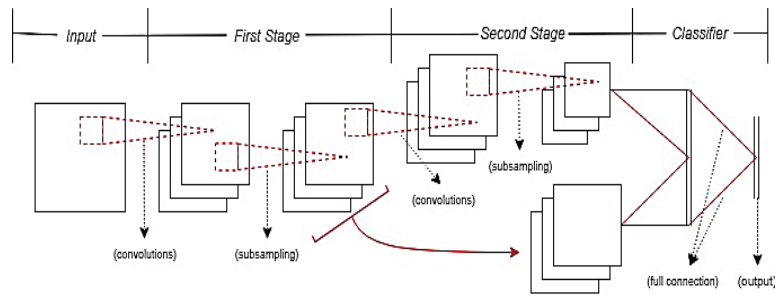
Fig. 4. A typical CNN block scheme [10]

N = Input height and width
k = kernel height and width
D = input depth
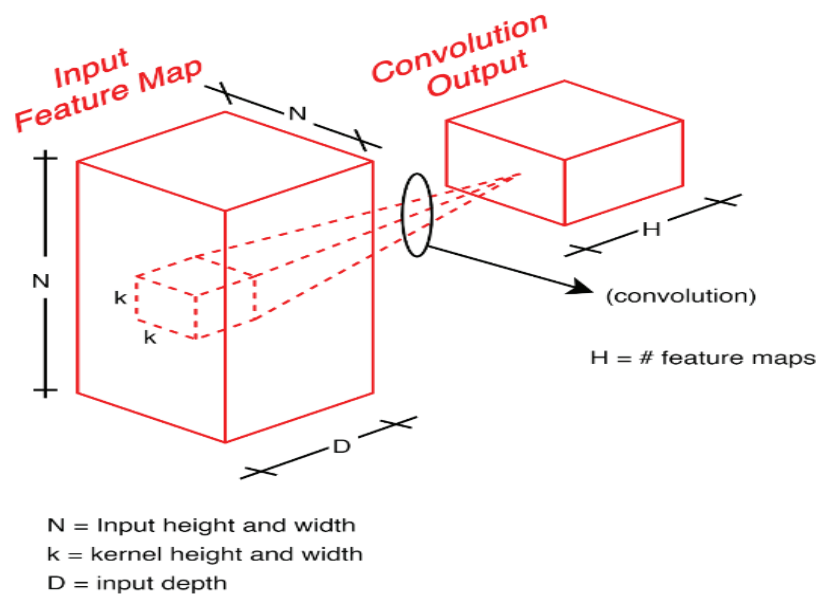
Fig. 5. Convolutional process representation [15]
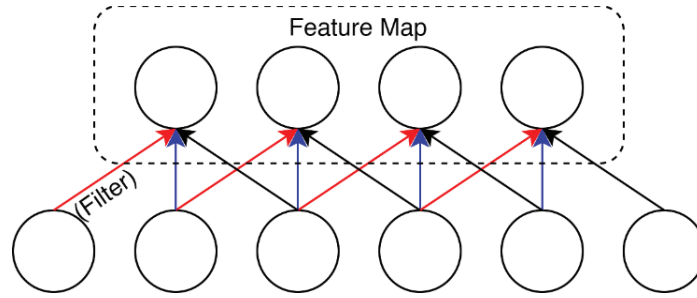
Fig. 6. The filters and maps are represented as neurons in a convolutional layer [15]
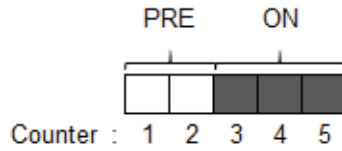
Fig. 7. Visualization of the data required to be trained in ANN

measured only in a single phase. The illustration of data measurement is shown in Figure 8.

Generally speaking, there are two types of feeders in Figure 3. The upper side of the 11 kV bus might be called a source feeder while the lower side is the load feeder. Figure 9 shows the illustration of the current reading for the whole relay with a variety of conditions, as stated in Section 2.2. Moreover, Figure 10 shows the illustration voltage and frequency reading in accordance with the data counter. In total, there are 193 symptoms constructed based on the combination of the power system operations and events.

3.1.1 Current flow analysis

Relay A and B could be grouped as the source feeder relay. For this type of relay, it might be known from Figure 9a. and Figure 9b. that there is a tremendous current spike when the LLL fault is occurring. The other current surge occurs when there is a motor starting. Especially for Relay A, the minor current increase happens when the DG is falling to outage condition. For sure, on the other perspective, Relay B will sense the current drop, as shown in Figure 9b. When the LG fault happens, both Relay A and B only sense a tiny deviation in terms of current reading.

Meanwhile, for Relay C and D that operate as a feeder type relay, the immense current drop occurs when the LLL fault is happening. This is due to there is no source feeding to the load during that occasion. A bit of current decrease happens during the motor starting. During the DG outage and LG fault, there is no current variation on the feeder line. Relay E and F belong to an induction machine that operates on 2.4 and 11 kV. During the LLL fault,
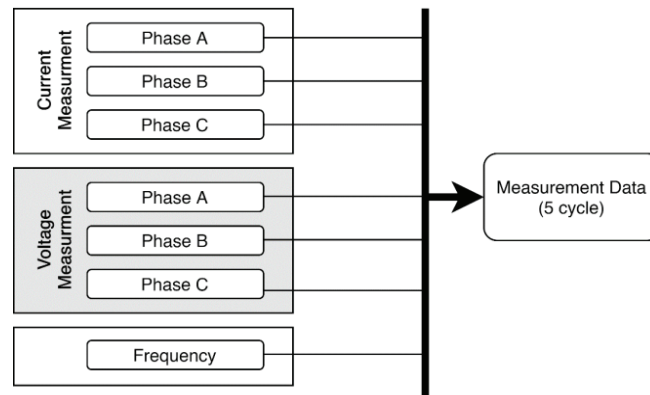
Fig. 8. Practical measurement data from the simulation
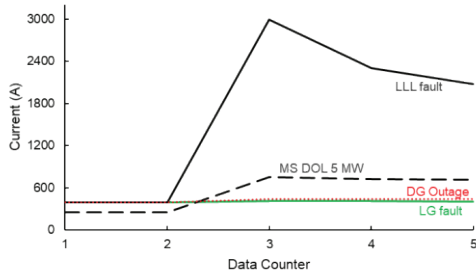
(a) Current reading on Relay A
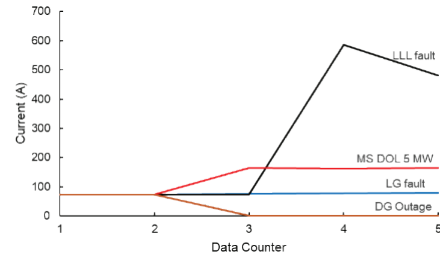
(b) Current reading on Relay B
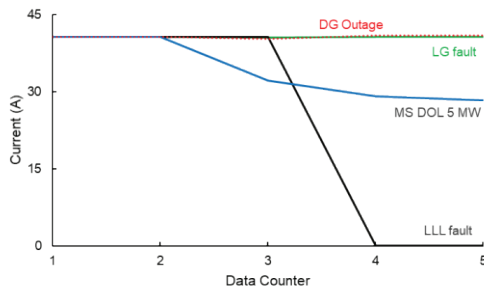
(c) Current reading on Relay C
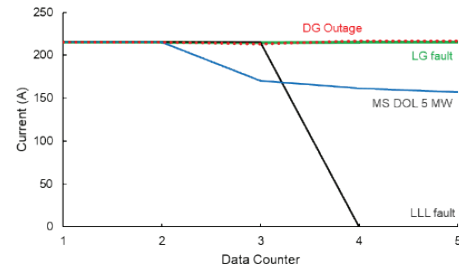
(d) Current reading on relay D
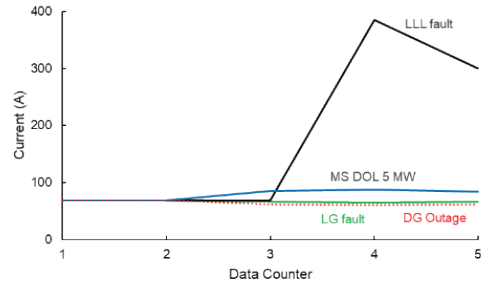
(e) Current reading on Relay E
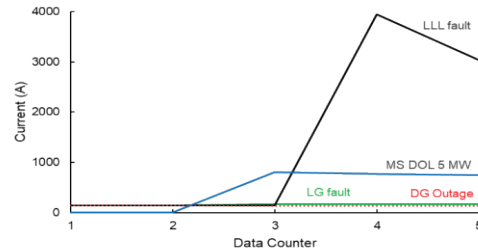
(f) Current reading on Relay F

Fig. 9. Voltage (a) and Frequency (b) reading on each relay with a varied event in 11 kV bus: LG fault, LLL fault, DG Outage, and Motor Starting (MS).

both relays sense a huge current spike since the motor is acting as a generator that feeds the current to the fault location. A minor current spike happens during the motor starting while there is such a big difference in terms of current reading during DG outage and LG fault.

3.1.2   *Voltage analysis*

Since all the relay is connected in parallel to the 11-kV bus, the voltage reading of the all-six relays must be the same. It might be known from

Figure 10.a. that the voltage collapse is immensely happening during the LLL fault. There is also a voltage collapse condition that happens during the motor starting, but not as severe as the LLL fault. In the event of a DG outage, the voltage reading shows if there is no deviation compared to the PRE-event condition. There is a minor increment of voltage during the LF fault.

3.1.3   *Frequency analysis*

Similarly, to the voltage measurement, the frequency

reading only needs a one-perspective measurement since the system is fully synchronized. Figure 10.b. shows that the major frequency collapse happens when the DG outage. A minor frequency collapse also happening when there are a motor starting and the LG fault. Meanwhile, during the LLL fault, the frequency is increasing dramatically.

3.2 Training and Classification using CNN

3.2.1 Implementation of CNN

The network input is a 135 × 35 matrix that is considered as a single data channel. The first layer, C1, conducts four input conversions with 2 × 2 kernels, creating four-function maps of size 133 × 33. In the second layer, C2, execute 2 × 2 kernels. The information is rescaled to suit the Keras sequential model's three-dimensional input criteria. For a simple univariate model, the input form is 35-time stages with one feature. In the convolutional layer, the sequence was not divided into several subsequences, but rather 32-time stages. Six neurons in the thick layer generate six outputs. One of the popular Recurring Neural Network (RNN) models is LSTM. As shown in, the schematic of LSTM and σ denotes a sigmoid feature. There are three basic gates on LSTM: i) an input, ii) output and iii) a forget gate. The procedure operation between these three doors allows LSTM able to fix long-term dependencies which are not learned by particular RNNs.

Both in Keras, a CNN-LSTM can be defined for training. A CNN LSTM can be described by bringing the first layer is CNN layers, and the second layer is followed by LSTM layers with a Dense layer at the output layer. It is helpful to think of this architecture as defining two sub-models. The CNN Model for features extraction and the LSTM Model for analysis of features over time phases. Figure 12 depicts the illustration of the feeding process from CNN to LSTM while the architecture based on CNN is summarized in Table 1. Figure 13 shows the Keras sequential model.

3.2.2 Experimental Result

Figure 14 shows the experimental result of the proposed CNN to recognize the symptoms of power system operations. It might be known that the model with 200 epochs might reach 69 % accuracy, as shown in Figure 14.a. An increasing epoch up to 350 shows that there is an accuracy spike that reaches 79 % at epoch 275 as depicts in Figure 14.b. This result later is confirmed by the heatmap of the dataset of features 1-35 (x-axis) with the value of each feature per row (y-axis) as shown in Figure 14.c. This indicates that CNN and LSTM can generalize and not just memorizing the pattern. Furthermore, this might be preliminary proof that CNN and LSTM might be helpful to supervise the power system operations.

Table 1. CNN based architecture

Layer	Kernel/Pooling Window	Layer Size
Input	-	1@135x35
Lstm (C1)	[32@2x2]	32@133x33
Lstm (C2)	[32@2x2]	32@122x31
Lstm (C3)	[32@2x2]	32@110x9
Dense (P2)	[6@2x2]	6@58
Full Out (F1)	-	58
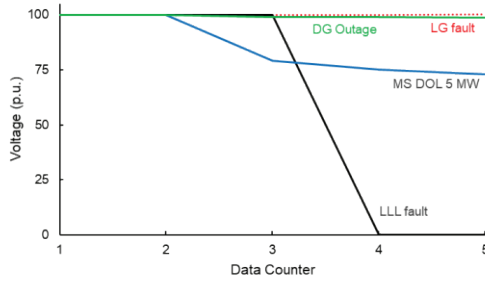
a) Voltage reading on 11 kV bus
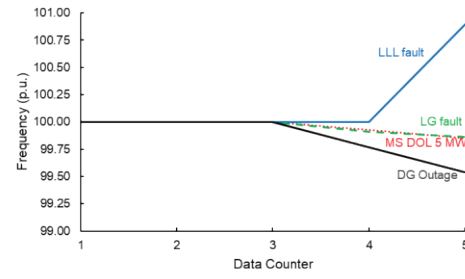
b) Frequency reading on 11 kV bus

Fig. 10. Voltage (a) and Frequency (b) reading on each relay with a varied event in 11 kV bus: LG fault, LLL fault, DG Outage, and Motor Starting (MS).
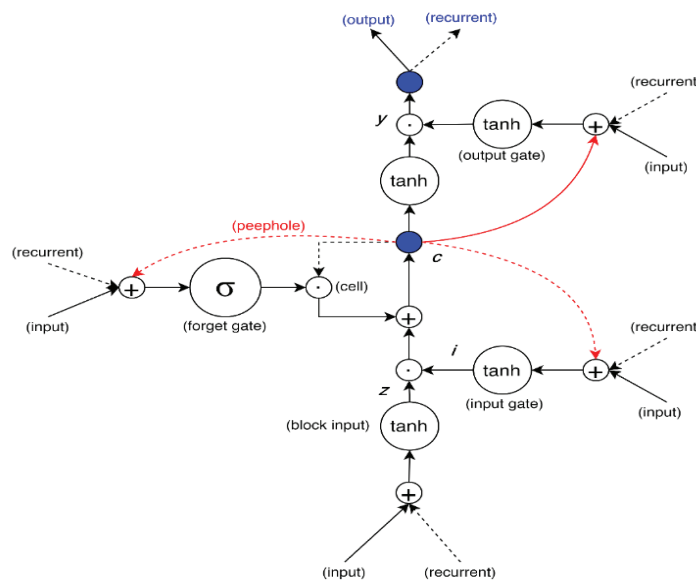
Fig. 11. LSTM Block
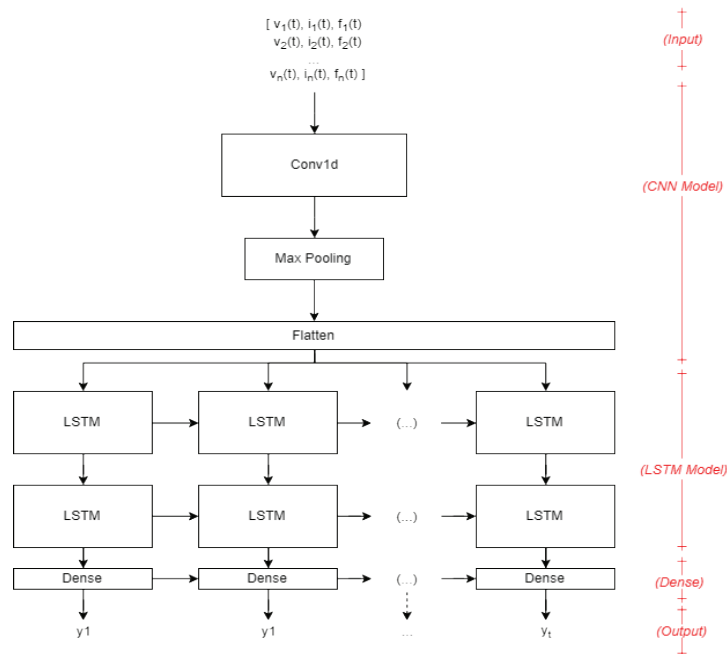
Fig. 12. Feeding into LSTM layers

```
from keras.layers import (
    Activation, Flatten, Dropout, LSTM,
    Dense,

model.add(LSTM(32, return_sequences=True,
               input_shape=(35, 1)))
model.add(LSTM(32, return_sequences=True))
model.add(LSTM(32))
model.add(Dense(6, activation='softmax'))

model.compile(loss='categorical_crossentropy',optimizer='adam',metrics=['acc'])
model.summary()
```

Fig. 13. Keras sequential model

(a)

(b)

(c)
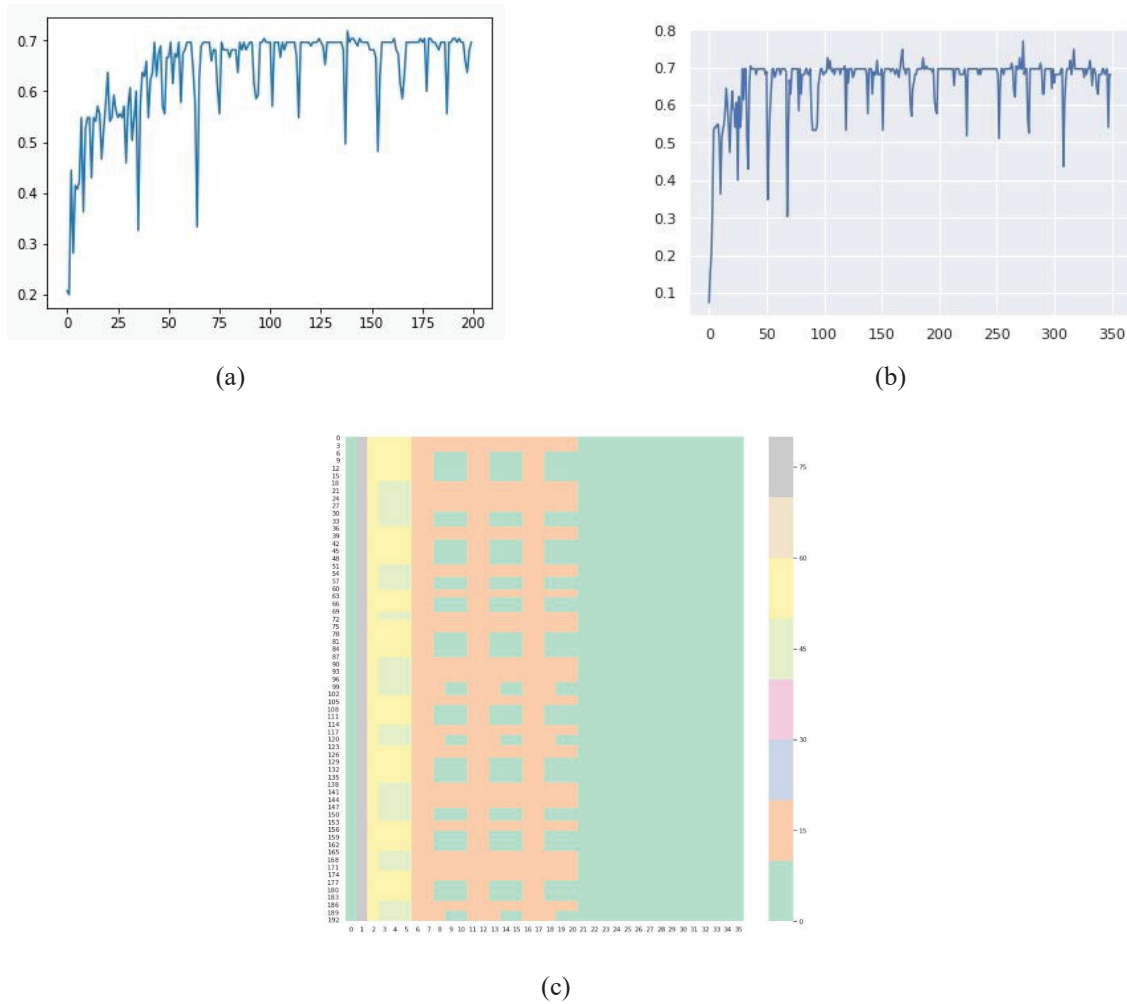
Fig. 14. Trial result of the CNN to recognize the symptoms of power system operations: (a) 200 epoch (b) 275 epoch, (c) heatmap dataset

4. CONCLUSION

The learning time would also improve proportionately if the conventional Neural Network (NN) were to be equal to a CNN, as the number of parameters would be much greater. With a significant reduction in parameters in a CNN, the learning period is reduced proportionately. In an ideal practice, a conventional NN might be built with the same performance as a CNN. A standard CNN-equivalent neural network would have more parameters that add to greater noise during the training stage. Therefore, the output of conventional CNN is always less efficient. In the future, it is expected that the expenditure of more time in a customized CNN architecture can result in an ideal model for the future task. Ensemble designs have shown that other classification activities are achieving stronger outcomes. Given that a model is better at rating specific event types, while its overall accuracy is low, multiple models can increase the classification performance. Lastly, the research was restricted to six events in power system operation with several kinds of circumstances of the case. A further kind of events and symptoms might be achieved by working with a greater number of the bus that could assist to develop stronger CNN models and produce precious fresh findings.

6. ACKNOWLEDGEMENTS

6. CONFLICT OF INTEREST

The authors declare no conflict of interest.

5. REFERENCES

1 D. Yang., J. Kim., Y.C. Kang., E. Muljadi., N. Zhang., J. Hong., and T. Zheng, Temporary Frequency Support of a DFIG for High Wind Power Penetration. *IEEE Transactions on Power Systems* 33(3): 3428–3437 (2018). DOI: 10.1109/TPWRS.2018.2810841

2 E. Muljadi., N. Samaan., V. Gevorgian., J. Li., and S. Pasupulati. Different factors affecting short circuit behavior of a wind power plant. *IEEE Transactions on Industry Applications,* 49(1): 284–292 (2013). DOI: 10.1109/TIA.2012.2228831

3 J. Kim., E. Muljadi., V. Gevorgian., and A.F. Hoke. Dynamic capabilities of an energy storage-embedded DFIG system. *IEEE Transactions on Industry Applications* 55(4): 4124–4134 (2019). DOI: 10.1109/TIA.2019.2904932

4 J.P. Holguin., D.C. Rodriguez., and G. Ramos. Reverse Power Flow (RPF) detection and impact on protection coordination of distribution systems. *IEEE Transactions on Industry Applications.* 56(3): 2393–2401 (2020). DOI: 10.1109/ TIA.2020.2969640

5 V.R. Mahindara., D.F.C. Rodriguez., M. Pujiantara, A. Priyadi., M. H. Purnomo., and E. Muljadi. Modern concerns and challenges of overcurrent protection coordination in distribution systems. Presented at the *2020 IEEE/IAS 56th Industrial and Commercial Power Systems Technical Conference (I&CPS)*, Virtual Conference, Apr. 2020.

6 A. Hooshyar, and R. Iravani. Microgrid Protection. *Proceedings of the IEEE* 105(7): 1332–1353 (2017), DOI: 10.1109/JPROC.2017.2669342

7 V.R. Mahindara., M.G. Istiqlal., M. Pujiantara., D.A. Asfani., A. Priyadi., and M. H. Purnomo. Obtaining the setting of inverse-curve overcurrent relay using serial computing modified particle swarm optimization in real system applications. In: 2*018 International Seminar on Intelligent Technology and Its Applications* (ISITIA), Aug., 187–192 (2018). DOI: 10.1109/ISITIA.2018.8710868

8 A. Prasad., J. Belwin Edward., and K. Ravi, A review on fault classification power transmission systems: Part—I, *Journal of Electrical Systems and Information Technology* 5(1): 48–60 (2018). DOI: 10.1016/j.jesit.2017.01.004

9 A. Prasad., J. Belwin Edward., and K. Ravi, A review on fault classification methodologies in power transmission systems: Part-II, *Journal of Electrical Systems and Information Technology* 5(1): 61–67, (2018). DOI: 10.1016/j.jesit.2016.10.003

10 Y. LeCun., Y. Bengio., and G. Hinton. Deep learning. *Nature* 521(7553): 436–444 (2015). DOI: 10.1038/nature14539

11 H. Chiroma, U.A. Abdullahi, S.M.Abdulhamid, A.A. Alarood, L.A. Gabralla, I.A.T. Hashem, D.E.

Gbenga, A.I. Abubakar, A.M. Zeki, and T. Herawan. Progress on artificial neural networks for big data analytics: A survey, *IEEE Access* 7: 70535–70551 (2019). DOI: 10.1109/ACCESS.2018.2880694

12 R.M. Vincentius, A.W. Nugraha., P.S. Talitha., P. Margo., P. Ardyono., and H.P. Mauridhi. Recognition of electric machines boundary as the constraint of over current relay coordination in real industrial application with serial firefly algorithm optimization. In *2019 IEEE 12th International Symposium on Diagnostics for Electrical Machines, Power Electronics and Drives* (SDEMPED), Aug. 153–159 (2019). DOI: 10.1109/DEMPED.2019.8864828

13. F.W. Rahmat., M. Pujiantara., V. Lystianingrum., V.R. Mahindara., and T.P. Sari. Self-Classification of multifunction relay based on neural network for industrial scale," in 2020 International Seminar on Intelligent Technology and Its Applications (ISITIA), Jul. 13–18 (2020),
 DOI: 10.1109/ISITIA49792.2020.9163719

14. N. Buduma. *Fundamentals of Deep Learning.* O'Reilly Media, Inc. Boston, MA (2017).

15. K. Ovtcharov., O. Ruwase., J. Kim., J. Fowers., K. Strauss., and E.S. Chung. Toward accelerating deep learning at scale using specialized hardware in the datacentre. *In 2015 IEEE Hot Chips 27 Symposium (HCS), Aug.* (2015), 1–38. DOI: 10.1109/ HOTCHIPS.2015.7477459

Reducing Energy and Water Consumption in Textile Dyeing Industry with Cleaner Production by Inlet-Outlet Modification to Reuse Wastewater

Erkata Yandri[1,2]*, Rinaldi Idroes[3], Roy Hendroko Setyobudi[1,4],
Carolus Boromeus Rudationo[1], Satriyo Krido Wahono[5], Rangga Kala Mahaswa[6],
Juris Burlakovs[7], and Herry Susanto[1]

[1]Graduate School of Renewable Energy, Darma Persada University, Jl. Radin Inten 2,
Pondok Kelapa, East Jakarta 13450, Indonesia
[2]Center of Renewable Energy Studies, Darma Persada University, Jl. Radin Inten 2,
Pondok Kelapa, East Jakarta 13450
[3]Department of Chemistry, Faculty of Mathematics and Natural Sciences,
Universitas Syiah Kuala, Kopelma Darussalam, Banda Aceh 23111, Indonesia
[4]Department of Agriculture Science, Postgraduate Program, University of Muhammadiyah
Malang, Jl. Raya Tlogomas No. 246, Malang, 65145, Indonesia
[5]Research Division for Natural Product Technology – Indonesian Institute of Sciences,
Jl. Jogja - Wonosari, km 31.5, Gunung Kidul, Special Region Yogyakarta 55861, Indonesia
[6]Faculty of Philosophy, Universitas Gadjah Mada, Jl. Olahraga, Caturtunggal, Depok,
Sleman, Yogyakarta 55281, Indonesia
[7]Department of Water Management, Estonian University of Life Sciences, Tartu, Estonia;
Friedrich Reinhold Kreutzwaldi 1a, 51014 Tartu, Estonia

Abstract: Dyeing Finishing (DF) textile industries which consume a lot of energy, chemicals, water, etc., then produce a lot of wastewater which creates significant environmental problems, can be anticipated by applying Cleaner Production. This paper is presented to discuss the technical modification process of dyeing production machines, which reuse process wastewater to save water and energy consumption in the production process. For that reason, there are three steps taken. First, understand the process flow of the textile dyeing industry. Second, understand in detail the dyeing process of the Jet Dyeing (JD) machine. Third, implement steps on the floor, focusing on the JD machine, starting from the initial conditions until the third step. As a result, savings in water consumption per day for 10 JD machines were achieved by almost 50 %, with details; at the initial status 700 000 L, 600 000 L in the first step, 430 000 L in the second step, and finally 400 000 L in the third step. A similar action can be carried out in other processes, such as washing, de-sizing, or in other industries which also consume a lot of water and energy.

Keywords: Energy Efficiency, Jet Dyeing, Waste and Water Management, Reuse Wastewater, Wastewater Treatment Plant, Water Efficiency.

1. INTRODUCTION

Sustainable development meets the needs of the present without compromising the ability of future generations to meet their own needs [1]. To increase awareness of global environmental problems, it is expected the wisely utilization of natural resources from all parties and sectors [2]. As an important natural resource, water faces a serious problem for its availability and quality [3] The industrial sector contributes to a major consumer of clean water resources as well as produces a lot of wastewater

[4]. The industry should always be assessed the environmental performance from process and product perspectives. The manufacturing sector interprets it as a process that requires fewer resources and no waste produced. Waste is an unwanted product or damage, defective during the manufacturing process.

Figure 1 shows the basic concept of action to reduce energy and water consumption [5]. As shown in Figure 1(a), to collect and interpret technological innovation, the data is distinguished between technical and organizational innovations. Technical innovations are divided into product and process. Process innovations focus to reduce input with a given amount of output. Product innovations improve goods and services by developing new goods. Organizational innovations apply to total quality management. Cleaner Production (CP) refers to process-related into end-of-pipe and integrated technologies.

As shown in Figure 1(b), CP defines as the continuous improvement to reduce the utilization of air, water, land, to prevent pollution and to reduce the waste generation in the process, products, and services, to improve the efficiency, better environmental performance, and increase competitive advantage. In short, CP is the continuous application of an integrated preventive environmental strategy to processes and products to reduce risks to humans and the environment [6]. CP encompasses a thorough review of all aspects of business operations and identifies opportunities where improvements will help the business's economy as well as the environment. CP avoids staff from undue accidents, increases the morale of staff, improves product compliance, prevents spills, and raises the business's image amongst competitors. CP also creates awareness for pollution, wastes and emissions.

Figure 1(c) shows a secondary source of waste generation as the excess energy required to process and treat any waste generated. In the manufacturing industry, there are three classes of waste. *Process wastes, the most costly waste:* are solid, liquid, vapour, and excess-energy-generated wastes from the lower-value feed materials to the higher-value products. *Utility wastes:* are solid, liquid, vapour, and excess-energy wastes from utility

systems to support the process, such as steam, electricity, water, compressed air, waste treatment, etc. Other wastes: are the results from start-ups and shutdowns, housekeeping, maintenance, etc. The textile industry, especially Dyeing Finishing (DF) consumes a lot of resources, such as energy, chemicals, and water during the process and produces a lot of wastewater contributing to environmental issues [7]. CP can be applied for DF focusing on the wet process in the Jet Dyeing (JD) machine. Reduction of water consumption with CP will reduce both the energy cost and also chemical cost.

CP has been widely studied and applied to the dyeing process in the textile industry to reduce water consumption and environmental impact. Lu *et al.* [8] combined a treatment system with two-stage anaerobic-aerobic treatment, biological aerated filter process (BAF), and membrane technology, resulting in the highest efficiency in terms of removal efficiency for COD, colour, and turbidity. Cesar da Silva *et al.* [9], conducted a survey and expert analysis for more than 100 large textile industries to established with data analysis structural equation modelling for hypothesis testing. They determined that cleaner production could give a good impact on operational, environmental and economic performance, as same as result, the same result has also been obtained by de Oliveira *et al.* [10].

Haji *et al.* [11] reviewed the effect of plasma treatment on surface modification of most used natural and synthetic fibres and the effects using natural dyes provide to reduce wastewater and toxic chemicals for CP. Fauzi *et al.* [12] analyzed the strategy to implement the CP concept in a batik industry by waste identified the dyeing, soaking, and rinsing processes were main contributors to the dye waste and suggested using natural dyes to minimized water pollution. Cinperi *et al.* [13] used composite wastewaters to treat the quality of reuse wastewaters in a pilot-scale MBR process and resulted in the high purification efficiency of textile wastewater. Núñez *et al.* [14] evaluated the electrocoagulation for efficient removal of pollutants in the industrial liquid waste with some variables to remove 86 % colour, 82 % turbidity, and 59 % COD without a negative effect on the dyed fabric quality. Chiarello *et al.* [15] evaluated

(a)

(b)

(c)
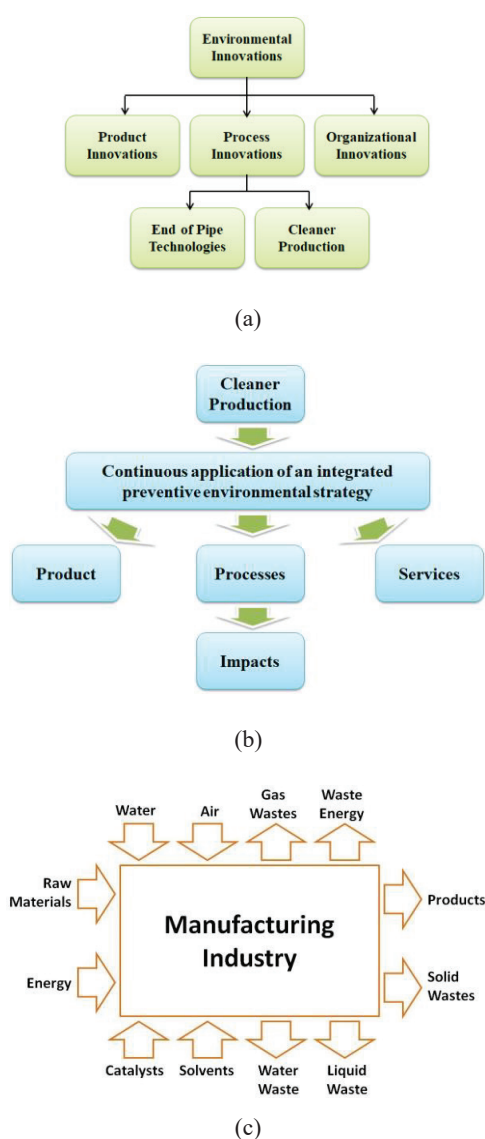
Fig. 1. The basic concept of action, a). From the Environmental Innovations to Cleaner Production, b). From the Cleaner Production to impacts, c). Basic input-output the manufacturing industry [5].

the number of reuse cycles of residual dyeing bath from reactive cotton dyeing treated with horseradish peroxide with 99 % colour removal. Forte and Prelog [16] evaluated the dye-house wastewater treatment with a flocculation method for re-use in further process, resulted in the high efficiency of dye-house wastewater treatment. Silva *et al.* [17] integrated two processes of a chemical-electrochemical oxidation process with a cationic exchange process using marine macro-algae, resulted successfully reused in other wet processes. Chen [18] evaluated the model of 10 indicators of advanced treatment technology for printing and

dyeing wastewater with the analytical hierarchy process (AHP), resulted in good consistency for further process.

Based on the literature review above, CP has been widely carried out in the textile DF industry in all processes, with the aim of environment, efficiency, etc. Most of the studies focus on restoring the condition of wastewater by chemical or biological processes to become water that meets production requirements. These two processes become separate production units supported by sophisticated technology, which requires a high initial investment and higher water treatment costs. However, not many papers have discussed in detail the technical steps taken. Also, no publication discusses the reuse of dyeing production wastewater directly with modifications and specific process strategies easily, quickly, and cheaply. The purpose of this paper is to discuss the technical modification process in dyeing machines, which reuse process wastewater to save water and energy in the production.

2. MATERIALS AND METHODS

The method of research was based on the regular daily operational activities and floor observations in a textile dyeing finishing which process polyester and rayon fabric. There are several steps taken. First, understand the process flow of the textile dyeing industry. The textile industry is a very diverse sector in terms of raw materials, processes, products, and equipment. It can be categorized roughly into dry and wet processing. Dry processing includes yarn manufacturing, fabric weaving, and knitting. Wet processing is the most water, energy, and pollution-intensive, especially for cotton as natural fibre. Generally, the flow of the wet process for dyeing can be shown in Figure 2. The process of Singeing, de-Sizing, Washing, Boiling, and Bleaching is categorized as the Preparation process. Preparation aims to remove impurities and foreign matters, clean and modify the fabric for follow up processing or provide certain qualities for end-use. About half of the total pollution and a significant amount of wastewater from wet processing comes from preparation. The Dyeing process in the wet process to be the highest priority concern which may cause a major environmental problem with colour, BOD (10 % to 20 %), most metals, salts, COD (>30 %), high water and energy

consumed [10]. Jet Dyeing (JD) machine is one of the popular for dyeing which consumes a lot of water. Environmental performance of the dyeing process is very much related to specific water and energy consumption, dyestuff fixation (%), liquid ratio (LR), heavy metals, use of environmentally hazardous chemicals, and shading.

Second, understand in detail the dyeing process of the JD machine. It was started from the analysis of the dyeing process by collecting data from each machine base on the individual step of the process, these included characteristics of colour processed by a JD machine, water required, and water wasted by the machine and the most important thing is the colour quality which only can get a result from Lab Dips.

Third, implement action on the floor. The actions are to understand the current process and status of water consumption. The first action was by utilizing the water used for cooling for the first dyeing process for a light colour. The second one was by utilizing the water used for Over Flow 2 (OF2) for the first dyeing process for a dark colour. The third one was by utilizing the water used for Over Flow 1 (OF1) for the first dyeing process of black colour.

3. RESULTS AND DISCUSSION

3.1 Pre-implementation

There are 10 Jet Dyeing (JD) machines with a capacity of 300 kg of raw fabric per batch for different processes and colour allocation. The daily dyeing output is 25 000 m. The standard ratio of water to the fabric from each JD is 7 L kg^{-1} to 10 L kg^{-1}, depending on the technology. The total water consumption per batch for 10 JD machines is about 199 015 L or about 600 000 L d^{-1} with 3.3 batches per machine d^{-1}. The details of step dyeing, colour allocation, and water consumption for each JD machine can be seen in Table 1. The washing step is as same as the dyeing process with additional cleaning using loop fabric and additional cooling. The total water consumed for cleaning 10 JD machines was 375 179 L. Since only 3.3 JD machines are washed daily, the water consumption is only 112 000 L. Table 2 shows the detailed step of washing and water consumption for each JD machine.

The first step of dyeing is dyeing itself which some dark colours can be started with hot water. To keep the stability of colour to be processed, each machine has a special task of colour. JD1, JD2, JD3 are used to process the light colour. JD4 is a small machine that is intended to be a re-process machine. JD5 is to process the medium colour. JD6 is to process the cationic colour. JD7 and JD8 are to process the dark colour. JD9 is to process the special colour and JD10 is to process the Black colour. JD1, JD2, JD3, JD6, JD7, JD8, JD9, JD10 have a set volume of water for 3 000 L batch^{-1} and JD4 and JD5 have a set volume of water for 1 850 L batch^{-1} and 7 000 L batch^{-1}.

Comparing to machines with the same capacity of dyeing, JD10 with the black colour processed consumed of water 63 191 L per batch, more water than the other JD machine except for JD4 with small capacity and JD5 with double capacity. Comparing to the process, the cooling process consumed 56 740 L of water for 10 JD machines, more than the other process. The total water consumed for
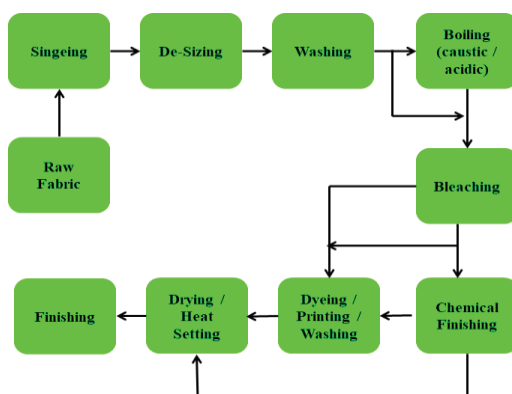
Fig. 2. General wet process flow of the dyeing [19]

Table 1. Step dyeing, colour allocation, and water consumption of JD machines per batch

JD	Process	Allocate	L batch⁻¹										
			Dyeing 1	Cooling	Over Flow 1	Filling Over Flow 2	Over Flow 2	Neutral	Over Flow 1	Filling Over Flow 2	Over Flow 2	Out	Total
1	Non RC	Light	3 000	4 149	700	3 000	1 000	-	-	-	-	3 000	14 849
2	Non RC	Light	3 000	4 149	700	3 000	1 000	-	-	-	-	3 000	14 849
3	Non RC	Light	3 000	4 149	700	3 000	1 000	-	-	-	-	3 000	14 849
4	1/2 RC	Repro	1 850	3 436	350	1 850	350	925	-	-	-	1 850	10 611
5	1/2 RC	Medium	7 000	13 000	5 000	7 000	5 000	3 500	-	-	-	7 000	47 500
6	Non RC	Cationic	3 000	5 571	1 000	3 000	1 000	-	-	-	-	3 000	16 571
7	RC	Dark	3 000	5 571	1 000	3 000	1 000	3 000	-	-	-	3 000	19 571
8	RC	Dark	3 000	5 571	1 000	3 000	1 000	3 000	-	-	-	3 000	19 571
9	RC	Special	3 000	5 571	1 500	3 000	1 000	3 000	-	-	-	3 000	20 071
10	RC	Black DB	3 000	5 571	2 000	3 000	1 000	3 000	3 000	3 000	1 000	3 000	20 571
	Total		32 850	56 740	13 950	32 850	13 350	16 425	3 000	3 000	1 000	32 850	199 015

Table 2. Steps of washing process and water consumption for JD machines

JD	Process	Allocate	L batch⁻¹												
			Dyeing 1	Cooling	Over Flow 1	Filling Over Flow 2	Over Flow 2	Neutral	Looper	Cooling	Over Flow 1	Filling Over Flow 2	Over Flow 2	Out	Total
1	Non RC	Light	4 000	4 149	700	3 000	1000	3 000	3 000	4 149	700	3 000	1 000	3 000	30 698
2	Non RC	Light	4 000	4 149	700	3 000	1 000	3 000	3 000	4 149	700	3 000	1 000	3 000	30 698
3	Non RC	Light	4 000	4 149	700	3 000	1 000	3 000	3 000	4 149	700	3 000	1 000	3 000	30 698
4	1/2 RC	Repro	2 850	3 436	350	1 850	350	1 850	1 850	3 436	350	1 850	350	1 850	20 371
5	1/2 RC	Medium	8 000	13 000	5 000	7 000	5 000	7 000	7 000	13 000	5 000	7 000	5 000	7 000	89 000
6	Non RC	Cationic	4 000	5 571	1 000	3 000	1 000	3 000	3 000	5 571	1 000	3 000	1 000	3 000	34 143
7	RC	Dark	4 000	5 571	1 000	3 000	1 000	3 000	3 000	5 571	1 000	3 000	1 000	3 000	34 143
8	RC	Dark	4 000	5 571	1 000	3 000	1 000	3 000	3 000	5 571	1 000	3 000	1 000	3 000	34 143
9	RC	Special	4 000	5 571	1 500	3 000	1 000	3 000	3 000	5 571	1 500	3 000	1 000	3 000	35 143
10	RC	Black DB	4 000	5 571	2 000	3 000	1 000	3 000	3 000	5 571	2 000	3 000	1 000	3 000	36 143
	Total 10 mc		42 850	56 740	13	32 850	13 350	32 850	32 850	56 740	13	32 850	13	32	375
	Total 3.33 mc d⁻¹		12 855	17 039	4 189	9 865	4 009	9 865	9 865	17 039	4 189	9 865	4 009	9 865	112

all JD machines is 199 015 L for one batch. JD machines which used to process the light colour consumed less water than a darker colour. JD10 which used to process the black colour consumed 36 143 L of water and it means the highest water consumer comparing to the other JD machines. Comparing with each step, Cooling consumed 56 740 L of water for 10 JD machines.

Figure 3 shows the piping scheme of the initial status of water consumption in the dyeing process of JD machines. All the inlet water for all steps in the dyeing process is supplied only from the water treatment plant (WTP) and also all the outlet water for all steps was carried out to the wastewater treatment plant (WWTP). The total water consumed from WTP and water wasted to WWTP for one day operation for 10 JD machines was about 700 000 L (See Table 1 and Table 2).

3.2 After Implementation

Figure 4 shows the piping scheme of the first action of water consumption in the dyeing process of JD machines. The action is to utilize the cooling water as the input water into the dyeing process. The temperature of the water after used as cooling for the machine can achieve around 85 °C. Utilizing a higher temperature will save both time and energy. By the first action, the total water consumed from WTP and water wasted to WWTP for a one-day operation for 10 JD is about 600 000 L. It saves 14 % of input from WTP.

Figure 5 shows the piping scheme of the second action of water consumption in the dyeing process of JD machines. The action was to utilize the outlet water of OF2 from JD1, JD2, and JD3 as the input water for JD7, JD8, and JD10. Because
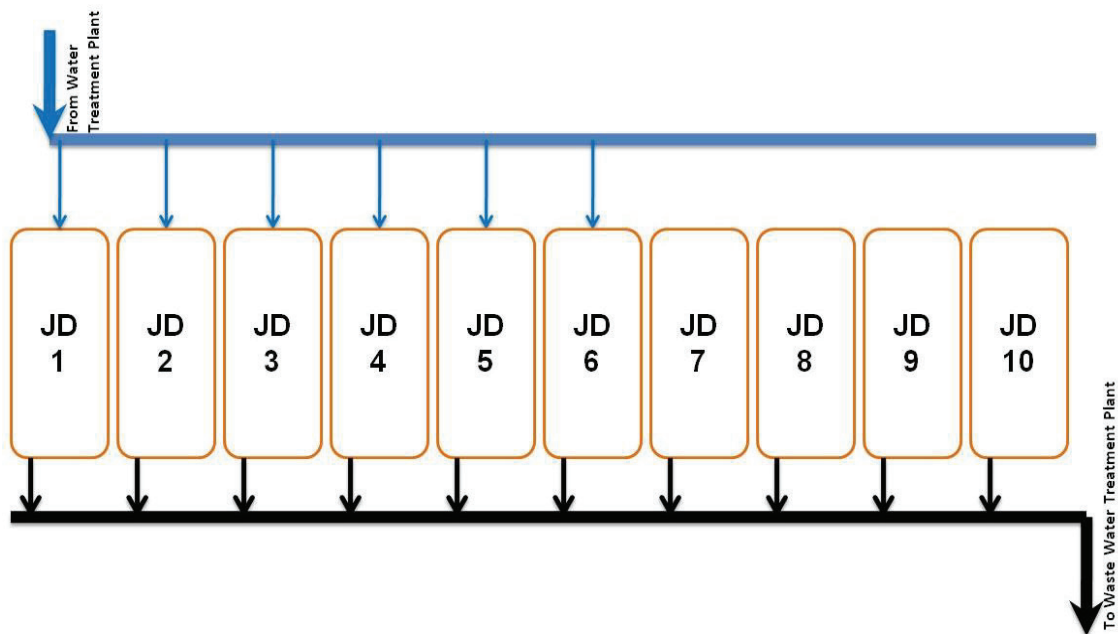
Fig. 3. Piping scheme of the initial status

JD1, JD2, JD3 only process the light colour and the outlet water of its OF2 was tolerated from colour residue and after checking in the Lab Dips. It is safe to use for the dark colour as can be processed by JD7, JD8, and JD10. By the second action, the total water consumed from WTP and water wasted to WWTP for a one-day operation for 10 JD machines was 430 000 L. It saves 39% of input from WTP.

Figure 6 shows the piping scheme of the third action of water consumption in the dyeing process of JD machines. This third action was the next action after the construction of the Hot Water Storage 2 (HWS2) to be finished. There were two works for this third action. The first work was the actions to utilize the outlet water of OF1 from the light colour processed machine, which are JD1, JD2, and JD3 as the input water for JD10 which specialized to process the black colour. The second work was the action to utilize the outlet water of OF2 as the cooling water for JD7, JD8, and JD10. The outlet water of JD7, JD8, and JD10 was stored in HWS2. According to the testing result in Lab Dips, especially for colour stability and colour fastness, there was no significant influence of colour stability and also fastness for the black colour. By the third action, the total water consumed from WTP and WWTP for a one-day operation for 10 JD machines was 400 000 L. It saves 43 % of input from WTP.

The more detailed results from the actions that

have been carried out are summarized in Table 3. It clarifies the pipes at the inlet and outlet to the JD machine, as follows; WTP, HWS1, OF2, HWS2, and WWTP. Besides, it also explains the stages of quality inspection at; Lap Dips, Final Quality Control (FQC), JD Quality Control (JDQC). The control system of the inlet and outlet on the JD machines was carried out with a standard program before making changes, as well as with an adjusted program.

Based on the results that have been obtained, there are three important things to discuss. First, understand the process and know where to save. The textile industry, especially for dyeing processing, consumes a lot of water and it also produces a lot of wastewater. The more water consumed will be the more wastewater produce, resulting in a more costly process both freshwater in WTP and wastewater in WWTP. Concerning the issue of environmental problems and also industry competitiveness, CP is one of the effective solutions. With the main process is dyeing itself which water is the main resource, CP can be started from this water demanded process. The most important to start CP in the dyeing process is by understanding the characteristic of colour to be processed in JD machines and also the steps of the dyeing process. Every step of dyeing required water then produces wastewater. After classifying the water required and the water wasted during the dyeing process and
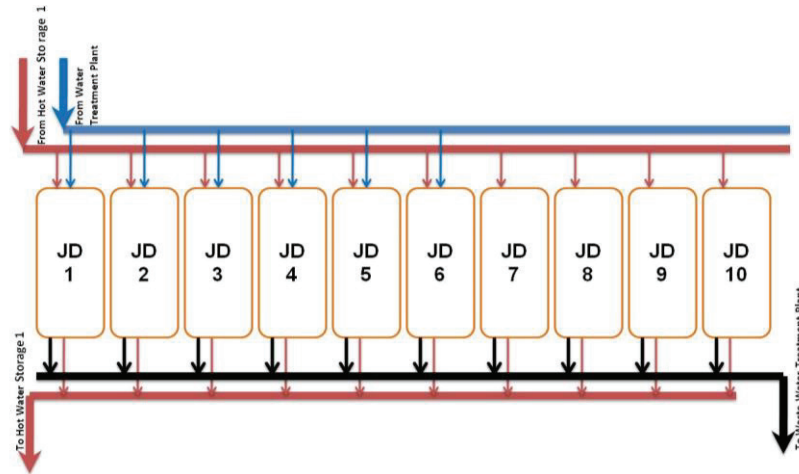
Fig. 4. Piping scheme of the first action
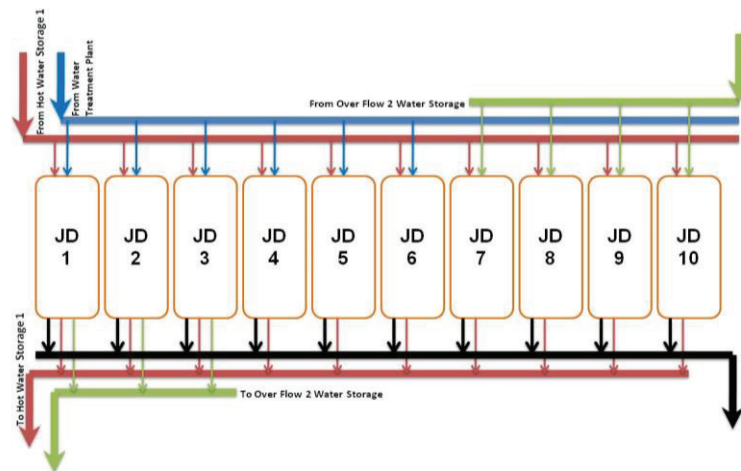
Fig. 5. Piping scheme of the second action

also combined with the characteristic colour to be processed. The next step is to understand how to store and re-use the water from the process.

Second, designing a construction system based on the process flow. This step requires water storage construction and piping installations, which are adapted to the reuse of process wastewater. To work automatically, the reprogramming needs to be done to each JD machine, according to the type of process being carried out. This process must be carried out carefully with high protection to anticipate errors in reusing the process wastewater, which will not affect the quality, productivity, or safety.

Third, monitoring and analyzing the results for further improvement. Reduction of fresh processed in WTP and wastewater processed in WWTP means the reduction of electricity consumed by electrical equipment in WTP, WWTP, and JD machines, and

also the reduction of chemical usage in WTP and WWTP. The less water consumption and energy required are the more ecological manufacturing itself. The water consumption in textile wet processing depends on the liquor ratio, as well as on the number of consecutive processes. The machine capacity should also be effectively used to reduce the consumption of process water and chemicals: the dyes are dosed per kg fabric, whereas the auxiliaries are dosed per one process liquor.

The practical application of reducing energy and water consumption that has been carried out in the JD machine can also be carried out in other processes in the DF textile industry, such as washing, de-sizing, or in a process in other industries that also consume the most water and energy. Of course, some things must be adjusted after being analyzed. For the companies, reducing water and energy consumption contribute to reducing production
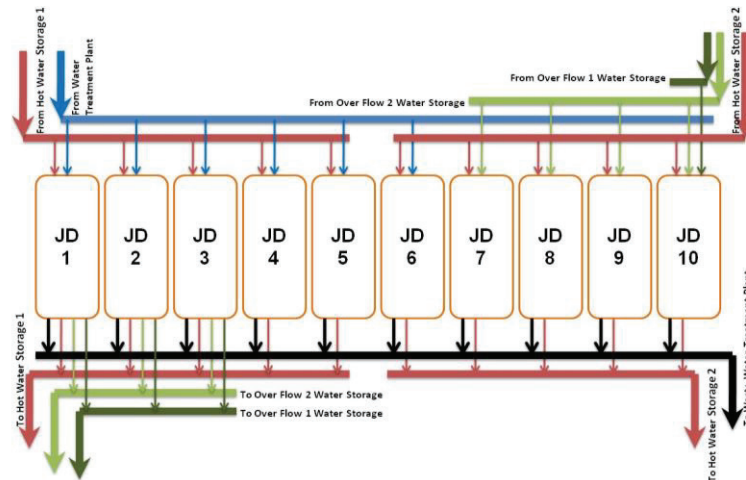
Fig. 6. Piping scheme of the third action

Table 3. Detail summary results of the actions for the dyeing process

Items	Initial Status	1st Action	2nd Action	3rd Action
Water consumption	700 000 L	600 000 L	430 000 L	400 000 L
Consp./JD a day	70 000 L	60 000 L	43 000 L	40 000 L
Input WTP saved	-	14 %	39 %	43 %
Piping: Inlet	WTP	WTP, HWS1	WTP, HWS1, OF2	WTP, HWS1, OF2, HWS2
Piping: Outlet	WWTP	HWS1, WWTP	HWS1, WWTP, OF2	HWS1, WWTP, OF2, HWS2
Quality Control	Lap Dip, FQC	Lap Dip, JDQC, FQC	Lap Dip, JDQC, FQC,	Lap Dip, JDQC, FQC
Automatic Process	Standard Program	Adjust Program	Adjust Program	Adjust Program

costs and their impact on the environment [20], and also strengthening energy security locally [21], which is powered by smart grid technology [22]. For future research direction, the development of smart and precise control mechanisms must be carried out for the appropriate water storage allocation process for a particular process. For cleaner and greener production, the textile industry must involve renewable energy sources in the production process, for example from solar energy using a Photovoltaic (PV) module to generate electricity [23], or a hybrid photovoltaic and thermal (PVT) collector that produces electricity and heat energy [24 - 26]. In addition, the treatment and utilization of other wastes such as exhaust gas [27] also need to be considered in hi-tech [28, 29]. Regarding cleaner and greener production, the textile industry also must be equipped with aerobic and anaerobic water treatment. Furthermore, to increase efficiency, the water treatment should be designed to produce biogas as renewable energy [30].

4. CONCLUSION

Before starting CP, the total water consumed from WTP and water wasted to WWTP for one-day operation for 10 JD was 700 000 L. After the 1st action, by utilizing the outlet cooling water, the total water consumed from WTP and water wasted to WWTP for a one-day operation for 10 JD machines was 600 000 L. In the 2nd action, by utilizing the outlet water of OF2, the total water consumed from WTP and WWTP for a one-day operation for 10 JD machines was 430 000 L. The 3rd action as the next action by utilizing the outlet water of OF1 from the light colour process for processing the black colour and also utilizing the outlet of OF2 for water cooling in the dark colour processing machines, it is predicted that the total water consumed from WTP and WWTP for a one-day operation for 10 JD machines was 400 000 L.

5. ACKNOWLEDGEMENTS

6. CONFLICT OF INTEREST

The authors declare no conflict of interest.

7. REFERENCES

1. R. Emas. Brief for GSDR. The concept of sustainable development: Definition and defining principles. Florida International University (2015).

2. R. Naz., M. Shah., A. Ullah., I. Alam, and Y. Khan. An assessment of effects of climate change on human lives in context of local response to agricultural production in district Buner. *Sarhad Journal of Agriculture,* 36(1): 110–119 (2020). DOI: 10.17582/journal.sja/2020/36.1.110.119

3. M.I. Meo, S. Haydar, O. Nadeem, G. Hussain, and H. Rashid. Characterization of hospital wastewater, risk waste generation and management practices in Lahore. *Proceedings of the Pakistan Academy of Sciences* 51 (4): 317–329 (2014).

4. B. Muchtasjar., H. Hadiyanto., M. Izzati., Z. Vincēviča–Gaile, and R.H. Setyobudi. The ability of Water Hyacinth (*Eichhornia crasipes* Mart.) and Water Lettuce (*Pistia stratiotes Linn.*) for reducing pollutants in batik wastewater. *E3S Web of Conferences 226*(00010): 1–6 (2021). DOI: 10.1051/e3sconf/202122600010

5. M. Frondel., J. Horbach, and K. Rennings. End-of-pipe or cleaner production? An empirical comparison of environmental innovation decisions across OECD countries. *Business strategy and the environment* 16(8): 571–584 (2017). DOI: 10.1002/bse.496

6. L. Shi., J. Liu., Y. Wang, and A. Chiu. Cleaner production progress in developing and transition countries. *Journal of Cleaner Production* 278:123763 (2021). DOI: 10.1016/j.jclepro.2020.123763

7. K.K. Samanta., P. Pandit., P. Samanta, and S. Basak. Water consumption in textile processing and sustainable approaches for its conservation. In: *Water in textiles and fashion,* S.S. Muthu (Ed.), UK: Woodhead Publishing, p. 41–59 (2019). DOI: 10.1016/B978-0-08-102633-5.00003-8

8. X. Lu., L. Liu., R. Liu., and J. Chen. Textile wastewater reuse as an alternative water source for dyeing and finishing processes: A case study. *Desalination* 258(1–3): 229–232 (2010). DOI: 10.1016/j.desal.2010.04.002

9. P.C. da Silva., G.C. de Oliveira Neto., J.M.F. Correia, and H.N.P. Tucci. Evaluation of economic, environmental and operational performance of the adoption of cleaner production: Survey in large textile industries. *Journal of Cleaner Production* 278:123855 (2020). DOI: 10.1016/j.jclepro.2020.123855

10. G.C. de Oliveira Neto., J.M.F. Correia., P.C. Silva., A.G. de Oliveira Sanches, and W.C. Lucato. Cleaner Production in the textile industry and its relationship to sustainable development goals. *Journal of Cleaner Production* 228, 1514–1525 (2019). DOI: 10.1016/j.jclepro.2019.04.334

11. A. Haji and M. Naebe. Cleaner dyeing of textiles using plasma treatment and natural dyes: A review. *Journal of Cleaner Production* 265:121866 (2020). DOI: 10.1016/j.jclepro.2020.121866

12. A.M. Fauzi, and R.L. Defianisa. Analysis for cleaner production implementation strategy in batik industry in Bogor. IOP Conf. Ser. *Earth and Environmental Science* 325(012005):1–8 (2019). DOI: 10.1088/1755-1315/325/1/012005

13. N.C. Cinperi., E. Ozturk., N.O. Yigit, and M. Kitis. Treatment of woolen textile wastewater using membrane bioreactor, nanofiltration and reverse osmosis for reuse in production processes. *Journal of Cleaner Production* 223:837–848 (2019).DOI: 10.1016/j.jclepro.2019.03.166

14. J. Núñez., M. Yeber., N. Cisternas., R. Thibaut., P. Medina, and C. Carrasco. *Journal of Hazardous* 371:705–711 (2019). DOI: 10.1016/j.jhazmat.2019.03.030

15. L.M. Chiarello., M. Mittersteiner., P.C. de Jesus., J. Andreaus, and I.O. Barcellos. Reuse of enzymatically treated reactive dyeing baths: Evaluation of the number of reuse cycles. *Journal of Cleaner Production* 267:122033 (2020). DOI: 10.1016/j.jclepro.2020.122033

16. P.F. Tavčer, and K. Prelog. Wastewater treatment using flocculation method and water reuse for dyeing of polyester fibers. *IOP Conference Series: Materials Science and Engineering* 827(012055):1–5 (2020). DOI: 10.1088/1757-899X/827/1/012055

17. L.G. Silva., F.C. Moreira., M.A.P. Cechinel., L.P. Mazur., A.A.U. de Souza., S.M.G.U. Souza, S.M.A.G.U. Souzaa., R.A.R. Boaventurab, and V.J.P. Vilar. Integration of Fenton's reactionbased processes and cation exchange processes in textile wastewater treatment as a strategy for water reuse. *Journal of Environmental Management* 272: 111082 (2020). DOI: 10.1016/j.jenvman.2020.111082

18. X. Chen. Evaluation of advanced treatment technology of dyeing wastewater based on analytic hierarchy process. *IOP Conference Series: Earth and Environmental Science* 508(012020):1–6 (2020). DOI: 10.1088/1755-1315/508/1/012020

19. C. Sahoo., A.K. Gupta, and I.M.S. Pillai. Heterogeneous photocatalysis of real textile

wastewater: evaluation of reaction kinetics and characterization. *Journal of Environmental Science and Health,* Part A, 47(13): 2109–2119. (2012). DOI: 10.1080/10934529.2012.695996

20. E. Yandri, R. Ariati, A.S. Uyun, and R.H. Setyobudi. Potential energy efficiency and solar energy applications in a small industrial laundry: A practical study of energy audit. *E3S Web of Conferences* 190(00008): 1–9. (2020). DOI: 10.1051/e3sconf/202019000008

21. E. Yandri., R. Ariati, and R.F. Ibrahim. Meningkatkan keamanan energi melalui perincian indikator energi terbarukan dan efisiensi guna membangun ketahanan nasional dari daerah [Improve energy security through detailed indicators of renewable energy and efficiency in order to build national resilience from the regions]. *Jurnal Ketahanan Nasional* 24(2): 239–260 (2018). [in Bahasa Indonesia]. DOI: 10.22146/jkn.30999

22. B. Novianto., K. Abdullah., A.S. Uyun., E. Yandri., N.S. Muhammad., H. Susanto., Z. Vincēviča-Gaile, R.H. Setyobudi, and Y. Nurdiansyah. Smart micro-grid performance using renewable energy. *E3S Web Conference* 188(00005): 1–11 (2020). DOI: 10.1051/e3sconf/202018800005

23. D. Faturachman., E. Yandri., E.T. Pujiastuti., O. Anne., R.H. Setyobudi., Y. Yani., H. Susanto., W. Purba, and S.K. Wahono. Techno-Economic analysis of photovoltaic utilization for lighting *and cooling system of ferry Ro/Ro ship 500 GT. E3S Web Conference,* 226(00012): 1–10 (2021).DOI: 10.1051/e3sconf/202122600012

24. E. Yandri. Development and experiment on the performance of polymeric hybrid Photovoltaic Thermal (PVT) collector with halogen solar simulator. *Solar Energy Materials and Solar Cells* 201:110066 (2019). DOI: 10.1016/j.solmat.2019.110066

25. E. Yandri. Methods for the development and testing of polymeric hybrid photovoltaic thermal (PVT) collector for indoor experiments. *MethodsX* 6:2620–2635 (2019). DOI: 10.1016/j.mex.2019.10.021

26. E. Yandri. The effect of Joule heating to thermal performance of hybrid PVT collector during electricity generation. *Renewable Energy* 111: 344–352 (2017). DOI: 10.1016/j.renene.2017.03.094

27. W. Purba., E. Yandri., R.H. Setyobudi., H. Susanto., S.K. Wahono., K. Siregar, Y.A. Nugroho., A. Yaro., K. Abdullah., Y. Jani, and D. Faturahman. Potentials of gas emission reduction (GHG) by the glass sheet industry through energy conservation. *E3S Web of Conferences* 226(00047): 1–12 (2021). DOI: 10.1051/e3sconf/202122600047

28. E. Yandri., B. Novianto., F. Fridolini., R.H. Setyobudi., H. Wibowo., S.K. Wahono., K.Abdullah., W. Purba, and Y.A. Nugroho. The technical design concept of hi-tech cook stove for urban communities using non-wood agricultural waste as fuel sources. *E3S Web of Conferences.* 226(00015):1–9(2021). DOI: 10.1051/e3sconf/202122600015

29. R.M. Rasool, M. Malik, and R. Khalid. Internet of things (IOT) based waste management in small cities. P*roceedings of the Pakistan Academy of Sciences: A. Physical and Computational Sciences* 56 (3): 67–74 (2019)

30. R. H. Setyobudi, E. Yandri, M.F.M. Atoum, S. M. Nur, I. Zekker, R. Idroes, T.E. Tallei, P.G. Adinurani, Z. Vincēviča-Gaile, W. Widodo, L. Zalizar, N. Van Minh, H. Susanto, R.K. Mahaswa, Y.A. Nugroho, S.K Wahono, and Z. Zahriah. Healthy-smart concept as standard design of kitchen waste biogas digester for urban households. *Jordan Journal of Biological Sciences,* 14(3):613–620 (2021).

Pakistan Academy of Sciences

Research Article

Custom Built of Smart Computing Platform for Supporting Optimization Methods and Artificial Intelligence Research

Indar Sugiarto[1*], Doddy Prayogo[2], Henry Palit[3], Felix Pasila[1],
Resmana Lim[1], Agustinus Noertjahyana[3], I Gede Widyadana[4],
Surya Hermawan[2], Agustinus Bimo Gumelar[5], and Bernardo Nugroho Yahya[6]

[1]Department of Electrical Engineering, Petra Christian University, Jl. Siwalankerto No.121-131, Surabaya, 60236, Indonesia
[2]Department of Civil Engineering, Petra Christian University Surabaya, 60236, Indonesia
[3]Department of Informatics, Petra Christian University, Surabaya, 60236, Indonesia
[4]Department of Industrial Engineering, Petra Christian University Surabaya, 60236, Indonesia
[5]Department of Information System, Narotama University, Jl. Arief Rachman Hakim 51, Sukolilo, Surabaya, 60117, Indonesia
[6]Department of Industrial and Management Engineering, Hankuk University of Foreign Studies, 107, Imun-ro, Dongdaemun-gu, Seoul, 130-791, Korea

Abstract: This paper describes a prototype of a computing platform dedicated to artificial intelligence explorations. The platform, dubbed as PakCarik, is essentially a high throughput computing platform with GPU (graphics processing units) acceleration. PakCarik is an Indonesian acronym for *Platform Komputasi Cerdas Ramah Industri Kreatif,* which can be translated as "Creative Industry friendly Intelligence Computing Platform". This platform aims to provide complete development and production environment for AI-based projects, especially to those that rely on machine learning and multiobjective optimization paradigms. The method for constructing PakCarik was based on a computer hardware assembling technique that uses commercial off-the-shelf hardware and was tested on several AI-related application scenarios. The testing methods in this experiment include: high-performance lapack (HPL) benchmarking, message passing interface (MPI) benchmarking, and TensorFlow (TF) benchmarking. From the experiment, the authors can observe that PakCarik's performance is quite similar to the commonly used cloud computing services such as Google Compute Engine and Amazon EC2, even though falls a bit behind the dedicated AI platform such as Nvidia DGX-1 used in the benchmarking experiment. Its maximum computing performance was measured at 326 Gflops. The authors conclude that PakCarik is ready to be deployed in real-world applications and it can be made even more powerful by adding more GPU cards in it.

Keywords: Artificial Intelligence, Machine Learning, Multi-objective Optimization, Graphics Processing Unit Accelerator, High Throughput Computing.

1. INTRODUCTION

In recent years, interest in Artificial Intelligence (AI) researches is increasing and showing its fruitful results in many areas including creative industry sectors. With the advent of Industrial Revolution 4.0, the need of implementing practical but robust AI becomes more and more demanding. Thus, researches in this area are blooming [1, 2].

However, running high-impact AI researches especially on Deep Learning (DL) requires a high-performance computing platform [3, 4]. This is an inevitable consequence since DL, like other machine learning approaches, usually works on massive data to automatically gain its working parameters.

Several dedicated computing platforms have

been produced by diverse vendors that target this ever-growing research field [5]. For example, Nvidia Corporate has several products that are capable of high-performance computing up to several hundred teraflops, scaled from a workstation level to a server-class [6, 7]. However, those platforms are either very expensive or a part of a cloud computing service that does not give any direct means of maintenance for the AI researcher. For example, the price for an entry-level one Nvidia DGX Station is USD 149 000, which is way above standard research grants in Indonesia (around USD 3 500 yr^{-1}). In this circumstance, the authors have developed a smart computing platform that can be built to support AI researches. The platform, dubbed as PakCarik, is essentially a high throughput computing platform with GPU (graphics processing unit) acceleration. PakCarik is an Indonesian acronym for *Platform Komputasi Cerdas Ramah Industri Kreatif*, which can be translated as "Creative Industry friendly Intelligence Computing Platform". This paper describes how PakCarik was built and tested on several application scenarios.

2.   MATERIALS AND METHODS

PakCarik aims to provide a complete development and production environment for AI-based projects, especially those that rely on optimization and machine learning paradigms. This research area is well-known for its challenging but intriguing methods for uncovering hidden information in massive unstructured data [8].

As a platform targeting industrial applications, PakCarik is equipped with various open-source libraries that enable the developer to quickly develop and deploy their projects. Special messaging service software is also installed in PakCarik, making it a complete framework for developing an IoT-based system. This software will act as an integrated IoT broker inside PakCarik that accommodates various messaging protocols such as MQTT and Kafka. The platform was designed such that the connection among different protocols is seamless. Such mechanisms are known to be challenging but very useful for developing complex IoT applications [9]. Figure 1 shows how PakCarik will be deployed as an IoT-based platform.

From a hardware perspective, PakCarik is a high throughput computer that is built using COTS (commercially off-the-shelf) components. Using COTS, the cluster can be customized to meet the customer budget whilst achieving high performance in a self-maintainable fashion [10]. Currently, PakCarik has two prototypes: PC1 and PC2. Table 1 shows the difference between PC1 and PC2.

3.   RESULTS AND DISCUSSION

PakCarik has undergone these preliminary tests: high-performance lapack (HPL) benchmarking, message passing interface (MPI) benchmarking, and TensorFlow (TF) benchmarking. Table 4 shows the benchmarking results on PakCarik using the only CPU without GPU acceleration.

From the experiments, this research gained some insight into the performance of PakCarik at normal speed (without overclocking). Although the two prototypes of PakCarik use different processors, the performance is not much different. This opens the possibility of combining both prototypes into one cluster. Currently, PakCarik is undergoing thorough tests in Turbo mode where researchers overclock the processors up to 5 GHz (or more). However, we haven't found the highest stable operating frequency since these tests require the presence of an advanced cooling system (only one of the prototypes, which is PC1, that has a liquid cooling system at the moment).

This paper also performed a benchmarking for the GPU accelerator with Deep Learning image processing applications. For this, the authors use two models: inception-3 [11] and restnet-50 [12]. The comparison was made by measuring how many images were processed during the training phase since this phase usually takes more resources and a longer time compared to the inference phase. In these models, the batch size for the training was set to 32. The results of these experiments were compared to the results of different machines whose data are available online [13]. Figure 2 and Figure 3 show the performance of PakCarik compared to the performance of other platforms.

The purpose of the experiment shown in Figure 2 and Table 2 was to compare head-to-head of this platform (PakCarik) to the other platforms that were restricted to use only a single GPU in the
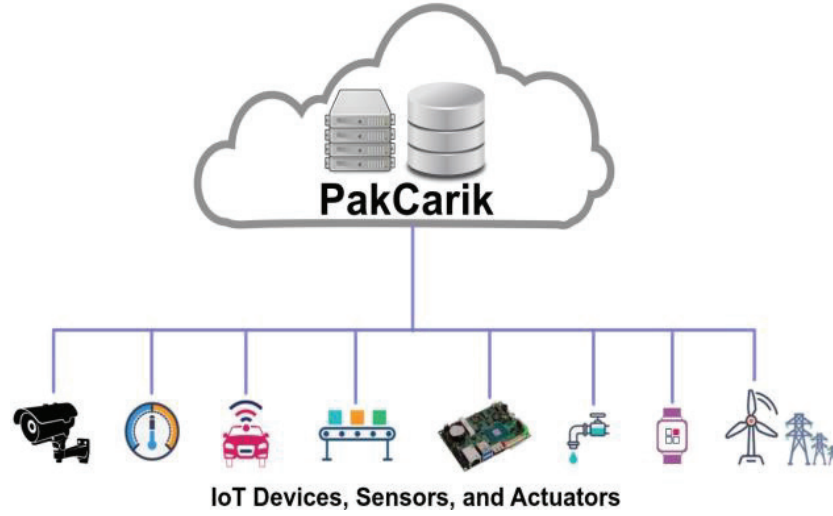
Fig. 1. IoT topology based on the PakCarik ecosystem. In this scenario, external IoT gateways are not necessary since they are embedded in PakCarik.

Table 1. Two protypes of PakCarik.

Component	PC1	PC2
Processor	Intel i9-7900X (10-cores) @3.30GHz	AMD Threadripper 2990WX (32-cores) @3.00GHz
Memory	40GB DDR4	32GB DDR4
Storage	500GB SSD SATA3	250GB SSD NVMe/PCIe
GPU	GTX 1070ti (2432 cores, 8GB DDR5)	TX 2080ti (4352 cores, 11GB DDR5)
PSU	1 000 W	1 200 W
Form factor	ATX-Tower	Rackmount 4U

Table 2. Platforms with a single GPU accelerator for the experiment.

Platform	Description
Platform-1	NVIDIA® DGX-1 with 1-GPU Tesla® P100
Platform-2	Google Compute Engine with 1-GPU NVIDIA® Tesla® K80
Platform-3	Amazon EC2 with 1-GPU NVIDIA® Tesla® K80
Platform-4	Dell Gaming Laptop G7 with 1-GPU GTX-1050ti
Platform-5	PC1 (PakCarik prototype 1), see Table 1
Platform-6	PC2 (PakCarik prototype 2), see Table 1

Table 3. Platforms with multiple GPU accelerators were used for the experiment.

Platform	Description
Platform-1	NVIDIA® DGX-1 with 8-GPU Tesla® P100
Platform-2	Google Compute Engine with 8-GPU NVIDIA® Tesla® K80
Platform-3	Amazon EC2 with 8-GPU NVIDIA® Tesla® K80
Platform-4	Dell Gaming Laptop G7 with 1-GPU GTX-1050ti
Platform-5	PC1 (PakCarik prototype 1), see Table 1
Platform-6	PC2 (PakCarik prototype 2), see Table 1

processing of Inception v3 and Restnet-50. This needs to be done since each prototype of PakCarik only has one GPU. The results show that the second prototype of PakCarik (PC2) outperforms the other platforms. This happens because PC2 uses a GPU card that has more cores and memory compared to the other platforms. Platform-2 and Platform-3, which are commonly used by cloud computing communities and when restricted only to using a single GPU, are quite similar to Platform-4, which is very common to be found in nowadays computer market.

The purpose of the experiment shown in Figure 3 and Table 3 was to compare head-to-head of this platform (PakCarik) to the other platforms with their maximum configuration. Platform-1 can have up to eight GPU cards, whereas Platform-2 and Platform-3 can have more cards but were restricted to use only eight cards in the experiment. On the other hand, PakCarik has a single GPU card in each prototype. The results show that Platform-1 (NVIDIA DGX-1) with eight GPU cards outperforms the other platforms.

This is a predicted result since more cards mean more computing power [14, 15]. However, even though PC2 has a single GPU card, its performance

Table 4. Result of the preliminary experiments on PakCarik.

Experiment	PC1	PC2
HPL	326 Gflops	317 Gflops
MPI	2.76 s	2.85 s
TF	133.96 fps	133.07 fps
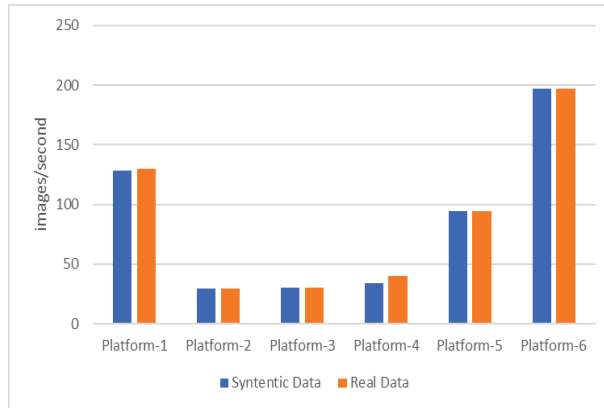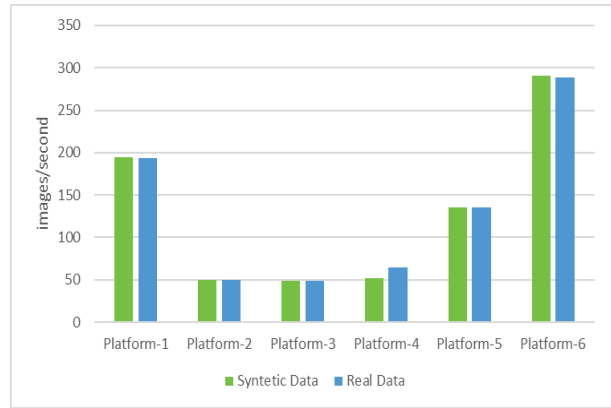
(a)   (b)

Fig. 2. Performance comparison when running (a) Inception v3 model and (b) Restnet-50 model using platforms described in Table 2. The higher the value (images s^{-1}) the better.
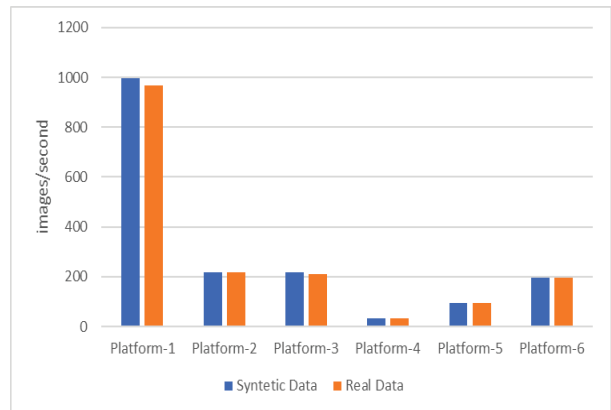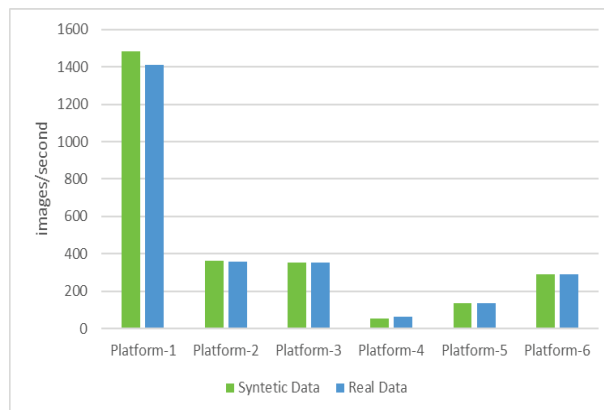
Fig. 3. Performance comparison when running (a) Inception v3 model and (b) Restnet-50 model using platforms described in Table 3. Similar to Fig.2, the higher the value (images s^{-1}) the better.

is quite similar to the commonly used cloud computing services: Google Compute Engine and Amazon EC2, each with eight GPU cards.

Knowing this, that this platform has a potential use case in future real-world applications especially in a country such as Indonesia since the access to the cloud computing services are expensive in long term scenario [16]. Arguably, this platform can easily outperform the dedicated Deep Learning computing engine such as Nvidia DGX-1 provided more similar cards were added to PakCarik, as shown by comparing Figure 2 and Figure 3 [17].

4. CONCLUSION AND SUGGESTIONS

After some experiments with PakCarik, we are convinced that PakCarik is ready to be deployed in real-world applications. In several scenarios as explained, PakCarik outperforms other similar but more expensive platforms available on the market. The authors measured its maximum computing performance at 326 Gflops. Furthermore, it can be inferred from the same experiment that PakCarik can be made even more powerful by adding more GPU cards.

5. ACKNOWLEDGEMENTS

6. CONFLICT OF INTEREST

The authors declare no conflict of interest.

7. REFERENCES

1. A. Ng, Baidu's *Chief Scientist on Intersection of Supercomputing,* Machine Learning. [Online] from www.nextplatform.com/2016/04/01/baidus-chief-scientist-intersection-supercomputing-machine-learning/ (2016). [Accessed on July 27th 2019].

2. H. Nasser, Y. Hafeer and S. Ali. Towards software testing as a service for software as a service based on cloud computing model. *Proceedings of the Pakistan Academy of Sciences A. Physical and Computational Sciences* 55 (4): 1–8 (2018)

3. S.L. Graham., M. Snir, and C.A. Patterson. *Getting Up to Speed: The Future of Supercomputing.* National Academies Press (2005). DOI: 10.17226/11148

4. U. Khan and U. Naeem. Practices for clients in the adoption of hybrid cloud. *Proceedings of the Pakistan Academy of Sciences A Physical and Computational Sciences.* 54 (1): 13–32 (2017)

5. V.V. Kindratenko., J.J. Enos., G. Shi., M.T. Showerman., G.W. Arnold, J.E. Stone., J.C. Phillips, and W.M. Hwu, GPU clusters for high-performance computing. IEEE International Conference on Cluster Computing and Workshops (CLUSTER'09), (2009) pp. 1–8. DOI: 10.1109/ CLUSTR.2009.5289128

6. *NVIDIA. NVIDIA DGX-1 With Tesla V100 System Architecture.* [Online] from http://images.nvidia. com/content/pdf/dgx1-v100-system-architecture-whitepaper.pdf (2018). [Accessed on July 27th 2019].

7. N.A. Gawande., J.A. Daily., C. Siegel., N.R. Tallent, and A. Vishnum, Scaling deep learning workloads: Nvidia dgx-1/pascal and intel knights landing. *Future Generation Computer Systems* 108:1162–1172 (2020). DOI:10.1016/j.future.2018.04.073

8. X. Glorot, and Y. Bengio. Understanding the difficulty of training deep feedforward neural networks. Thirteenth International Conference on Artificial Intelligence and Statistics (AISTATS), (Sardinia, Italy, 2010).

9. C. Berry., G. Hall., B. Matuszewski, and L.K. Shark. A comparison of architectures and evaluation of metrics for in-stream machine learning algorithms in industry 4.0 applications. 30th International Conference on Condition Monitoring and Diagnostic Engineering Management. (Preston and Grange-Over-Sands, UK, 2017).

10. L.Y. Joo., T.S. Yin., E. Xu., E. Thia., P.F. Chia., C.W.K. Kuah, and K.K. He, A feasibility study using interactive commercial off-the-shelf computer gaming in upper limb rehabilitation in patients after stroke. *Journal of Rehabilitation Medicine,* 42(5):437–441 (2010). DOI: 10.2340/16501977-0528

11. C. Szegedy., V. Vanhoucke., S. Ioffe, J. Shlens, and Z. Wojna. Rethinking the inception architecture for

computer vision. The IEEE conference on computer vision and pattern recognition, pp. 2818–2826. (2016).

12. H. Kaiming., X. Zhang., R. Shaoqing, and J. Sun. Deep residual learning for image recognition. The IEEE conference on computer vision and pattern recognition, pp. 770–778. (2016).

13. Tensorflowx.org. Benchmarks. [Online] from https://www.tensorflow.org/guide/performance/benchmarks [Accessed on August 9th 2019].

14. A.Lee, C. Yau, M.B. Giles, A. Doucet and C.C. Holmes. On the utility of graphics cards to perform massively parallel simulation of advanced Monte Carlo methods. *Journal of Computational and Graphical Statistics*, 19(4): 769–789 (2010).

15. S. Shi, Q. Wang, P. Xu and X. Chu. Benchmarking state-of-the-art deep learning software tools. 7th

International Conference on Cloud Computing and Big Data (CCBD), 2016, pp. 99–104. (2016). DOI: 10.1109/CCBD.2016.029.

16. R. Makhlouf,. Cloudy transaction costs: A dive into cloud computing economics. *Journal of Cloud Computing,* 9 (1):1–11. (2020). DOI: 10.1186/s13677-019-0149-4

17. O. Adjoua L. Lagardère, L.H. Jolly, A. Durocher, T. Very , I. Dupays, Z. Wang, T.J. Inizan , F. Célerse, P. Ren , J.W Ponder, J.P. Piquemal Tinker-HP: Accelerating molecular dynamics simulations of large complex systems with advanced point dipole polarizable force fields using GPUs and multi-GPU systems. *Journal of Chemical Theory and Computation,* 17 (4), 2034–2053 (2021). DOI: 10.1021/acs.jctc.0c01164

A Novel Approach of Controlling Stoppage of Drip Infusion Using Image Processing on Raspberry PI Platform

Hartono Pranjoto[1*], Lanny Agustine[1], Diana Lestariningsih[1],
Yesiana Dwi Wahyu Werdani[2], Widya Andyardja[1], Jose Maria Leao Filipe[1],
Manar Fayiz Mousa Atoum[3], and Abubakar Yaro[4,5]

[1]Department of Electrical Engineering, Faculty of Engineering, Widya Mandala Catholic
University, Jl. Kalisari Selatan No.1, Surabaya 60112, Indonesia, Surabaya, Indonesia
[2]Faculty of Nursing, Widya Mandala Catholic University Surabaya, Indonesia
[3]Department of Medical Laboratory Science, Faculty of Applied Health Science,
The Hashemite University, PO Box 330127, 13133 Zarqa, Jordan
[4]Strathclyde Institute of Pharmacy & Biomedical Sciences (SIPBS), University of Strathclyde,
SPBBS, 161 Cathedral St, Glasgow G4 0RE, Scotland, United Kingdom
[5]Dr Yaro Laboratory & AHRO Institute of Health Sciences and Research, 272 Bath Street,
Glasgow, Scotland, G2 4JR, United Kingdom

Abstract: Intravenous drip diffusion is a common practice to treat patients in hospitals. During treatment, nurses must check the condition of the infusion bag frequently before running out of fluid. This research proposes a novel method of checking the infusion bag using an image processing technique on a compact Raspberry PI platform. The infusion monitoring system proposed here is based solely on capturing the image of the infusion bag and the accompanying bag/ tube. When the infusion fluid enters the patient, the surface of the liquid will decrease, and at the end will reach the bottom of the infusion bag. When the image of the fluid surface touches the bottom of the infusion bag, a mechanism will trigger a relay, and then activate a pinch valve to stop the flow of the infusion fluid before it runs out. The entire system incorporates a digital camera and Raspberry as the image processor. The surface of the liquid is determined using the Canny Edge Detection algorithm, and its relative position in the tube is determined using the Hough Line Transform. The raw picture of the infusion bag and the processed image are then sent via a wireless network to become part of a larger system and can be monitored via a simple smartphone equipped with the proper application, thus becoming an Internet of Things (IoT). With this approach, nurses can carry on other tasks in caring for the patients while this system substitutes some work on checking the infusion fluid.

Keywords: Canny Edge Detection, Health Care, Hough Line Transform, Infusion Control, Internet of Things

1. INTRODUCTION

Intravenous therapy in patients is one of the most widely used treatments in hospitals for the healing process of a patient. There are two methods of doing so, namely using an infusion pump and using drip IV (intravenous) delivery that has been used since 1944 [1]. Since the first use, there are many methods implemented to monitor the flow of the infusion fluid by measuring the weight, counting the number of drops, using ultrasonic wave TDR, infrared detection, and RFID [2–10].

Ogawa *et al.* [2] and Amano *et al.* [3] used three pieces of electrodes to form capacitors then compare the impedance to detect the fluid droplets. The same group then extended the work with a BlueTooth network for the reporting method. Every drip infusion set must be equipped with three electrodes before the system can be used for patients in this system. Baros and dos Santos [4] used an optical sensor and motor actuator to detect the

infusion fluid's droplets and then regulate the flow with the motor. The fluid regulation flow utilized an integrated design of software and hardware developed within their research group.

Cataldo *et al.* [5] used time-domain reflectometry to detect the amount of infusion fluid inside the infusion tube by attaching a two-stip probe to the infusion tube's surface. This method had good results, but every infusion tube requires a two-stip probe attached to the surface, and the position of the probe will significantly determine the accuracy of the result. Huang and Lin [6] used a similar RF (radio frequency) approach to detect the level of infusion fluid by attaching an RFID (radio frequency identification) tag. When an infusion tube containing liquid is full, the RFID tag will not respond to the signal sent by the RFID reader. However, when the fluid level inside the bag is below the RFID tag, it worked as usual and echoes the signal to the RFID reader.

Further, Ting *et al.* [7] studied the electrical characteristics of how the RFID tag is suitable to echo the signal from the RFID reader and how the reader should detect the signal. They use two different modes of application, one for the low fluid warning and the other for the inventory control. This approach required an attachment process of the RFID tag to the infusion fluid, and the placement can be crucial in determining the low-level detection.

Gupta *et al.* [8] utilized four LED (light-emitting diodes) to detect the number of fluid droplets inside the drip chamber. The LEDs are attached outside the drip chamber at different levels, accompanied by four light detectors. This work showed promises, but when the drip chamber wall has some droplet splash, then the LED cannot detect the infusion droplet correctly. A study by Gil *et al.* [9] also utilized a light source and light sensor to detect the droplet inside the drip chamber and then report the result to the nurse station using a wireless local area network. Other more straightforward system development uses a simple optical sensor, a digital counter with reset, and two seven-segment displays to show the flow rate of the infusion fluid.

Tharian *et al.* [11] controlled the infusion fluid flow using a DC motor and disk-spring mechanism. The result of the work shows minimal effectiveness in regulating the infusion fluid while Rashid *et al.* [12] used an optical sensor to detect the infusion droplets and a servo motor valve to control the flow. The result showed that the system is working, although it is sensitive.

The above review indicates that the infusion set (infusion tube with the infusion set) requires some modification for use. This method proposed here requires no change at all to the system. Nurses only need to place the infusion tube onto the stand, set the roller clamp according to the requirement, and hang it as usual.

Figure 1 shows the gravity drip infusion set. The set consists of four main components, namely, a vented spike to connect it to the infusion tube, an IV drip chamber to see the droplets of liquid entering the patient's body, the infusion line to drain fluid, and a roller clamp to regulate the fluid infusion. The end is the IV catheter to connect to the catheter in the patient. The infusion tube that provides intravenous fluids is hung on the infusion pole
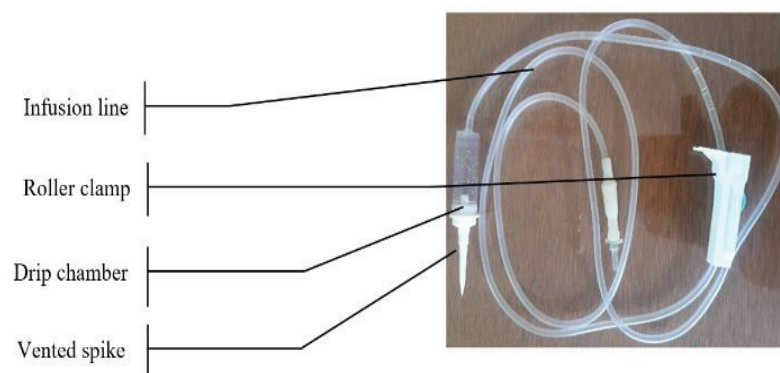
Fig. 1. Gravity drip infusion set.

In this drip system, the infusion liquid will drip from the vented spike output into the IV drip chamber slowly, depending on the position of the roller clamp. The liquid droplet volume based on the infusion set is 20 drops mL^{-1}. Therefore, the droplet count can be used to monitor the amount of fluid entering the patient's body.

In this study, monitoring the amount of fluid that comes out of the IV tube by using an image processing technique by detecting the surface of the liquid. As the amount of liquid decreases, the surface will go down until it reaches the bottom of the infusion tube. At this time, then the computer that processes the image will execute a pinch mechanism to stop the flow of liquid. As the infusion fluid is delivered to the patient, the surface level of it will go lower will reach the bottom of the tube when it runs out. As the surface level reaches the bottom of the infusion tube, the computer will trigger a mechanism to stop the delivery of the fluid to the patient similar to [8], and at the same time will trigger an alert to the nurse station to take action of the infusion tube.

2. MATERIALS AND METHODS

The experimental setup comprises a digital camera to capture the image of the infusion tube together with the infusion fluid, a Raspberry PI computer to process the image, and a wireless network to send the data. The implementation of the system will include two infusion tubes running at the same time with one unit detecting both infusion fluids. Figure 2a is the photograph of the setup with the infusion pole standing at the center of the picture. Two infusion bags are hanging on top of the pole, similar to a traditional infusion with two infusion lines going to the patient. Instead of going directly to the patient, the infusion line is inserted into the unit that will stop the flow of the fluid when it is almost out. There are two buttons to start the process of monitoring the infusion for the left and right sets. There are two LED indicators to track the status of the monitoring also for the two infusions. At the bottom are the power button and also a button to shut down the system gracefully since it is a Raspberry PI running Linux operating system. The digital camera is a standard USB camera compatible with the Raspberry PI and is mounted in front of the infusion set. Figure 2b shows the photograph of the setup from the side to provide clarity. Figure 2c is the inside of the Raspberry PI control box which consists of the single-board computer.

Figure 3 describes the functional block diagram of the system. The camera captures the image of the infusion tube with the fluid and then sends the data into the Raspberry PI via the USB data connection.
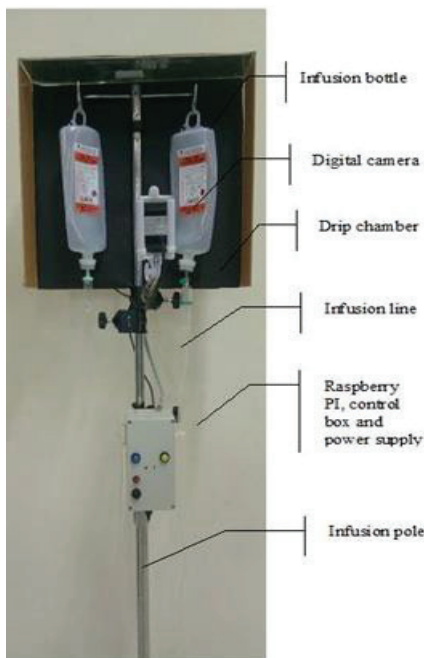
Fig. 2a. Experimental setup front view

Fig. 2b. Side view with the digital camera
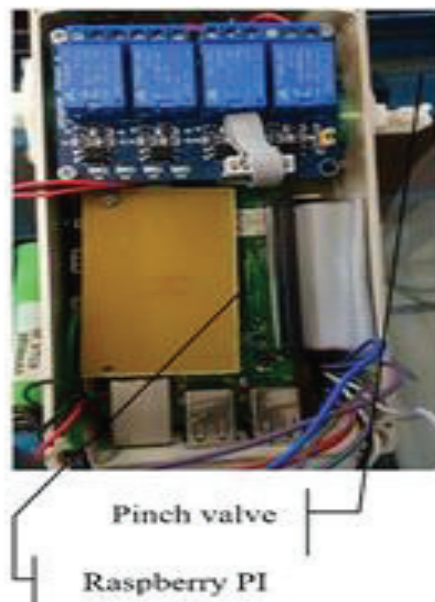
Fig. 2c. Control box with Raspberry PI, pinch valve, and relay

The Raspberry PI processes the data, determines the position of the surface of the fluid, computes the estimated volume of the remaining liquid. When the liquid is about to run out (determined/ calculated less than 20 mL) then it will activate the pinch valve to stop the flow and raise the alarm. During the process of monitoring, the Raspberry PI also updates the data of the fluid condition to a web server nearby using a wireless connection every minute. An operator can monitor the situation continuously either via a workstation located at the nurse station or using a smartphone connected to the server either via a local wireless connection or via the Internet.

Figure 3 illustrates the entire set, which consists of a Raspberry PI computer, a camera, and a web/ database server. The process starts when the nurse presses the start button after setting the infusion tube on the infusion pole. The USB camera captures the image from the infusion set and then sends the image to the Raspberry PI computer via a USB connection. The Raspberry PI computer processes the image the using Canny Edge Detection algorithm along with Hugh Line Transform to detect the surface of the liquid and then computes the amount of volume already transferred to the patient and at the same time determines the remaining fluid left in the tube. When there is less than 20 mL of fluid left, the computer will activate the pinch valve to stop the flow of infusion to the patient. The process described above is repeated every minute.

The computer will send the data from the image processing result to the web/ database server every 5 min via a wireless connection, which is already embedded in the Raspberry PI. The picture of the infusion tube, along with the data of the amount of fluid remaining, a marker of the edge of the tube, and surface-level via a smartphone connected to the server or via a workstation. Figure 4 shows the result of the image processing together with the marker that is available for viewing via a smartphone.

3. RESULTS

The experimental setup uses an actual infusion tube used in a typical hospital which is normal saline NaCl 500 mL. The experiment uses the same material, although they are from different batch numbers and dates of expiration. The volume of the fluid leaving the tube is measured using a graduated cylinder while – at the same time – the Canny Edge detection and Hough Line Transform determines the location of the surface of the liquid in the picture [13–17]. This work is carried out using Open CV with Raspberry PI model 3B+. At the start of measurement after the infusion tube is placed at the infusion stand, the top surface levels are set at pixel coordinate 550, and the bottom of the tube is at pixel coordinate133. When the surface level of the fluid goes down due to the decrease of the volume, the volume is measured. Figure 5 is the correlation graph of the amount of fluid leaving the tube and the surface level of the fluid in the picture.
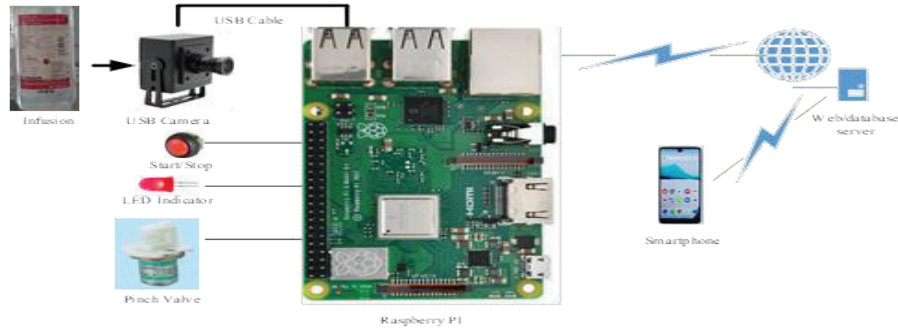
Fig. 3. System setup with USB camera, Raspberry PI, pinch valve, and webserver

The digital camera captures the entire infusion bottles and then crops the picture into a height of 650 pixels for image processing. There are two methods used for image processing. The edges of the infusion bottle and the surface of the liquid use the Canny Edge detection algorithm and Hough Line transform algorithm to detect the straight line of the surface of the liquid.

Figure 4a to Figure 4f depicts the process of image processing to locate the surface of the liquid. The start of the fluid surface detection uses the standard Canny Edge Detection method, which involves six distinct steps starting from the original image (Fig 4a) as follows:

i.   Grayscale conversion from color image (Fig 4b);
ii. Noise reduction of the image using a simple smoothing technique with Gaussian filter (Fig 4c.);
iii. Normalization to extract the intensity gradient of the grayscale image;
iv. Removing spurious response of the edge

detection using non-maximum suppression;
v.   Determining the potential edges using a double threshold (Fig 4d.);
vi. Tracking the edges using hysteresis and remove the weak and the non-connected.

Line detection of the surface of the fluid is performed by the Hough line transform, which is a technique of image analysis to find straight edges in conjunction with the method mentioned above. Figure 4e is the inverse of Figure 4d for easy observation. After the line transformation, as shown in Figure 4f (at the point of the arrow), the surface of the infusion fluid is detected, and the marker is superimposed to the first image.

In Figure 4f, on the left-hand side of the tube, there is a long line (green in color), which shows the edge of the infusion tube. This line is the reference line to determine the location of the fluid level since the surface level will be located 25 pixels to the right of the line. The horizontal line (red) is the processed indicator of the surface of the fluid. This red line is the parameter to determine the amount of

(a)   (b)   (c)   (d)   (e)   (f)
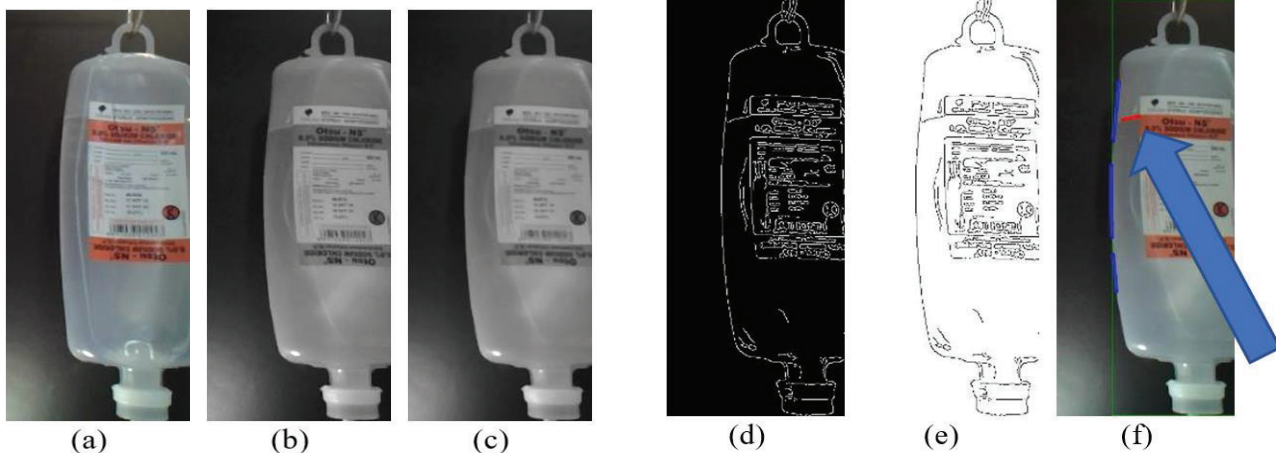
Fig. 4. The process of image liquid processing detection
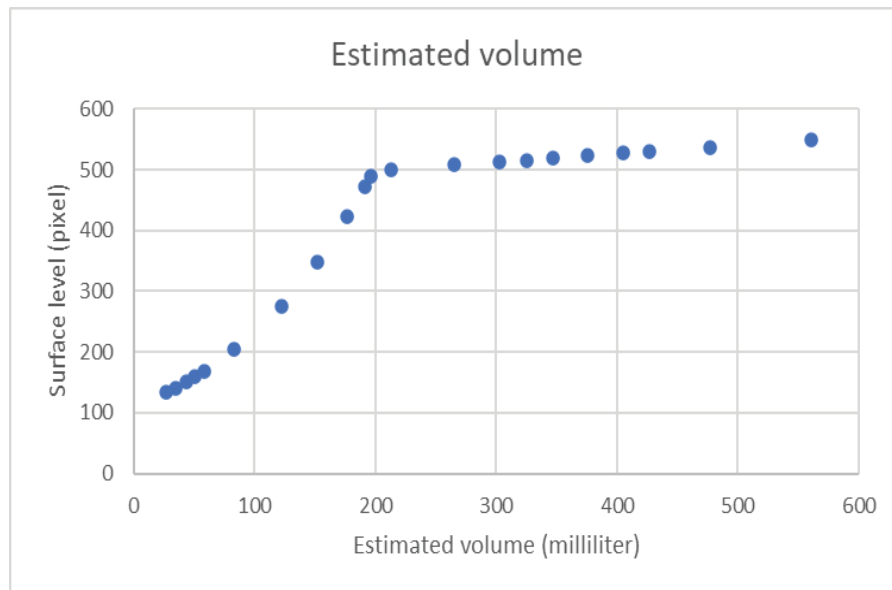
Fig. 5. Relationship of the surface level in pixel coordinate and the volume of the liquid.

volume left in the bottle as emphasized at the top of the arrow.

The amount of fluid leaving the tube will decrease the level of the surface of the fluid. The amount of liquid left in the tube is calculated by subtracting the initial volume of infusion fluid from the fluid, leaving the tube measured using a graduated cylinder.

4. DISCUSSION

Figure 5 shows the relationship between surface level in pixel coordinate as a function of leftover infusion fluid inside the tube. There are ten measurements conducted to obtain this figure. During the observation, the amount of infusion fluid left inside the tube and the surface level height are recorded. The plot is the average of the ten observations mentioned previously, and the most significant deviation is ± 20 pixels at a volume level of 270 mL. The change of pixel height is not proportional to the leftover volume because the infusion tube itself deforms due to the lack of fluid, and there is no air replacing it. Figure 5 clearly shows a clean break at 200 mL volume in the tube due to this condition.

The amount of fluid in the tube is estimated using two different empirical models for the upper part (from 200 to 550 pixel coordinate) and for

the bottom part (from 25 to 200 pixel coordinate). The upper estimation of the fluid follows a linear equation using a curve fitting by Microsoft Excel with a correlation coefficient of 1, as stated in Equation (1). The bottom part of the data uses exponential curve fitting since the plot shows exponential curvature. Equation (2) results from arbitrary curve fitting provided by Microsoft Excel and is always consistent with the result. Estimation of the amount of fluid left in the bottle is within 10 mL – which is the essential part because the line must be stopped – uses this model. This model fits very well and will stop the fluid level consistently Upper part:

$$y=0.1378x+47.3 \tag{1}$$

Bottom part:

$$y=107.8\exp(0.0077x) \tag{2}$$

Where:

y = the estimated volume left in the infusion tube
x = the pixel coordinate

The computer always monitors the level of the liquid with the technique mentioned above, and when the level reaches below 133-pixel coordinate, it triggers a signal to activate the pinch valve to stop the flow of the infusion liquid completely. At

the same time, there is also a visual alarm via the LED to alert the nurse that the infusion process has stopped.

The picture similar to Figure 4f is available in the Raspberry PI computer controlling the system and also sent to a web server to be filed and also viewed remotely. There is no display monitor on the Raspberry PI at the infusion set. Therefore there is no means to see the picture of the processed image. Data send to the webserver uses JSON (Javascript Object Notation), which is lightweight in format. This feature allows the processed images monitored from anywhere as part of the Internet of Things.

Results of sending the image of the infusion bottle via a wireless network are not implemented just for one infusion set [18-21] (one infusion pole and two infusion bottles), but for the entire room comprising several beds. In this work, ten infusion poles are monitored at the same time, and the image data are sent with tags so that each picture is identified correctly based on the bed and in turn, based on the patient. Figure 6 is the implementation of the system viewed using a smartphone.

The health care people can observe the pictures obtained from the process. A web page monitor is available to view the images via a wireless local area network along with a detailed description of the infusion condition. The system mentioned above uses a Raspberry PI platform.

5. CONCLUSION

A novel approach of controlling the stoppage of drip infusion using image processing uses the Canny Edge Detection method and Hough Line Transform to find the edges of the image and then determine the surface of the liquid. The pixel position of the surface is then used to predict the amount of infusion volume left. This method has been shown to work correctly and reliably based on the image itself. Together with the Hough line transform, the Canny Edge detection can predict the amount of infusion fluid left in the infusion tube.

6. ACKNOWLEDGEMENTS

7. CONFLICT OF INTEREST

The authors declare no conflict of interest.

8. REFERENCES

1. D. Kelly, and S.J. Brull. The cost of modern technology, *Journal of Clinical Anesthesia.* 180(7):80–81 (1995). DOI: 10.1016/0952-8180(94)00022-V

2. H. Ogawa, H. Maki, S. Tsukamoto, Y. Yonezawa, H. Amano, W. Morton Caldwell, A new drip infusion solution monitoring system with a free-flow detection function. *Proceedings of the 2010 Annual International Conference of the IEEE Engineering in Medicine and Biology Society (EMBC 2010).* p.1214–1217 (2010).

3. H. Amano., H. Ogawa., H. Maki., S. Tsukamoto., Y. Yonezawa, and W.M. Caldwell. A remote drip infusion monitoring system employing Bluetooth. *Proceedings of the Annual International Conference of the IEEE Engineering in Medicine and Biology Society, EMBS,* (2012). DOI:10.1109/ EMBC.2012.6346356

4. E. Barros, and M.V.D. dos Santos. A safe, accurate

Fig. 6. Two infusion bottles viewed from a smartphone.

intravenous infusion control system. *IEEE Micro*, p. 12–21 (1998). DOI:10.1109/40.735940

5. A. Cataldo., G. Cannazza., N. Giaquinto., A. Trotta, and G. Andria. Microwave TDR for real-time control of intravenous drip infusions, *IEEE Transactions on Instrumentation and Measurement.* 61(7):1866–1873 (2012). DOI: 10.1109/TIM.2012.2192346

6. C. Huang., and J. Lin. A warning system based on the RFID technology for running-out of injection fluid. International Conference *IEEE EMBS.* p. 2212–2215 (2011). DOI:10.1109/IEMBS.2011.6090418

7. S.H. Ting., C.K. Wu, and C.H. Luo. Design of dual mode RFID antenna for inventory management and IV fluid level warning system. *International Journal of Antennas and Propagation* 2470291:1–7 (2017). DOI:10.1155/2017/2470291

8. R.C. Gupta., S.R. Taneja., K.K. Thariyan, and S. Verma. Design and implementation of controlled drug infusion system. *Journal of Scientific and Industrial Research* 64:761–766 (2005).

9. R.A. Gil Jr, J.N. Padilla, and B.T.T. Iii. Intravenous piggyback infusion control and monitoring system using wireless technolog. *International Journal of Advanced Technology and Engineering Exploration,* 3(17): 50–57 (2016).

10. V.V. Kamble., P.C. Pandey., C.P. Gadgil, and D.S. Choudhary. Monitoring of intravenous drip rate. *Proceeding Iinternational Conference on Biosciences & Medical Engineering,* Vol. I, (2001).

11. K.K. Thariyan., S.R. Taneja, R.C. Gupta, and S.S. Ahluwalia. Design and development of a unique drop sensing unit for infusion pump, *Journal of Scientific and Industrial Research.* 61: 798–801 (2002).

12. H. Rashid, S. Shekha, S.M.T. Reza, I.U. Ahmed, Q. Newaz, A low cost automated fluid control device using smart phone for medical application. *International Conference on Electrical, Computer and Communication Engineering.* p. 809–814 (2017).

13. B. Raghavendra., K. Vijayalakshmi, and M. Arora. Intravenous drip meter & controller, *8th COMSNETS.* p. 1–5 (2016). DOI: 10.1109/COMSNETS.2016.7440024

14. B. Wang, and S. Fan. An Improved CANNY Edge Detection Algorithm, *2009 Second International Workshop on Computer Science and Engineering, Qingdao.* p. 497–500 (2009) DOI: 10.1109/WCSE.2009.718

15. A. Haghi., U.U Sheikh., and M.N. Marsono. A hardware/ software co-design architecture of canny edge detection. *Computational Intelligence Modelling and Simulation (CIMSiM) 2012, Fourth International Conference on Computational Intelligence, Modelling and Simulation,* p. 214–219 (2012). DOI: 10.1109/CIMSim.2012.18

16. D.N. Reddy., V.V. Yerigeri, and H. Sanu. Design and simulation of canny edge detection. *International Journal of Engineering Sciences & Research Technology* 3(11):304–311 (2014).

17. X. Zhang., D. Wang, and X. Li. Recognition and measurement of drug-release hole based on machine vision algorithms, *4th International Congress on Image and Signal Processing,* p.1950–1953 (2011). DOI: 10.1109/CISP.2011.6100595

18. X. Wen. Design of medical infusion monitor and protection system based on wireless communication technology, *2nd International Symposium on Intelligent Information Technology Application.*, p. 755–759, (2008). DOI: 10.1109/IITA.2008.47

19. H. Zhu. New algorithm of liquid level of infusion bottle based on image processing. *2009 International Conference on Information Engineering and Computer Science* p. 1–3 (2009). DOI: 10.1109/ICIECS.2009.5363597

20. M. Xiao., L. Zhang., and C.Z. Han. A moving detection algorithm based on space-time background difference. In: D.S. Huang, X.P. Zhang, G.B. Huang (Eds.) Advances in Intelligent Computing. ICIC 2005. *Lecture Notes in Computer Science* 3644: 146–154 (2005). DOI: 10.1007/11538059_16

21. R. Duvvuru., P.J. Rao, and S.K. Singh. Improvising security levels in WLAN via novel BSPS. *International Conference on Emerging Trends in Communication, Control, Signal Processing and Computing Applications* (C2SPCA). p. 1–6 (2013). DOI: 10.1109/C2SPCA.2013.6749426

Pakistan Academy of Sciences

Research Article

Probabilistic Static Voltage Stability of Power System with Integration of PV Generators using Monte Carlo Simulations

Awan Uji Krismanto[1*], Hafizhul Ayyasi Khairullah[1], Irrine Budi Sulistiawati[1], Abraham Lomi[1], and Dipu Sarkar[2]

[1]Department of Electrical Engineering, National Institute of Technology Malang,
Jl. Raya Karanglo, Km. 2, Malang 65143, Indonesia
[2]National Institute of Technology, Chumukeidma, Dimapur, Nagaland 797103, India

Abstract: As a renewable source, the uncertainties and intermittencies of solar irradiance have become the main concern in developing and integrating such power generation into an electricity network. In power system operation, it is important to maintain a stable voltage profile under random power injection from renewable power generations. The effect of photovoltaic (PV) power plants on the static voltage stability of the interconnected power system is presented in this paper. The probabilistic study was conducted through Monte Carlo Simulation (MCS) to investigate the fluctuation of voltage profiles under uncertain power injection from PV power plants. The standard test system of IEEE 14 bus and practical test system of Lombok, West Nusa Tenggara electricity network are investigated. It was noticed that the installation of a photovoltaic power plant affected the voltage profiles. The fluctuated condition of power injection from PV power plant resulted in more fluctuation of voltage profiles as indicated by higher standard deviation values. Moreover, distributed location of the PV power plant also influenced the circumstances of voltage fluctuation, providing less fluctuated condition of voltage profiles. Eventually, it can be observed that the voltage fluctuation would influence the static voltage stability of the interconnected power system.

Keywords: Photovoltaic Generator, Probability Distribution, Renewable Energy, Solar Energy, Voltage Fluctuation, Voltage Profiles.

1. INTRODUCTION

Massive development of technologies drastically changes the necessity of society. In few decades, electricity has become an essential thing for human life since most of the appliances and facilities need electrical energy to operate. Therefore, the dependences of humans live on electricity has been increasing enormously. With the fast growth of electricity demand, the invention and development of novel energy resources to ensure sufficient electricity supplies are critical. On the other hand, the deposits of fossil fuels are continuously decreasing due to extensive exploration and consumption [1, 2]. Moreover, the usage of fossil fuels introduces detrimental effects on the environment. With the limitations and drawbacks of fossil fuel, renewable energy is the promising option to overcome the energy concern. One of

the most developing renewable energy resources is solar energy. By 2020, around 500 GW solar PV facilities are installed throughout the world. It is expected that in 2050, 15 % of world energy demand are fulfilled by solar energy [3].

The implementation of PV-based power plants brings economic beneficial effects due to the abundant amount and cheap energy resources. Moreover, it is also environmentally friendly as a result of the non-emission operation and the usage of non-polluting materials [4]. Despite those advantages, the integration of PV-based power plants also alters the power system operation and control. Recently, the increased penetration rate of PV generation has raised concerns over utility due to the possible negative impact on the stability of the power system [5]. The generation of electricity from the sun has a challenge because

the availability of the sun on the earth's surface depends on the sun's position which varies due to differences in latitude [5, 6]. Furthermore, the dependency of solar power on environmental and weather circumstances increases the uncertainty and unpredictable operating condition of the power system. It potentially affects the stable operating point of the power system [6, 7].

Fluctuating power injection from PV-based power plants may change the power flow direction, transmission line congestion, and hence the power losses. Eventually, it potentially influences the system voltage. The bus voltage is considered an important parameter in the power system since it significantly influences system stability and safety. The variations in P and Q affect the voltages across all the buses in the system as well. Therefore, a voltage stability analysis can be applied to decide whether the voltage levels across the buses are at an acceptable level or not [8, 9].

Power system voltage stability refers to all buses in the system that can maintain a steady voltage after a fault. However, from a system planning and operating point of view, the stress stability analysis is to find the distance of the system to the voltage drop in normal operation and to identify areas where the stress is weak when the voltage drops. This is called static voltage stability [10]. With the increasing trend of PV integration in power systems, it is important to investigate the effects of having of such renewable power generation on static voltage stability. Researchers monitored that PV location and size have a profound impact on system voltage stability [3]. It might have either adverse or advantage impacts on voltage stability. The effect of the partially solar-PV system on long-term voltage stability was investigated in [11, 2]. It was observed that the integration of PV power plants might improve the system voltage stability.

Even though many kinds of research have been conducted to investigate PV effects on voltage stability, however, it was only using the deterministic approach. The main drawback of the deterministic approach is the limited number of cases [1, 13]. Therefore it would not reflect the actual condition of system voltage profiles under random power injection from PV power generation. With the limitation of the deterministic

approach, it is important to conduct a probability analysis approach. This paper concentrates on the analysis of PV plant installations in interconnected power systems using a probabilistic approach. A probabilistic study using the Monte Carlo simulation method is implemented to provide a realistic scenario of uncertain conditions of power injection from a PV power plant.

2. MATERIALS AND METHODS

2.1 Monte Carlo Simulation

Voltage stability is concerned with the ability of the power system to maintain acceptable voltages across all buses in the system under normal conditions and after failure. The system enters a state of voltage instability when a disturbance occurs, an increase in load demand, or a change in system condition causes a progressive and uncontrolled voltage drop. A major factor causing instability is the inability of the power system to meet reactive power demands [9].

As power injection from the renewable power plant is continuously fluctuating due to unpredictable weather conditions, it would introduce the uncertain operation of the power system. Under uncertain power injection from a PV power plant, a deterministic power flow analysis is not sufficient to represent the actual power system condition. Therefore, a probabilistic analysis approach is required to capture the behavior of the power system in particular voltage stability circumstances under random power injection from the PV power plant.

Probabilistic power flow (PLF) based on numerical methods (such as Monte Carlo simulations) or analytical methods (such as convolutional techniques) was developed in the 1970s to deal with power system uncertainty due to variations in grid variables [13].

The active bus load is an independent random variable and the transmission system is represented by a DC network model (so that the reactive power flow is negligible). The generation delivery procedure is modeled by allocating the variation of the total electric charge for the generation bus. Since the active electric load variable on each bus is

assumed to be independent, the probability density function of the circuit current can be calculated by a series of convolutions. Later, this basic method was extended and also applied to the AC network model [14].

The probabilistic distribution function is estimated from the solar irradiation data collected respectively using the Gaussian mixture distribution function. [15] The Gaussian mixture model is useful for modeling data that comes from one of several groups that may differ from one another, but data points in the same group can be modeled well by the Gaussian distribution. [13] The formula for determining the Gaussian value in Equation (1):

$$PX^{(x)} = \frac{1}{\sigma\sqrt{2\pi}} e^{-(x-\mu)^2/2\sigma^2} \tag{1}$$

The variable x represents the value of the random variable and for the variable μ represents the expectation of an experiment, for the variables σ^2 or σ represents the standard deviation. For some of the different formulas, here it is written in Equation (2):

$$Px^{(x)} = N\ (x; \mu, \sigma^2) \tag{2}$$

which the variable N describes the normal value.

Once a statistical model is defined in terms of a probability density function, a Monte Carlo simulation is performed which involves repeating the simulation process using in each simulation a set of specific values of the random variable [16]. Various methods have been proposed to study the effect of uncertainty on stress stability. Among the proposed probabilistic analytical methods, the Monte Carlo simulation has become a popular method due to its ability to handle a large number of samples with great accuracy and flexibility. As the power output of the generation unit varies due to the uncertainty of the renewable energy system, the power-sharing scheme in the microgrid changes accordingly which might disrupt the power generation and load demand balance [15].

Load Flow results based on Monte Carlo Simulation in terms of power flow in various parts of the system and voltage profiles in all network buses can be treated statistically, and statistical estimation and inference methods can be applied [15].

In uncertainty analysis, the relationship between the dependent and independent variables can be expressed in Equation (3):

$$v = h(z) \tag{3}$$

h represents a function describing the correlation between the dynamic behavior of the output variables and the uncertain values of the input variables. The input and output vector variables can be represented as

v =[v_1, v_2…] ^ t and z = [z_1, z_2…] ^ t of their respective values [15].

The purpose of Monte Carlo analysis is to estimate the uncertainty of the output or the dependent variable resulting from the uncertainty of the input or the independent variable through certain complex functions [12].

For modeling the power generation in PV, there are several models of system problems that do not need to be considered, such as not considering the system configuration and line impedance values. The purpose of modeling the power distribution function in PV is to schedule the generator by considering the solar energy system by determining the optimal amount of generating power for the solar energy system units during the study period so that the total cost can be minimized by the power balance equation, requirements for power reserves, and other constraints [17].

Calculation of changes in the duration of radiation can be converted to power using Equation (4):

$$P_{PV}(G_t) = \begin{cases} P_{sn} \dfrac{(G_t)^2}{G_{std} R_c} \\ P_{sn} \dfrac{G_t}{G_{std}} \end{cases} \tag{4}$$

G_t = Forecast radiation per hour
G_{std} = Solar radiation in a standard environment is set with a value of 1 000 W m^{-2}
R_c = The point of radiation is defined as 150 W m^{-2}
P_{sn} = Average PV power output

These values can only be known through short-term forecasting. Because the demand for system load and solar radiation depends on the social behavior of the customer and weather variables [18].

2.2 Photovoltaic Model

In this manuscript, probabilistic analysis of system voltage profiles under PV power uncertainty is conducted using DigSILENT Power Factory analytical software. Therefore, the default PV model provided in Power Factory software is considered in this study. The template model of PV with additional features and control is comprising of multiple control blocks and functionalities.

The PV-based power plant is modeled as a static generator with MPPT, control system, and DC link capacitor as depicted in Figure 1. The inverter system of the PV model employs Udc-Q which maintains the voltage of DC capacitor constant to ensure stable operation of the PV system by suppressing power and voltage fluctuations. The voltage controller is providing direct (Id_ref) and quadrature (Iq_ref) current reference values to control switching stages of the inverter. While PLL model ensures synchronized operation between the PV system and the other generator units during grid-tied operation.

For the static voltage stability study, the dynamic model of the PV power plant is simplified as follows [19, 20]: The dynamic of the MPPT controller is neglected and it is assumed that the PV array model

provided reference values for the Udc-Q controller. Due to the high-frequency switching features of the inverter system, the fast response of the inverter inner control loop is neglected.

3. RESULTS AND DISCUSSION

Two test systems are considered in this paper to investigate the impact of uncertain power injection from PV systems. The first investigated test system is IEEE 14 as depicted in Figure 2. To investigate the effects of PV power uncertainty on system voltage profiles, the PV power plants are connected in bus 4, 5, and 10.

The second study case considers the electrical system of Lombok, West Nusa Tenggara, Indonesia as depicted in Figure 3. the Lombok electricity system consists of seven generating units, which operate at a voltage of 150 kV, and consists of 17 buses and 19 channels connected to load centers. Multiple PV-based power plants are connected in three buses which are located in Sengkol, Pringgabaya, and Paokmotong with a capacity of 3×5 MW. By integrating PV sequentially, it will be done by randomizing the PV radiation capacity to analyze the voltage profile of the transmission system.

The Lombok network was selected in this research due to the high solar potential energy in the island while most of the conventional power generations were powered by diesel engines. The penetration of PV generation in Lombok island has been significantly increasing, replacing a certain
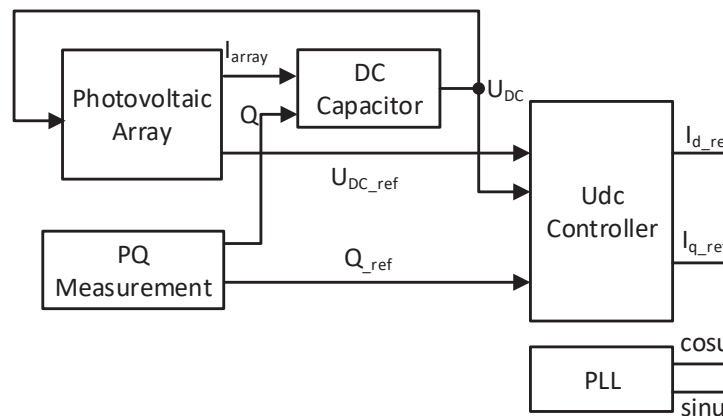
Fig.1. PV system model in DigSILENT power factory
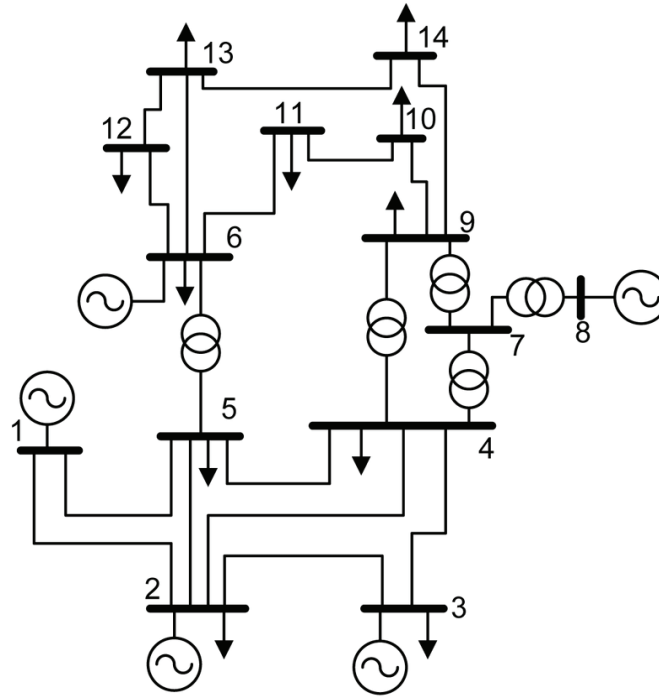
Fig 2. Single line diagram of IEEE 14 Bus
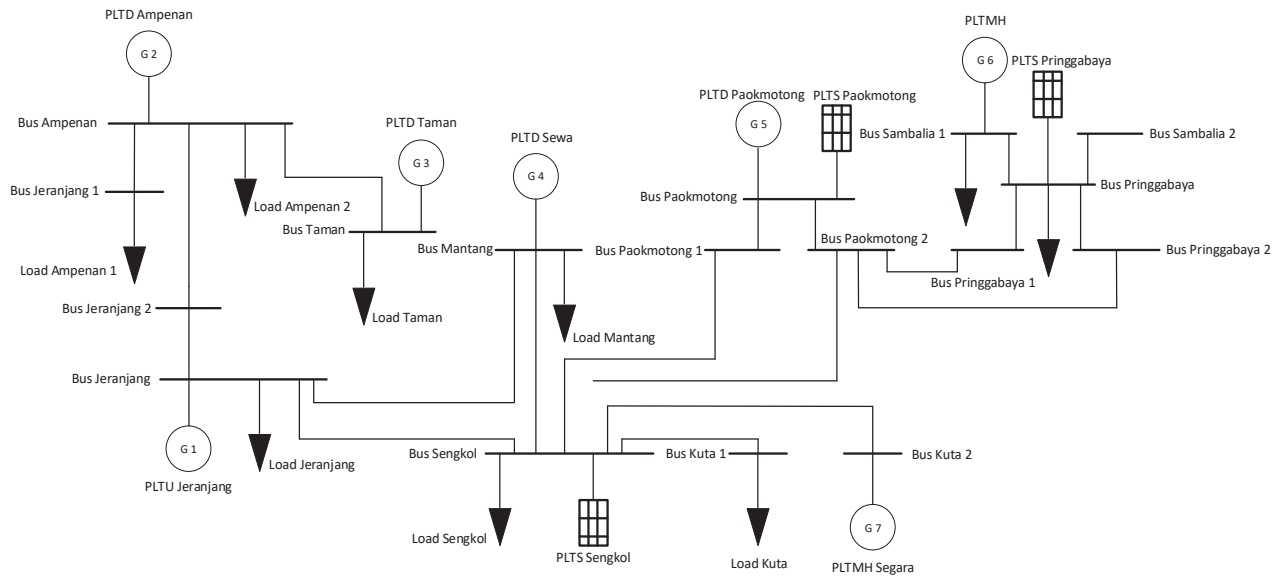
Fig. 3. Single line diagram of Lombok 150 kV

portion of diesel engine-based power generation. Therefore, it is necessary to investigate the impacts of PV integration on static voltage stability in this island electricity network.

To realize the uncertain condition of PV power plant power injection in the investigated test systems, 1 000 data of PV power are randomly generated and sampled through the Monte Carlo simulation method. The 1 000 random scenarios

of PV power injections from different regions are then implemented in DigSILENT power factory analytical software. Fluctuation of voltage profiles of the selected bus is statistically investigated through average and deviations values of the selected buses.

The dynamic model of PV generation developed in DigSILENT power factory is considered to provide more realistic system dynamic behavior

under the different generations of PV generations.

3.1 Analysis of Voltage Profiles in IEEE 14 bus

In the first study case, two scenarios were considered. The first scenario investigates the effects of integrating one PV power plant to bus 4 of the IEEE 14 bus system. The 1 000 data of random power injection from the PV power plant are considered, resulting in 1 000 values of bus voltage fluctuations.

Figure 4 shows the fluctuation of bus 5, 8, and 9 in the IEEE 14 bus system after the integration of the PV power plant on bus 4. It was monitored that when one PV power plant is integrated, bus 5 V fluctuated moderately as depicted in Figure 4a. The bus voltage of bus 5 has an average value of 0.967 5, a maximum value of 0.968 02, a minimum value of 0.966 97, and the standard deviation value on bus 5 is 0.000 74. The less fluctuating condition was observed in bus 8 as shown in Figure 4b.

It was monitored that the voltage of bus 8 has

an average value of 0.958 03, a maximum value of 0.958 30, a minimum value of 0.957 76, and the standard deviation value on bus 8 is 0.000 37. More stable bus voltage under different power injections from one PV power plant is monitored in bus 9 as presented in Figure 4c. It was observed that the voltage of the corresponding bus has an average value of 0.947 02, a maximum value of 0.947 13, a minimum value of 0.946 91, and with lower standard deviation value on bus 9 is 0.000 15.

The second scenario considers the integration of three PV power plants on bus 12, 14, and 15 in the IEEE 14 bus system. Integration of three PV power plants in the existing power system network would inject more power into the system. Therefore more voltage enhancements were expected. On the other hand, the distributed energy sources would provide a more stable power flow in the network, resulting in less fluctuation of system voltage profiles.

The investigated result from the IEEE 14 bus system with the integration of PV generators is depicted in Figure 5. The voltage of bus 5 has an
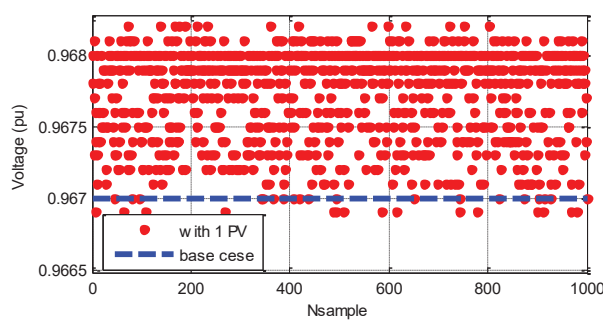
a) Bus 5
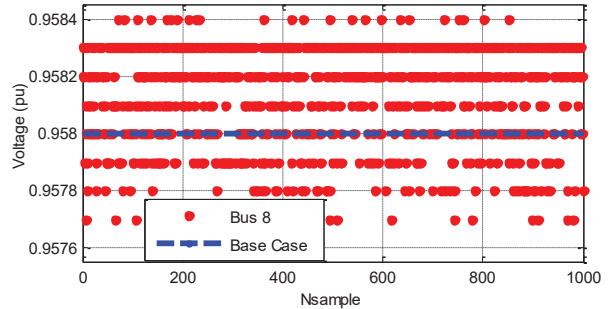
b) Bus 8
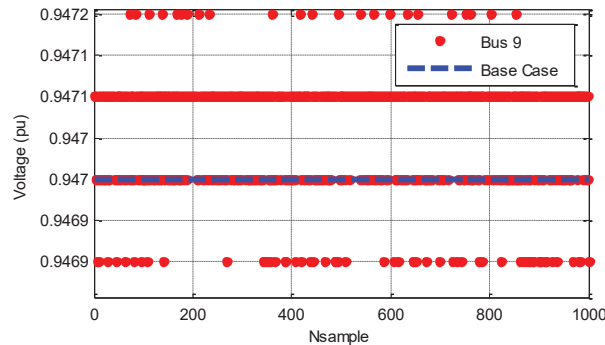
c) Bus 9

Fig. 4. Bus Voltage of selected bus of IEEE 14 bus with the integration of 1 PV power plant.

a) Bus 5

b) Bus 8

c) Bus 9
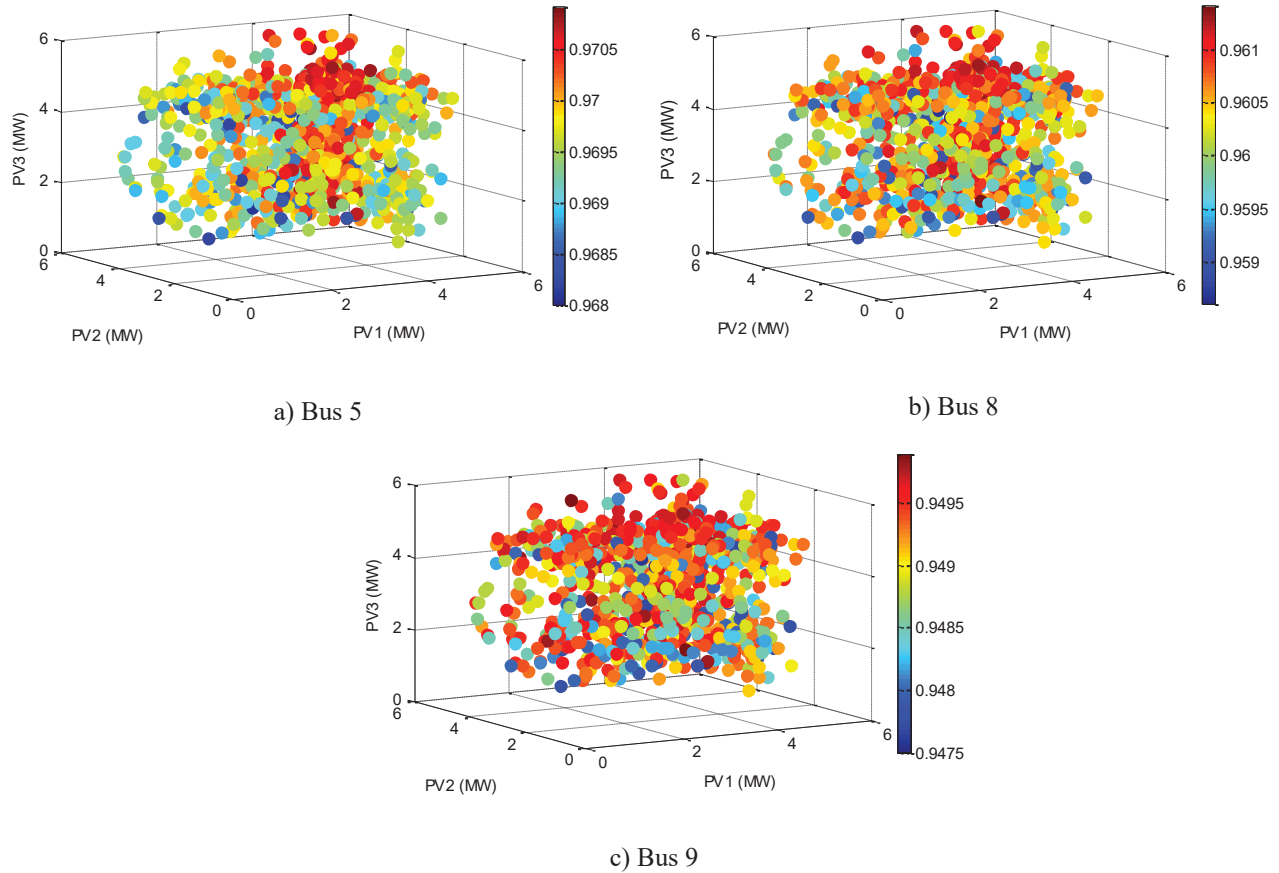
Fig. 5. Bus Voltage of selected bus of IEEE 14 bus with the integration of 3 PV power plants.

average value of 0.969 66, a maximum value of 0.969 90, a minimum value of 0.969 42, and the standard deviation value on bus 5 is 0.000 34. Enhancement of voltage profile is also monitored in bus 8 and 9. After integration of three PV power plants, the voltage of bus 8 has an average value of 0.960 4, a maximum value of 0.960 58, a minimum value of 0.960 40, and the standard deviation value on bus 8 is 0.000 12. While the voltage of bus 9 has an average value of 0.949 27, a maximum value of 0.949 28, a minimum value of 0.949 27, and the standard deviation value on bus 9 is 0.000 13.

From the two scenarios, it can be noticed that integration of one PV system results in a slight change of voltage profile and hence a small fluctuation in voltage values. In the second scenario of integrating three PV power plants, the voltage profiles of the investigated buses are less fluctuating than in the first scenario with one PV power plant. The placement of PV power plants close to each other results in the less fluctuating condition of power flow and hence enhanced the voltage stability. Additional power injection from

three locations of PV power plants results in more stable voltage profiles of the investigated bus.

3.2 Lombok Network Power Flow Analysis

Similar scenarios were implemented in the second practical test system of the Lombok interconnected power system. In the first scenario, one PV power plant is integrated. The rated capacity of a 5 MW PV system is considered.

Figure 6 represents the fluctuation of bus Ampenan, Jeranjang, and Mantang in the Lombok system after the integration of one PV power plant. It was monitored that when one PV power plant is integrated, the bus voltage of Ampenan fluctuated significantly. The bus voltage of bus Ampenan has an average value of 0.987 9, a maximum value of 0.988 1, a minimum value of 0.987 8, and the standard deviation value on the Ampenan bus is 6.045 1. Similarly, the fluctuating condition was observed in bus Jeranjang. It was monitored that the voltage of bus Jeranjang has an average value of 0.991 9, a maximum value of 0.992 1, a minimum

a) Bus Ampenan

b) Bus Jeranjang

c) Bus Mantang
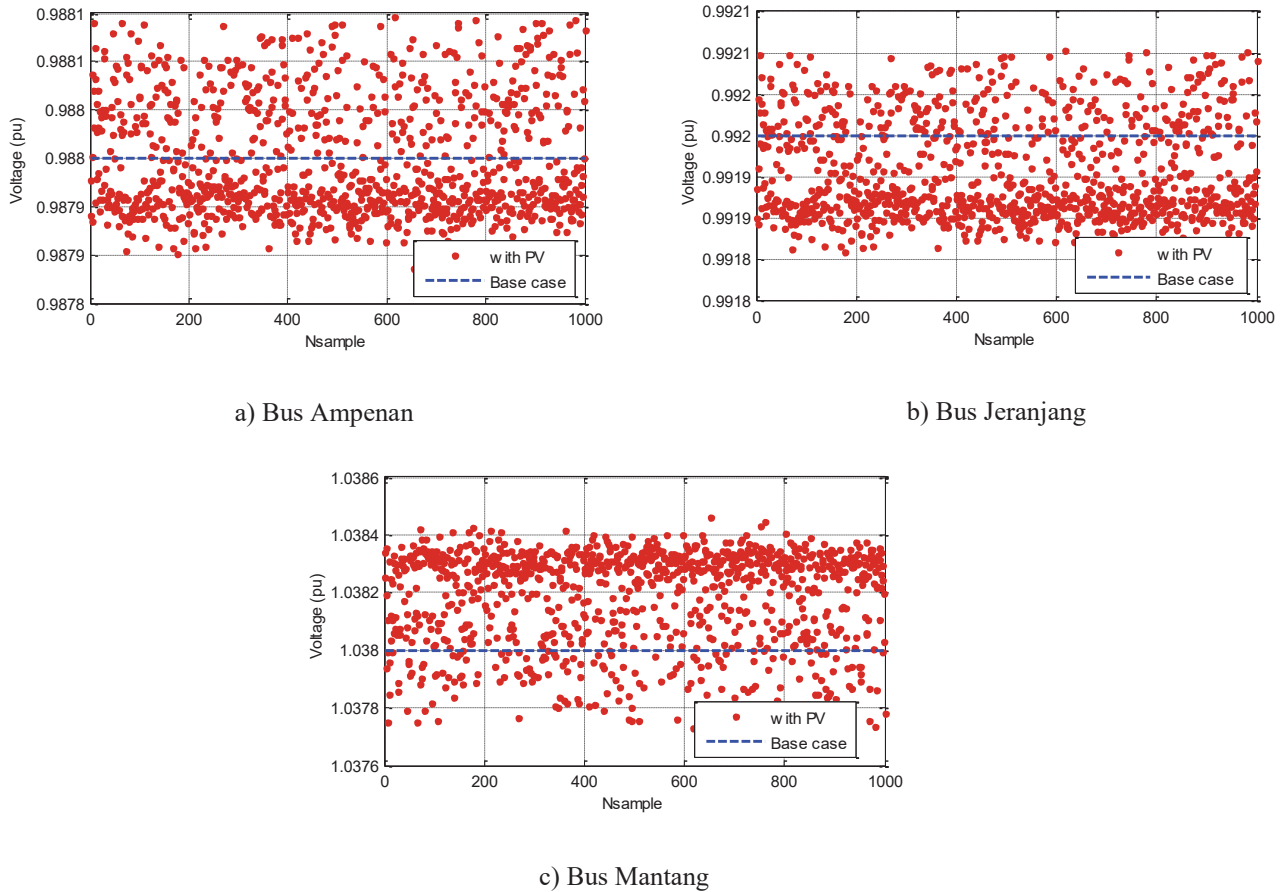
Fig. 6. Bus Voltage of selected bus of Lombok system with integration of one PV power plant.

value of 0.991 8, and the standard deviation value on the Jeranjang bus is 6.015 4.

More stable bus voltage under different power injections from one PV power plant is shown in bus Mantang. It was observed that the voltage of the corresponding bus has an average value of 1.038 1, a maximum value of 1.038 4, a minimum value of 1.038 4, and the standard deviation value on the Mantang bus is 0.000 1.

Fig. 6. Bus Voltage of selected bus of Lombok system with integration of one PV power plant. The second scenario considers the integration of three PV power plants in Sengkol, Pringgabaya, and Paokmotong with a capacity of 3 × 5 MW. Figure 7 shows the fluctuation of bus 5, 8, and 9 voltages under uncertain power injection from three PV power plants.

Additional power injection from three locations of PV power plants results in more stable voltage profiles of the investigated bus. More power

injection from three distributed PV power plants enhanced the voltage profiles of the system and also reduced the voltage fluctuation.

The bus voltage of Ampenan is indicated by an average value of 0.987 6, a maximum value of 0.9879, a minimum value of 0.987 3, and the standard deviation value on the Ampenan bus is 0.000 122. The average value of the voltage profile is higher and the standard deviation is lower than the scenario with one PV system. These conditions indicate the improvement of static voltage stability. Similar results are observed in bus Jeranjang and Mantang. In detail, the voltage profile of bus Jeranjang has an average value of 0.986 7, a maximum value of 0.987 1, a minimum value of 0.986 5, and the standard deviation value on the Jeranjang bus is 0.000 123. While bus voltage of Mantang has an average value of 1.039 113 a maximum value of 1.03 96, a minimum value of 1.038 3, and the standard deviation value on the Mantang bus is 0.000 256.

a) Bus Ampenan

b) Bus Jeranjang

c) Bus Mantang
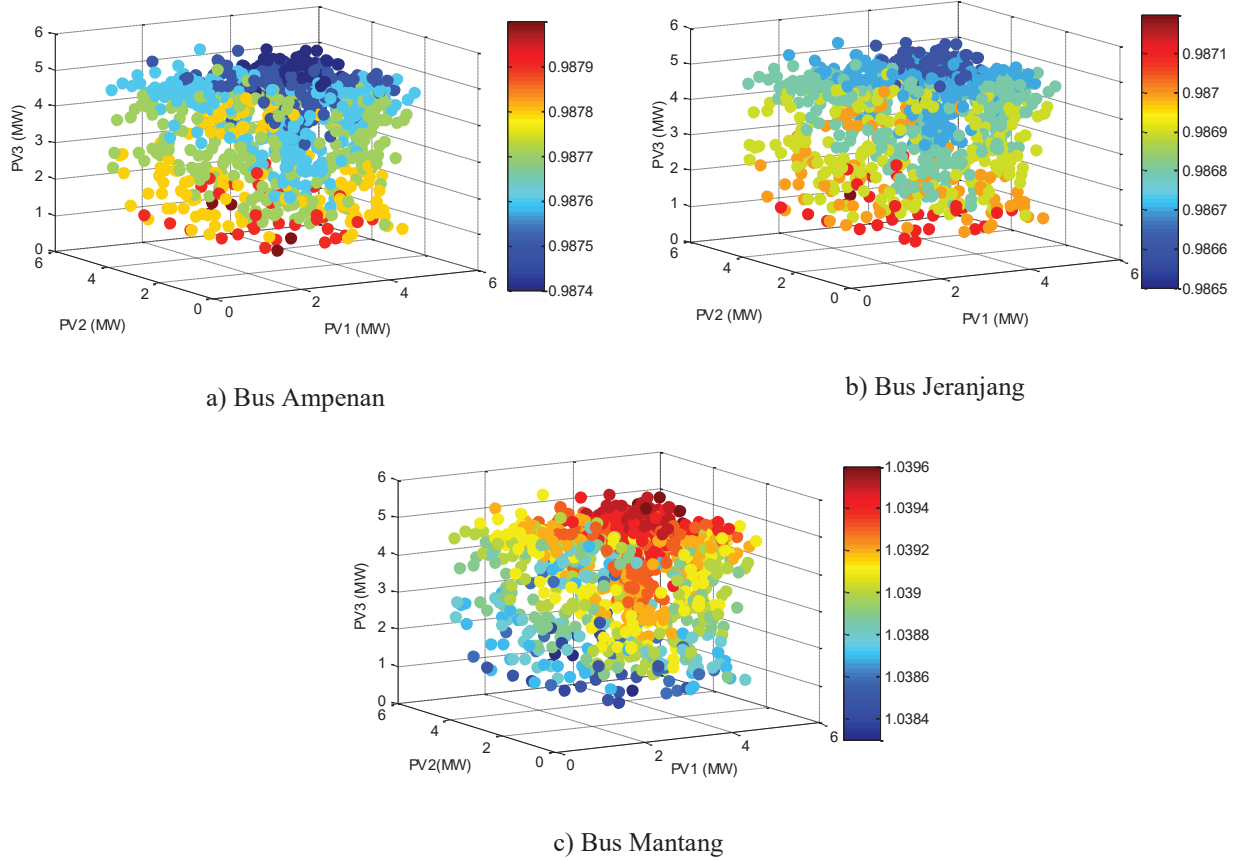
Fig. 7. Bus voltage of selected bus of Lombok system with integration of three PV power plants.

From the presented results, integrating more PV power plants in some locations provides beneficial effects on power system operation. Since the function of the PV power plant is to support the power demand without reducing existing power generation from conventional power generation. Eventually, it would improve the voltage profiles of the system. The static voltage stability of the power system is enhanced with the increase of PV power plant penetrations. It can be observed from the presented research that most of the voltage profiles had higher values than in the base case scenario without penetration of the PV power plant. Moreover, distributed location of the power system would reduce congestions of transmission lines and power losses. It would provide a more stable voltage profile as indicated by lower values of standard voltage deviation. With these results, it can be suggested that more distributed PV power plant installation would provide a more stable situation of voltage profiles. The obtained results can be implemented to planning the PV allocation and transmission line expansion. Hence, the effect of

uncertainties of solar irradiance can be minimized and more stable system voltage profiles can be maintained.

In this research, Monte Carlo Simulation is considered to provide the probabilistic study of system voltage variations under random power injection from PV generations. To obtain more realistic results, the number of data can be increased. However, it should be considered the computational time when a large number of data were considered in the studies. In the future, more detailed data resolution can be considered to perform the probabilistic analysis and more renewable energy sources such as wind power generation can be involved in the study.

4. CONSLUSION

A probabilistic study of voltage profiles of the interconnected power system has been addressed in this paper. It was clearly shown from standard test systems and practical test systems that the integration

of PV power plants and additional power injection from those renewable power sources enhanced the system voltage profiles. It was also observed that more distributed power sources would maintain the static voltage stability conditions even though the power system was operated under uncertain circumstances of power injection from PV.

5. CONFLICT OF INTEREST

The authors declare no conflict of interest.

6. REFERENCES

1. A.U. Krismanto and N.Mithulanthan. Probabilistic small signal stability analysis of autonomous wind-diesel microgrid. *ISGT Asia Pacific* 2017. Auckland, New Zealand, (2017). DOI: 10.1109/ISGT-Asia.2017.8378359

2. Anindhita, I. Rahardo, I. Fitriana, R.E.P. Dewi, E. Siregar, N. Niode, Yudiartono, A. Sugiyono, L.O.M.A. Wahid, P.T. Wijaya, and A.K. Paminto. *Outlook Energi Indonesia 2018 - Energi Berkelanjutan untuk Transportasi Darat* [Indonesia Energy Outlook 2018 - Sustainable Energy for Land Transportation]. Pusat Pengkajian Industri Proses dan Energi (PPIPE), Badan Pengkajian dan Penerapan Teknologi (BPPT). Jakarta, Indonesia (2018) [in Bahasa Indonesia]

3. REN21, Renewables 2020 Global Status Report, (2018).

4. E. Yandri. The effect of Joule heating to thermal performance of hybrid PVT collector during electricity generation. *Renewable Energy*, 111: 344–352 (2017). DOI: 10.1016/j.renene.2017.03.094

5. R. Shah., M. Nadarajah., R. Bansal., K. Lee, and A. Lomi. Influence of large-scale PV on voltage stability of sub-transmission system. *International Journal on Electrical Engineering and Informatics* 4(1): 148–161 (2012). DOI: 10.15676/ijeei.2012.4.1.12

6. N. Dhlamini, and S.P.D. Chowdhury. Solar photovoltaic generation and its integration impact on the existing power grid. *IEEE PES/IAS Power Africa,* (2018) p. 710–715. DOI: 10.1109/PowerAfrica.2018.8521003

7. F.A. Khalil, M. Asif, S. Anwar, Sana ul Haq, and F. Illahi. Solar tracking techniques and implementation in photovoltaic power plants: A review. P*roceedings of the Pakistan Academy of Sciences A. Physical and Computational Sciences* 54 (3): 231–241 (2017)

8. R. Bayindir., Ş. Demirbaş., E. Irmak., U. Cetinkaya., A. Ova, and M. Yeşil. Effects of renewable energy sources on the power system. *IEEE International Power Electronics and Motion Control Conference* (PEMC) (2016). p. 388–393. DOI: 10.1109/EPEPEMC.2016.7752029

9. P. Kundur., N.J. Balu, and M.G. Lauby. *Power System Stability and Control* (Vol. 7). McGraw-hill, New York (1994).

10. D. Wang., X. Yuan., M. Zhao, and Y. Qian. Impact of large-scale photovoltaic generation integration structure on static voltage stability in China's Qinghai province network. *The Journal of Engineering* 2017(13): 671–675 (2017). DOI: 10.1049/joe.2017.0414.

11. E. Munkhchuluun, and L. G. Meegahapola. Impact of the solar photovoltaic (PV) generation on long-term voltage stability of a power network. *Conference: 2017 IEEE Innovative Smart Grid Technologies - Asia* (ISGT-Asia), 1–6. 2017. DOI: 10.1109/ISGT-Asia.2017.8378456.

12. W. Suampun. Voltage stability analysis of grid-connected photovoltaic power systems using CPFLOW. *Procedia Computer Science,* 86: 301–304, 2016. DOI: 10.1016/j.procs.2016.05.082

13. A. U. Krismanto, N. Mithulananthan, and I. Kamwa, Oscillatory stability assessment of microgrid in autonomous operation with uncertainties. *IET Renewable Power Generation,* 12(4): 494–504, 2018. DOI: 10.1049/iet-rpg.2017.0579

14. R. Sridharan. Gaussian Mixture Models and the EM Algorithm, (Lecture Notes - MIT CSAIL). (2017). https://people.csail.mit.edu/rameshvs/content/gmm-em.pdf (Accessed on 15 January 2021).

15. G. Stefopoulos., A.P. Meliopoulos, and G.J. Cokkinides. Advanced probabilistic power flow methodology. *15th Power Systems Computation Conference.* (PSCC) 2005, (2005) p. 22–26.

16. A.U. Krismanto., N. Mithulananthan, and I. Kamwa. Oscillatory stability assessment of microgrid in autonomous operation with uncertainties. *IET Renewable Power Generation*, 12(4): 494–504. (2018). DOI: 10.1049/iet-rpg.2017.0579

17. S. Conti, and S. Raiti. Probabilistic load flow using Monte Carlo techniques for distribution networks with photovoltaic generators. *Solar Energy* 81(12): 1473–1481 (2007). DOI: 10.1016/j.solener.2007.02.007

18. R. Liang, and J. Liao. A fuzzy-optimization approach for generation scheduling with wind and

solar energy systems. *IEEE Transactions on Power Systems* 22(4): 1665–1674 (2007). DOI: 10.1109/TPWRS.2007.907527

19. J. Park., W. Liang., J. Choi., A.A. El-Keib., M. Shahidehpour, and R. Billinton. A probabilistic reliability evaluation of a power system including Solar/Photovoltaic cell generator. *IEEE Power &* *Energy Society General Meeting,* 2009, pp. 1–6. DOI: 10.1109/PES.2009.5275722

20. Q. Linan., Z. Dawei., S. Tao., C. Ning, and D. Jie. Photovoltaic generation model for power system transient stability analysis. *International Journal of Computer and Electrical Engineering* 5(3): 289–300 (2013). DOI: 10.7763/IJCEE.2013.V5.717

Utilization of Chicken Eggshells as Catalyst in Biodiesel Synthesis from Waste Cooking Oil

Lizda Johar Mawarani[1*], Thomas Andherson Sihombing[1], Doty Dewi Risanti[1],
Muhannad Illayan Massadeh[2], and Dwi Prananto[3]

[1]Department of Engineering Physics, Institut Teknologi Sepuluh Nopember, Kampus ITS
Sukolilo Surabaya, Indonesia 60111
[2]Department of Biological Science and Biotechnology, Faculty of Science,
The Hashemite University 13133, Zarqa, Jordan
[3]Materials Science Program, Faculty of Engineering, Niigata University, Niigata City,
Niigata 950-2181, Japan

Abstract: Solid oxides are the most used catalyst for the synthesis of biodiesel, one of which is calcium oxide (CaO). This research reports the synthesis of CaO catalysts sourced from chicken eggshells through the calcination process. Chicken eggshells were cleaned and dried for 24 h at 120 °C. The eggshells were then calcined at temperatures varying from 600 °C to 900 °C for 6 h and the resulted sample were characterized by FTIR and XRD. The biodiesel synthesis was conducted at 65 °C with a reaction time of 2 h and the concentration of catalyst was varied at 3 wt%, 6 wt%, and 9 wt%. The optimal biodiesel synthesis was obtained at a concentration of CaO catalyst formed at a calcination temperature of 900 °C at 9 wt%. The yield of biodiesel conversion was obtained at 81.43 % and glycerol was produced as a by-product.

Keywords: Alternate Feedstock, Calcination, Environmentally Friendly Catalyst, Reduce Production Cost, Renewable Energy, Reuse Waste Material

1. INTRODUCTION

Sustainable biodiesels are usually made from vegetable oils, inedible oils, fats, algae, and waste cooking oil. The vegetable oil is more efficient for biodiesel production due to the low content of free fatty acids (FFA) [1–3]. The high content of FFA in biodiesel synthesis can trigger a saponification reaction and reduces the quality of biodiesel [4]. Biodiesel synthesis from vegetable oil requires more expensive production costs than waste cooking oil since waste cooking oil is easy to obtain [5]. Thus, waste cooking oil is more attractive for biodiesel synthesis [6].

A calcium oxide (CaO) catalyst is a heterogeneous base catalyst that can be used as an accelerator in biodiesel synthesis reactions.

One of the CaO catalysts can be synthesized through the calcination process of $CaCO_3$. One of the many wastes containing $CaCO_3$ is chicken eggshells. Chicken eggs are widely consumed in Indonesia, so chicken eggshells are quite abundant. Eggshells have many advantages, among them are biodegradable, recyclable, and biocompatible [7]. Eggshells consist of 94 % $CaCO_3$, 1 % $Ca_3(PO_4)_2$, 1 % $MgCO_3$, and 4 % of organic ingredients [8]. The solid waste of chicken eggshells is harmless to the environment, it is generally disposed of in landfills without any pretreatment.

2. MATERIALS AND METHODS

This research used the waste of chicken eggshells as feed stock to produce CaO catalysts. The eggshells were cleaned then dried at 100 °C for 24 h and

crushed to reduce their particle size up to 60 mesh.

CaO catalysts were made through the calcination process of sieved eggshell particles. The process is intended to remove carbon dioxide compounds through the decomposition reaction of calcium carbonate ($CaCO_3$) contained in eggshells so that calcium oxide compounds are obtained. Equation (1) shows the reaction during the calcination process [9]:

$$CaCO_3 \quad CaO + CO_2 \qquad (1)$$

The chicken eggshell powder was then calcined for 6 h at a varied temperature of 600 °C, 700 °C, 800 °C, and 900 °C. The resulted sample was analyzed and characterized using X-ray Diffractometer (XRD) and the Fourier Transform Infra-Red (FT-IR) spectroscopy.

The next step was the pretreatment process to reduces the content of FFA in the waste cooking oil sample. In this study, the desired FFA content is < 1 %. The process was started by heating waste cooking oil (300 mL) at a temperature of about 55 °C to 65 °C. Then a mixed solution of methanol (15% of the mass waste cooking oil) and H_2SO_4 catalyst (1% of the mass waste cooking oil) was put into the waste cooking oil sample at 60 °C for 2 h. After the reaction finished, the waste cooking oil was washed using distilled water. The waste cooking oil was then reheated at 120 °C for 10 min. Then to prepare a lye solution, the CaO catalyst from chicken eggshells was mixed with methanol with a molar ratio of 6:1. The added lye solution to the pretreated waste cooking oil with a varied concentration of 0 wt%, 3 wt%, 6 wt%, and 9 wt% and heated at 65 °C for 2 h for transesterification reaction. After the transesterification reaction was completed, the biodiesel sample was left for one night to separate the upper layer containing biodiesel. Glycerol in the lower layer must be washed to neutralize the biodiesel from glycerol.

3. RESULTS AND DISCUSSION

The physical formation of CaO can be seen from the color change of the eggshell after the calcination process. Calcination at 600 °C produced a dark gray powder, at 700 °C produced a pale gray powder, at 800 °C produced a pale gray with a little white,

and at 900 °C produced a white powder with a little gray. The higher the calcination temperature, the more metal oxides formed which is indicated by the color change of the chicken eggshells powder to white [9].

The results of XRD for the chicken eggshells powder after calcination at a temperature of 600 ºC to 900ºC, are shown in Figure 1. The XRD pattern for calcination at 900 °C shows the successful formation of the crystalline CaO structure as indicated by the appearance of a sharp peak at $2\theta = 32.2°$, 37.4°, 53.9°, 64.2°, and 67.4° that indicate an increase in the resulting CaO digitality. Commercial CaO also has the same peaks on the XRD pattern. However, there are still peaks associated with the $CaCO_3$ phase which appeared at $2\theta = 29.4°$ and 47.3° also the $Ca(OH)_2$ which appeared at $2\theta = 28.6°$, 34.2°, 47.2°, and 50.9°.

The compound fraction is calculated using the Reference Intensity Ratio (PERR) shown in Equation (2) [10]:

$$Fraction\ R\ (\%) = \frac{\sum \dfrac{I_i}{I_{max}}}{\sum \dfrac{I_p}{I_{max}}} x\ 100\ \% \qquad (2)$$

Figure 1 shows that at calcination temperature of 600 ºC, 700 ºC, and 800 ºC high composition of $CaCO_3$ was formed with compound fraction around 68 % to 86 % along with the minor composition of CaO, $Ca(OH)_2$, and impurity with respective compound fraction around 7 % to 8 %, 3 % to 5 %, and 11 % to 19 %. This indicates that at calcination temperatures of 600 ºC, 700 ºC, 800 ºC only a small amount of $CaCO_3$ is converted to CaO. For 900 ºC calcination temperature, the composition of CaO was optimally formed with a fraction compound of 85.02 % with 3.73 % of $CaCO_3$, 11.24 % of $Ca(OH)_2$, and is already clean from impurity.

FTIR analysis of the CaO catalyst was carried out at 4 000 cm^{-1} to 400 cm^{-1} wave numbers as shown in Figure 2 [11]. The OH band appeared at a wave number of 3 639.06 cm^{-1} to 3 760.21 cm^{-1} for the calcination temperature of 800 ºC and appeared very sharply at 900 ºC, but did not appear at temperatures of 600 ºC and 700 ºC. The OH band is considered as a CaO characteristic [12] so that the appearance of the OH group indicates

a peak fit between the three samples. However, the emergence of these OH groups cannot merely be used to justify that the sample analyzed is CaO because the presence of $Ca(OH)_2$ also causing the emergence of a dip in the area of about 3 643 cm^{-1} as shown by previous research [13]. The presence of such dip may be due to the adsorbent of water on the CaO surface because of its nature as an absorber of water from the air [13].

The CaO is detected by referring to the wave number at the area around 400 cm^{-1} in the sample. Referring to the standard CaO, $CaCO_3$, and $Ca(OH)_2$ spectrum, the CaO spectrum appeared to broaden at that wave number. Dips in the region of about 400 cm^{-1} to 500 cm^{-1} are connected with the stretching of Ca-O bonds. The sample with a calcination temperature of 900 ºC indicates more CaO formation, due to the broadened dip at the wave number.

The calcination temperature greatly influences the structure of the catalyst and its catalytic properties. Therefore, the catalytic activity of the sample of eggshell powder was then tested through a process of transesterification to convert triglycerides to biodiesel (free acid methyl esters/ FAME). The FFA level of the waste cooking oil is reduced from 4.045 % to 0.775 % by the CaO catalyst; a significant reduction of 80.84 %.

This research found that only eggshell powder produced by calcination at 900 ºC can form glycerol after the transesterification reaction with the waste cooking oil. This is mainly because eggshell powder with calcination temperatures of 600 ºC, 700 ºC, and 800 ºC was not producing enough CaO and was mainly dominated by $CaCO_3$ or calcite. Previous studies also found that if the eggshell powder is dominated by $CaCO_3$, it was not able to catalyze and eliminate energy during the transesterification reaction [14].

The CaO catalyst from eggshell Powder with calcination temperatures of 900 ºC produced a fraction of biodiesel of about 66.76 %. This can prove that a higher calcination temperature increases the catalytic properties of the transesterification process. In addition, the formation of glycerol after the transesterification process also justifies the presence of biodiesel because it has fulfilled the

transesterification reaction. This is also confirmed by previous research which discussed its calcination temperature at 900 ºC and found that the catalyst that was very active in the transesterification reaction process [15].

In biodiesel synthesis, the concentration of catalyst is also very much influences the transesterification process. Figure 3 shows the biodiesel yield at different catalyst concentrations.

Figure 3 shows that the biodiesel yield increases monotonically with increasing calcium oxide (CaO) catalyst concentration. This increase is consistently occurring in all samples of chicken eggshell powder. From the results, it was found that the CaO catalyst produced at 900 ºC calcination temperature gave the largest contribution in converting triglycerides to biodiesel by 81.43 % with a concentration of 9 wt%. The synthesis of biodiesel with a commercial catalyst was also carried out to compare the biodiesel produced with a catalyst from the eggshell. The highest biodiesel production was obtained on the 9 % catalyst concentration which was 83.59 %. This yield is higher than the catalyst from eggshells at the same concentration. However, for the 3 wt% and 6 wt% eggshell catalysts, the biodiesel yield was higher than the commercial CaO catalyst. This is caused by the increase in the reaction rate at a high concentration of catalyst which reduces the activation energy [12].

The yield of biodiesel is higher than the results of Muhammad et. al. [16] that synthesized biodiesel from used cooking oil using a microwave and CaO catalyst from chicken eggshells and duck eggshells. The catalyst composition varied from 1 % to 10 % and showed the maximum amount of yield of biodiesel at a composition of 5 % CaO from chicken and duck eggshells, respectively 40.74 % and 67.07 %. From this known that used cooking oil biodiesel with CaO catalyst from chicken eggshells and through common transesterification in this study gives better results.

The biodiesel produced in the experiment was then tested to determine whether it is suitable with the available standards for use. The tests carried out were among others to determine the kinematic viscosity, density, pour point, flash point, and fog point. The biodiesel characteristics are shown
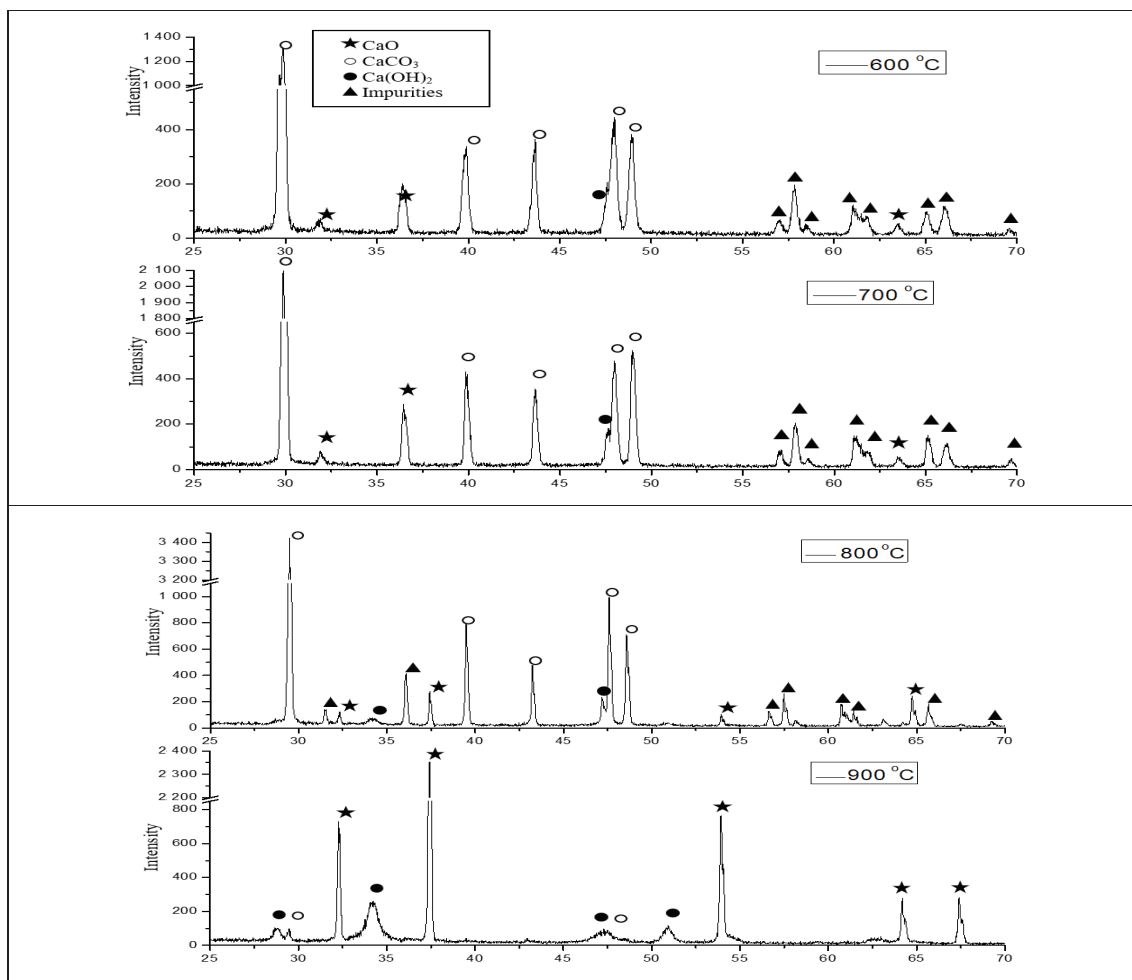
Fig. 1. XRD diffraction pattern of 6 h calcined eggshells
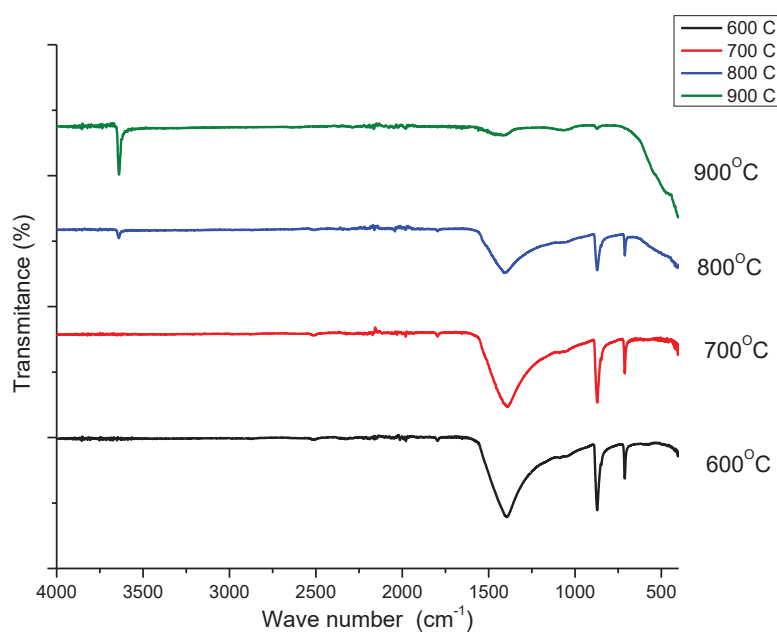
Fig. 2. Graph of FTIR results of chicken eggshells powder with 6 h calcination

in Table 1. Density test of the biodiesel samples produced with CaO catalyst formed by calcination temperatures at 800 ºC and 900 ºC, commercial CaO, and without catalyst were met with SNI and ASTM standards for all concentrations. But for the samples produced with CaO formed by calcination temperature at 600 ºC and 700 ºC the density of the biodiesel of which has not met with the standard for all catalyst concentrations.

The results of the kinematic viscosity test of the biodiesel samples with CaO catalyst formed at 900 ºC calcination temperature and commercial CaO catalysts were met with the SNI and ASTM standards and were characterized by a rather thin physical property. When compared to conventional diesel the kinematic viscosity value of the biodiesel samples that met the standard is not much different, which is around 4.6 mm^2 s^{-1}. This means that CaO catalyst formed with calcination temperature of 900 ºC and commercial CaO can reduce the kinematic viscosity of biodiesel.

Flashpoint of all the biodiesel samples was met with SNI standards (minimum 100 ºC) and ASTM (minimum 130 ºC) so that all biodiesel samples were within safe limits of fire hazards during storage, handling, and transportation. But the flashpoint value of the biodiesel samples produced by CaO catalyst formed at a calcination temperature of 900 ºC and commercial CaO and CaO catalyst formed at 600 ºC, 700 ºC, 800 ºC, for the same process. The case without catalyst has a very significant difference with a ratio of about 1: 2. It should be noted that the flashpoint that is too high is also not good to be used because biodiesel will be difficult to light itself [17].

The test results of the cloud points of all biodiesel samples were met with the two standards. For the pour points, test CaO catalyst formed at calcination temperatures of 800 ºC and 900 ºC and
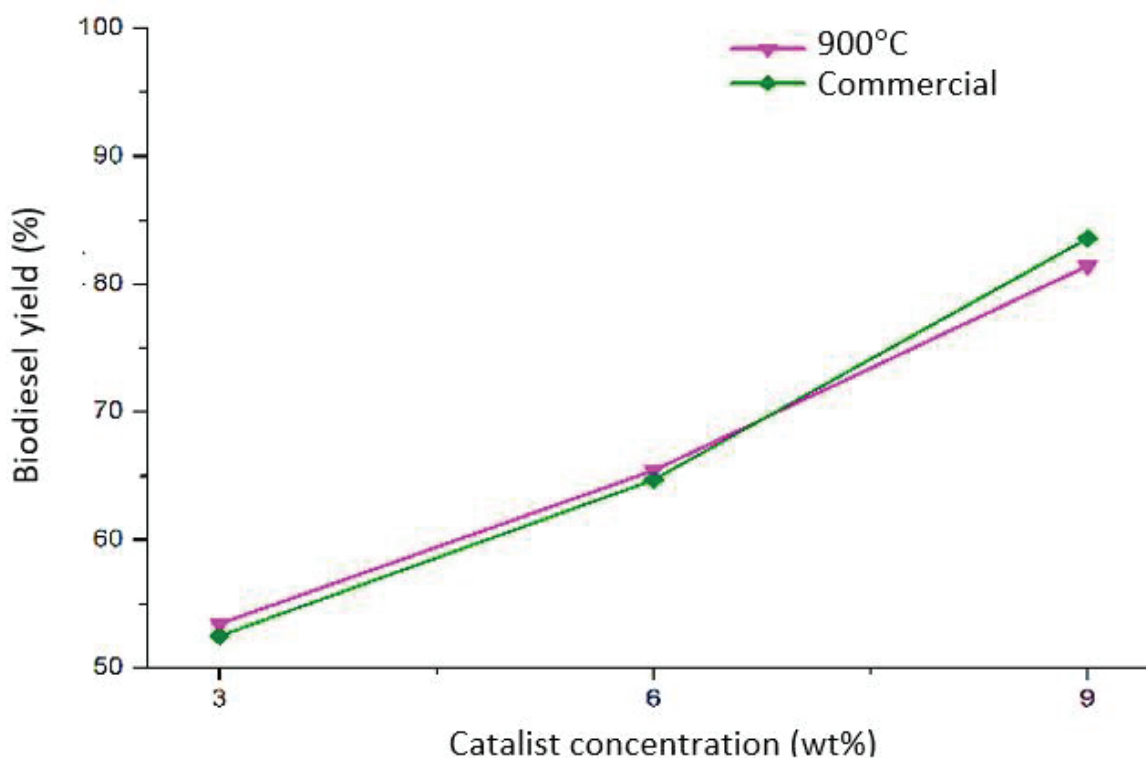
Fig. 3. Graph of the yield of biodiesel at a different catalyst concentration

Table 1. Biodiesel sample characteristics based on SNI and ASTM

Characteristics			Density (kg m^{-3})	Kinematic viscosity (mm^2 s^{-1})	Point (^{o}C)		
					flash	pour	cloud
ASTM D6751			800 to 880	1.90 to 6.00	Min. 100	Max. 18	Max. 18
SNI-04-7182:2015			850 to 890	2.30 to 6.00	Min. 120	Max. 18	Max. 18
Without catalist		**0**	880	25.02	326.5	18.3	15.1
		3	910	34.39	328.3	21.6	17.6
	600 ^{o}C	**6**	900	34.23	336.8	20.8	16.5
		9	900	34.22	327.7	21.4	16.3
		3	910	36.37	334.7	20.1	16.4
	700 ^{o}C	**6**	900	33.72	330.9	18.9	16.6
		9	890	32.96	327.2	18.3	16.7
CaO catalist		**3**	870	33.6	332.6	16.1	14.8
concentration	**800 ^{o}C**	**6**	850	34.32	326.7	17.7	14.6
(wt%)		**9**	850	33.9	318.7	17.1	13.7
		3	870	3.88	175.5	15.4	11.3
	900 ^{o}C	**6**	860	4.41	178.3	16.7	11.7
		9	870	4.58	175.8	17.8	10.7
		3	860	3.99	185.4	16.1	11.8
	Commercial	**6**	870	4.39	186.7	17.5	11.5
		9	860	4.53	184.6	17.7	11.6

commercial CaO were met with SNI (maximum 18 ºC) and ASTM (maximum 18 ºC). Whereas for the CaO catalyst formed at a calcination temperature of 600 ºC and 700 ºC, and without catalyst were not meet with the standards so it is not recommended.

4. CONCLUSION

Based on the results of the characterization and analysis carried out on the CaO catalyst and biodiesel samples, this article concluded that the CaO catalyst formed with calcination at a temperature of 900 ºC can be used as a reference for the production of biodiesel where the concentration of 9 wt% yields the highest biodiesel formation of about 81.43 %. The results of the test to characterize the biodiesel samples that met with the qualifications of SNI-04-7182: 2015 and ASTM D6751 were obtained from the biodiesel samples Synthesized by CaO catalyst form chicken eggshell with calcination temperature of 900 ºC and commercial CaO with 3 wt%, 6 wt%, and 9 wt% catalyst concentration.

5. CONFLICT OF INTEREST

The authors declare no conflict of interest.

6. REFERENCES

1. F. Ullah., A. Nosheen., I. Hussain., and A. Bano. Base catalyzed transesterification of wild apricot kernel oil for biodiesel production. *African Journal of Biotechnology* 8(4): 3289–3293 (2009)

2. A.H.K. Khichi. Bioethanol and biodiesel from second generation feedstocks: A promising solution to energy shortages in Pakistan. *Proceedings of the Pakistan Academy of Sciences B. Life and Environmental Sciences* 54 (2): 79–88 (2017).

3. H.H. Senousy., and S.A. Ellatif. Mixotrophic cultivation of *Coccomyxa subellipsoidea microalga* on industrial dairy wastewater as an innovative method for biodiesel lipids production. *Jordan Journal Biology Sciences* 13(1): 47–54 (2020).

4. E.I. Rhofita. Penurunan kadar Free Fatty Acid (FFA) pada reaksi esterifikasi dalam proses produksi biodiesel: Kajian waktu reaksi dan temperatur reaksi. [Decreasing levels of Free Fatty Acid (FFA) in the esterification reaction in the biodiesel production process: Study of reaction time and reaction temperature]. *Jurnal Ilmu-Ilmu Teknik Sistem* 11: 39–44 (2015). [in Bahasa Indonesia].

5. B. Supple., R. Howard-Hildige., E. Gonzalez-Gomez, and J. Leahy. The effect of steam treating

waste cooking oil on the yield of methyl ester. *Journal of the American Oil Chemists* 79: 175–178 (2002). DOI: 10.1007/s11746-002-0454-1

6. M. Canakci. The potential of restaurant waste lipids as biodiesel feedstocks. *Bioresource Technology* 98: 183–190 (2007). DOI: j.biortech.2005.11.022

7. Z. Wei., C. Xu, and B. Li. Application of waste eggshell as low-cost solid catalyst for biodiesel production. *Bioresource Technology* 100(11): 2883–2885 (2009). DOI: 10.1016/j.biortech.2008.12.039.

8. W. Stadelman. *Encyclopedia of Food Science and Technology,* 2nd ed. John Wiley and Sons, New York, USA. p. 593–599 (2005)

9. H. Santoso., I. Kristianto, and A. Setyadi. *Pembuatan biodiesel menggunakan katalis basa heterogen berbahan dasar kulit telur.* [The making biodiesel using heterogeneous base catalysts from eggshell]. Research Report Engineering Science - LPPM Universitas Katolik Parahyangan, Bandung, Indonesia (2013). [in Bahasa Indonesia].

10. J.D. Martín-Ramosm, and J. Díaz-Hernández. *Pathways for Quantitative Analysis by X-Ray Diffraction.* Instituto Andaluz de Ciencias de la Tierra (IACT, CSIC-UGR), Spain (2011). DOI: 10.5772/36256

11. S. Rahmawati., R. Ediati, and D. Prasetyoko. *Sintesis partikel nano CaO dengan metode kopresipitasi dan karakterisasinya* [Synthesis of nano CaO particles by coprecipitation method and their characterization]. University Scientific Paper, ITS, Surabaya, Indonesia (2012). [in Bahasa Indonesia].

12. S. Martinez., L. Romero., R. Lopez, and J. Romero. Preparation and Characterization of CaO nanoparticles/NaX zeolite catalysts for the transesterification of sunflower oil. Industrial and *Engineering Chemistry Research* 50(5): 2665–2670 (2010). DOI: 10.1021/ie1006867

13. B. Yoosuk., P. Udomsap., B. Puttasawat, and P. Krasae. Modification of calcite by hydration–dehydration method for heterogeneous biodiesel production process: The effects of water on properties and activity. *Chemical Engineering Journal* 162(1): 135–141 (2010). DOI: 10.1016/j.cej.2010.05.013

14. N. Tangboriboon., R. Kunanuruksapong, and A. Sirivat. Preparation and properties of calcium oxide from eggshells via calcination. *Materials Science-Poland* 30(4): 313–322 (2012). DOI: 10.2478/s13536-012-0055-7

15. J.A. Kinast. *Production of biodiesels from multiple feedstocks and properties of biodiesels and biodiesel/diesel blends:* Final report. Report 1 in a Series of 6 (No. NREL/SR-510-31460). National Renewable Energy Lab., Golden, CO., USA. (2003).

16. Muhammad, R. D., Umar, A., Budiawan, B., Bakri, R., and Sihombing, R. Utilization of duck eggshell and chicken eggshell as catalyst for biodiesel synthesis from waste cooking oil. *AIP Conference Proceedings* 2168 (020071):1–8 (2019). DOI: 10.1063/1.5132498.

17. H. Yasin., R. Mamat., A.F. Yusop., R. Rahim, and A. Aziz. Fuel Physical characteristics of biodiesel blend fuels with alcohol as additives. *Procedia Engineering* 53: 701–706 (2013). DOI: 10.1016/j.proeng.2013.02.091

Pakistan Academy of Sciences

Research Article

Analysis of the Sand Drying Process in the Biomass-Energized Rotary Drying Machine

Herry Susanto[1,2]*, Roy Hendroko Setyobudi[2,3], Danny Faturachman[4],
Erkata Yandri[2], Asep Hendiarko Priyatna[2], Asyari Daryus[1], Zane Vincevica Gaile[5],
Satriyo Krido Wahono[6], Rangga Kala Mahaswa[7], and Maizirwan Mel[8]

[1]Department of Mechanical Engineering, Darma Persada University,
Jl. Taman Malaka Selatan No.22, Jakarta 13450, Indonesia
[2]Graduate School of Renewable Energy, Darma Persada University, Jakarta, Indonesia
[3]Department of Agriculture Science, Postgraduate Program, University of Muhammadiyah
Malang, Jl. Raya Tlogomas No.246, Malang 65145, Indonesia
[4]Department of Marine Engineering, Darma Persada University, Jakarta, Indonesia
[5]Department of Environmental Science University of Latvia, Jelgavas Street 1, Room 302,
Riga LV-1004, Latvia
[6]Research Division for Natural Product Technology – Indonesian Institute of Sciences,
Jl. Jogja - Wonosari, km 31.5, Gunung Kidul, Yogyakarta - Special Region 55861, Indonesia
[9]Faculty of Philosophy, Universitas Gadjah Mada, Jl. Olahraga, Caturtunggal, Depok, Sleman,
Yogyakarta 55281 - Special Region, Indonesia
[8]Department of Biotechnology Engineering, Kulliyyah of Engineering,
International Islamic University Malaysia, P.O. Box 10, 50728 Kuala Lumpur, Malaysia

Abstract: Hebel brick (also known as a lightweight brick) is a product of modern building materials because it has a lighter weight but it is stronger than cement bricks and red bricks. Hebel bricks can withstand pressures of more than 4 MPa and are suitable as building wall materials, and speed up construction, and save on cement material costs. One of the most important materials is silica sand in the manufacture of Hebel bricks. The silica sand used in the manufacture of Hebel bricks must have a moisture content of 10 % to 15 %. The purpose of this study is to provide a solution in the form of a drying technique design using a rotational speed control method and a machine that uses biomass-based energy sources. This rotary drying machine is designed to be able to dry wet silica sand into silica sand with water content according to standards. The development of this drying machine begins with making an initial design and parameter analysis. Then proceed to the design, manufacture, and performance testing. The calculation results show that the wet base moisture content has decreased from 33.17 % to 16.58 %, the dry base moisture content decreased from 49.63 % to 19.88 % and drying efficiency also decreased from 63.11 % to 17.11 %. Hence it can be seen that the percentage of wet base moisture content reduced by 50 %, the percentage of dry base moisture content reduced by 59.94 %, and the percentage of drying efficiency reduced by 72.9 %.

Keywords: Building Material, Drying Heat, Hebel Brick, Increase Cost Efficiency, Renewable Energy, Silica Sand.

1. INTRODUCTION

Modern buildings are characterized by the efficient use of raw materials and costs. Hebel brick is a building material that has shifted the role of cement brick and red brick because it has a lighter

weight but is stronger than cement brick and red brick. Hebel brick has a dry density of about 520 kg m^{-3} and a normal density of about 650 kg m^{-3} and is also able to withstand pressures of more than 4 MPa and has a thermal conductivity of 0.14 W m^{-1} k^{-1}. Proven to be very strong for

building wall materials, accelerate construction and save costs of using cement materials [1].

In the manufacture of the Hebel bricks, one of the most important materials is silica sand (SiO_2). Silica sand mining areas are usually close to rivers or beaches, hence after being taken from the mining area, the silica sand still has high moisture content ranging from 60 % to 80 %. Meanwhile, the silica sand used in the manufacture of Hebel bricks must have a slight moisture content ranging from 10 % to 15 %. Hence to get silica sand with moisture content (10 % to 15 %), a drying process is required. To get fast drying results, the silica sand drying process needs to be done using a drying machine. At this time many types of drying machines have been developed, ranging from conveyor-shaped drying machines, oven-shaped drying machines, and some even developing rotary drying machines. Most of these drying machines are still operated using sources of electrical energy and some are using fossil fuel generators. And in recent years, various studies have been conducted by making drying machines that use heat energy from renewable energy sources.

Several researchers have developed drying machines for various purposes, such as Susanto *et al.* [2] has developed the solar-energized drying machine for drying foodstuffs. Sandra [3] has developed a conveyor-shaped drying machine for drying cocoa beans. Estiasih *et al.* [4] has developed the oven-shaped drying machine for the development of food processing technology. Susanto [5, 6] have developed the renewable-energized drying machine for drying silica sand. Hussain *et al.* [7] has developed a drying machine for drying wood. Latifah *et al.* [8] has developed the shoe drying system. Atnaw *et al.* [9] and Yassen *et al.* [10] have developed solar biomass drying systems. Kirar *et al.* [11] has developed the solar cloth drying machine. Nyzam *et al.* [12] has developed a heating system to disinfect rice lice using radiofrequency and microwaves. Macieira *et al.* [13] has developed dry and wet systems to rehabilitate buildings. Rabidin *et al.* [14] has developed the vacuum drying system using kilns and radiofrequency. And Wutthithanyawat *et al.* [15] has developed a drying process by controlling the temperature in the heating zone. Hanif *et al.* [16] have discussed drying for chilies, while Abdullah

et al. [17], Suwati *et al.* [18], and Siskawardani *et al.* [19] discussed seaweed drying. Hence with the increasingly widespread development of renewable-energized drying machines, It is hoped that it can reduce the use of fossil fuels, hence in the future, it can reduce the occurrence of environmental pollution.

2. MATERIALS AND METHODS

2.1 Flow Diagram of Research

The research process was carried out in several stages, namely the first stage by making an initial design and parameter analysis based on heat transfer properties, thermodynamics, and engine elements. The second stage is to optimize the design process. If the results are optimal, it will proceed to the third stage by making the drying machine design drawing. Meanwhile, if the results are not optimal, it will be repeated to the initial design process and parameter analysis. After making the drying machine design drawing is complete, it will proceed to the fourth stage by carrying out the fabrication process for the manufacture of the dryer machine. After the dryer machine is fabricated, it will proceed to the next stage by testing the performance and drying process on the dryer machine. Completely, Figure 1. shows stages carried out in this research.
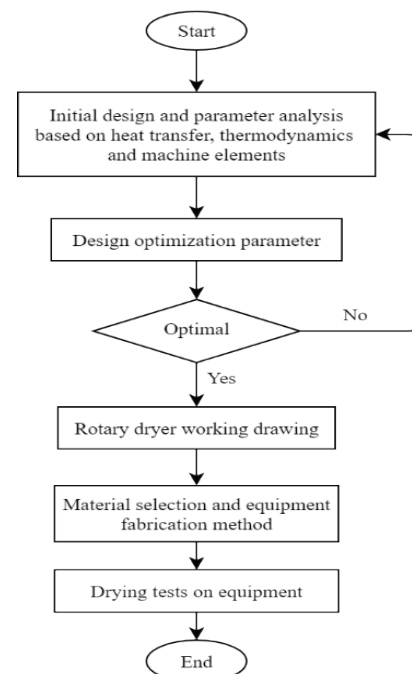
Fig. 1. Flow diagram of the research.

2.2 Working Principle of Biomass-Energized Drying Machine

In the research design of the biomass-energized rotary drying system, the heat used from biomass energy allows the drying process to take place continuously. The silica sand to be dried still has a high moisture content ranging from 60 % to 80 %. Meanwhile, the silica sand used in the manufacture of Hebel bricks must have a slight moisture content ranging from 10 % to 15 %. Hence it takes the amount of wood biomass waste as much as 15 kg h^{-1} with a specific heat of 19.94 kJ kg^{-1}. Figure 2 shows the components of the rotary dryer machine:

The first step in the drying process using the biomass-energized rotary dryer system is by inserting wet silica sand material through the inlet hopper to be channeled into the drying chamber. Drying process of wet silica sand material, by turning the drying chamber using drive motor and flowing hot air generated from the combustion process that occurs in the furnace of biomass. A combination of the drying chamber rotation and hot airflow will facilitate the drying process of wet silica sand material.

The drying chamber rotation will cause stirred and spread the wet silica sand material in the drying chamber, and facilitate the flow of hot air to release the moisture content present in the wet silica sand materials and remove it from the drying chamber. In addition, the drying chamber rotation will facilitate the wet silica sand material to move from the initial entry to exit the drying chamber. The hot air flowed from the biomass furnace, generated from the combustion of biomass waste in the biomass furnace combustion chamber. The heat generated from the combustion chamber is then transferred to the drying air chamber through a heat transfer process. The heat transfer process in the biomass furnace is shown in Figure 3.

3. RESULTS

3.1 Drying Process on the Rotary Drying Machine

To find out the drying process of this rotary dryer machine, it can be known through the following equation. The first step is to calculate the wet base moisture content of silica sand using Equation (1) [2, 5, 6]:

$$MC_{wb} = \frac{W_a}{W_b} \; x \; 100 \; \% \tag{1}$$

Then using Equation (2) to calculate dry base moisture content of silica sand:

$$MC_{db} = \frac{100MC_{wb}}{100 - MC_{wb}} \tag{2}$$

Equation (3) is used to calculate drying rate of silica sand:

$$M = \frac{M_0 - M_t}{\Delta t} \tag{3}$$

Equation (4) is used to calculate the amount of silica sand drying heat:

$$Q = Q_1 + Q_2 + Q_3 \tag{4}$$

Equation (5) is used to calculate Q1 (silica sand
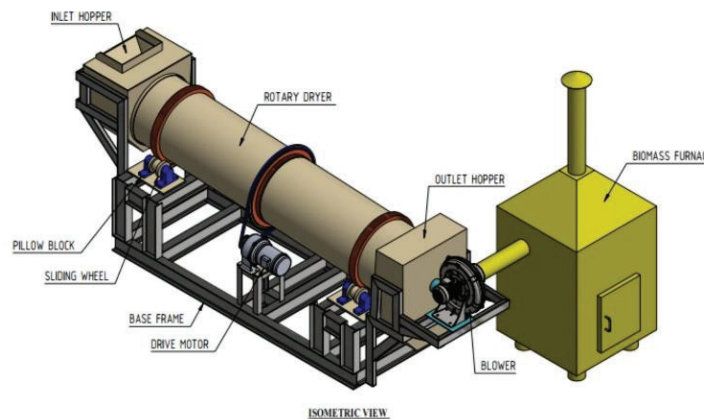
Fig. 2. The rotary dryer machine components.
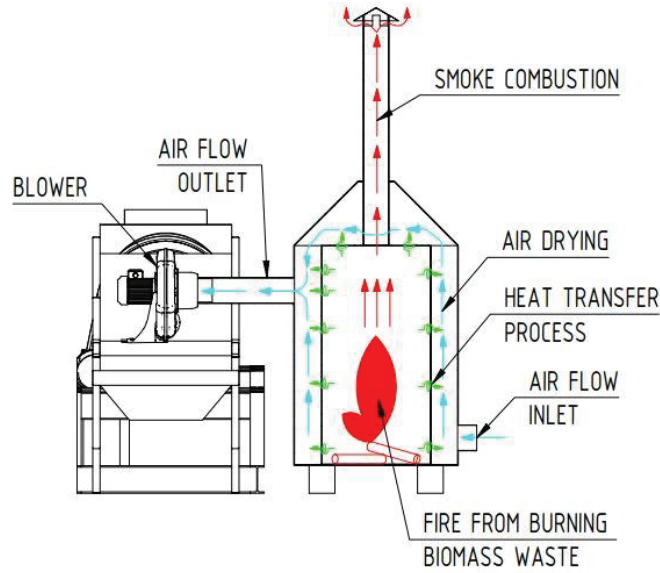
Fig. 3. The heat transfer process occurs in the furnace of biomass.

sensible heat):

$$Q_1 = m_k \cdot c_p \cdot (T_1 - T_0) \qquad (5)$$

Equation (6) is used to calculate Q2 (water sensible heat) and it is used to increase the water temperature in silica sand:

$$Q_2 = m_a \cdot c_a \cdot (T_1 - T_0) \qquad (6)$$

Equation (7) is used to calculate Q3 (water evaporation latent heat) which is the amount of heat used to evaporate water from silica sand:

$$Q_3 = m_w \cdot h_{fg} \qquad (7)$$

Equation (8) is used to calculate the amount of heat received by silica sand:

$$q = \rho \cdot V \cdot c_u \cdot (T_{in} - T_{out}) \qquad (8)$$

Equation (9) is used to calculate the drying efficiency of silica sand:

$$\eta = \frac{Q}{q} \; x \; 100\,\% \qquad (9)$$

Where:

MC_{wb} = Wet base moisture content (%)
MC_{db} = Dry base moisture content (%)
W_a = Silica sand water mass (kg)
W_b = Silica sand wet mass (kg)
M = Drying rate of silica sand (kg s^{-1})

M_0 = Silica sand initial mass (kg)
M_t = Silica sand final mass (kg)
Δ_t = Time interval of drying (s)
Q = Silica sand drying heat (kJ)
Q_1 = Silica sand sensible heat (kJ)
Q_2 = Water sensible heat (kJ)
Q_3 = Water evaporation latent heat (kJ)
q = Heat received by silica sand (kJ)
m_k = Dry silica sand mass (kg)
m_a = Water mass in silica sand (kg)
m_w = Water evaporated mass (kg)
c_p = Silica sand specific heat (J kg^{-1} °C^{-1})
c_a = Water specific heat (J kg^{-1} °C^{-1})
c_u = Air specific heat (J kg^{-1} °C^{-1})
h_{fg} = Water evaporation specific heat (J kg^{-1})
ρ = Silica sand density (kg m^{-3})
V = Drying chamber volume (m3)
T_0 = Silica sand initial temperature (°C)
T_1 = Silica sand final temperature (°C)
T_{in} = Burner intake temperature (°C)
T_{out} = Burner exit temperature (°C)
η = Silica sand drying efficiency (%)

3.2 Drying Process Data Analysis

The following data shows the drying process in the drying machine. Table 1 shows the initial data of the drying machine.

Equations (1) to Equation (9) are used to calculate the drying process and drying efficiency using the data in Table 1. Furthermore, Table 2 and

Table 3 show the calculation results.

Table 2 shows the calculation results of wet base moisture content, dry base moisture content, and drying rate. While Table 3, it shows the calculation results for drying heat and drying efficiency. The calculation results graphs of the drying process and drying efficiency are shown in Figure 4 and Figure 5:

The Figure 4 graph shows that with variations in the rotation of the rotary dryer chamber from 6.6 rpm to 13.2 rpm, the wet base moisture content decreased from 33.17 % to 16.58 % and the dry base moisture content also decreased from 49.63 % to 19.88 %.

The Figure 5 graph shows that with variations in the rotation of the rotary dryer chamber from 6.6 rpm to 13.2 rpm (in SI: 1 rpm = 1/60 Hz), the drying efficiency decreased from 63.11 % to 17.11 %.

4. DISCUSSION

In designing the biomass-energized rotary dryer system, several things must be considered carefully, namely: (i) the material being dried is silica sand, hence it must take into account the erosion of the drying chamber shell. Therefore, it is necessary to design the drying chamber shell with the appropriate thickness and safety with a relatively long lifetime [4, 5]. (ii) To anticipate this equipment used in areas that have not yet received electricity, a generator or renewable-energized power plant must be prepared in advance [2, 5, 6]. (iii) Since heat for the drying process is generated by the furnace of biomass, the fuel from the waste biomass used also affects

Table 1. The initial data of the drying machine.

No	Parameters	Value	Unit
i	Drying chamber Area (A)	0.272	m^2
ii	Drying chamber Length (L)	3	m
iii	Drying chamber Volume (V)	0.81	m^3
iv	Drying air speed (v_u)	11	$m\ s^{-1}$
v	Total volume of the outflow (Q_u)	0.050	$m^3\ min^{-1}$
vi	Wet silica sand mass (m_b)	100	kg
vii	Total mass of the outflow ($\dot{m}$)	4.5	$kg\ min^{-1}$
viii	Air specific heat (c_u)	1 004	$J\ kg^{-1}\ °C^{-1}$
ix	Water specific heat (c_a)	4 180	$J\ kg^{-1}\ °C^{-1}$
x	Silica sand specific heat (c_p)	664	$J\ kg^{-1}\ °C^{-1}$
xi	Water evaporation specific heat (h_{fg})	2 260	$J\ kg^{-1}$
xii	Silica sand initial temperature (T_0)	20	°C
xiii	Silica sand final temperature (T_1)	35	°C
xiv	Burner intake temperature (T_{in})	80	°C
xv	Burner exit temperature (T_{out})	50	°C

Table 2. Drying process calculation results.

n_r	V	m_a	m_k	MC_{wb}	MC_{db}	M
(rpm)*	(m^3)	(kg)	(kg)	(%)	(%)	$(kg\ min^{-1})$
6.6	0.367	33.17	66.83	33.17	49.63	5
7.9	0.306	27.64	72.36	27.64	38.20	5
9.2	0.262	23.69	76.31	23.69	31.05	5
10.6	0.229	20.73	79.27	20.73	26.15	5
11.9	0.204	18.43	81.57	18.43	22.59	5
13.2	0.183	16.58	83.42	16.58	19.88	5

*) In SI: 1 rpm = 1/60 Hz

Susanto et al

Table 3. Drying efficiency calculation results.

n_r	Q_1	Q_2	Q_3	Q	q	η
(rpm)*	(kJ)	(kJ)	(kJ)	(kJ)	(kJ)	(%)
6.6	665.63	2 079.73	74.96	2 820.32	4 468.73	63.11
7.9	720.69	1 733.10	62.47	2 516.27	5 806.06	43.34
9.2	760.02	1 485.52	53.54	2 299.09	7 143.39	32.18
10.6	789.52	1 299.83	46.85	2 136.20	8 480.72	25.19
11.9	812.46	1 155.40	41.65	2 009.51	9 818.05	20.47
13.2	830.82	1 039.86	37.48	1 908.16	11 155.38	17.11

*) in SI: 1 rpm = 1/60 Hz
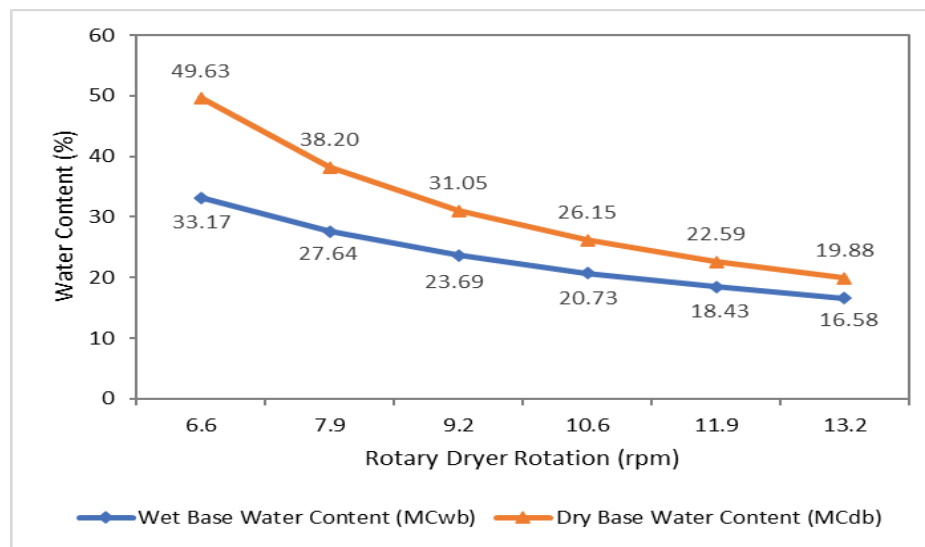
Fig. 4. Graphs of water content (%) vs rotary dryer rotation (rpm) [in SI: 1 rpm=1/60 Hz]
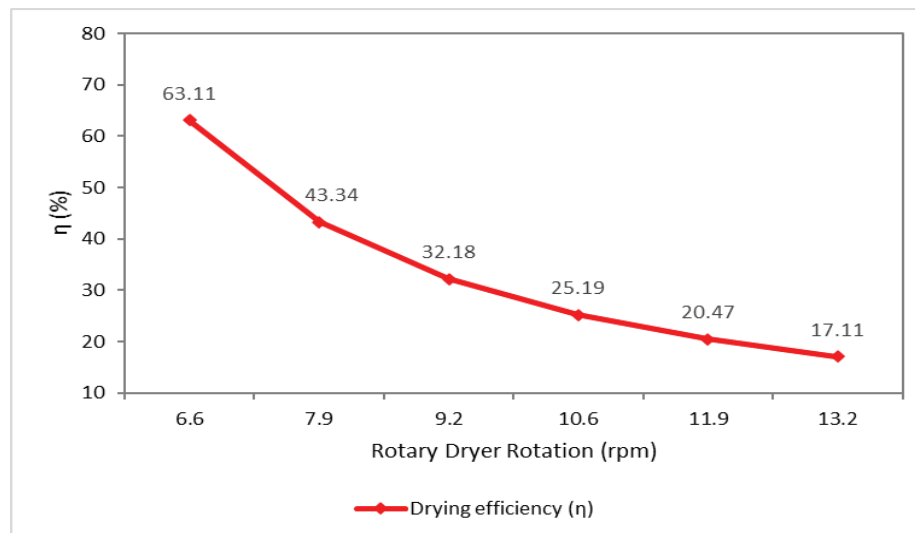
Fig. 5. Graph of drying efficiency (%) vs rotary dryer rotation (rpm [1 rpm = 1/60 Hz]).

the heat generated. The wet biomass waste used will not burn easily, hence it causes combustion in the furnace of biomass to take longer to reach the ideal drying temperature in the drying chamber. Conversely, the dry biomass waste used will burn easily, hence it causes combustion in the furnace of biomass to take faster to reach the ideal drying temperature in the drying chamber. In addition, because the drying process using the rotary dryer machine is carried out for 8 h d^{-1}, the availability of biomass waste is an important thing that must be available. And the amount of biomass waste required for burning in a biomass furnace is around 120 kg d^{-1} [4].

5. CONCLUSION

The biomass-energized rotary drying machine is designed to dry silica sand to make Hebel bricks. This drying machine is used to dry silica sand which has an initial moisture content of 80 % to a moisture content of 15 %. With variations in the rotation of the rotary dryer chamber from 6.6 rpm to 13.2 rpm. The calculation results show that wet base moisture content was reduced by 50 % and dry base moisture content was reduced by 59.94 %. In addition, drying efficiency was also reduced by 72.9 %. Therefore, it is known that drying efficiency gets better when the rotary dryer chamber rotates more slowly.

6. ACKNOWLEDGEMENTS

7. CONFLICT OF INTEREST

The authors declare no conflict of interest.

8. REFERENCES

1. S. Farooq, and I. Yaqoob. Awareness towards efficiency of green and conventional building materials used in Pakistan. *Proceedings of the Pakistan Academy of Sciences A. Physical and Computational Sciences* 56(3):75–84 (2019).

2. H. Susanto, R.H. Setyobudi, Y. Chan., S.M. Nur, E. Yandri, J. Burlakovs, H. Asbanu, Y.A. Nugroho, and Y. Jani. Development of the solar-energized foodstuff drying system for urban communities. *IOP Conference Series: Earth and Environmental Science,* 490(012009):1–11 (2020). DOI: 10.1088/1755-1315/490/1/012009

3. M.P. Sandra, Andasuryani, Santosa, and R. Ekaputri. *Rancang Bangun Alat Pengering Tipe Konveyor Otomatis Untuk Peningkatan Mutu Biji Kakao Hasil Pengeringan.* [Design of Automatic Conveyor Dryers for Quality Improvement of Cocoa Beans from Drying], Universitas Andalas, Indonesia (2009). [in Bahasa Indonesia].

4. T. Estiasih, and K. Ahmadi. *Teknologi Pengolahan Pangan.* [Food Processing Technology], Bumi Aksara, Malang (2011). [in Bahasa Indonesia].

5. H. Susanto, R.H. Setyobudi, D. Sugiyanto, Y. Chan, E. Yandri, S.K. Wahono, K. Abdullah, J. Burlakovs, W. Widodo, Y.A. Nugroho, and A. Yaro. Design of rotary dryer for sand drying using biomass energy sources. *E3S Web of Conferences* 226(00024):1–12 (2021). DOI: 10.1051/e3sconf/202122600024

6. H. Susanto, K. Abdullah, A.S. Uyun, S.M. Nur, and T.M.I. Mahlia. Turbine design for low heat organic rankine cycle power generation using renewable energy sources. *MATEC Web of Conferences* 164(01012):1–17 (2018). DOI: 10.1051/matecconf/201816401012

7. T. Hussain, M. Shamraiz, and S.U. Abrar. Effect of temperature and vacuum on the drying rate and various parameters of wood samples, using an indigenously designed and developed vacuum drying system. *International Journal of Technology* 5:795–809 (2016). DOI: 10.14716/ijtech.v7i5.2135

8. A. Latifah, H. Aulawi, and M.A. Ramdhani. Design of the automatic shoe dryer. *MATEC Web of Conferences* 197(11009):1–6 (2018). DOI: 10.1051/matecconf/201819711009

9. S.M. Atnaw, C.K.M. Faizal, and A.J. Oumer. Development of solar biomass drying system. *MATEC Web of Conferences* 97(01081):1–7(2017). DOI: 10.1051/matecconf/20179701081

10. T.A. Yassen, H.H. Al-Kayiem, and K. Habib. Evaluation of hybrid solar – biomass dryer with no load. *MATEC Web of Conferences* 13(06007):1–5 (2014). DOI: 10.1051/matecconf/20141306007

11. D.S. Kirar, H.S. Bhadoria, and R. Pandey. Configuration and development of a solar cloth dryer. *MATEC Web of Conferences* 57(01019):1–5 (2016). DOI: 10.1051/matecconf/20165701019

12. S.Z.A. Nyzam, R.A. Rahim, and H.A. Rahim. Review article of radio frequency and microwave heating treatment to disinfest kutu beras in Malaysian

rice. *MATEC Web of Conferences* 140(01023):1–6 (2017).
DOI: 10.1051/matecconf/201714001023

13. M. Macieira, and P. Mendonca. Building rehabilitation with dry and wet systems – embodied water comparison. *MATEC Web of Conferences* 68(13009):1–7 (2016).DOI: 10.1051/matecconf/20166813009

14. Z.A. Rabidin, G.K. Seng, and M.J.A. Wahab. Characteristics of timbers dried using kiln drying and radio frequencyvacuum drying systems. *MATEC Web of Conferences* 108(10001):1–5 (2017). DOI: 10.1051/matecconf/201710810001

15. C. Wutthithanyawat, and N. Srisiriwat. Temperature control of heating zone for drying process: effect of air velocity change. *MATEC Web of Conferences* 65(03002):1–3 (2016). DOI: 10.1051/matecconf/201665030

16. M. Hanif, M.K. Khattak, M. Rahman, M. Aamir, M. Ramzan, M. Amin, M. Khan, and S. Shiekh. Convective drying of chilies using a concentrating solar collector. *Proceedings of the Pakistan Academy of Sciences* 52 (2): 103–107 (2015).

17. K. Abdullah, A.S. Uyun, R. Soegeng, E.Suherman, H. Susanto, R.H. Setyobudi, J. Burlakovs, and Z. Vincēviča-Gaile. Renewable energy technologies for economic development. *E3S Web of Conference* 188(00016): 1–8 (2020). DOI:10.1051/e3sconf/202018800016

18. S. Suwati, E. Romansyah, S. Syarifudin, Y. Jani, A.H. Purnomo, D. Damat and E. Yandri. Comparison between natural and cabinet drying on weight loss of seaweed *Euchuema cottonii* Weber-van Bosse. *Sarhad Journal of Agriculture,* Special issue 1:1–8 (2021). DOI: 10.17582/journal.sja/2021/37.s1.01.08

19. D.D. Siskawardani, S. Winarsih and K. Khawwee. The antioxidant activity of Kelor (*Moringa oleifera* Lam.) leaves based on drying method. *Jordan Journal of Biological Sciences* 14(2): 291–295 (2021).

Pakistan Academy of Sciences

Research Article

Facility Planning Optimization Platform, GGOD, for Expandable Cluster-type Micro-grid Installations and Operations

Kazuaki Iwamura[1*], Yosuke Nakanishi[1], Udom Lewlomphaisarl[2], Noel Estoperez[3], and Abraham Lomi[4]

[1]Waseda University, Graduate School of Energy and Environment, 3-4-1 Okubo,
Shinjuku-ku, Tokyo 169-8555, Japan
[2]National Advanced Automation and Electronics Research Unit, 112 Phahonyothin Road,
Khlong Nueng, Khlong Luang District, Pathumthani 12120, Thailand.
[3]Mindanao State University, Illigan Institute of Technology, Illigan City, Andres Bonifacio Ave,
Iligan City, 9200 Lanao del Norte, Philippines
[4]Renewable Energy Research Center, National Institute of Technology Malang,
Jl. Raya Karanglo, Km. 2, Malang 65143, Indonesia

Abstract: This paper describes the architecture and the utilization for a facility planning optimization platform called GGOD, "Grid of Grids Optimal Designer" and applies it to expandable cluster-type micro-grid installations and operations. The expandable cluster-type micro-grid is defined as a group of micro-grids that are connected by bi-directional power transfer networks. Furthermore, power sources are also networked. Especially, by networking among power sources, powers necessary for social activities in-demand areas are secured. The proposed architecture is based on service-oriented architecture, meaning that optimization functions are executed as services. For flexibility, these services are executed by requests based on extensible mark-up language texts. The available optimizations are written in meta-data, which are accessible to end-users from the meta-data database system called clearinghouse. The meta-data are of two types, one for single optimization and the other for combined optimization. The processes in GGOD are conducted by the management function which interprets descriptions in meta-data. In meta-data, the names of optimization functions and activation orders are written. The basic executions follow sequential, branch, or loop flow processes, which execute combined optimizations, compare more than two kinds of optimization processes, and perform iterative simulations, respectively. As an application of the proposed architecture, the power generation sites and transmission networks are optimized in a geospatial integrated-resource planning scenario. In this application, a structure and a method for the combination of component functions in GGOD are exemplified. Moreover, GGOD suggests promotions of a lot of applications by effective combinations of basic optimization functions.

Keywords: Clearinghouse, Grid of Grids Optimal Designer, Power Generation Sites, Service-Oriented Architecture, Transmission Networks.

1. INTRODUCTION

A micro-grid is a feasible power supply system [1, 2] with sustainable power generation; accordingly, it has been introduced in many areas of the world. Moreover, new micro-grid concepts, the cluster-type micro-grids [3, 4], are expected to be introduced in non-electrified areas. Cluster-type micro-grids offer local power generation, resilient and sustainable operation using renewable powers, and power transfer with other micro-grids to balance power generations and consumptions over a large area.

However, reducing the installation and operation costs of micro-grids is imperative. This can be achieved by optimizing the installation and operation in simulations. Two well-known planning

optimization simulators are Hybrid Optimization Models for Multiple Energy Resources (HOMER) [5] and the Wien Automatic System Planning Package (WASP) [6].

HOMER, developed by National Renewable Energy Laboratory (NREL) in the USA, optimizes the installation and operation costs of various renewable power generators within a designated operation period. However, it does not optimize the facility specifications.

WASP considers the construction and operation costs in power-generation planning but ignores the construction costs of transmission networks that connect the power generating sites to the main grids or demand areas.

To resolve the above optimization problems, this study proposes a new planning optimization simulator called GGOD, "Grid of Grids Optimal Designer. GGOD is an evolving simulator, and the planning simulation platform and testbed have been developed in the current stage. This paper explains the GGOD architecture and presents an example of its application.

2. MATERIALS AND METHODS

2.1 Architecture of GGOD

The GGOD simulator is developed according to service-oriented architecture (SOA), which stores and executes the optimization functions as services. GGOD is incorporated into a total structure comprising three layers: the end-user layer, the service-manager layer, and the service execution layer. Figure 1 shows the architecture of GGOD. The functions of each layer are described below.

- End-user layer: The end-user layer represents the client systems, which send optimization requests to and receive optimization results from the service-manager layer.

- Service manager layer(broker): The service-manager layer includes web-adjusted interface functions and management functions. The web-adjusted interface functions comprise the clearinghouse function for storing meta-data, the data conversion function, and the acceptance-and-

dispatch functions. The meta-data provided by the clearinghouse function explain optimization and analysis components to end-users. The data conversion function converts a request data sent by end-users to a command sequence of optimization and analysis. The acceptance-and-dispatch function receives requests from end-users and returns optimization results to requesting client systems (result dispatch). The manager function activates optimization and/or analysis components in the service execution layer, and monitors and manages the progress of the optimization processes.

- Service execution layer(supplier). The service execution layer contains optimization and/or analysis components, which are registered in a database called a repository. There are two types of components: wrapped functions for automatic execution, and non-wrapped functions that enable the use of commercial software packages by manual operation. Examples of optimization and analysis components are shown in Table 1. As GGOD is an evolving system, the registration of new components enables the execution of new optimizations and analyses.

Table 1. Examples of components

Component Classification	Component name	Content of functions
Optimization	Facility installation and operation	Introduction cost minimization for micro-grid power facilities
	Renewable power generation site selection	Clustering of renewable sites based on geographical portfolio theory
	Transmission network generation	Transmission network generation based on cost minimization of facility construction
	Economical estimation	Techno-economical transmission expansion analysis
	Combinatorics	Shortest path finding, Minimum spanning tree search
Analysis	Power flow analysis	Stochastic power flow analysis
	Impact analysis	Impact assessment on the environment and social activities

2.2 Optimization Method and Process in GGOD

Optimizations and analyses in GGOD are executed by two processing flows, the meta-data reference, and the optimization. The optimization execution is shown in Figure 2.

2.2.1 Meta-data based method for optimizations process

The clearinghouse function in the web-adjusted interface provides the meta-data for optimization and analysis to end-users. The meta-data explain the optimization/analysis processing and indicate the input and output data specifications. Optimization component suppliers register the optimization/ analysis components into the repository and the meta-data into the meta-database. The end-users confirm the meta-data and decide optimization processes to be executed.

Meta-data are written in the extensible mark-up language (XML) format. XML data are expressed by a start-tag (<*>), the contents, and an end-tag (</*>), for instance, <Name> Content </Name>. Meta-data of single components differ from those of combinations of more than two single components. Meta-data for single components give the name of optimization, the explanation of optimization processing, and the input and output data forms and specifications. The meta-data of combined components provide the names of the single components and their execution order. Multiple optimizations can be ordered in three basic ways (Figure 3): sequential process type for executing the multiple optimizations in series, branch process type for performance comparisons of more than two types of optimization components, and loop process type for iterative executions.

2.2.2 Optimization process

The optimization service starts when a request arrives from the acceptance-and-dispatch function in the web-adjusted interface. The management
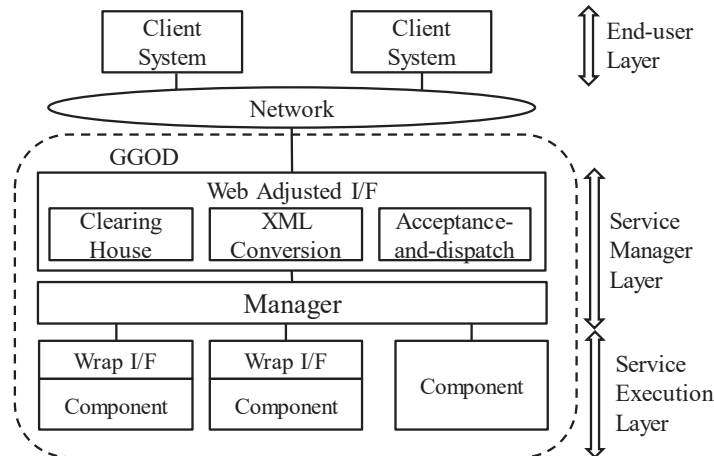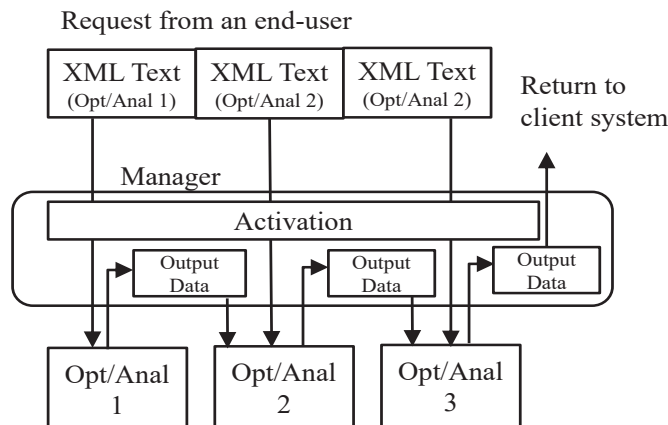

Fig. 1. Optimization process in GGOD.

Fig. 2. Optimization process in GGOD.

function analyzes the request texts, converts the single optimizations into a group of requests, and determines the optimization processing order, thereby monitoring and managing the optimization processes. After the optimization process, the output of processing results is temporarily stored in the memory for use by the subsequent optimization/analysis components.

3. RESULTS

GGOD optimization is applied to geospatial integrated-resource planning (GIRP), a facility installation planning of renewable power generation clusters and power transmission networks that transfer renewable powers to the access points (APs) of main grids or demand areas. The GIRP planning corresponds to geospatial planning in the International Renewable Energy Agency report [7]. The objectives of GIRP are (i) optimizing the selection of renewable power generation sites to minimize the total variance of generated powers, and (ii) optimizing transmission routes to minimize the total construction cost. In the present application, the power is generated from winds. The optimization processing order, contents of input and output data are shown in Figure 4.

3.1 Renewable Power Selection

Wind power generation sites are obtained based on the modern portfolio selection theory in financial research [8]. First, feasible wind power generation areas are determined using three-dimensional geographic data (terrain data) and wind velocity data. Terrain geographic data are ground-height data that corresponds to a digital elevation model (DEM), which also provides mesh data. All meshes are regular squares and the height values are assigned at four corner points. The wind velocities are measured at observation stations. The velocities at the centers of all squares in the DEM mesh are calculated by interpolating at least four measured data.

Next, a mesh of the highest velocities is selected. Then, the neighboring meshes are gathered to minimize the fluctuation variance of power generations among the selected meshes. The selection processes are iterated [9] until the variances at the wind power generation areas and

wind farm (WF) sites are minimized.

3.2 Shortest-Transmission Route-Finding

Step 1 of the proposed flow selects the wind power generation sites. The power transmission routes are then searched using the shortest-transmission route-finding algorithm in the DEM. This scheme applies the Dijkstra algorithm [10] to obtain the power transmission routes among the WFs searched in the renewable power selection, and the APs (i.e., the connection points in the existing transmission network or demand areas). Thus, all routes that combine the WFs and AP points are calculated.

3.3 Transmission Network Selection

The final optimization process is transmission network selection. All WF candidates are selected by renewable power selection, and all candidates of the transmission routes are searched by shortest-transmission route finding. The transmission networks without loops are then selected and connected to the APs or demand areas. The selection is constrained by insisting that the total power generation capacity of the WFs exceeds the target capacity. The objective is to select the transmission networks that minimize the total facility construction costs of both WFs and transmission network lines [11, 12].

The total number of selections of 100 WF sites is 2^{100}. As checking all selections is impractical, the appropriate WFs and their transmission networks are found by meta-heuristics based on the genetic algorithm. The genetic algorithm minimizes objective functions (of the construction costs in this example) by performing crossover, mutations, and selections to achieve its goal [10]. The final optimized selections of WFs and transmission network networks are shown in Figure 5.

The target value of total power selection is set to 2 GW previously. The main results by optimization are as follows.

- Selected total power capacity: 2.02 GW.
- The total length of transmission networks: 279.2 km

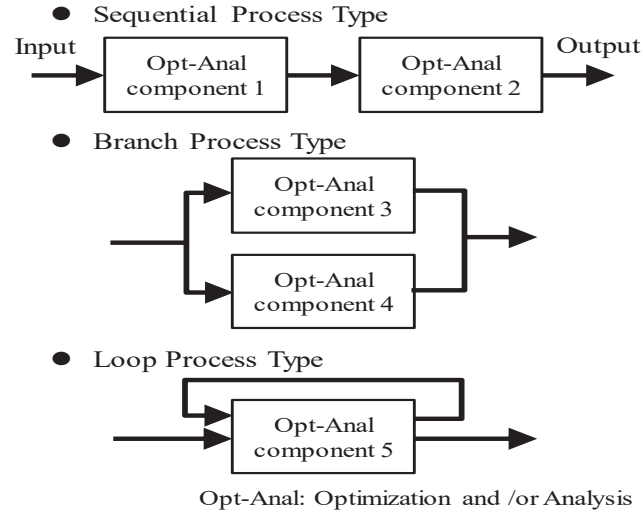The target of the power selection is satisfied.

Fig. 3. Processing orders for basic optimizations in GGOD.
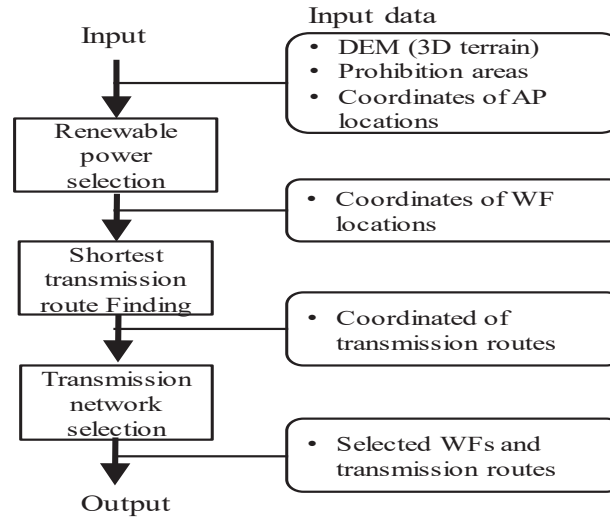
Fig. 4. The optimization process of GGOD.
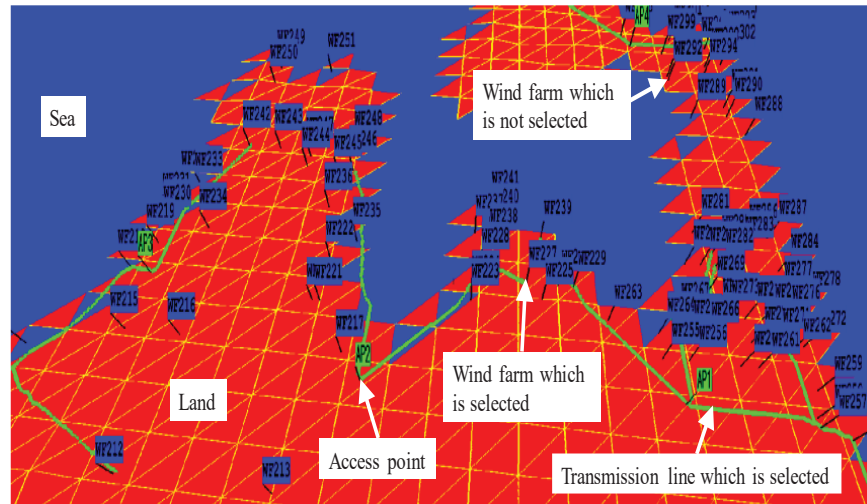
Fig. 5. Results of GIRP (Optimized selections of WFs and Transmission networks).

The total length changes according to the selection of power sites. In other power selection cases, the total lengths of transmission networks are more than 298.1 km. Thus the optimization is accomplished. Total processing time is optimization processing times. The time of processing management by GGOD is negligible.

4. DISCUSSION

The GGOD executed optimization processes based on meta-data interpretation. The important points are described below.

- Optimization processes are decomposed into basic functions, renewable power selection, shortest-transmission route finding, and transmission network selection. These functions can be developed separately and each function would be utilized in other applications. A combination of basic functions generates interesting results. By enriching basic functions, application fields would be expanded.
- The management function properly analyzes meta-data and activates optimization and analysis functions.
- Optimization and analysis functions are developed by a lot of researchers and engineers. The availability of these functions depends on meta-data description. Especially, accuracies for descriptions of input/ output data specifications are important.
- Geographical processing is an important characteristic of GGOD.

5. CONCLUSION

This paper introduced an SOA-based facility planning optimization platform called GGOD, a flexible optimization service that offers many kinds of optimization services. GGOD is composed of three layers: the end-user layer, the service manager layer, and the service execution layer. The end-user layer is composed of client systems, while the service manager and service execution layers are implemented in GGOD. The service manager layer is the broker function that activates and manages the optimization functions in the service execution layer. The service execution layer includes

optimization and analysis tools.

The important characteristics of GGOD are listed below. (i) By registering various optimization and analysis components in GGOD, GGOD will become more available to many applications. (ii) The stored geospatial data enables analyses of real-world conditions. (iii) GGOD is an evolving system that registers and applies new optimization/ analysis components. These components are easily incorporated by updating the previous components and meta-data.

The optimization processing comprises meta-data selection and optimization steps. The meta-data is written in the XML format, which flexibly states the optimization name, an explanation of the optimization, and the specifications of the input and output data.

To demonstrate the usefulness of the platform, GGOD was applied to GIRP. The GIRP was executed by sequentially executing three optimization/ analysis components: renewable power selection, shortest-transmission route finding, and transmission network selection. The result shows that optimization is executed successfully. The processing capability and processing time depend on the effectiveness of optimization components.

In future work, the available optimization/ analysis components will be extended to distribute optimal components to various power researchers and engineers.

6. ACKNOWLEDGEMENTS

7. CONFLICT OF INTEREST

The authors declare no conflict of interest.

8. REFERENCES

1. C. Schwaegerl, and L. Tao. The microgrids concept. In: *Microgrids: Architecture and control.* N. Hatziargyriou (Ed). Wiley, New Jersey, USA. p. 4–7 (2014). DOI: 10.1002/9781118720677.ch01

2. B. Novianto., K. Abdullah., A.S. Uyun., E. Yandri., N.S. Muhammad., H. Susanto., Z. Vincēviča-Gaile, R.H. Setyobudi, and Y. Nurdiansyah. Smart micro-grid performance using renewable energy. *E3S Web Conference* 188(00005): 1–11 (2020). DOI: 10.1051/e3sconf/202018800005

3. K. Iwamura., Y. Nakanishi., H. Takamori., U. Lewlomphaisarl., N. Estoperez, and A. Lomi. Optimal design suite for expandable micro-grid clusters. *7th International Conference on Renewable Energy Research and Applications,* Paris, France, 2018, p. 354–359 (2018). DOI: 10.1109/ICRERA.2018.8566707

4. S. Ahmad., M.H. Zafar., M. Ashraf., I. Khan, and F.Q. Khan. Energy-Efficient TDMA based Clustering Scheme for WSN. *Proceedings of the Pakistan Academy of Sciences: A. Physical and Computational Sciences* 55 (3): 53–65 (2018)

5. Homer. *HOMER page website.* [Online] from https://www.homerenergy.com, (2019) [Accessed on July 27th, 2019].

6. WASP. *WASP page website*. [Online] from https://www.energyplan.eu. (2019) [Accessed on July 27th, 2019].

7. International Renewable Energy Agency. *Planning for the renewable future: Long-term modelling and tools to expand variable renewable power in emerging economies.* [Online] from https://www.irena.org/publications/2017/Jan/Planning-for-the-renewable-future-Long-term-modelling-and-tools-to-expand-variable-renewable-power.* (2017) [Accessed on July 27th, 2019].

8. S.D. Stewart., C.D. Piros, J.C. Heisler. *Portfolio Management: Theory and Practice.* John Wiley & Sons, US (2019).

9. K. Nishiyama., K. Iwamura, and Y. Nakanishi. Optimized site selection for new wind farm installations based on portfolio theory and geographical information. *8th IEEE PES Innovative Smart Grid Technologies Conference North America* (Washington, USA, 2019). DOI: 10.1109/ISGT.2019.8791636

10. B. Korte, and J. Vygen. *Combinatorial Optimization, Theory and Algorithms.* Springer Nature, Switzerland AG. (2018).

11. B.R. Phillips, and R.S. Middleton, SimWIND: A geospatial infrastructure model for optimizing wind power generation and transmission. *Energy Policy* 43:291–302(2012). DOI: 10.1016/j.enpol.2012.01.006

12. K. Iwamura., R. Kobayashi., K. Nishiyama, and Y. Nakanishi. A combined geospatial approach to extension planning of wind farms and transmission networks. *8th IEEE PES Innovative Smart Grid Technologies Conference Europe* (Sarajevo, Bosnia-Herzegovina, 2018). p. 1–6 (2018). DOI: 10.1109/ISGTEurope.2018.8571437

Pakistan Academy of Sciences

Research Article

Design and Simulation "Ha"-Slot Patch Array Microstrip Antenna for WLAN 2.4 GHz

Sotyohadi Sotyohadi[1*], I Komang Somawirata[1], Kartiko Ardi Widodo[1], Son Thanh Phung[2], and Ivar Zekker[3]

[1]Department of Electrical Engineering, National Institute of Technology (ITN) Malang,
Jl. Raya Karanglo Km. 2, Malang 65145, East Java, Indonesia
[2]Faculty of Electrical and Electronics Engineering (FEEE), Ho Chi Minh City University of
Technology and Education (HCMUTE), 01 Vo Van Ngan Street, Thu Duc District,
Ho Chi Minh City, Vietnam
[3]Institute of Chemistry, University of Tartu, Ravila 14a, 50411 Tartu, Estonia

Abstract: This paper presents a linear 1 × 2 "Ha (ᨀ)"–slot patch array microstrip antenna. The proposed design of an array microstrip antenna is intended for Wireless Local Area Network (WLAN) 2.4 GHz devices. From the previous research concerning the single patch "Ha (ᨀ)"–slot microstrip antenna, the gain that can be achieved is 5.77 dBi in simulation. This value is considered too small for an antenna to accommodate WLAN devices if compare to a Hertzian antenna. To enhance the gain of microstrip antenna, some methods can be considered using linear 1 × 2 patch array and T-Junction power divider circuit to have matching antenna impedance. The distances between two patches are one of the important steps to be considered in designing the patch array microstrip antenna. Thus, the minimum distance between the patch elements are calculated should be greater than $\lambda/2$ of the resonance frequency antenna. If the distance less than $\lambda/2$ electromagnetically coupled will occur, vice versa when it is to widen the dimension of the antenna will less efficient. Epoxy substrate Flame Resistant 4 (FR4) with dielectric constant 4.3 is used as the platform designed for the array antenna and it is analyzed using simulation software Computational Simulation Technology (CST) studio suite by which return loss, Voltage Standing Wave Ratio (VSWR), and gain are calculated. The simulation result showed that the designed antenna achieve return loss (S11) -25.363 dB with VSWR 1.1 at the frequency 2.4 GHz, and the gain obtained from simulation is 8.96 dBi, which is greater than 64.4 % if compared to the previous one. The proposed antenna design shows that increasing the number of patches in the array can technically improve the gain of a microstrip antenna, which can cover a wider area if applied to WLAN devices.

Keywords: CST Studio Suite, Flame Resistant 4, Return Loss (S11), T-junction, Voltage Standing Wave Ratio.

1. INTRODUCTION

Antenna can be classified as the transducer, which is able to transfer energy from one form to another [1–3]. From this meaning, the antenna has a very important role in wireless telecommunication, because the antenna is a metal conductor that can radiate and harvest radio waves [4]. Along with the rapid development of wireless communication devices, the need for an antenna in a small size, compact, lightweight, and the ability to work in a wide band frequency is required. One type of antenna which suitable for this requirement is a

microstrip antenna [5]. Besides some advantages possessed by microstrip antenna, there are also disadvantages such as poor efficiency, narrow bandwidth, and low gain, which becomes a major problem for mobile communication designers [6]. From previous research on the single patch "Ha (ᨀ)"-slot microstrip antenna, the gain obtained is 5.77 dBi for simulation, and the gain from the antenna after fabrication and measurement it reaches only 3.576 dBi [7]. This value is relatively low if compared to other types of antenna such as Hertzian antenna [8]. To accommodate WLAN devices, the gain of the single patch microstrip

antenna should be improved, thus it can operate in the 2.4 GHz frequency and can cover a wider area [9]. Some considerable methods and techniques can be used to overcome this problem. One method that has been utilized to improve the gain of microstrip antenna is the patch arrangement in an array [10]. An antenna array is a combination of several connected antennas arranged to form a single antenna [11]. The main benefits of array microstrip antenna are the increase of overall gain, providing reception of diversity, and interference canceling from a common set of directions [9].

In this research a linear 1×2 "Ha (ᴖᴔ)"-slot patch array microstrip antenna is designed and simulated, as the development and improvement of a single patch "Ha (ᴖᴔ)"-slot microstrip antenna [7]. Thereafter, the design was simulated using CST studio suite student version software to have the result of return loss (S11), VSWR, and antenna gain.

2. MATERIALS AND METHODS

2.1 "Ha(ᴖᴔ)"-slot Microstrip Antenna

The linear 1×2 "Ha (ᴖᴔ)"-slot patch array microstrip antenna is designed to work for frequency 2.4 GHz. This frequency is an ISM (Industrial, Scientific, and Medical) which is not regulated and can be freely used [12]. Material parameters for the simulation are set for the dielectric substrate FR4, which has the dielectric permittivity constant $(\varepsilon_r) = 4.3$ and the substrate thickness (h) = 1.5 mm.

The basic design of the linear 1×2 "Ha (ᴖᴔ)"-slot patch array microstrip antenna is based on a single patch "Ha (ᴖᴔ)"-slot microstrip antenna, which can be shown in Figure 1 [7].

The dimension and annotation of the single patch microstrip antenna can be explained in the Table 1 [7].

2.2 Patch Array Microstrip Antenna Design

Based on the single patch "Ha (ᴖᴔ)"-slot microstrip antenna design, the "Ha (ᴖᴔ)"-slot patch array was developed in a corporate feed network. The design of the two-element microstrip patch array antenna with the "Ha (ᴖᴔ)"– slot can be shown in Figure 2.

In order to achieve the design shown in Figure 2, three steps need to be carried out. Namely, obtaining the distance between two patches, the width dimensions, and the length of the microstrip antenna patch array two-element.

The first step is to determine the distance between patch array elements. The minimum distance between the elements for the patch array is $\lambda/2$ of the resonance frequency antenna in Equation (1) [13].

$$d = \lambda/2 = v/(2 \times f) \tag{1}$$

Where d is the distance between patches, v is the velocity of light in free space $(3 \times 10^8 \text{ m s}^{-1})$, and f is the resonance frequency of the antenna.

The estimation of the minimum distance between elements is due to the effect of electromagnetically coupled which occurs if the distance between elements is less than $\lambda/2$. However, the microstrip antenna substrate dimension will result in less efficiency if the distance is too wide.

The second step is to determine the width of the ground plane (W_g) microstrip patch array antenna of two elements. The Wg can be calculated by Equation (2):

$$W_g = (2 \times c) + (2 \times W_p) + d \tag{2}$$

Where W_p is the width of the patch, c is the distance between the edge of the substrate and the patch, and d is the distance between patches.

The third step is to determine the length of the ground plane (L_g). The L_g can be calculated with the consideration of the T-Junction dimension in Equation (3). To ease the calculations of dimension T- Junction, notation #1 to #6 is added, which is shown in Figure 2.

$$L_g = a + L_p + d' + L_{\#5} + (L - 0.695\,5) \tag{3}$$

Where a is the distance between the edge of the upper side of the microstrip antenna and the patch, L_p is patch length which both of them have the same length, d' is the length of the microstrip feed line which has an impedance of 50 Ω, $L_{\#1}$ and $L_{\#5}$ are the T-junction lengths of the power divider and
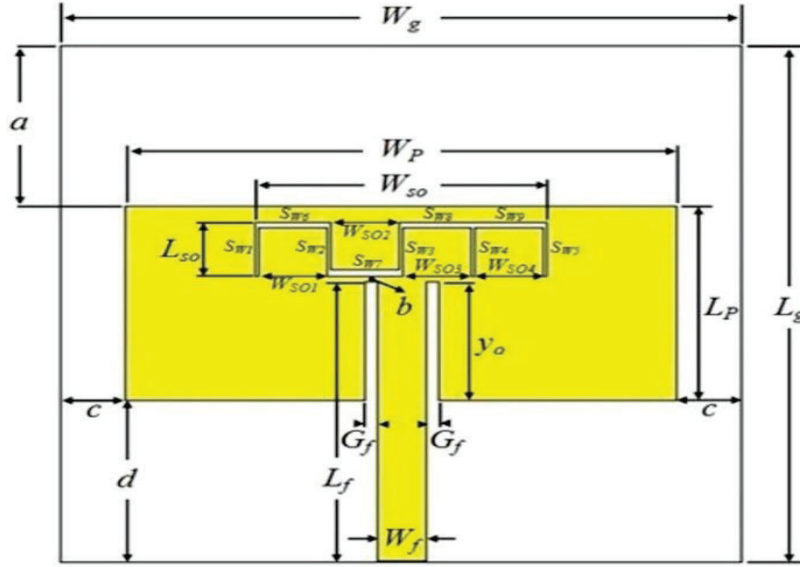
Fig. 1. Single patch "Ha"-slot microstrip antenna.
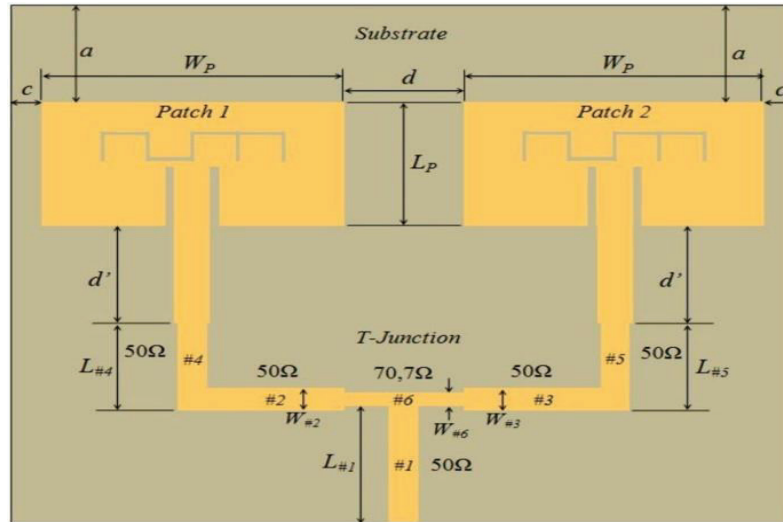
Fig. 2. 1×2 "Ha"-slot patch array microstrip antenna in a corporate feed.

matching impedance and 0.695 5 (mm) is the width difference between $L_{\#6} - L_{\#2}$ or $L_{\#6} - L_{\#3}$ because the width of $L_{\#2}$ and $L_{\#3}$ are equal.

2.3 T-Junction Power Divider

T-Junction is a method to connect the two patch microstrip antenna as a radiating element arranged in a row (corporate feed). The utilization of the T-Junction power divider method as a feeder and signal distributor to both patches is on the simplicity of matching by adjusting the position of the inset feeding and it is relatively easy to model it [14]. Figure 3 shows the standard form of the T-Junction power divider [14].

From the T-Junction design shown in Figure 3, the procedure to obtain the dimensions of the microstrip feed line for Power Divider are as follows:

i. For designing two-element array or 1×2 patch array microstrip antenna arranged incorporate feed, a power divider is needed to connect the two elements of the microstrip antenna array with a transmission line, which generally has a 50 Ω impedance. To calculate both impedance matching can be obtained using Equation (4) [15].

$$Z = Z_0 \times \sqrt{N} \qquad (4)$$

Table 1. Dimension of single patch "Ha"-slot microstrip antenna.

Antenna Dimension	Annotation	Value (mm)
L_p	Patch Length	18
W_p	Patch Width	38.393 4
L_g	Ground plane Length	48
W_g	Ground plane Width	47.393 4
L_f	Microstrip feed line Length	26
W_f	Microstrip feed line Width	3.363 9
G_f	Inset feed Gap	0.9
y_o	Inset feed line Length	11.035 6
a	Distance between top edge with patch	15
b	Gap between slot with microstrip feed line	0.464 4
c	Distance between side edge with patch	4.5
d	Distance between bottom edge with patch	15
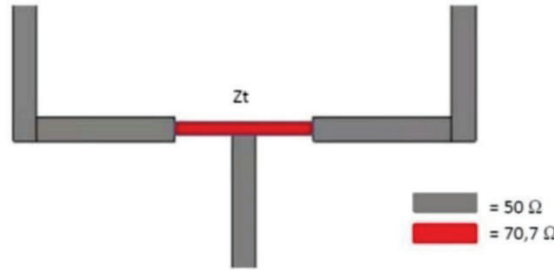
Fig. 3. T-Junction power divider.

Where Z is the required impedance value according to the number of microstrip antenna element arrays, Z_0 is the input impedance of the microstrip (Z_{in}) antenna, and N is the number of elements or arrays of microstrip antennas.

ii. After the value of Z is obtained, the next step is to calculate the dimensions of the microstrip line input impedance Z_{in}. The width (W) and length (L) of the microstrip line 50 Ω can be calculated. Start calculating the susceptance (B) [2] of the microstrip line using Equation (5).

$$B = (60 \times \pi^2) / (Z_0 \times \sqrt{\varepsilon_r}) \qquad (5)$$

Where B is the value of susceptance, π is a constant value of 3.14, Z_0 is the impedance of the transmission line and the 50 Ω antenna channel (Z_{in}) and ε_r is the relative permittivity of the substrate material of the antenna.

After calculating the value of B, the next step is calculating the width (W) [4] of the power divider by using Equation (6).

$$W = \frac{2h}{\pi}\left\{B - 1 - ln(2B - 1) + \frac{\varepsilon_r - 1}{2.\varepsilon_r}\left[ln(B - 1) + 0.39 - \frac{0.61}{\varepsilon_r}\right]\right\} \qquad (6)$$

iii. Length (L) of impedance 50 Ω microstrip line can be obtained with Equation (10). However, before calculating the length of the microstrip line 50 Ω, the ratio of the width microstrip feed line to the thickness of the substrate (W/h) should be examined by Equation (7) [4].

$$W / h > 1$$

If the requirement of $W/h > 1$ is met, then the dielectric constant value (ε_{eff}) can be calculated using Equation (7) as follows [24].

$$\varepsilon_{eff} = \frac{(\varepsilon_r + 1)}{2} + \frac{(\varepsilon_r - 1)}{2}\left[\frac{1}{\sqrt{1 + 12\left[\frac{h}{W}\right]}}\right] \quad (7)$$

As a result of the microstrip antenna effective area, the effective wavelength of the antenna is obtained using Equation (8):

$$\lambda_0 = v/f \quad (8)$$

Where, v is the velocity or speed of light in free space (v_0) 3×10^8 m s^{-1} and f is the resonance or operating frequency of the antenna in units (Hz) or cycle per second (c s^{-1}).

Moreover, the effective length (λ_g) of the microstrip antenna can be obtained by Equation (9).

$$\lambda_g = \lambda_0 / \sqrt{\varepsilon_{eff}} \quad (9)$$

Finally, the length (L) of the microstrip feed line can be calculated in Equation (10) with an impedance of 50 Ω. The effective length of the antenna is a quarter lambda (λ/4) of the effective wavelength, according to Equation (10).

$$L = \lambda_g / 4 \quad (10)$$

The microstrip line 70.7 Ω can be obtained using the calculation in step 2 and step 3.

2.3 Proposed Antenna

The proposed design of the linear 1×2 "Ha (ꡧ)"-slot patch array microstrip antenna is shown in Figure 4.

The calculation results obtained for ground plane length (L_g) as follows:

$$Lg = 15 + 18 + 15 + 17.291\ 5 + (17.715 - 0.695\ 5)$$
$$L_g = 82.311 \text{ mm}$$

The width of the ground plane (W_g) is obtained as follows:
$$W_g = (2 \times 45) + (2 \times 38.393\ 4) + 62.5$$
$$W_g = 229.286\ 8 \text{ mm}$$

The dimension of Figure 4 and the power divider is given in the following Table 2.

Besides the design of the patch array microstrip antenna, the antenna power divider becomes the essential part of the design. In order to have the matching impedance of both patch array microstrip antennas, it is necessary to calculate the value of the T-Junction power divider, which can be explained in four steps.

i. Determine the impedance of power divider Z. From Equation (4) the value of required impedance for two elements can be obtained. If Z0 = 50 Ω, and the number of patch element N = 2, then the value of impedance Z is equal to:

$$Z = 50 \times \sqrt{2} = 70.71 = 70.7 \text{ Ω}$$

ii. In this research, the relative permittivity ε_r of FR4 (epoxy) material generally varies from 4.3 to 4.4 (which then the value 4.3 is used for designed calculations) in Equation (6).

$$B = \frac{60 \times (3.14)^2}{50 \times \sqrt{4.3}} = \frac{591.576}{103.682} = 5.706$$

After calculating the value of B, the next step is calculating the width (W) [2] of the power divider by using Equation (6).

The FR4 thickness h of the substrate is 1.5 mm.

$$W = \frac{2 \times 1.5}{3.14}\left\{5.706 - 1 - ln(2 \times 5.706 - 1)\right.$$
$$\left. + \frac{4.3 - 1}{2 \times 4.3}\left[ln(5.706 - 1) + 0.39 - \frac{0.61}{4.3}\right]\right\}$$
$$W = 2.92 \text{ mm}$$

iii. After the width (W) of the power divider is obtained, the next step is to examine the ratio between the width (W) and the height of the substrate using Equation (7).

$$\frac{W}{h} > 1$$

$$\frac{2.92}{1.5} = 1.946\ 7 > 1$$

Because $W/h > 1$, the dielectric constant value (ε_{eff}) uses Equation (7) as follows [2]. Thus,
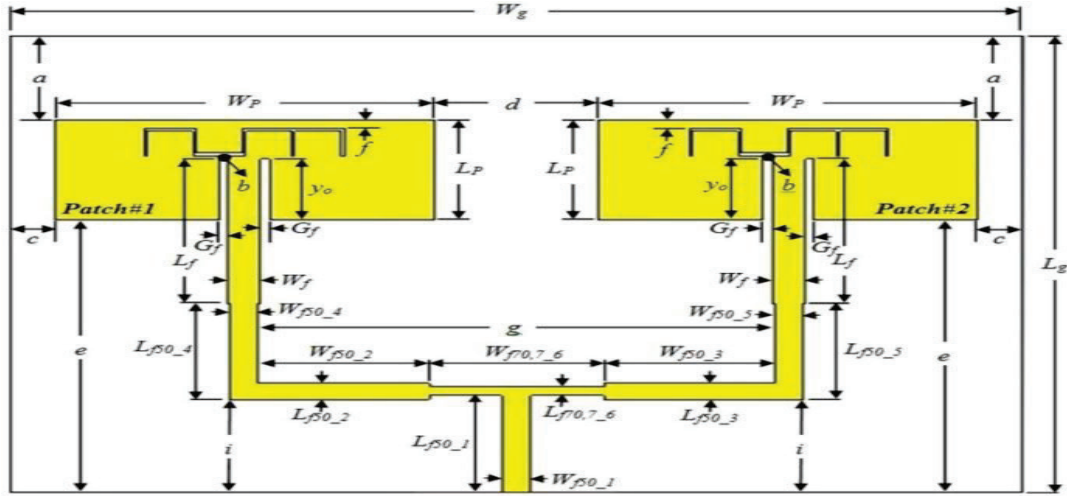
Fig. 4. 1 × 2 "Ha"-slot patch array microstrip antenna in a corporate feed.

Table 2. Dimension of 1 × 2 "Ha"-slot patch array microstrip antenna.

Antenna Dimension	Annotation	Value (mm)
L_g	Ground plane Length	82.311
W_g	Ground plane Width	229.286 8
$L_{f50\_1, 2, 3, 4, 5}$	Length 50 Ω matching impedance 1, 2, 3, 4, 5	17.291 5
$W_{f50\_1, 2, 3, 4, 5}$	Width 50 Ω matching impedance 1, 2, 3, 4, 5	2.92
$L_{f70.7\_6}$	Length 70.7 Ω matching impedance 6	17.715
$W_{f70.7\_6}$	Width 70.7 Ω matching impedance 6	1.529

$$\varepsilon_{eff} = \frac{(4.3 + 1)}{2} + \frac{(4.3 - 1)}{2} \left[\frac{1}{\sqrt{1 + 12\left[\frac{1.5}{2.92}\right]}} \right]$$

$$\varepsilon_{eff} = 2.65 + 1.65\,[0.373\,6] = 3.266\,4$$

Soon after the value of the antenna effective area is obtained, then calculate the effective wavelength using Equation (8).

Therefore,

$$\lambda_0 = \frac{3 \times 10^8}{2.4 \times 10^9} = 0.125\,mm$$

$$\lambda_0 = 0.125\,m \times 1\,000 = 125\,mm$$

Built upon the result of effective wavelength, the effective length (λ_g) of the microstrip antenna can be calculated by applying Equation (9).

$$\lambda_g = 125/\sqrt{3.266\,4} = 69.166\,mm$$

Finally, the length (L) of the microstrip feed

line can be calculated in Equation (10).

$$L = 69.166\,/\,4 = 17.291\,5\,mm$$

Finally, as a result for the dimension of 70.7 Ω microstrip line is $W = 1.529$ mm, $L = 17.715$ mm.

3. RESULTS

The design of the linear 1 × 2 "Ha (ꞁꞁ)"-slot patch array microstrip antenna is simulated on the CST Studio software. The patch array design in the simulation software is shown in Figure 5.

3.1 Return Loss

For a better quality of the antenna, the return loss (S11) should be less than -10 dB. Figure 6 shows the simulation result for return loss (S11) at a frequency of 2.4 GHz.

Figure 6 shows that the measurement results

for return loss (S11) patch array microstrip antenna is as low as -25.363, which means that the design of the antenna has a very small reflection or VSWR ≈ 1.

3.2 Gain Antenna

In the following Figure 7, it shows the gain of the antenna.

Figure 7 above, shows that the result of gain measurement from simulation. In which the main lobe direction of the antenna is 25.0 degrees, and the maximum gain antenna is 8.96 dBi.

Therefore, the simulation comparison between a single "Ha (ᴨᴫ)"-slot patch and 1 × 2 "Ha"-slot patch array microstrip antenna is shown in Table 3.

Fig. 5. Design and simulation 1 × 2 "Ha"-slot patch array microstrip antenna.
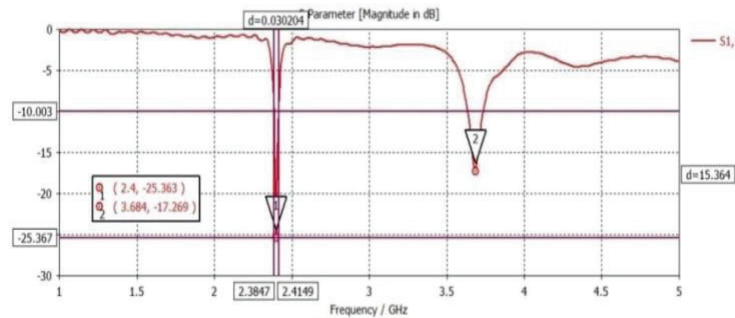
Fig. 6. The result of the return loss (S11) simulation.

Theta / Degree vs. dBi

Frequency = 2.4
Main lobe magnitude = 8.96 dBi
Main lobe direction = 25.0 deg.
Angular width (3 dB) = 67.0 deg.
Side lobe level = -8.8 dB

Fig. 7. The gain results in simulation.

Table 3. Simulation comparison single and patch array.

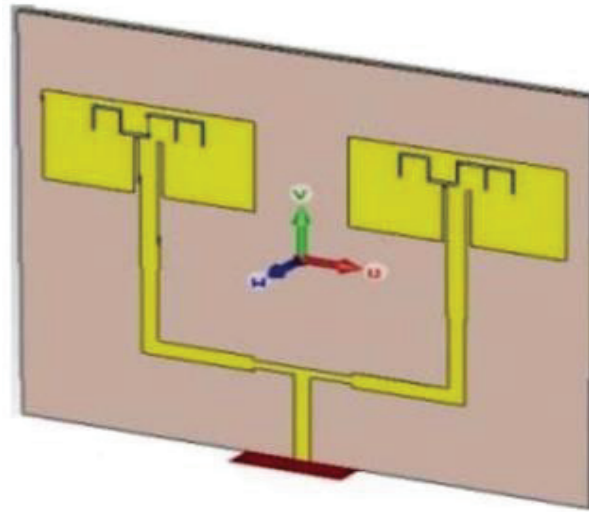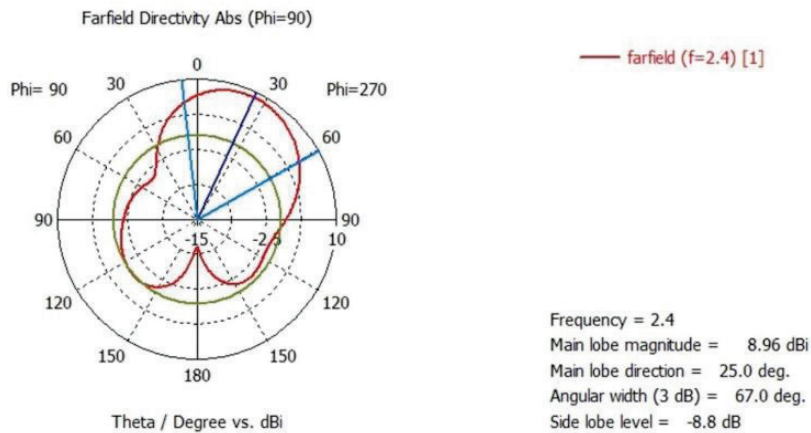| Parameter	Single Patch	1 x 2 Patch Array
Resonance Frequency (GHz)	2.408	2.4
Return Loss / S11 (dB)	-23.8	-25.363
Gain (dBi)	5.77	8.96

4. DISCUSSION

This research discusses the design and simulation of linear 1 × 2 "Ha (ꀎ)"-slot patch array microstrip antenna. The simulation result can help to take the next step for fabrication. To ensure that the fabrication can be achieved successfully, calculation in designing the patch array antenna is needed. After obtaining each value parameter based on calculation and achieving the antenna dimensions, the next step is to design the antenna in CST simulation. The CST studio suite is utilized to simulate a patch array microstrip antenna to measure the return loss (S11) and antenna gain.

In designing the patch array microstrip antenna, there are two critical part that needs to be consider and optimized. The first part is the distance between two array patches, which should be not less than λ/2 of the resonance frequency antenna. And then the next part is the T-Junction power divider, which will determine the impedance of both patch array.

5. CONCLUSION

A linear 1 × 2 "Ha (ꀎ)"-slot patch array microstrip antenna is designed and simulated. The simulation's result shows that the patch array configuration can achieve return loss (S11) -25.363 dB with VSWR 1.1 at the frequency 2.4 GHz and the value for gain can reach 8.96 dBi. Hence, the result of the gain in patch array increased by 64.4 % if compared to the gain value of the single patch"Ha (ꀎ)"-slot microstrip antenna.

6. CONFLICT OF INTEREST

The authors declare no conflict of interest.

7. REFERENCES

1. R.D.Tamas. Antenna and propagation: A sensor approach. *Sensors,* 21(4920):1–4 (2021). DOI: 10.3390/s21144920.

2. G. Ahmad, A. Sultan, M.I.K. Babar, M. Ashraf, and T. Jan. Fabrication and analysis of a triple band patch antenna. *Proceedings of the Pakistan Academy of Sciences A. Physical and Computational Sciences,* 55 (3): 45–51 (2018).

3. Najvia and S. Bashir. Broadband reflectarray antenna with high gain for X band (8 to 12GHz) applications. *Proceedings of the Pakistan Academy of Sciences: A. Physical and Computational Sciences*, 55(3), 21–33 (2018).

4. C.A. Balanis. *Antenna Theory: Analysis and Design,* 4rd Edition. John Willey and Sons, New Yersey, USA (2016).

5. S. Gupta and T. Srivastava. A review on microstrip patch antenna and its miniaturisation techniques. *International Journal of Engineering and Technical Research,* 7(7): 81–84 (2017).

6. H. Yon, N. H. Abd Rahman, M. A. Aris, and H. Jumaat. Developed high gain microstrip antenna like microphone structure for 5G application. *International Journal of Electrical and Computer Engineering,* 10(3): 3086–3094 (2020), DOI: 10.11591/ijece.v10i3.pp3086-3094.

7. S. Sotyohadi, S.H. Pramono, and M. Sarosa. Design and fabrication of "Ha ( )" shape-slot microstrip antenna for WLAN 2.4 GHz. Proceedings of Second International Conference on Electrical Systems, Technology and Information 2015 (ICESTI 2015). *Lecture Notes in Electrical Engineering,* 365: 383–391 (2016). DOI: 10.1007/978-981-287-988-2_41

8. M. Mynuddin and Md.Z. Rahman. Design and simulation of half wave-dipole antenna for LTE applications using CST microwave studio. J*ournal of Electrical Engineering and Electronics Technology,* 9(4):1–4 (2020). DOI: 10.37532/jeeet 2020.9(2)e.175.

9. M. Stanley, Y. Huang, H. Wang, H. Zhou, A. Alieldin, and S. Joseph. A capasitive coupled patch antenna array with high gain and wide coverage for 5G smartphone applications. *IEEE Access*, 6:1–13(2018). DOI: 10.1109/ACCESS.2018.2860795

10. V. Midasala, and P. Siddaiah. Microstrip patch antenna array design to improve better gains. *Procedia Computer Science,* 85:401–409 (2016).

DOI: 10.1016/j.procs.2016.05.181.

11. D.I. Kaklamani, A. D. Panagapoulos, P.K. Gkonis. Antennas and propagation aspects for emerging wireless communication technologies. *Electronics* 10 (964):1–3 (2021). DOI:10.3390/electronics10080964.

12. R.M. Sandoval, A.J. Garcia-Sanchez, F. Garcia-Sanchez, J. Garcia-Haro. Evaluating the more suitable ISM frequency band for IoT-based smart grids: A quantitative study of 915 MHz vs. 2400 MHz. *Sensors*, 17(76):1–15 (2017). DOI:10.3390/s17010076.

13. B. Singh, N. Sarwade, K.P. Ray. A compact modified corporate feed network for antenna arrays with non-identical rectangular microstrip antenna elements. In: *2016 International Symposium on Antennas and Propagation (APSYM),* Cochin, India. Institute of Electrical and Electronics Engineers. Curran Associates, Inc. USA, p. 17–20. (2016).

14. U. Nissanov. THz equal and unequal 1 to 8 T-Junction power dividers. *Sensors International,* 2(100113):1–8 (2021). DOI: 10.1016/j.sintl.2021.100113

15. Y.A. Rayisiwi, T. Hariyadi. Design of A 1:12 power divider at 5 GHz for ground surveillance radar application. *IOP Conf. Series: Materials Science and Engineering*, 384 (012053): 1–6 (2018). DOI: 10.1088/1757-899X/384/1/012053

Pakistan Academy of Sciences

Research Article

Resolving Economic Dispatch with Uncertainty Effect in Microgrids Using Hybrid Incremental Particle Swarm Optimization and Deep Learning Method

Nasyith Hananur Rohiem[1], Adi Soeprijanto[1], Dimas Fajar Uman Putra[1], Mat Syai'in[2], Irrine Budi Sulistiawati[3*], Muhammad Zahoor[4], and Luqman Ali Shah[5]

[1]Department of Electrical Engineering, Sepuluh Nopember Institute of Technology (ITS),
1st Campus ITS Keputih, Gedung B, C & AJ, Sukolilo, Surabaya 60111, Indonesia
[2]Department of Marine, Shipbuilding Institute of Polytechnic Surabaya,
1st Campus ITS Keputih, Sukolilo, Jl. Teknik Kimia, Surabaya 60117, Indonesia
[3]Department of Electrical Engineering, National Institute of Technology (ITN) Malang,
2nd Campus ITN, Jl. Raya Karanglo, Malang 65145, Indonesia
[4]Department of Biochemistry, University of Malakand, Lower Dir 18800, Pakistan
[5]National Center of Excellence in Physical Chemistry (NCE),
University of Peshawar 25120, Pakistan

Abstract: Microgrids are one example of a low voltage distributed generation pattern that can cover a variety of energy, such as conventional generators and renewable energy. Economic dispatch (ED) is an important function and a key of a power system operation in microgrids. There are several procedures to find the optimum generation. The first step is to find every feasible state (FS) for thermal generator ED. The second step is to find optimum generation based on FS using incremental particle swarm optimization (IPSO), FS is assumed that all units are activated. The third step is to train the input and output of the IPSO into deep learning (DL). And the last step is to compare DL output with IPSO. The microgrids system in this paper considered 10 thermal units and a wind plant with power generation based on probabilistic data. IPSO shows good results by being capable to generate a total generation as the load requirement every hour for 24 h. However, IPSO has a weakness in execution times, from 10 experiments the average IPSO process takes 30 min. DL based on IPSO can make the execution time of its ED function faster with an 11 input and 10 output architecture. From the same experiments with IPSO, DL can produce the same output as IPSO but with a faster execution time. From the total cost side, wind energy is affecting to reduce total cost until USD 22.86 million from IPSO and USD 22.89 million from DL.

Keywords: Conventional Thermal Generator, Economic Dispatch, Low Voltage Distribution, Power System Operation, Probabilistic, Renewable Energy.

1. INTRODUCTION

Microgrids are one example of low voltage distributed generation with a variety of energy sources, such as conventional thermal generators and renewable energy (RE) [1, 2]. RE like a wind turbine (WTs) [3–11] has big uncertainty and produces unstable generation because of nature. With probabilistic data, it can give important information about the RE plant area also information about the power generation produced by WTs [11]. A microgrid has a lower cost of energy supply with less carbon emission because the system can be operated to handle some level load or to support the main grid with a small source [1, 2]. One of the main functions of microgrid generation control is to decide unit commitment (UC) and the economic dispatch (ED) but this research will concern ED [1, 2].

Economic dispatch (ED) is the key to power system operation to find the optimum generation from every feasible initial of unit combination [6, 9, 12–14]. To find a better feasible solution, a priority list (PL) is a good initializer and has shown promising results [6, 15–18]. Optimum generation from every feasible solution can be defined by some promising method [15–18] such as particle swarm optimization (PSO), genetic algorithm (GA), Lagrange relaxation (LR), etc. hybrid models which are compared one method with another may have a better result than individuals method.

In this manuscript, proposed incremental particle swarm optimization (IPSO) to solve ED in a microgrid system. IPSO is a combination of PSO and ISL (incremental social learning) [19] to improve the performance of PSO and to eliminate local optimal [20–25]. The feasibility state is assumed that all units are activated both before and after WTs are affected. Feasibility state and output generation from IPSO is trained into a DL [26, 27] to speed up the execution time. Not only to speed up the execution time, but DL also to be a promising algorithm to make quickly and precisely decisions maker function with large training data [28–32].

2. MATERIALS AND METHODS

A microgrids system consists of a conventional generator or thermal plant and RE based on the generator [1, 2].

2.1 Generator

The thermal plant in this paper used a 10 unit generator with a 24 h load [1, 2] for the unit generates. For the wind plant, the total capacity installed [1, 2] of wind power is 560 kW from four generators and each capacity is 140 kW. In this manuscript, a detailed model for the simulation of wind power generation is often used in the field.

Wind plant converts from wind speed or kinetic energy to electric energy and equation [1, 2, 4, 5] to convert power from a wind plant is shown in Equation (1).

$$P = 0.5 \, \rho \, A \, C_p \, V^3 \qquad (1)$$

Where P is power (W), ρ is air density (kg m^{-3}),

A is rotor area (m^2), C_p is coefficient power and V^3 is wind speed (m s^{-1}).

In this research-based on wind plant data, equation [1, 2] power output of the wind generator can be presented as shown in Equation (2):

$$P_{out} = aV^4_w + bV^3_w + cV^2_w + dV_w + e \qquad (2)$$

Where Pout is power generated (W) and V is wind speed (m s^{-1}).

2.2 Constraint

In this research, ED is determined based on several constraints with the mathematical [1, 2, 6] equations as shown in Equation (3) to Equation (6)

2.2.1 Thermal Cost

$$F_i \left(P_{Ti} (t) \right) = a_i + b_i \, P_{Ti} (t) + c_i \, P_{Ti}(t)^2 \qquad (3)$$

Where, ai, bi and ci are quadratic cost coefficients, T_i^{down} is minimum downtime (hr), T_i^{up} is minimum uptime (hr), $T_{i,cold}$ is cold start hours (hr), and $T_{i,0}$ is unit first initialize (hr).

2.2.2 Generation Limit

$$P_{i,min} \, X_{i,t} \leq P^s_{i,t} \leq P_{i,max} \, X_{i,t} \qquad (4)$$

Where, $P_{i,min}$ is minimum power generation (W), $P_{i,t}$ is the output power of unit i at time t (W), $P_{i,max}$ is maximum power generation (W).

2.2.3 Spinning Reserve

$$\sum_{i=1}^{n} P_T(t) + P_R(t) \leq I_i(t) P_{T_i}^{max} \qquad (5)$$

2.2.4 Net Load

$$Load(t) = Thermal \ load(t) - Wind(t) \qquad (6)$$

2.3 Load

The wind speed probability data [23, 24] used is wind data in December 2015 as shown in Figure 1 at an altitude of 50 m above ground in the Sidrap wind plant [24] with a geographical position between 03043′ to 04009 *S* 11 & 119041′ to 120010′*E* or *Long*: 3 980, *Lat* 119 710.

WTs generation [(determined by Equation (2)] as shown in Figure 2 (blue line) is determined based on hourly wind speed probability data on 25 December 2015 and thermal load [1, 2] before WTs is affected as shown in Figure 2 (orange line). Based on Equation (6), the new loads after the wind turbine effect are shown in Figure 2 (grey line).

2.4 Initial State

All states are based on PL defined by FLAC [6] to sort generators from the lowest to the highest. Table 1 is a table of the priority list.

Table 1. PL generator microgrid.

Unit	1	2	3	4	5	6	7	8	9	10

The feasibility state is determined based on the Pmax value which must be greater than the load. The feasibility state in this paper takes into account the spinning reserve by 10 %. Pmax is the sum of the maximum active generator limits. In this section, all units are assumed to be active. If all units are active, the generation limit has a minimum value of 800 kW and a maximum of 3 200 kW as shown in Table 2.

Table 2. Initial unit.

Unit										Limit (kW)	
1	2	3	4	5	6	7	8	9	10	Min	max
1	1	1	1	1	1	1	1	1	1	800	3 200

2.5 IPSO based solution method for ED

IPSO used in this paper is developed by Oca et al. [20]. IPSO is combined by ISL [20] to schedule time for adding particles [20, 21] to the population and PSO. For growing the new population from IPSO [25] can be calculated using Equation (7).

$$x'_{new,j} = x'_{new,j} + U (p_{mode\,el,j} - x_{new,j}) \qquad (7)$$

Where $x'_{new,j}$ new,j is new particle's update position, $x'_{new,j}$ is new particle's original random position, $p_{mode\,el,j}$ is the model particle's position and U is a random number (0–1).

As shown in Figure 3 of the IPSO process, it is the overall process. FLAC data input is used to determine all state PL and the result as shown in Table 3. Then based on the load at a certain hour IPSO determines the feasibility state. There are two cases to determine feasibility state in this paper, before wind turbines, and after WTs are affected. The feasibility state before and after the wind turbine effect is shown the same as Table 4, then the IPSO optimization process starts. The optimal solution to determine the generation value of an active unit based on state conditions that can meet the load supply at certain times in every iteration. The generation value is adjusted to the Pmin and Pmax limits. The objective function from each iteration of the new individual should be compared with another one in the next iteration and the lower cost from the objective function at all iterations is used as local best condition and global best condition after all particles were evaluated.

2.6 Deep Learning (DL) based on IPSO

DL used in this paper is constructed from 11 input describe load then feasibility state and 10 output describe power generation of active generator. DL construction is shown in Figure 4.

DL training input is determined from the load and feasible combination of generators while the data output for DL training is taken from IPSO generation output based on a combination of generators that allow at certain hours. The DL training process uses MATLAB software as shown in Figure 4.
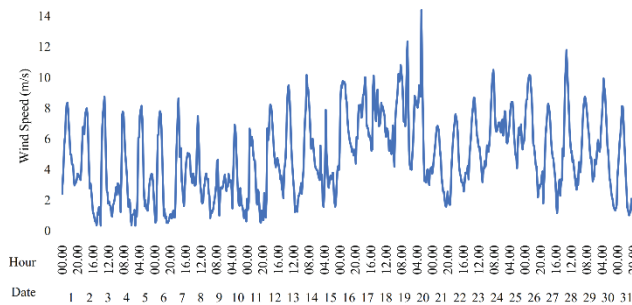

Fig. 1. Wind speed during December 2015.

3. RESULTS AND DISCUSSION

There are several experiments and simulations have been carried out in this study, including ED based on IPSO, ED DL based on IPSO, total cost results, comparison of ED IPSO and ED DL before and after being affected by WTs. For the thermal unit data [1, 2] as shown in Table 5 and wind generator data as shown in Table 6.

Table 6. Plant data of wind generator.

P_r	V_{ci}	V_r	V_{co}	a	b	c	d	e
140	3	15.01	17	-0.02	0.033	-0.9	-2.1	7.1

Where, P_r is rate power (kW), V_{ci} is wind speed cut in (m s^{-1}), Vco is wind speed cut off (m s^{-1}) and V_r is rating speed (m s^{-1}).

3.1 Output generation IPSO

IPSO in this paper construct by a total of 1 500 particles in the last iterations, 1 000 iterations. The incremental function which makes a new population in every iteration of the IPSO process makes this method out from the local optimum and makes the output generation shows good result. Total power generation is equal to load at a certain hour, both before and after the wind turbine effect as shown in Figure 2. Table 4 shows all hours of loading results. All of them are from both cases based on feasibility state.

3.2 Output generation DL

DL in this paper has been trained using 2 700 data based on the output process from IPSO. DL training input as shown in Table 3 and output data in Table 7. Sorted by the smallest to largest load both before and after being affected by WTs. DL

Table 5. Thermal unit data.

Unit	$P_{i,max}$ (kW)	$P_{i,min}$ (kW)	a_i (USD hr^{-1})	b_i (USD kWh^{-1})	c_i (USD kWh^{-2})
1	600	100	5	4	10
2	400	100	5	6	20
3	400	100	20	8	25
4	400	100	20	10	25
5	300	50	30	10	20
6	300	100	30	12	20
7	200	100	40	14	15
8	200	50	40	16	15
9	100	50	55	15	12
10	100	50	55	17	12

Fig. 2. Load pattern.

```
                    ┌──────────────┐
                    │    Start     │
                    └──────┬───────┘
                           │
                       ╱────────╱
                      ╱  FLAC  ╱
                     ╱────────╱
                           │
                ┌──────────────────────┐
                │ Determination of All  │
                │        State          │
                └──────────┬───────────┘
                           │
                ┌──────────────────────┐
                │        Load           │
                │      i =1 to 24       │
                └──────────┬───────────┘
                           │
                ┌──────────────────────┐
                │ Find Feasibility State│
                └──────────┬───────────┘
                           │
                ┌──────────────────────┐
                │   Iteration = 1 –     │
                │    Max Iteration      │
                └──────────┬───────────┘
                           │
                ┌──────────────────────┐
                │   Particle = 1 –      │
                │    Max Particle       │
                └──────────┬───────────┘
                           │
                ┌──────────────────────┐
                │ - Update Velocity      │
                │ - Check Limit Generation│
                │ - Check Total Load     │
                │ - Check P best         │
                └──────────┬───────────┘
                           │
                     ◇ Max Particle ?  ◇
                           │ Yes
                ┌──────────────────────┐
                │     Global Best       │
                └──────────┬───────────┘
                           │
                ┌──────────────────────┐
                │     Add particle      │
                └──────────┬───────────┘
                           │
                     ◇ Max Iteration ? ◇
                           │ Yes
                    ┌──────────────┐
                    │     End      │
                    └──────────────┘
```
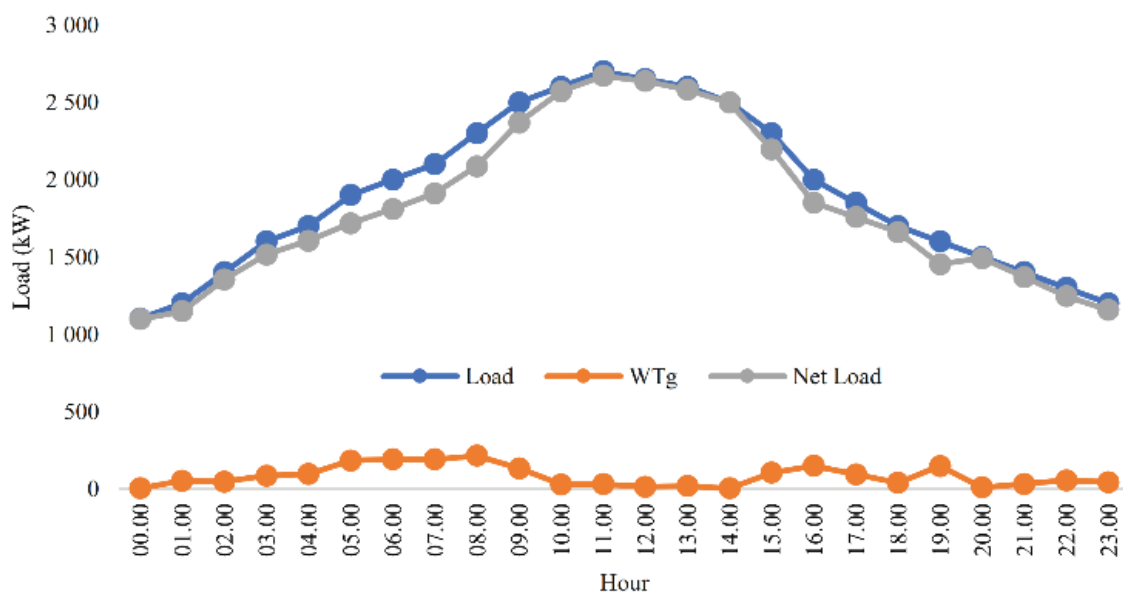
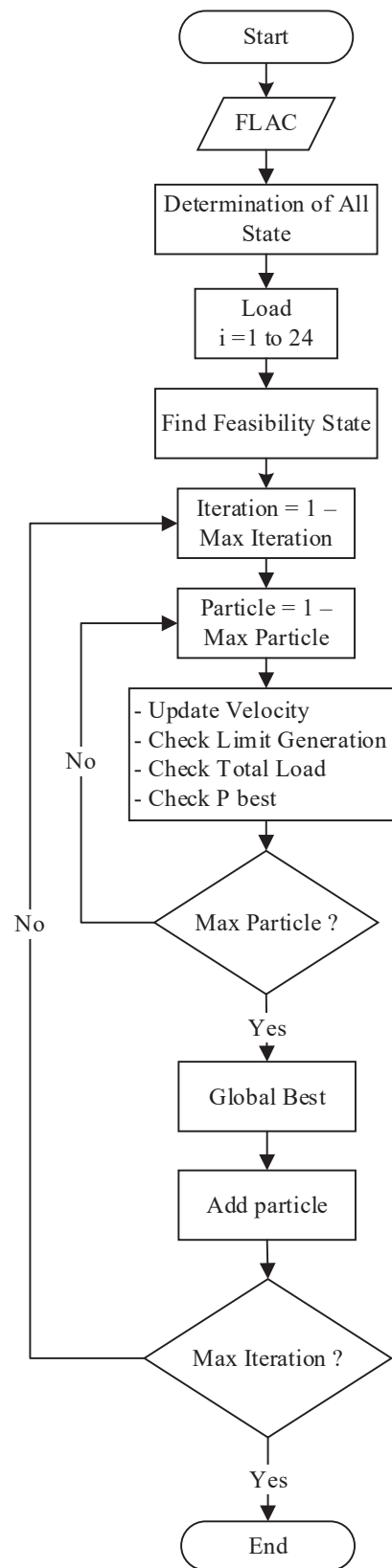**Fig. 3.** IPSO flowchart.
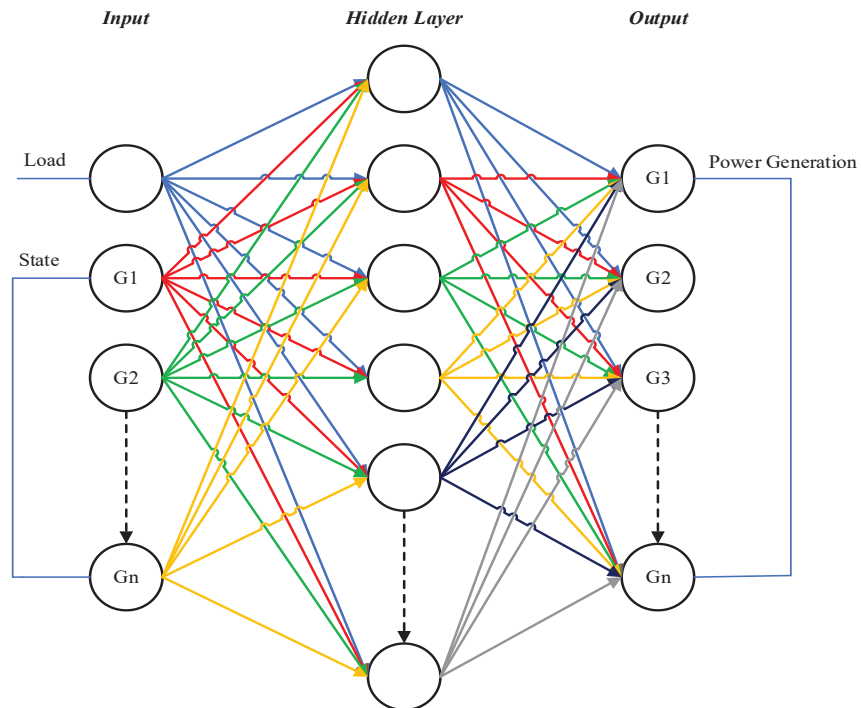
Fig. 4. DL construction.
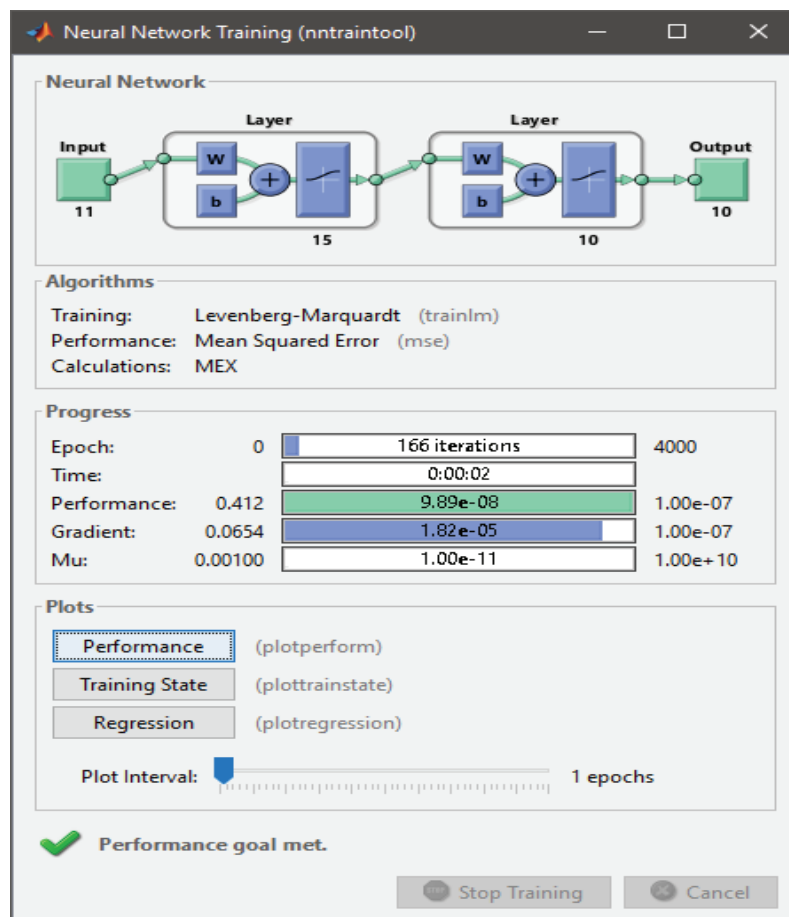
Fig. 5. DL train proses.

Table 3. Data of input train DL.

Load (kW)	1 055	1 072	1 097	1 100	>>	2 637	2 650	2 670	2 700
Unit 1	1	1	1	1		1	1	1	1
Unit 2	1	1	1	1		1	1	1	1
Unit 3	1	1	1	1		1	1	1	1
Unit 4	1	1	1	1		1	1	1	1
Unit 5	1	1	1	1	>>	1	1	1	1
Unit 6	1	1	1	1		1	1	1	1
Unit 7	1	1	1	1		1	1	1	1
Unit 8	1	1	1	1		1	1	1	1
Unit 9	1	1	1	1		1	1	1	1
Unit 10	1	1	1	1		1	1	1	1

Table 4. IPSO output both before and after WTs is affected.

Time (hours)	Before wind is affected		After wind is affected	
	Load (kW)	IPSO	Load (kW)	IPSO
1	1 100	1 100	1 097	1 097
2	1 200	1 200	1 148	1 148
3	1 400	1 400	1 355	1 355
4	1 600	1 600	1 515	1 515
5	1 700	1 700	1 604	1 604
6	1 900	1 900	1 717	1 717
7	2 000	2 000	1 809	1 809
8	2 100	2 100	1 910	1 910
9	2 300	2 300	2 086	2 086
10	2 500	2 500	2 368	2 368
11	2 600	2 600	2 572	2 572
12	2 700	2 700	2 670	2 670
13	2 650	2 650	2 637	2 637
14	2 600	2 600	2 582	2 582
15	2 500	2 500	2 498	2 498
16	2 300	2 300	2 197	2 197
17	2 000	2 000	1 852	1 852
18	1 850	1 850	1 757	1 757
19	1 700	1 700	1 661	1 661
20	1 600	1 600	1 452	1 452
21	1 500	1 500	1 491	1 491
22	1 400	1 400	1 369	1 369
23	1 300	1 300	1 246	1 246
24	1 200	1 200	1 156	1 156

Table 7. Data of output train DL.

Load (kW)	1 055	1 072	1 097	1 100	>>	2 637	2 650	2 670	2 700
Unit 1	355	372	397	400		600	600	600	600
Unit 2	100	100	100	100		600	600	600	600
Unit 3	100	100	100	100		400	400	400	400
Unit 4	100	100	100	100		387	400	400	400
Unit 5	50	50	50	50	>>	300	300	300	300
Unit 6	100	100	100	100		100	100	120	150
Unit 7	100	100	100	100		100	100	100	100
Unit 8	50	50	50	50		50	50	50	50
Unit 9	50	50	50	50		50	50	50	50
Unit 10	50	50	50	50		50	50	50	50

Table 8. DL output both before and after WTs is affected.

Time (hr)	Before wind is affected		After wind is affected	
	Load (kW)	DL	Load (kW)	DL
1	1 100	1 100	1 097	1 097
2	1 200	1 201	1 148	1 148
3	1 400	1 401	1 355	1 356
4	1 600	1 601	1 515	1 515
5	1 700	1 700	1 604	1 605
6	1 900	1 901	1 717	1 717
7	2 000	2 000	1 809	1 809
8	2 100	2 100	1 910	1 910
9	2 300	2 301	2 086	2 086
10	2 500	2 500	2 368	2 368
11	2 600	2 599	2 572	2 572
12	2 700	2 700	2 670	2 670
13	2 650	2 651	2 637	2 638
14	2 600	2 600	2 582	2 582
15	2 500	2 500	2 498	2 498
16	2 300	2 301	2 197	2 198
17	2 000	2 000	1 852	1 852
18	1 850	1 850	1 757	1 758
19	1 700	1 700	1 661	1 661
20	1 600	1 601	1 452	1 452
21	1 500	1 500	1 491	1 491
22	1 400	1 401	1 369	1 369
23	1 300	1 300	1 246	1 246
24	1 200	1 201	1 156	1 156
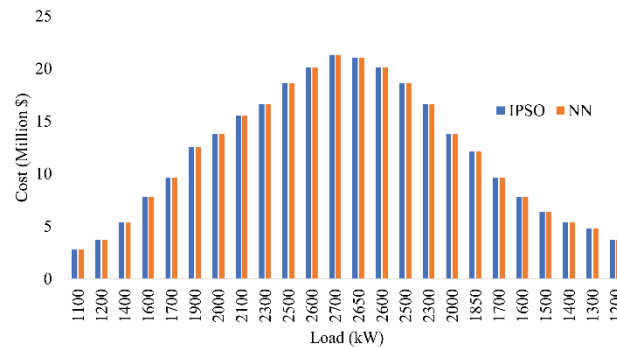
Fig. 6. Total cost before the wind is affected
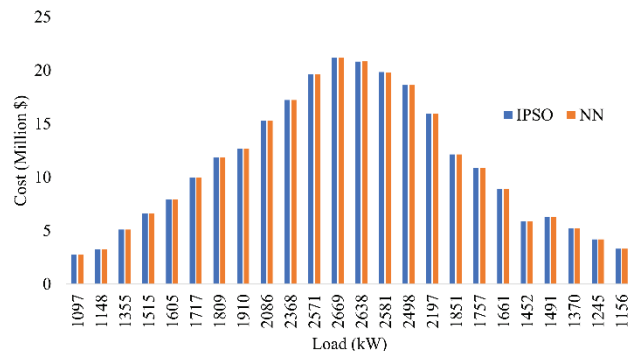
Fig. 7. Total cost after the wind is affected

structure is regulated with 15 neurons. The training process needs almost 2 h to finish. After the training process is successful, DL is tested as an economic dispatch function that replaces IPSO both before and after the WTs are affected. As shown in Table 8, all hour load both before and after WTs is affected, DL can produce a total load according to each hour of loading. DL can produce total power generation equal to or slightly higher than the load should be.

3.3 Total Cost Results

After checking the total generation process in this chapter shown the results of the total cost data as the objective function in this research from before wind is affected the system as shown in Figure 6 and after as shown in Figure 7. Because the total generation from both methods is quite the same, the total cost from both methods too in every each hour. The reduction of total cost from before wind is affected and after are USD 22.86 Million for IPSO and USD 22.89 Million for DL.

3.4 Comparison of ED IPSO and ED DL

Based on the test results of IPSO and DL is shown a good result but the execution time from these two methods are very different. IPSO produces an average execution time of more than 30 min in 10 ED tests with 24 h of loading and DL managed to speed up ED IPSO execution time to 3.5 s on average in 10 tests. The effect of WTs has an impact on the total load that must be generated by the thermal generator and the total cost generated by the thermal generator.

3.5 Future research

The wind turbine (WTs) in this study is one of the RE. In future research, the application of a microgrid with several other REs will be studied, including solar panels, biogas, and others [33–41].

5. CONCLUSION

AIPSO shows good results in the ED process, being able to generate according to the feasibility state with total generation according to the total targeted load, but IPSO produces a long enough execution time of 30 min on average in 10 tests. DL structure in this research successfully replaces the ED function

in the IPSO method, by producing the same output with load or slightly higher than the load should be and being able to accelerate execution time to 3.5 s on average in 10 tests. From the total cost side, wind energy is affecting the reduction cost for USD 22.86 Million as the result of IPSO and USD 22.89 Million as the result from DL.

6. CONFLICT OF INTEREST

The authors declare no conflict of interest.

7. REFERENCES

1. R.D.Tamas. Antenna and propagation: A sensor 1. R. Effatnejad, H. Hosseini, and H. Ramezani. Solving unit commitment problem in microgrids by harmony search algorithm in comparison with genetic algorithm and improved genetic algorithm. *International Journal on Technical and Physical Problems of Engineering*, 6(4):61–65 (2014).

2. T. Logenthiran, and D. Srinivasan. Short term generation scheduling of a microgrid. *TENCON 2009 - 2009 IEEE Region 10 Conference* (2009). DOI: 10.1109/TENCON.2009.5396184

3. Y. Zhang, B. Chen, Y. Zhao and G. Pan. Wind speed prediction of IPSO-BP neural network based on lorenz disturbance. *IEEE Access*, 6: 53168–53179 (2018). DOI: 10.1109/ACCESS.2018.2869981

4. C.M. Baby, K. Verma, and R. Kumar. Short term wind speed forecasting and wind energy estimation: A case study of Rajasthan. *2017 International Conference on Computer, Communications and Electronics (Comptelix)* (2017). DOI: 10.1109/COMPTELIX.2017.8003978

5. V. Reddy, S.M. Verma, K. Verma, and R. Kumar. Hybrid approach for short term wind power forecasting. *2018 9th International Conference on Computing, Communication and Networking Technologies (ICCCNT)* (2018). DOI: 10.1109/ICCCNT.2018.8494034

6. H. Quan, D. Srinivasan, and A. Khosravi. Incorporating wind power forecast uncertainties into stochastic unit commitment using neural network-based prediction intervals. *IEEE Transactions on Neural Networks and Learning Systems,* 26(9):2123–2135 (2015). DOI: 10.1109/TNNLS.2014.2376696

7. J. Wang, M. Shahidehpour, and Z. Li. Security-constrained unit commitment with volatile wind power generation. *IEEE Transactions on Power*

System, 23(3):1319–1327 (2008). DOI: 10.1109/TPWRS.2008.926719

8. R. Billinton, B. Karki, R. Karki and G. Ramakrishna. Unit commitment risk analysis of wind integrated power systems. *IEEE Transactions on Power Systems,* 24(2):930–939 (2009). DOI: 10.1109/TPWRS.2009.2016485

9. J.F. Restrepo, and F.D. Galiana. Assessing the yearly impact of wind power through a new hybrid deterministic/stochastic unit commitment. IEEE Transactions on Power Systems, 26(1):401–410 (2011). DOI: 10.1109/TPWRS.2010.2048345

10. Q.P. Zheng, J. Wang, and A.L. Liu. Stochastic optimization for unit commitment–A review. *IEEE Transactions on Power Systems,* 30(4):1913–1924 (2015). DOI: 10.1109/TPWRS.2014.2355204

11. P. Pinson, H. Madsen, and H.A. Nielsen. From probabilistic forecasts to statistical scenarios of short-term wind power production. *Wind Energy,* 12(1):51–62 (2009).DOI: 10.1002/we.284

12. M.N. Heris, B.M. Ivatloo, and G.B. Gharehpetian. A comprehensive review of heuristic optimization algorithms for optimal combined heat and power dispatch from economic and environmental perspectives, *Renewable and Sustainable Energy Reviews,* 81(2):2128–2143 (2018). DOI: 10.1016/j.rser.2017.06.024

13. B. Zhao, C.X. Guo, B.R. Bai, and Y.J. Cao. An improved particle swarm optimization algorithm for unit commitment. *International Journal of Electrical Power & Energy Systems,* 28(7):482–490 (2006). DOI: 10.1016/j.ijepes.2006.02.011

14. Y.K. Wu, H.Y. Chang, and S.M. Chang. Analysis and comparison for the unit commitment problem in a large-scale power system by using three meta-heuristic algorithms. Energy Procedia, 141:423–427 (2017).DOI: 10.1016/j.egypro.2017.11.054

15. T. Logenthiran, and D. Srinivasan. Particle swarm optimization for unit commitment problem. 2010 *IEEE 11th International Conference on Probabilistic Methods Applied to Power Systems* (2010).DOI: 10.1109/PMAPS.2010.5528899

16. C.P. Cheng, C.Y. Liu, and G.C. Liu. Unit commitment by Lagrangian relaxation and genetic algorithms. *IEEE Transactions on Power Systems*, 15(2):707–714 (2000).DOI: 10.1109/59.867163

17. P.H. Chen. Two-level hierarchical approach to unit commitment using expert system and elite PSO. *IEEE Transactions on Power Systems,* 27(2):780–789 (2011).DOI: 10.1109/TPWRS.2011.2171197

18. V.Arora,and S.Chanana. Solution to unit commitment problem using Lagrangian relaxation and Mendel's GA method. *2016 International Conference on Emerging Trends in Electrical Electronics & Sustainable Energy Systems (ICETEESES)* (2016). DOI: 10.1109/ICETEESES.2016.7581372

19. A. Haydlaar, A. Musyafa, A. Soeprijanto, M. Syaiin, G. Suhardjito, B. Herijono, R.Y. Adhitya, H. A. Widodo, and E. A. Zuliari. Optimization of power coefficient (Cp) in variable low rated speed wind turbine using increamental particle swarm optimization (IPSO). *2017 International Symposium on Electronics and Smart Devices (ISESD)* (2017). DOI: 10.1109/ISESD.2017.8253305

20. M.A.M.d. Oca, T. Stutzle, K.V.d. Enden, and M. Dorigo. Incremental social learning in particle swarms. *IEEE Trans Syst Man Cybern B Cybern*, 41(2):368–384 (2011).DOI: 10.1109/tsmcb.2010.2055848

21. M.A.M.d. Oca, K.V.d. Enden, and T. Stützle. Incremental particle swarm-guided local search for continuous optimization. *Conference: Proceedings of the 5th International Workshop on Hybrid Metaheuristics* (2008). DOI: 10.1007/978-3-540-88439-2_6

22. M.A.M.d. Oca, and T. Stützle. Towards incremental social learning in optimization and multiagent systems. *GECCO '08: Proceedings of the 10th Annual Conference Companion on Genetic and Evolutionary Computation,* p.1939–1944 (2008). DOI: 10.1145/1388969.1389004

23. EMD International. Wind prospecting, implemented for the Ministry of Energy and Mineral Resources, Indonesia, and ESP3. The Environmental Support Programme 3 (ESP3)/ Danida (2017) http://indonesia.windprospecting.com (accessed 01 May 2019).

24. UPC Renewables Asia I Ltd. Sidrap Wind Farm Project Phase 1. *Project Report* (2016).https://www.upcrenewables.com/indonesia/ (accessed 01 May 2019).

25. M. Syai'in, and A. Soeprijanto. Combination of generator capability curve constraint and statistic-fuzzy load clustering algorithm to improve nn-opf performance. *Journal of Electrical Systems - Paris,* 8(2):198–208 (2012).

26. E. Mocanu, P.H. Nguyen, and M. Gibescu. Deep learning for power system data analysis. *Big Data Application in Power Systems*, 125–158 (2018). DOI: 10.1016/b978-0-12-811968-6.00007-3

27. A.K. Ozcanli, F. Yaprakdal, M. Baysal. Deep learning methods and applications for electrical power systems: A comprehensive review. *International Journal of Energy Research,* 44(10):7136–7157 (2020).DOI: 10.1002/er.5331

28. Y. Hong, Y. Zhou, Qibin Li, W. Xu, and X. Zheng, A deep learning method for short-term residential load forecasting in smart grid. *IEEE Access*, 8: 55785–55797 (2020) DOI: 10.1109/ACCESS.2020.2981817

29. Q. Chen, M. Xia, T. Lu, X. Jiang, W. Liu, and Q. Sun short-term load forecasting based on deep learning for end-user transformer subject to volatile electric heating loads. *IEEE Access* 7: 162697–162707(2019). DOI: 10.1109/ACCESS.2019.2949726

30. A. Gensler, J. Henze, B. Sick, N. Raabe. Deep Learning for solar power forecasting — An approach using auto encoder and LSTM neural networks. in *2016 IEEE International Conference on Systems, Man, and Cybernetics (SMC)* (2016). DOI: 10.1109/SMC.2016.7844673

31. R. Zhang, M. Feng, W. Zhang, S. Lu and F. Wang. Forecast of solar energy production - A deep learning approach. *2018 IEEE International Conference on Big Knowledge (ICBK),* 2018, pp. 73–82, DOI: 10.1109/ICBK.2018.00018.

32. H. Wang, Z. Lei, X. Zhang, B. Zhou, J. Peng. A review of deep learning for renewable energy forecasting. *Energy Conversion and Management,* 198:111799. DOI: 10.1016/j.enconman.2019.111799.

33. F.A. Khalil, M. Asif, S. Anwar, S. ul Haq, and F. Illahi. Solar tracking techniques and implementation in photovoltaic power plants: A review. *Proceedings of the Pakistan Academy of Sciences A. Physical and Computational Sciences*, 54(3):231–241 (2017).

34. H.E. Gelani, N. Mashood, D. Faizan and H. Haseeb. Efficiency comparison of alternating current (AC) and direct current (DC) distribution system at residential level with load characterization and daily load variation. *Proceedings of the Pakistan Academy of Sciences A. Physical and Computational Sciences,* 54(2):111–118 (2017).

35. K. Abdullah, A.S. Uyun, R. Soegeng, E. Suherman, H. Susanto, R.H. Setyobudi, J. Burlakovs, and Z. Vincēviča-Gaile. Renewable energy technologies for economic development. *E3S Web of Conference,* 188(00016):1–8 (2020).DOI:10.1051/e3sconf/202018800016

36. R. H. Setyobudi, E. Yandri, M.F.M. Atoum, S. M. Nur, I. Zekker, R. Idroes, T.E. Tallei, P.G. Adinurani, Z. Vincēviča-Gaile, W. Widodo, L. Zalizar, N. Van Minh, H. Susanto, R.K. Mahaswa, Y.A. Nugroho, S.K Wahono, and Z. Zahriah. Healthy-smart concept as standard design of kitchen waste biogas digester for urban households. *Jordan Journal of Biological Sciences*, 14(3):613–620 (2021).

37. B. Novianto., K. Abdullah., A.S. Uyun., E. Yandri., S.M. Nur., H. Susanto, Z. Vincēviča-Gaile., R.H. Setyobudi, and Y. Nurdiansyah. Smart micro-grid performance using renewable energy. *E3S Web of Conferences,* 188(00005):1–11 (2020).DOI: 10.1051/e3sconf/202018800005

38. A. Dolatabadi, M. Jadidbonab, and B. Mohammadi-ivatloo, Short-term scheduling strategy for wind-based energy hub: A hybrid stochastic/IGDT approach, IEEE Transactions on Sustainable Energy 10 (1): 438–448 (2019). DOI: 10.1109/TSTE.2017.2788086.

39. Y. Lin, M. Yang, C. Wan, J. Wang, and Y. Song, A multi-model combination approach for probabilistic wind power forecasting. *IEEE Transactions on Sustainable Energy* 10(1): 226–237 (2019). DOI: 10.1109/TSTE.2018.2831238.

40. Y. Wang, N. Zhang, C. Kang, M. Miao, R. Shi and Q. Xia. An efficient approach to power system uncertainty analysis with high-dimensional dependencies. *IEEE Transactions on Power Systems,* 33 (3): 2984–2994 (2018).DOI: 10.1109/TPWRS.2017.2755698.

41. M.I. Khan, and M. Amir. Design and stability analysis of a proposed microgrid for on campus diesel and photovoltaic power sources. *Proceedings of the Pakistan Academy of Sciences A. Physical and Computational Sciences:* 58(1): 47–60 (2021). DOI: 10.53560/PPASA(58-1)723

Pakistan Academy of Sciences

Research Article

Techno-economic Analysis of Rooftop Photovoltaic System (RPVS) using Thin-Frameless Solar Panels for Household Customers in Indonesia

Carolus Boromeus Rudationo[1], Bangun Novianto[1,2]*, Erkata Yandri[1,2],
Herry Susanto[1,3], Roy Hendroko Setyobudi[1,4], Aep Saepul Uyun[1,2],
Syukri Muhammad Nur[1,2], Satriyo Krido Wahono[5], Wahyu Widodo[4], Ivar Zekker[6],
and Abraham Lomi[7]

[1]Graduate School of Renewable Energy, Darma Persada University,
Jl. Taman Malaka Selatan No. 22, Jakarta 13450, Indonesia
[2]Center of Renewable Energy Studies, Darma Persada University, Jakarta, Indonesia
[3]Department of Mechanical Engineering, Darma Persada University, Jakarta, Indonesia
[4]Department of Agriculture Science, Postgraduate Program, University of Muhammadiyah
Malang, Jl. Raya Tlogomas No.246, Malang 65145, Indonesia
[5]Research Division for Natural Product Technology – Indonesian Institute of Sciences,
Jl. Jogja - Wonosari, km 31.5, Gunung Kidul, Special Region Yogyakarta 55861, Indonesia
[6]Institute of Chemistry, University of Tartu, Ravila 14a, 50411 Tartu, Estonia
[7]Renewable Energy Research Center & Power and Energy System Simulation Laboratory,
National Institute of Technology Malang, JL. Raya Karanglo KM. 2, Malang 65153, Indonesia

Abstract: The availability of thin-frameless solar panels on the market today makes the installation of rooftop Photovoltaic (RPVS) systems more attractive. The purpose of this research is to analyze financially the use of thin-frameless solar panels for on-grid RPVS by household electricity customers in Indonesia. The investment cost, the maintenance costs, and the electricity cost savings were involved for the financial analysis, such as Internal Rate of Return (IRR), Net Present Value (NPV), and Pay Back Period (PBP). The calculation is carried out for ideal conditions, the direction of a non-ideal rooftop and the yearly increase of electricity prices is 15 %. The analysis results show that the minimum available rooftop area is still sufficient for the rooftop area needs for solar panel placement, the thin solar panels are safer than standard solar panels, and savings on electricity payments for the return on investment of the RPVS is to be attractive with the IRR > 12 %. The average investment cost of the non-ideal condition is 8 % higher than the ideal condition. This study provides an overview to the policymakers and developers in exploiting the potential of RPVS, especially in Indonesia. For future research directions, this study needs to analyze the technical and economic feasibility of using hybrid smart-grid technology with batteries.

Keywords: Clean Energy, Economic of Solar Energy, Energy Saving, Net Metering, Renewable Energy

1. INTRODUCTION

Indonesia's fossil energy reserves are dwindling due to increasing consumption from year to year. The formation of fossil energy takes millions of years. For this reason, fossil energy consumption must be reduced by utilizing alternative energy sources such as renewable energy. Renewable energy sources can be converted into ready-to-use energy without the greenhouse effect. Renewable energy sources are solar energy, wind energy, water energy, geothermal energy, and biomass energy. As a country located on the equator, Indonesia has abundant solar energy potential [1]. Solar

energy can be converted into electricity using solar photovoltaic [2] and solar thermal power [3], or into thermal energy with a solar thermal collector [4], or both electricity and thermal with a hybrid photovoltaic and thermal collector [5–7]. Indonesia is targeting renewable energy sources of 23 % by 2025 and 31 % by 2050 in the national energy mix. In 2018, the renewable energy mix only reached 15.2 % with a 3 % contribution from solar energy. This is due to regulatory constraints for installation such as panel weight, rooftop PV aesthetics, as well as operations related to on-grid and off-grid storage systems. Based on customer data from the State-Owned Electricity Company (PLN), the most electricity consumption from 2012 to 2017 was household customers. In this case, the role of the community as a customer is very important. Thus, the use of rooftop PV systems (RPVS) in reducing the electricity consumption of household customers is very relevant to achieving Indonesia's renewable energy mix target [8]. Then, the Minister of Energy and Mineral Resources issued regulations No. 49/2018 and No. 16 /2019, accompanied by a PLN Policy since 2019, making it easier to install RPVS [9]. Thus, the on-grid RPVS becomes more attractive. In addition, PLN also provides regulations and export-import measuring tools for grid-connected, making RPVS for household and commercial buildings more attractive [10].

To utilize the potential of solar energy into electrical energy, the RPVS was developed. This system converts solar energy into electrical energy [11–13]. There are several kinds of solar cell materials, including mono-crystalline (m-si), poly-crystalline (p-si), amorphous-crystalline (a-si), and thin layers of CIS (Cu, Cd, and Zn) [14]. For protection, the surface of the solar panel is covered with glass or plastic. This material must be able to transmit irradiance close to 100 % with low physical weight. In addition, different silicon materials lead to different module efficiency, such as; mono-crystalline 16 %, poly-crystalline 13 %, amorphous-crystalline 8 %, and CIS thin film 10 % [15].

The use of on-grid RPVS in Indonesia by the customers has great potential for achieving the national energy mix target of 23 % by 2025. The simulations for economic analysis were carried out by Subarianto for the implementation of the RPVS

by the customers using the Minister of Energy and Mineral Resources regulations No. 49 / 2018 and using import-export kWh and the thick aluminum-framed solar panels [16]. The impact of using the on-grid rooftop PV system in Indonesia has been discussed in both economic and environmental aspects. The environmental aspects are discussed by calculating the reduction of greenhouse gas emissions [17]. The economic aspect was carried out to analyze the cost of a household-scale rooftop PV system [18]. The economic aspect is discussed by calculating the IRR, BEP, Life cycle cost, and benefit-cost ratio [19, 20]. Furthermore, the innovation of solar panel products with the thin-frameless technology. Hopefully, the installation of RPVS will be even more attractive. This innovation does not need to consider additional costs for strengthening the roof truss or changing the existing roof construction. The installation only uses double-adhesive without perforating the roof, to avoid the risk of a leaking roof.

Based on the review above, the financial calculation of the RPVS installation has never been investigated and the relationship between the influence of the usage of RPVS by the household customers with available rooftop area, as well as the technology used that takes into account the weight of solar panels so that they can be installed massively in Indonesia. For this reason, this research aims to analyze financially the usage of thin-frameless solar panels as a prospect for the usage of the rooftop PV system by household electricity customers in Indonesia.

2. MATERIALS AND METHODS

First, conducted survey for the household customers from 450 W to 3 500 W in Jakarta with surrounding cities (Jabodetabek = Jakarta, Bogor, Depok, Tangerang, Bekasi or JMA = Jakarta Metropolitan Area), Bandung, Yogyakarta, Makassar and Pontianak. The survey data taken included the installed power, monthly electricity payments, and the basic electricity price is the basic electricity price that applies from 2019 to June 2020, the number of family members in the house, the size of the house, household electrical equipment used during the day, household electrical equipment used in the afternoon and evening. The electrical power data for household equipment used assumptions as
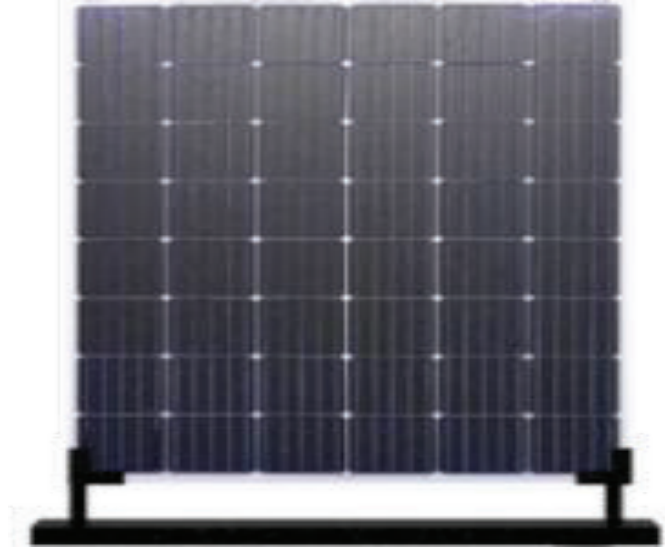
Fig. 1. Thin-frameless solar panel of JLeaf m-si 255 Wp [21]

shown in Table 1.

Another assumption was electricity costs, taken by the average value of payments from all customers per class of the PLN electricity. The upper limit for the RPVS power consumption was 90 % of the installed power according to the board of directors' regulations in 2018. The daily average electricity consumption (DAEC), Ce,day [kWh] can be calculated by Equation (1):

$$C_{e,day} = \frac{B_{e,month}/30}{P_e} \quad (1)$$

where B$_{e,month}$ is the cost of monthly electricity bill [IDR], and P$_e$ [IDR/kWh] is the basic price of electricity.

Second, the capacity of the on-grid RPVS for the household customer's consumptions was calculated. This was to provide an overview of the required rooftop area with the thin-frameless solar panel as shown in Figure 1. As shown in Figure 1(a), the panel is protected with 2.0 mm thin glass without an aluminum frame. Thin glass produces a more perfect irradiance transmission and has a lighter mass [21]. The detailed specification of the thin-frameless solar panels is shown in Table 2 [22].

Third, provided financial analysis on the installation of the on-grid RPVS by the household customers and the potential for saving electricity costs per month using the RPVS. Financial calculation scenarios were carried out using the Internal Rate of Return (IRR) and Pay Back Period (PBP). IRR and PBP from most of the power of the RPVS used up to a maximum of 90 % of the installed power. The investment cost was calculated using components of thin-frameless solar panels with some available power, quality affordable inverters, locally made cables, and other affordable accessories that are but of high quality according to Indonesian national standards as shown in Table 3.

The Inv$_{tot}$ as the total investment can be calculated by Equation (2) and Equation (3):

$$Inv_{tot} = Mat_{tot} + InCom_{tot} \quad (2)$$

$$Mat_{tot} = \sum_{1}^{n} C_n \times P_n \quad (3)$$

where Mat$_{tot}$ [IDR] is the total material cost, C$_n$ is the component item, P$_n$ [IDR] is the price of n component item, and InCom$_{tot}$ [IDR] is the installation and commissioning cost. The total investment costs were divided into Equation (2), namely in ideal conditions and non-ideal conditions. Ideal conditions occur where the direction of the rooftop and the rooftop slope is under the ideal conditions of the solar-energized power plants installation to the angle of incidence of solar rays, hence no additional costs are needed to change and add costs to the rooftop for the installation of the RPVS. Meanwhile, non-ideal conditions occur

Table 1. The electrical power data for household equipment

No	Load items	Power (Watt)
1	Television	100
2	Refrigerator	100
3	Electric stove	400
4	Iron	300
5	Rice cooker	300
6	Water pump	300
7	Fan	75
8	Lamp	50
9	Air conditioning (AC)	350
	Total load (Watt)	1 975

Table 2. Technical specification of JLeaf m-si 255 Wp [22]

	Technical specification	
1	Modul type	ST48M255TGP
2	P_{max} (Wp)	255
3	Power tolerance (%)	± 3
4	V_{mp} (V)	27.22
5	I_{mp} (A)	9.39
6	V_{oc} (V)	31.68
7	I_{sc} (A)	10.26
8	Efficiency (%)	19.2
9	Dimension L x W x H (mm)	1 334 x 997 x 3
10	Weight (kg)	7.3
11	Frameless	
12	Screw-free installation	
13	Product warranty	10 yr
14	Power warranty	10 yr ≥ 90 %
		25 yr ≥ 80 %

Table 3. Components - Specifications - Cost of the on-grid RPVS of 500 Wp

No	Description	Cost (IDR)	Unit (pcs)	Total Cost (IDR)
1	Solar panels of 255 Wp	1 750 000.00	2	3 500 000.00
2	Jtape adhesive of PV	50 000.00	1	50 000.00
3	Solar Charge Controller	1 300 000.00	1	1 300 000.00
4	Inverter	2 000 000.00	1	2 000 000.00
5	ATS	150 000.00	1	150 000.00
6	MCB AC & DC	100 000.00	2	200 000.00
7	Contactor	200 000.00	2	400 000.00
8	Relay	75 000.00	2	150 000.00
9	Cable protection	100 000.00	1	100 000.00
10	Timer	200 000.00	1	200 000.00
11	Panel box	300 000.00	1	300 000.00
12	Cable and schoen	1 400 000.00	1	1 400 000.00
13	Change exim meter	800 000.00	1	800 000.00
14	Installation cost	500 000.00	1	500 000.00
	Total installation cost			**11 050 000.00**

where the direction of the rooftop and the rooftop slope do not match and cannot generate electricity from solar energy. IRR [%] and PBP [yr] are calculated with Equation (4) and Equation (5) [23]:

$$IRR = I_h + \frac{NPV.I_l}{NPV.I_h - NPV.I_l} x (I_h - I_l) \qquad (4)$$

$$PBP = \frac{T_C}{NCF/P} \qquad (5)$$

where I_l [%] is the lowest rate, I_h [%] is the highest rate, NPV [IDR] is the Net Present Value, NCF [IDR] is the net cash flow, and P [yr] is the period. If the net positive cash flow is uneven, the following Equation (6) can be used:

$$PBP = A + \frac{B}{C} \qquad (6)$$

where A [years] is the last period number with negative cumulative cash flow, B [IDR] is the absolute value (that is, the value without a negative sign) of the cumulative net cash flows at the end of period A, and C [IDR] is the total cash inflows during the period after period A. The customer monthly electricity costs for households, customer electricity consumption used during the day.

3. RESULTS

The potential for electrical power that may be generated by the RPVS was calculated based on survey results from customers spread over five cities, namely Jabodetabek, Bandung, Yogyakarta, Makassar, and Pontianak as shown in Table 4.

Figure 2 explains the investment value of the RPVS installation for household customers. Figure 2(a) shows the relationship of installation costs with the RPVS installation capacity. The

(a)   (b)
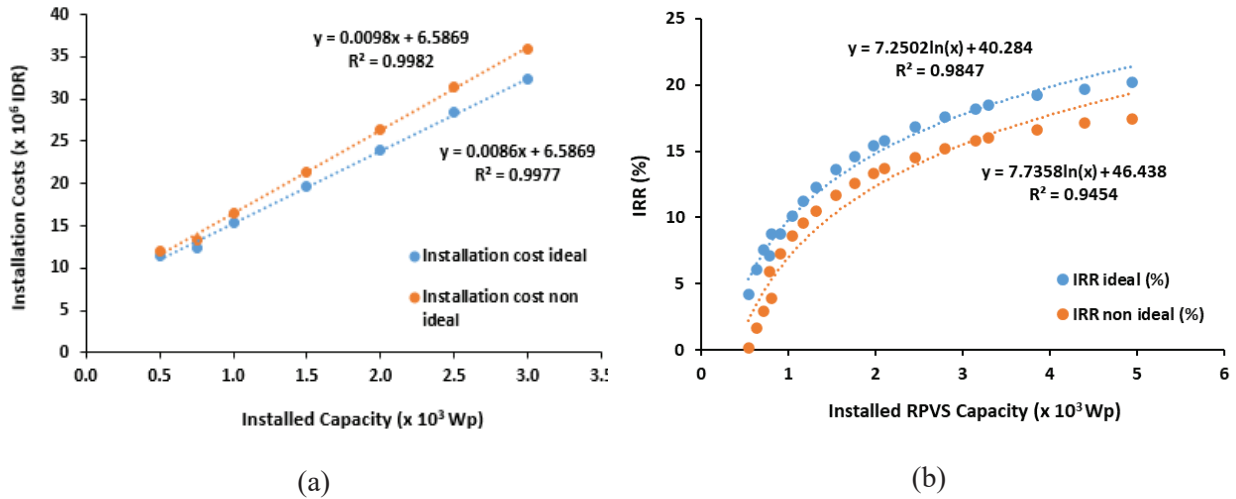
Fig. 2. Economic analysis, a). Installation cost (IDR) vs installed capacity (Wp), b). IRR (%) vs installed RPVS capacity (Wp)
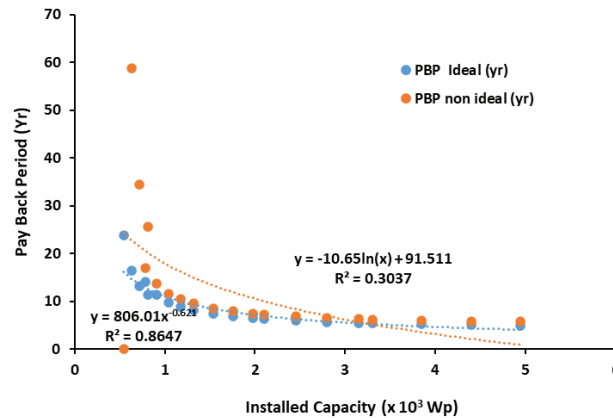
Fig. 3. Relationship between PBP and installation capacity (Wp)

RPVS installation costs follow the equation $y = 0.0098x + 6.5869$ for ideal rooftop conditions, and $y = 0.0086x + 6.5869$ for non-ideal rooftop conditions. Attractive investment conditions show that the IRR of ideal conditions was greater than the IRR of non-ideal conditions.

The ideal IRR following the equation, $y = 7.2502\ln(x) – 40.284$. The IRR non-Ideal following the equation $y = 7.7358\ln(x) – 46.438$, where x is the installed RPVS capacity (Wp). Figure 2(b) explains the relationship IRR (%) versus the rooftop solar-energized power plants installation capacity. If an attractive IRR standard was used, the IRR is > 12 %, From the graph, it can be concluded at the point of the rooftop RPVS capacity that attracts the household customers to install it.

Figure 3 shows the PBP versus installed capacity of RPVS. PBP shows the time at which the total value of NPV = 0 (Zero). This means that the NPV of expenditures (investment plus periodic maintenance expenses) was the same as the NPV of income (savings on the electricity payments). The calculation of PBP was used as a benchmark for how long the investment spent will return from the income that comes from saving on electricity payments. The calculation of the PBP was done by calculating the NPV of both investment and savings income. PBP was summed up in the equation, $y = 806.01x-0.621$ for the ideal condition of the house rooftop. While $y = -10.65\ln(x) + 91.511$ is for the non-ideal conditions.

The average PBP for the installed RPVS capacity was 90 % of the purchasing power. That is for 7.5 yr for ideal rooftop conditions and 11 yr for non-ideal rooftop conditions. The larger the installed RPVS capacity, the smaller the PBP value will be. This means that the investment costs incurred will return in a shorter time as shown in Table 5.

Savings occurred during the day when solar radiation becomes a source of electricity generation from the RPVS. Then, the electrical energy was used for the electrical load of all electrical equipment used during the day. By using a power source from the RPVS, the electricity payment was only to meet the electricity used from the electricity source when the RPVS did not produce electricity (occurs at night if it did not use batteries or when the weather did not allow the RPVS to produce electricity). If viewed from five cities the percentage of electricity cost savings based on installed capacity, all of these cities had considerable savings potential as shown in Figure 4.

The use of the RPVS for household customers caused potential savings in electricity costs. Get the optimum value of savings from the power consumption of the installed RPVS will be determined by regulations and then tested by the financial aspect. The calculation of the savings obtained by assuming the usage of electricity during the day was 30 % of the electricity cost and 90 % of the maximum power.

4. DISCUSSION

Based on the results described above, there are at least three important things that need to be discussed further here. First, related to the installation costs of the RPVS. Under ideal conditions, RPVS has the advantage of not requiring additional costs. This allows RPVS investments to be more attractive to electricity consumers [20]. As shown in Figure 2(a), the investment cost for RPVS installation between ideal and non-ideal conditions had a significant difference to the increase in installation capacity. Therefore, the ideal roof condition can be used as an initial benchmark. This needs to be considered in building a house.

Second, related to PBP as an important indicator in investment. PBP becomes more attractive if its value is less than equal to 10 yr [16]. For non-ideal roof conditions, the minimum installation limit occurred at 1 170 Wp for 1 300 VA customers, as shown in Figure 3 and Table 5.

Third, related to the cost savings of electricity consumption. The most important goal of RPVS installation is to save electricity costs per month [18]. As shown in Figure 4, Jabodetabek had the lowest average savings compared to other cities. This is because the monthly cost of electricity consumption in Jabodetabek was higher than in other cities, which is influenced by the number of household electrical appliances.

The practical application of this study is

Table 4. The PLN household customer survey results data

Region	Installed Power (VA)	Electricity Price (IDR kWh⁻¹)	Electricity Cost (IDR mo⁻¹)	kWh/ Daytime (Hour 8 to 16)	Afternoon Electric Power (W)
Jabodetabek	900	1 352	283 333	2.10	800
	1 300	1 467	519 565	3.54	1 000
	2 200	1 467	811 628	5.53	1 500
	3 500	1 467	1 807 292	12.32	2 500
Yogyakarta	900	1 352	210 417	1.56	800
	1 300	1 467	310 000	2.11	1 000
	2 200	1 467	650 000	4.43	1 500
	3 500	1 467	1 500 000	10.22	2 500
Bandung	450	1 174	75 000	0.64	350
	900	1 467	181 250	1.24	800
	1 300	1 467	313 889	2.14	1 000
	2 200	1 467	408 333	2.78	1 500
	3 500	1 467	875 000	5.96	2 500
Makassar	450	1 174	150 000	1.28	350
	900	1 467	263 636	1.80	800
	1 300	1 467	228 125	1.56	1 000
	2 200	1 467	681 250	4.64	1 500
Pontianak	900	1 467	285 000	1.94	800
	1 300	1 467	495 000	3.37	1 000
	2 200	1 467	777 778	5.30	1 500
	3 500	1 467	625 000	4.26	2 500

Table 5. The PBP ideal and non-ideal of RPVS capacity is 90 % of the purchasing power

PLN power(VA)	RPVS Capacity (Wp)	Ideal PBP (Year)	Non-ideal PBP (Year)
900	810	11.36	25.64
1 300	1 170	8.93	10.42
2 200	1 980	6.49	7.52
3 500	3 150	5.49	6.33
5 500	4 950	4.95	5.75
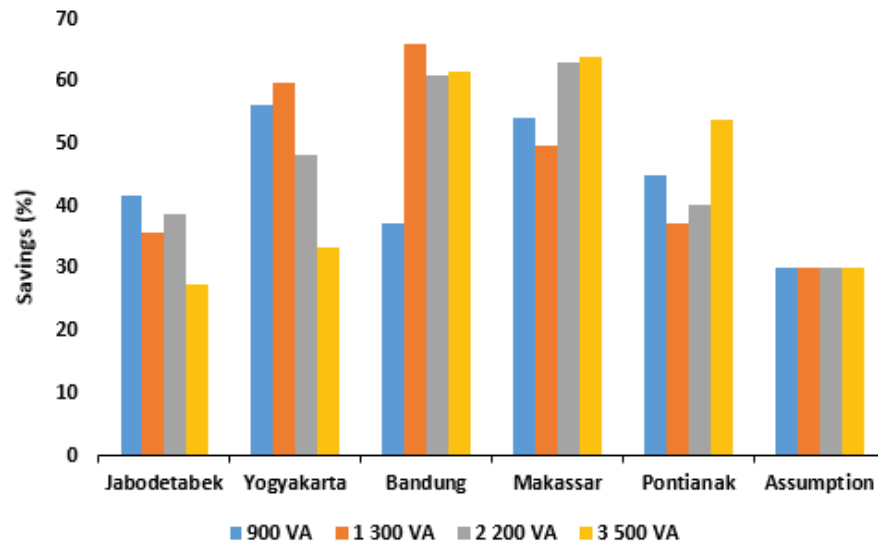
Fig. 4. Monthly electricity cost savings (%)

to provide an overview to policymakers and developers in exploiting the potential of rooftops as an energy producer. This must take into account current and future building standards. In addition, off-grid connected RPVS can also be applied to remote areas [17]. This study contributes to saving electricity costs individually and nationally by utilizing renewable energy sources. The thin-frameless solar panels' technology also reduces installation costs due to minimal modification of the roof construction [22, 23]. In addition, for renewable energy applications in rural areas [24], this type of Thin-frameless PV module can still be used because it is not a hassle in building construction and can reduce installation costs. For future research directions, this study needs to analyze the technical and economic feasibility of using hybrid smart-grid technology with batteries.

5. CONCLUSION

The survey data illustrates the situation of the average electricity consumption in five cities and the monthly costs to pay the electricity to the PLN. The existence of regulations from the Indonesian government is a good step in supporting the usage of renewable energy through the RPVS. The amount of the initial investment of RPVS installation has the potential for substantial savings in monthly financing. In addition, the long service life of the RPVS and the relatively short initial return on investment (PBP) make the RPVS attractive. The RPVS of the household customer that is not ideal affects the economic value of the RPVS investment. The difference in the average investment cost for a non-ideal rooftop has a value of 8 % more expensive than the ideal rooftop. Furthermore, the difference in the average PBP of a non-ideal RPVS has a PBP value of 1 yr longer than the ideal RPVS above 900 Wp of installed capacity.

6. ACKNOWLEDGEMENTS

7. CONFLICT OF INTEREST

The authors declare no conflict of interest.

8. REFERENCES

1. R.A. Wahyuono, and M.M. Julian. Revisiting renewable energy map in Indonesia: Seasonal hydro and solar energy potential for rural off-grid electrification (provincial level). *MATEC Web of Conferences* 164(01040):1–11 (2018). DOI: 10.1051/matecconf/201816401040

2. M.B. Hayat, D. Ali, K.C. Monyake, L. Alagha, and N. Ahmed. Solar energy – A look into power generation, challenges, and a solar-powered future. *International Journal of Energy Research* 43(3):1–19 (2018). DOI: 10.1002/er.4252

3. N.R. Avezova, A.E. Khaitmukhamedov, and A.Y. Usmanov. Solar thermal power plants in the world: The experience of development and operation. *Economy and Ecology of Heliotechnics* 53:72–77 (2017).DOI: 10.3103/S0003701X17010030

4. K.R. Kumar, N.V.V.K. Chaitanya, N.S. Kumar. Solar thermal energy technologies and its applications for process heating and power generation – A review. *Journal of Cleaner Production* 282(125296) (2021). DOI: 10.1016/j.jclepro.2020.125296

5. E.Yandri. The effect of Joule heating to thermal performance of hybrid PVT collector during electricity generation. *Renewable Energy* 111: 344–352 (2017). DOI: 10.1016/j.renene.2017.03.094

6. E.Yandri. Development and experiment on the performance of polymeric hybrid Photovoltaic Thermal (PVT) collector with halogen solar simulator. *Solar Energy Materials and Solar Cells* 201(110066):1–11 (2019). DOI: 10.1016/j.solmat.2019.110066

7. E.Yandri. Methods for the development and testing of polymeric hybrid photovoltaic thermal (PVT) collector for indoor experiments. *Methods* X 6:2620–2635 (2019). DOI: 10.1016/j.mex.2019.10.021

8. D. Watts, M. F. Valdés, D. Jara, and A. Watson. Potential residential PV development in Chile: The effect of schemes for grid-connected PV systems. *Renewable and Sustainable Energy Reviews* 41:1037–1051 (2015). DOI: 10.1016/j.rser.2014.07.201

9. D. Setyawati. Analysis of perceptions towards the rooftop photovoltaic solar system policy in Indonesia. *Energy Policy* 144: 111569 (2020). DOI: 10.1016/j.enpol.2020.111569

10. A. Hidayatno, A.D. Setiawan, I.M.W. Supartha, A.O. Moeis, I. Rahman, and E. Widiono. Investigating policies on improving household rooftop photovoltaics adoption in Indonesia.

Renewable Energy 156:731–742 (2020). DOI: 10.1016/j.renene.2020.04.106

11. M.A. Sihotang and K. Okajima. Photovoltaic power potential analysis in equator territorial: Case study of Makassar City, Indonesia. *Journal of Power and Energy Engineering* 5(1):15–29 (2017). DOI: 10.4236/jpee.2017.51002

12. B. Novianto, K. Abdullah, A.S. Uyun, E. Yandri, S.M. Nur, H. Susanto, Z.V. Gaile, R.H. Setyobudi, and Y. Nurdiansyah. Smart micro-grid performance using renewable energy. *E3S Web of Conferences* 188(00005):1–11 (2020). DOI: 10.1051/e3sconf/202018800005

13. F.A. Khalil, M. Asif, S. Anwar, S. ul Haq, and F. Illahi. Solar tracking techniques and implementation in photovoltaic power plants: A review. *Proceedings of the Pakistan Academy of Sciences A. Physical and Computational Sciences* 54 (3): 231–241 (2017).

14. S. Sharma, K.K. Jain, A. Sharma. Solar cells: In research and applications – A review. *Materials Sciences and Applications* 06(12):1145–1155 (2015). DOI: 10.4236/msa.2015.612113

15. E. Płaczek-Popko. Top PV market solar cells 2016. *Opto-Electronics Review* 25(2):55–64 (2017). DOI: 10.1016/j.opelre.2017.03.002

16. W.S. Nababan, H.V. Sihombing, and H. Ambarita. Techno-economic analysis of a solar rooftop: A case study in Medan city, Indonesia. *IOP Conference Series: Earth and Environmental Science* 452(012106):1–8 (2020). DOI: 10.1088/1755-1315/452/1/012106

17. A.K. Shukla, K. Sudhakar, and P. Baredar. Design, simulation and economic analysis of standalone roof top solar PV system in India. *Solar Energy* 136:437–449 (2016). DOI: 10.1016/j.solener.2016.07.009

18. J. Windarta, S. Saptadi, Denis, D.A. Satrio, and J.S. Silaen. Economic feasibility analysis of rooftop solar power plant design with household-scale on-grid system in Semarang City. *E3S Web of Conferences* 202(09002):1–15 (2020). DOI: 10.1051/e3sconf/202020209002

19. D. S. Williams, C. Susilawati, and G. Walker. Value of residential investment in photovoltaics and batteries in networks: A techno-economic analysis. *Energies* 11(4):1–25 (2018). DOI: 10.3390/en11041022

20. Subarianto. *Simulasi Potensi Aplikasi PLTS Atap Pelanggan PLN Tipe R-1 dan R-2 dengan Skenario Ekspor / Impor.* [Simulation of Potential Applications of Rooftop PV System for PLN Customers Types R-1 and R-2 with Export / Import Scenarios]. Master Thesis, Universitas Darma Persada (2019). [in Bahasa Indonesia].

21. S.C. Hermosa, G. Lucarelli, M. Top, M. Fahland, J. Fahlteich, and T. M.Brown. Perovskite photovoltaics on roll-to-roll coated ultra-thin glass as flexible high-efficiency indoor power generators. *Cell Reports Physical Science* 1(5) (100045):1–17 (2020). DOI: 10.1016/j.xcrp.2020.100045

22. A. Nicholls, R. Sharma, dan T.K. Saha. Financial and environmental analysis of rooftop photovoltaic installations with battery storage in Australia. *Applied Energy* 159:252–264 (2015).DOI: 10.1016/j.apenergy.2015.08.052

23. J. Ahmad. Techno-economic analysis of a wind-photovoltaic-biomass hybrid renewable energy system for rural electrification: A case study of Kallar Kahar. *Energy* 148:208–234 (2018).DOI: 10.1016/j.energy.2018.01.133

24. M. Rumbayan. Development of power system infrastructure model for the island communities: A case study in a remote island of Indonesia. Proceedings of the 2017 International Conference on Advanced Mechatronic Systems, p. 1–4. Xiamen, China, December 6-9, 2017. IEEE (2017). DOI: 10.1109/ICAMechS.2017.8316470

Instructions for Authors

Manuscript Format

The manuscript may contain Abstract, Keywords, INTRODUCTION, MATERIALS AND METHODS, RESULTS, DISCUSSION (or RESULTS AND DISCUSSION), CONCLUSIONS, ACKNOWLEDGEMENTS, CONFLICT OF INTEREST and REFERENCES, *and any other information that the author(s) may consider necessary*.

Abstract (font size 10; max 250 words)**:** Must be self-explanatory**,** stating the rationale, objective(s), methodology, main results, and conclusions of the study. Abbreviations, if used, must be defined on the first mention in the Abstract as well as in the main text. Abstract of review articles may have a variable format.

Keywords (font size 10)**:** Three to eight keywords**,** depicting the article.

INTRODUCTION: Provide a clear and concise statement of the problem, citing relevant recent literature, and objectives of the investigation.

MATERIALS AND METHODS: Provide an adequate account of the procedures or experimental details, including statistical tests (if any), concisely but sufficient enough to replicate the study.

RESULTS: Be clear and concise with the help of appropriate Tables, Figures, and other illustrations. Data should not be repeated in Tables and Figures, but must be supported with statistics.

DISCUSSION: Provide interpretation of the RESULTS in the light of previous relevant studies, citing published references.

ACKNOWLEDGEMENTS: (font size 10)**:** In a brief statement, acknowledge the financial support and other assistance.

CONFLICT OF INTEREST: State if there is any conflict of interest.

REFERENCES (font size 10)**:** Cite references in the text **by number only** in **square brackets**, e.g. "Brown et al [2] reported ..." or "... as previously described [3, 6–8]", and list them in the REFERENCES section, in the order of citation in the text, Tables and Figures (not alphabetically). Only published (and accepted for publication) journal articles, books, and book chapters qualify for REFERENCES.

Declaration: Provide a declaration that: (i) the results are original; (ii) the same material is neither published nor under consideration elsewhere; (iii) approval of all authors have been obtained; and (iv) in case the article is accepted for publication, its copyright will be assigned to *Pakistan Academy of Sciences*. Authors must obtain permission to reproduce, where needed, copyrighted material from other sources and ensure that no copyrights are infringed upon.

Manuscript Formatting

Manuscripts must be submitted in Microsoft Word (2007 Version .doc or .docx format); **pdf** files not acceptable. Figures can be submitted in Word format, TIFF, GIF, JPEG, EPS, PPT. Manuscripts, in *Times New Roman*, 1.15spaced (but use single-space for Tables, long headings, and long captions of tables & figures). The text must be typed in a double-column across the paper width. The Manuscript sections must be numbered, i.e., **1. INTRODUCTION, 2. MATERIALS AND METHODS,** and so on… (a) **Title** of the article **(**Capitalize initial letter of each main word; font-size 16; **bold**), max 160 characters (no abbreviations or acronyms), depicting article's contents; (b) Author' first name, middle initial, and last name (font size 12, **bold**), and professional affiliation (i.e., each author's Department, Institution, Mailing address and Email; but no position titles) (font size 12); (c) Indicate the corresponding author with *; (d) **Short running title**, max 50 characters (font size 10).

Headings and Subheadings (font size 11): All flush left

      LEVEL-1: **ALL CAPITAL LETTERS; Bold**

      Level-2: **Capitalize Each Main Word (**Except prepositions**); Bold**

      Level-3: Capitalize each main word (Except prepositions)***; Bold, Italic***

      Level-4: *Run-in head*; *Italics, in the normal paragraph position. Capitalize the initial word only and end in a colon (i.e., **:**)*

List of REFERENCES must be prepared as under:

a. Journal Articles *(Name of journals must be stated in full)*

1. I. Golding, J. Paulsson, S.M. Zawilski, and E.C. Cox. Real time kinetics of gene activity in individual bacteria. *Cell* 123: 1025–1036 (2005).

2. W. Bialek, and S. Setayeshgar. Cooperative sensitivity and noise in biochemical signaling. *Physical Review Letters* 100: 258–263 (2008).

3. R.K. Robert, and C.R.L.Thompson. Forming patterns in development without morphogen gradients: differentiation and sorting. *Cold Spring Harbor Perspectives in Biology* 1(6) (2009).

4. D. Fravel. Commercialization and implementation of biocontrol. *Annual Reviews of Phytopathology* 43: 337359 (2005).

b. Books

5. W.R. Luellen. Fine-Tuning Your Writing. *Wise Owl Publishing Company, Madison, WI, USA* (2001).

6. U. Alon, and D.N. Wegner (Ed.). An Introduction to Systems Biology: Design Principles of Biological Circuits. *Chapman & Hall/CRC, Boca Raton, FL, USA* (2006).

c. Book Chapters

7. M.S. Sarnthein, and J.D. Stanford. Basal sauropodomorpha: historical and recent phylogenetic developments. In: The Northern North Atlantic: A Changing Environment. P.R. Schafer, & W. Schluter (Ed.), *Springer, Berlin, Germany*, pp. 365–410 (2000).

8. J.E. Smolen, and L.A. Boxer. Functions of Europhiles. In: Hematology, 4th ed. W.J. Williams., E. Butler and M.A. Litchman (Ed.), *McGraw Hill, New York, USA*, pp. 103–101 (1991).

d. Reports

9. M.D. Sobsey, and F.K. Pfaender. Evaluation of the H2S method for Detection of Fecal Contamination of Drinking Water, Report WHO/SDE/WSH/02.08, *Water Sanitation and Health Programme, WHO, Geneva, Switzerland* (2002).

e. Online references

These should specify the full URL for reference and give the date on which it was consulted. Please check again to confirm that the work you are citing is still accessible:

10. L. Branston. SENSPOL: Sensors for Monitoring Water Pollution from Contaminated Land, Landfills and Sediment (2000). http://www.cranfield.ac.uk/biotech/senspol/ (accessed 22 July 2005)

Tables and Figures

Insert all tables as editable text, not as images. Number tables consecutively following their appearance in the text, Figures should appear in numerical order, be described in the body of the text, and be positioned close to where they are first cited. Each figure should have a caption that describes the illustration, and that can be understood independently of the main text (Caption Table 1. and Fig 1. font size 10; Bold; Captions should be in sentence case; left-aligned). All Figures should have sufficiently high resolution (minimum 1000 pixels width/height, or a resolution of 300 dpi or higher) to enhance the readability. Figures may be printed in two sizes: column width of 8.0 cm or page width of 16.5 cm; number them as **Fig. 1**, **Fig. 2**, … in the order of citation in the text. Parts in a figure can be identified by A, B, C, D, ... and cited as Figure 2A, Figure 2B, Figure 2C. Captions to Figures must be concise but self-explanatory. Laser printed line drawings are acceptable. Do not use lettering smaller than 9 points or unnecessarily large. Photographs must be of high quality. A scale bar should be provided on all photomicrographs.

Tables: with concise but self-explanatory headings must be numbered according to the order of citation (like **Table 1.**, **Table 2.**). *Do not* abbreviate the word "Table" to "Tab.". Round off data to the nearest three significant digits. Provide essential explanatory footnotes, with superscript letters or symbols keyed to the data. Do not use vertical or horizontal lines, except for separating column heads from the data and at end of the Table.

Figures: Figures may be printed in two sizes: column width of 8.0 cm or page width of 16.5 cm; number them as **Fig. 1**, **Fig. 2**, … in the order of citation in the text. Captions to Figures must be concise but self-explanatory. Laser printed line drawings are acceptable. Do not use lettering smaller than 9 points or unnecessarily large. Photographs must be of high quality. A scale bar should be provided on all photomicrographs.

Note: The template of the manuscript is available at http://www.paspk.org/proceedings/; http://ppaspk.org/

Reviewers: Authors may suggest four relevant reviewers, two National and two International (with their **institutional E-mail** addresses).

SUBMISSION CHECKLIST

The following list will be useful during the final checking of an article before sending it to the journal for review.

Ensure that the following items are present:

One author has been designated as the corresponding author with contact details:

• E-mail address (Correct and valid)

• Full address of Institute/organization

• Keywords

• All figure captions

• All tables (including title, description, footnotes)

Further considerations

• Manuscript has been 'spell-checked' and 'grammar checked'

• References are in the correct format for this journal

• All references mentioned in the Reference list are cited in the text, and vice versa

• Permission has been obtained for the use of copyrighted material from other sources (including the Internet)

In case of any difficulty while submitting your manuscript, please get in touch with:

Editor
Pakistan Academy of Sciences
3-Constitution Avenue, Sector G-5/2
Islamabad, Pakistan
Email: editor@paspk.org
Tel: +92-51-920 7140
Websites: http://www.paspk.org/proceedings/; http://ppaspk.org/

CONTENTS